CP-64173
Revision 0

QUANTITATIVE STRUCTURAL EVALUATION

Prepared for the U.S. Department of Energy
Assistant Secretary for Environmental Management

Contractor for the U.S. Department of Energy
under Contract DE-AC06-08RL14788

CH2MHILL
Plateau Remediation Company

P.O. Box 1600
Richland, Washington 99352

Approved for Public Release;
Further Dissemination Unlimited

CP-64173
Revision 0

QUANTITATIVE STRUCTURAL EVALUATION

Program/Project: CPRM

T. E. Bratvold
CH2M HILL Plateau Remediation Company

Date Published
October 2019

Prepared for the U.S. Department of Energy
Assistant Secretary for Environmental Management

Contractor for the U.S. Department of Energy
under Contract DE-AC06-08RL14788

CH2MHILL
Plateau Remediation Company
P.O. Box 1600
Richland, Washington 99352

APPROVED
By Janis D. Aardal at 10:25 am, Oct 18, 2019

Release Approval | Date

Approved for Public Release;
Further Dissemination Unlimited

TRADEMARK DISCLAIMER

Reference herein to any specific commercial product, process, or service by tradename, trademark, manufacturer, or otherwise, does not necessarily constitute or imply its endorsement, recommendation, or favoring by the United States Government or any agency thereof or its contractors or subcontractors.

This report has been reproduced from the best available copy.

Printed in the United States of America

LPI, Inc. Consulting Engineers

Advanced Analysis & Fitness for Service
Failure & Materials Evaluation
Nondestructive Engineering

Est. 1885

STRUCTURAL ASSESSMENT OF AGING LEGACY BURIED CRIBS AND TANKS AT THE HANFORD CENTRAL PLATEAU

Report No.: LA181779-R-001
Revision No: 0

October 7, 2019

Prepared For
TERRAGRAPHICS ENVIRONMENTAL ENGINEERING, INC.
Pasco, WA

Prepared By
LPI, Inc.

EXECUTIVE SUMMARY

LPI, Inc. (LPI) was requested to provide engineering services for the assessment of below-grade facilities located within the Central Plateau of the Hanford site that were determined to have the highest combined risk of failure [1]. Table ES-1 summarizes the scope for the structural analyses, which were performed to determine if margin from collapse still exists in the structural members (the amount of remaining factor of safety in the designs from collapse). The structural margin of the aging structures was assessed using requirements provided in the American Concrete Institute (ACI) [4, 5], American Institute of Steel Construction (AISC) [6], American Society of Civil Engineers/Seismic (ASCE/SEI 41) [11], ASCE 7 [24], International Building Code (IBC) [3] Codes, and the Wood Handbook [12]. These documents are generally design documents and do not necessarily present failure limits. However, they provide acceptable strength limits that can provide useful information to assess the fitness of structural components.

ANSYS ® software was used to perform the structural evaluations of the below-grade structures and is a general-purpose finite element computer code [7]. This software is widely used in the nuclear industry for thermal and structural analyses of structural and mechanical components and includes a wide range of capabilities for simulation and analysis of various material models and loading conditions. ANSYS Workbench Version 18.0 was used in the present evaluations. This software was validated and verified for the specific computers used in the analysis by means of a set of verification problems provided by ANSYS.

Information collection and review efforts were conducted to identify the different types of material properties and applied loads to be considered in the structural evaluations. Materials representing the 11 highest-risk facilities (one structure for each of the 11 structure categories in the scope of work) primarily include wood (Douglas Fir, and creosote-treated), concrete, wrought iron and mild carbon steel. Most material properties were obtained from publicly available reports, many of which involved previous assessments of Hanford degraded structures including, but not limited to, the PUREX Tunnel 1 Engineering Evaluation [14 and 21], Hanford Double-Shell Tanks [17], and Hanford Single-Shell Tanks [16, and 22]. As shown in Table ES-1, all structures are buried in or surrounded by soil. The 216-Z-2 structure is the only timber crib box having a cavity depth (14 ft) greater than the soil overburden (7 ft).

Applied loads in the present structural evaluations consist of dead weight, waste pressure (as applicable), lateral soil pressure, snow, and seismic loads identified in [5, 14, 24].

ANSYS is a trademark of ANSYS, Inc., Canonsburg, Pennsylvania.

Consistent with the analysis of the PUREX Tunnel 1 [14], and given that barricades (light-duty post and chain fence) and signage (i.e., “Cave-In Potential”, and “Caution Underground Radioactive Material” signage) are currently employed at the ground surface for many of these underground structures [18], live loads were not considered. As such, the structural calculations presented herein address the overall structural stability, and should not be used to justify worker safety.

Factored load combinations were used to determine structural demand. A detailed description of the loading is included in Appendix A. In this regard, several assumptions were necessary in order to perform the evaluations because some of the facilities had limited information regarding dimensions, reinforcement details, and prestressing data. For structures with documented evidence of subsidence, corrosion, or water intrusion, the structural evaluations also simulated degradation in structural members by employing reduced concrete thickness, reduced rebar surface area, or increased structural response to the applied loads.

Table ES-2 summarizes the results of the structural evaluations, which indicates that several structures have adequate margin against failure, while other structures likely experienced or potentially will experience some level of structural failure. Additional analysis should be performed using the results herein to determine whether local failures identified can lead to progressive failure and larger damage. Additional analysis using nonlinear analysis should also be performed to define and quantify failures more accurately.

The analyses performed herein are based on current code requirements for load factors, load combinations, and strength reductions for concrete and steel materials. The assessment of the original design requirements was not in the scope of work; therefore, the results of this report should not be used to characterize the adequacy of the original design. The impact of structural failure for structures shown in Table ES-3 was qualitatively evaluated in the “RL-40 Aging Structures Risk Assessment” report (Rev. 2) [18].

Table ES-1: Scope of Aging Legacy Buried Structures

Group	Structure	Description	Waste Level[1]
C1	216-Z-2	Timber crib box constructed in 1948; 12 x 12 x 14 ft; 7 ft overburden	N/A
C2	216-B-12	Timber crib box constructed in 1951; 16 x 16 x 10 ft; 15 ft overburden	N/A
C3	216-Z-6	Timber trench box constructed in 1945, 50 x 6.5 x 3.46 ft; 6 ft overburden	N/A
C4	216-Z-7	Timber trench box constructed in 1946; 8 x 150 x 3 ft; 6 ft overburden	N/A
C5	216-Z-9	Concrete covered crib constructed in 1955; 90 x 120 ft roof; earth walls slanted inward to 60 x 30 ft bottom; No overburden	N/A
T1	241-T-361	Upright cylindrical concrete tank constructed in 1944; Prestressed concrete; 20 ft OD x 19 ft tall; 6-in. wall thickness; 6 ft overburden	10.8 ft
T2	241-Z-361	Rectangular concrete tank constructed in 1948; 28 x 15 x 19 ft tall; 2 ft overburden	8 ft
T3	241-Z-8	Horizontal cylindrical steel tank constructed in 1954; 40 ft long x 8 ft OD; 6 ft overburden	N/A[2]
O1	PUREX deep bed filters[3]	Rectangular concrete vault constructed in 1954; 82 x 52 x 13 ft; 4 ft overburden and 4 in. shotcrete	N/A
O2	REDOX sand filter	Rectangular concrete vault constructed in 1950; 85 x 85 x 20 ft; No overburden	N/A
O3	241-CX-70	Upright cylindrical concrete tank constructed in1951; 20 ft ID x 15 ft tall; 13 in. thick wall and 1 ft thick roof; 11 ft overburden	N/A[4]

[1] Waste level is based on the documents retrieved and summarized in the Risk Assessment Report (Rev. 2) [18].

[2] Free-standing liquids were removed in 1974 from the 241-Z-8 tank, and approximately 7 in. (500 gal) of sludge remain [18].

[3] Appendix B of this document shows results for an additional structural evaluation of the PUREX deep bed filters based on 4 ft of soil overburden and 8 in. of shotcrete (instead of the existing 4 in. of shotcrete).

[4] Free-standing liquids and sludge were removed in 1992 from the 241-CX-70 tank, tank was dried, and is considered empty [18].

Table ES-2: Structural Evaluation Margin-to-Failure Results

Group	Structure	Acceptable (Y/N)	Discussion
C1	216-Z-2	Y	-
C2	216-B-12	N	Bending and shear stresses are above failure limit.
C3	216-Z-6	N	Overstress in shear
C4	216-Z-7	Y	-
C5	216-Z-9	N	Overstress in slab and column flexure
T1	241-T-361	Y	No information is available for the prestressing and rebar.
T2	241-Z-361	N	Moment and shear limits are exceeded at bottom of long walls. This will likely cause limited local failure. Failure will not progress due to the redundancy available in the box structure.
T3	241-Z-8	Y	Some yielding may take place.
O1	PUREX deep bed filters[5]	Y	-
O2	REDOX sand filter	Y	-
O3	241-CX-70	N	Local yielding of top radial rebar in the roof at the wall junction and in the wall at the top. The yielding may cause relieving of local stresses and limit damage progression.

[5] Appendix B of this document shows that the PUREX deep bed filter margin is still acceptable using 4 ft of soil overburden and 8 in. of shotcrete (instead of the existing 4 in. of shotcrete).

Table ES-3: RL-40 Aging Structures Evaluated in [18] (2 Sheets)

Group	Structure	Date Constructed	Caved-In, Subsidence	Depth of Soil Overburden	Type of Construction	Approximate Size (ft)	Facility Hazard Classification
C1	216-B-7A/B	1945	No	24 feet	Timber Crib Box	12W x 12W x 4H	Exempt
	216-B-8	1944	Yes	16 feet	Timber Crib Box	12W x 12W x 7H	Exempt
	216-B-9	1948	No	22 feet	Timber Crib Box	14W x 14W x 7H	Exempt
	216-B-10A/B	1948	Yes	16 feet	Timber Crib Box	12W x 12W x 3.5H	Exempt
	216-T-6	1945	Yes	16 feet	Timber Crib Box	12W x 12W x 4H	Exempt
	216-T-7	1947	No	19 feet	Timber Crib Box	12W x 12W x 7H	Exempt
	216-T-8	1949	Yes	16 feet	Timber Crib Box	12W x 12W x 4H	Exempt
	216-T-19	1950	Yes	21 feet	Timber Crib Box	12W x 12W x 9H	Exempt
	216-T-32	1945	No	22 feet	Timber Crib Box	12W x 12W x 4H	Exempt
	216-U-1	1950	No	16 feet	Timber Crib Box	12W x 12W x 4H	Exempt
	216-U-2	1950	No	16 feet	Timber Crib Box	12W x 12W x 4H	Exempt
	216-U-8	1951	Yes	16 feet	Timber Crib Box	16W x 16W x 10H	Exempt
	216-Z-1	1948	Yes	6 feet	Timber Crib Box	12W x 12W x 14H	Exempt
	216-Z-2	1948	No	6 feet	Timber Crib Box	12W x 12W x 14H	Exempt
	216-Z-5	1945	No	14 feet	Timber Crib Box	12W x 12W x 4H	Exempt
C2	216-B-12	1951	Yes	15 feet	Timber Crib Box	16W x 16W x 10H	Exempt
C3	216-Z-6	1945	Yes	6 feet	Timber Trench Box	50L x 6.5W x 4H	Exempt
C4	216-Z-7	1946	No	6 feet	Timber Trench Box	150L x 8W x 3H	Exempt
C5	216-Z-9	1955	No	None	Concrete Covered Crib	120L x 90W x 20H	2
T1	241-B-361	1944	No	6 feet	Cylindrical Concrete Tank	20D x 19H	Exempt
	241-T-361	1944	No	6 feet	Cylindrical Concrete Tank	20D x 19H	Exempt
	241-U-361	1951	No	6 feet	Cylindrical Concrete Tank	20D x 19H	Exempt
T2	241-Z-361	1948	No	2 feet	Rectangular Concrete Tank	28L x 15W x 19H	2

Table ES-3 RL-40 Aging Structures Evaluated in [18] (2 Sheets)

Group	Structure	Date Constructed	Caved-In, Subsidence	Depth of Soil Overburden	Type of Construction	Approximate Size (ft)	Facility Hazard Classification
T3	241-Z-8	1954	No	6 feet	Cylindrical Steel Tank	40L x 8D	Exempt
O1	PUREX Deep Bed Filters	1954	No	4 feet	Rectangular Concrete Vault	82L x 52W x 13H	2
O2	REDOX Sand Filter	1950	No	None	Rectangular Concrete Vault	85L x 85W x 20H	2
O3	241-CX-70	1951	Yes	11 feet	Cylindrical Concrete Tank	20D x 15H	Exempt

DOCUMENT RECORD

Document Type:	☐ **Calculation** ☒ **Report** ☐ **Procedure**
Document No:	LA181779-R-001
Document Title:	Structural Assessment of Aging Legacy Buried Cribs and Tanks at the Hanford Central Plateau
Client:	TerraGraphics Environmental Engineering, Inc.
Client Facility:	428 W. Shoshone St, Pasco, WA 99301
Client PO No:	Subcontract No. S18-1055, Task Order 1
Quality Assurance:	**Nuclear Safety Related?** ☒ **No** ☐ **Yes**
Computer Software Used:	☐ **No**[1] ☒ **Yes**[2] — 1. Check NO when EXCEL, MathCAD and/or similar programs are used since algorithms are explicitly displayed. 2. Include Software Record for each computer program utilized
Instrument Used	☒ **No** ☐ **Yes**[3] — 3. Include Document Instrument Record.

Revision	Approval Date	Preparer[5]	Checker[5]	Design Verification[5]	Approver[4,5]
0	10/07/19	*R. Siddiqui* *E. Cheifet* *B. Elaidi*	*E. Cheifet* *R. Siddiqui* *C. Guzmán-Leong*	*n/a*	*R. S. Vecchio*

[4] The Approver of this document attests that all project examinations, inspections, tests and analysis (as applicable) have been conducted using approved LPI Procedures and are in conformance to the contract/purchase order.

[5] Electronic signatures may be used only with prior concurrence.

Page	8	of	233	Total Pages	(include any Title Sheet and Attachments in page count. Document Back Cover, if utilized, not included in page count)

This document is rendered upon the condition that it is not to be reproduced wholly or in part for advertising or other purposes over our signature or in connection with our name without special permission in writing. Be advised that all materials submitted for evaluation will be retained for six months. After such time, all material will be discarded unless otherwise notified in writing to retain beyond six months.

Form: LPI-3.1-Rev-10-Fig-5-2

Record of Revision

Revision No.	Date	Description of Change	Reason
0	10/07/19	N/A	Original Issue

Form: LPI-3.1-Rev-10-Fig-5-7

Document Software Record[1] (include separate sheet for each software package used)			
1	**Computer Software Used** (Code/Version)	ANSYS Workbench 18.0 [7]	
2	**Software Supplier**	ANSYS, Inc.	
3	**Software Update Review**	☒ Error notices; describe: Reviewed error notices on ANSYS website ☒ Other; describe: Refer to [8 & 10]	
4	**Nuclear Safety Related Software**	☐ NO ☒ YES[2]	[2] If YES, complete the following: Computer 1 type: Dell Precision 7910-1 Computer1 S/N: HQ83XM2 Computer 1 O/S: Windows 10 Pro for Workstations V & V (include as ref): [8 & 10]
5	**Bases for Application**	Identify the bases that support use of this software for the application herein; may be separately discussed elsewhere in this document (indicate section) and/or may be addressed in the V&V (identify reference number):	See Section 3
6	**Input Listing/Summary[3]**	☐ Input listing and/or summary attached: ☒ Not attached; identify File/Disc ID: C1 – 1-29-2019 3;15;20 PM EST –ds.dat O1 Rev1 - 5-13-2019 10;47;44 AM EST - ds.dat (4 in. shotcrete) O1 Rev2 - 5-13-2019 11;37;35 AM EST - ds.dat (8 in. shotcrete) O2 – 2-15-2019 12;09;06 AM EST –ds.dat O2 – 2-15-2019 8;49;30 AM EST –post.dat T1 buckling LC1 – 2-14-2019 8;09;28 PM EST –ds.dat T1 buckling LC2 – 2-14-2019 8;48;35 PM EST –ds.dat T1 static – 2-14-2019 2;29;12 PM EST –ds.dat T1 static – 3-5-2019 4;08;02 PM EST –post.dat T2 static – 2-12-2019 10;41;52 AM EST –ds.dat T2 static – 2-14-2019 9;15;16 PM EST –post.dat T3 buckling LC1 – 2-15-2019 2;00;55 PM EST –ds.dat T3 buckling LC2 – 2-15-2019 2;09;08 PM EST –ds.dat T3 static – 2-15-2019 1;51;45 PM EST –ds.dat T1 buckling ldhi file – 2-14-2019 3:25;47 PM EST – file.ldhi	
7	**Output Data/Identifier(s)[3]**	☒ Output results attached: Selected relevant output is included herein ☐ Not attached; identify File/Disc ID:	
	[3]e.g., run date/time; use for reference, as appropriate, within body of calculation		
8	**Comments**	NA	
9	**Keywords[4]**	SOLID185, SOLID186, SOLID187, BEAM189, SHELL181, SHELL281, TARGE170, SURF154, CONTA174, CONTA175, CONTA177	

	[4]For use in describing software features used in this calculation; use common terms based on software user manual and/or help files.	
10	**Project Manager Name:**	Consuelo Guzmán-Leong

[1] If computer software is used on project, complete form with required information.
Update the LPI Computer Software Use List per LPI Procedure 13.1 requirements.

Form: LPI-3.1-Rev-10-Fig-5-8

Document Software Record[1]

(include separate sheet for each software package used)

1	**Computer Software Used** (Code/Version)	ANSYS Workbench 18.0 [7]
2	**Software Supplier**	ANSYS, Inc.
3	**Software Update Review**	☒ Error notices; describe: Reviewed error notices on ANSYS website ☒ Other; describe: Refer to [8 & 10]
4	**Nuclear Safety Related Software**	☐ NO ☒ YES[2] [2] If YES, complete the following: Computer 2 type: Dell Precision 7500-2 Computer 2 S/N: 13WTBM1 Computer 2 O/S: Windows 7 Professional V & V (include as ref): [8 & 10]
5	**Bases for Application**	Identify the bases that support use of this software for the application herein; may be separately discussed elsewhere in this document (indicate section) and/or may be addressed in the V&V (identify reference number): See Section 3
6	**Input Listing/Summary[3]**	☐ Input listing and/or summary attached: ☒ Not attached; identify File/Disc ID: C2 - 05-14-2019 12;32;50 PM EST– ds.dat C3 – 02-22-2019 02;22;15 PM EST – ds.dat C4 – 02-25-2019 10;18;45 PM EST – ds.dat C5 – 03-05-2019 04;38;17 PM EST – ds.dat O3 – 09-10-2019 11;53;33 AM EST – ds.dat O3 – 09-10-2019 04;25;24 PM EST – post.dat
7	**Output Data/Identifier(s)[3]**	☒ Output results attached: Selected relevant output is included herein ☐ Not attached; identify File/Disc ID:
	[3]e.g., run date/time; use for reference, as appropriate, within body of calculation	
8	**Comments**	NA
9	**Keywords[4]**	SOLID185, SOLID186, SOLID187, BEAM189, SHELL181, SHELL281, TARGE170, SURF154, CONTA174, CONTA175, CONTA177
	[4]For use in describing software features used in this calculation; use common terms based on software user manual and/or help files.	
10	**Project Manager Name:**	Consuelo Guzmán-Leong

[1] If computer software is used on project, complete form with required information.
Update the LPI Computer Software Use List per LPI Procedure 13.1 requirements.

Form: LPI-3.1-Rev-10-Fig-5-8

CERTIFICATION PAGE

I, the undersigned, being a registered Professional Engineer competent in the modeling and structural evaluation of various concrete, steel, and wood structures and acceptance criteria in the ACI 318/349, AISC Manual of Steel Construction, ASCE/SEI 41-13, ASCE 7-10, and IBC Codes and recognized methods for evaluation of timber structures and using the drawings cited herein, do hereby certify that to the best of my knowledge and belief the structural evaluations performed and documented in LPI Report No. LA181779-R-001, Rev. 0 are complete and accurate and comply with methods that are universally recognized for analysis of similar structures and determination of strength levels.

Certified by:	Robert S. Vecchio, Ph.D., PE		
Registration No.:	48689	State:	Washington

ROBERT S. VECCHIO
STATE OF WASHINGTON
48689
REGISTERED
PROFESSIONAL ENGINEER

EXPIRES 17-JAN-21

Table of Contents

Document Record 8
Record of Revision 9
Document Software Record 10
Certification Page 13
Table of Contents 14
1. INTRODUCTION 16
2. SCOPE 16
3. METHODOLOGY 17
3.1 Structure 216-Z-2, Group C1 21
3.2 Structure 216-B-12, Group C2 25
3.3 Structure 216-Z-6, Group C3 29
3.4 Structure 216-Z-7, Group C4 33
3.5 Structure 216-Z-9, Group C5 37
3.6 Structure 241-T-361, Group T1 39
3.7 Structure 241-Z-361, Group T2 42
3.8 Structure 241-Z-8, Group T3 45
3.9 Structure PUREX Deep Bed Filters, Group O1 46
3.10 Structure REDOX Sand Filters, Group O2 55
3.11 Structure 241-CX-70, Group O3 61
4. EVALUATION OF FINITE ELEMENT RESULTS 66
4.1 Structure 216-Z-2, Group C1 67
4.2 Structure 216-B-12, Group C2 71
4.3 Structure 216-Z-6, Group C3 74
4.4 Structure 216-Z-7, Group C4 77
4.5 Structure 216-Z-9, Group C5 80
4.6 Structure 241-T-361, Group T1 91
4.7 Structure 241-Z-361, Group T2 101
4.8 Structure 241-Z-8, Group T3 111
4.9 Structure PUREX Filters, Group O1 114
4.10 Structure REDOX Filter, Group O2 122
4.11 Structure 241-CX-70, Group O3 147

5. SUMMARY 159
6. REFERENCES 163

APPENDIX A: CRITERIA, MATERIAL PROPERTIES, ASSUMPTIONS.....23

APPENDIX B: PUREX FILTER WITH 8 IN. OF SHOTCRETE 10

APPENDIX C: RCR DOE COMMENTS AND ADDITIONAL PLOTS 30

1. INTRODUCTION

LPI, Inc. (LPI) was requested to provide engineering services for the assessment of below-grade facilities located within the Central Plateau of the Hanford site that were determined to have the highest combined risk of failure [1]. To that end, this report documents the structural evaluations of selected legacy aging buried cribs and tanks in accordance with the Master Service Agreement with TerraGraphics Environmental Engineering, Inc. [1]. The "RL-40 Aging Structures Risk Assessment" report [18] was conducted to identify aging buried structures most prone to structural degradation or collapse. Based on the results of this report [18], structural evaluations were performed for select structures. The intent of the structural evaluations is to determine whether margin from collapse exists in the highest risk structures.

2. SCOPE

Table 2-1 lists the structures included in this study and provides a summary description for each structure; the level of waste stored (as applicable) is also indicated. As shown in Table 2-1Table ES-1, all structures are buried in or surrounded by soil. The 216-Z-2 structure is the only timber crib box having a cavity depth (14 ft) greater than the soil overburden (7 ft).

Table 2-1: Scope of Aging Legacy Buried Structures

Group	Structure	Description	Waste Level[6]
C1	216-Z-2	Timber crib box constructed in 1948; 12 x 12 x 14 ft; 7 ft overburden	N/A
C2	216-B-12	Timber crib box constructed in 1951; 16 x 16 x 10 ft; 15 ft overburden	N/A
C3	216-Z-6	Timber trench box constructed in 1945, 50 x 6.5 x 3.46 ft; 6 ft overburden	N/A
C4	216-Z-7	Timber trench box constructed in 1946; 8 x 150 x 3 ft; 6 ft overburden	N/A
C5	216-Z-9	Concrete covered crib constructed in 1955; 90 x 120 ft roof; earth walls slanted inward to 60 x 30 ft bottom; No overburden	N/A
T1	241-T-361	Upright cylindrical concrete tank constructed in 1944; Prestressed concrete; 20 ft OD x 19 ft tall; 6-in. wall thickness; 6 ft overburden	10.8 ft
T2	241-Z-361	Rectangular concrete tank constructed in 1948; 28 x 15 x 19 ft tall; 2 ft overburden	8 ft
T3	241-Z-8	Horizontal cylindrical steel tank constructed in 1954; 40 ft long x 8 ft OD; 6 ft overburden	N/A[7]
O1	PUREX deep bed filters[8]	Rectangular concrete vault constructed in 1954; 82 x 52 x 13 ft; 4 ft overburden and 4 in. shotcrete	N/A
O2	REDOX sand filter	Rectangular concrete vault constructed in 1950; 85 x 85 x 20 ft; No overburden	N/A
O3	241-CX-70	Upright cylindrical concrete tank constructed in1951; 20 ft ID x 15 ft tall; 1 ft thick roof; 13 in. thick wall; 11 ft overburden	N/A[9]

3. METHODOLOGY

ANSYS ® software was used to perform the structural evaluations of the below-grade structures located within the Central Plateau of the Hanford site. ANSYS is a general-purpose finite element computer code [7] that is widely used in the nuclear industry for thermal and structural analyses of structural and mechanical components, and includes a

[6] Waste level is based on the documents retrieved and summarized in the Risk Assessment Report (Rev. 2) [18].

[7] Free-standing liquids were removed in 1974 from the 241-Z-8 tank, and approximately 7 in. (500 gal) of sludge remain [18].

[8] Appendix B of this document shows results for an additional structural evaluation of the PUREX deep bed filters based on 4 ft of soil overburden and 8 in. of shotcrete (instead of the existing 4 in. of shotcrete).

[9] Free-standing liquids and sludge were removed in 1992 from the 241-CX-70 tank, tank was dried, and is considered empty [18].

wide range of capabilities for simulation and analysis of various material models and loading conditions. ANSYS Workbench Version 18.0 was used in the present evaluations. This software was validated and verified as documented in [10].

Finite element models that were developed to assess margin-to-failure are described in the following subsections. Concrete structures were modeled as linear elastic solid and as such, rebar was not included in the modeling but were incorporated into the associated ACI Code evaluations. Internal liners, stiffeners and miscellaneous steel elements within concrete tanks were not credited since their structural integrity could not be verified. Material properties, load descriptions, and degradation modeling assumptions are provided in Appendix A of this report. Several models incorporate simulated degradation that was postulated based on the description of current conditions and historical events. Table 3-1 describes the simulated degradation and Appendix A provides additional discussion on the rational of the assumed degradation. The degree of degradation shown in Table 3-1 were assumed values in the absence of any information that may allow the determination of the actual degradation present in the structures (as applicable). In addition, missing information for member sizes, reinforcement details, and prestressing data were substituted using qualified assumptions. A summary of modeling assumptions is provided in Table 3-2.

The loading and load combinations in the finite element analyses are also described in Appendix A of this report. Loads include deadweight (DW), waste pressure (F), earth lateral load, (LE), snow load (S), and seismic load (E). Thermal loads were not postulated since any remaining radioactive contents were assumed to have insignificant potential for heat generation. Consistent with the analysis of the PUREX Tunnel 1 [14], and given that barricades (light-duty post and chain fence) and signage (i.e., “Cave-In Potential”, and “Caution Underground Radioactive Material” signage) are currently employed at the ground surface for many of these underground structures [18], live loads were not included in the present structural evaluations for any of the structures. The limiting load combinations are defined in Appendix A and include one non-seismic load combination and one seismic load combination.

Acceptance criteria from the American Concrete Institute (ACI) [4, 5], American Institute of Steel Construction (AISC) [6], American Society of Civil Engineers/Seismic (ASCE/SEI 41) [11], ASCE 7 [24], and International Building Code (IBC) [3] Codes, and the Wood Handbook [12] were used to assess margin to failure. Finite element stresses for steel and timber were compared to strength values. Finite element stresses for concrete were integrated over the cross section to obtain section axial force, bending moment, and shear force. These quantities were compared to the corresponding strength from the ACI code using concrete geometry and rebar. ACI 318 and ACI 349 provide very similar requirements for the structural components evaluated herein and, therefore, both documents were used as appropriate. For every structure, only critical and highly stressed components were

evaluated for margin. Slender structural components were evaluated for stability by performing Eigen value buckling analysis and comparing the critical buckling load to the postulated loads.

The analyses performed herein are based on current code factored load combinations and strength reductions for steel and concrete. The intent of the analysis is to assess margin for failure. An assessment of the original design requirements was not in the scope of work; therefore, the results documented herein should not be used to characterize the adequacy of the original design.

Table 3-1: Simulated Damage/Degradation

Group	Structure	Simulated Degradation
C1	216-Z-2	Response of roof elements was increased by 20% because subsidence has been observed in other structures within the group, and 216-Z-1 (neighbor crib) already collapsed [18]
C2	216-B-12	Response of roof elements was increased by 20% because subsidence has been observed [18]
C3	216-Z-6	Response of roof elements was increased by 20% because collapses have been observed [18]
C4	216-Z-7	N/A
C5	216-Z-9	Concrete thickness was reduced by 1 in. because concrete degradation has been observed [18]
T1	241-T-361	Concrete thickness was reduced by 0.6 in. (10%) and rebar area by 10% - assuming that degradation is present due to harsh environment
T2	241-Z-361	Roof and wall thickness were reduced by 1 in., rebar area was reduced by 20%[10] because steel liner corrosion and roof cracking has been observed [18]
T3	241-Z-8	N/A
O1	PUREX deep bed filters	Rebar area was reduced by 10% and roof slab and external wall thickness was reduced by 1 in. because water intrusion has been observed [18]
O2	REDOX sand filter	Similar to the water intrusion concerns for the PUREX deep bed filters, concrete cover rebar area was reduced by 10% and roof slab and external wall thickness was reduced by 1 in.
O3	241-CX-70	N/A [27]

[10] The initial degradation estimate was a 10% rebar area reduction, but was later increased to 20% to account for the observed cracking in 241-Z-361.

Table 3-2: Summary of Model Assumptions

Group	Structure	Assumptions
C1	216-Z-2	None
C2	216-B-12	None
C3	216-Z-6	None
C4	216-Z-7	None
C5	216-Z-9	1. Thickness of acid split brick lining on the slab bottom face and columns was assumed to be 1 in. 2. Soil beneath and around the perimeter concrete ledge was assumed adequate for supporting vertical and lateral structural reactions.
T1	241-T-361	1. Rebar and prestressing details were not available.
T2	241-Z-361	None
T3	241-Z-8	None
O1	PUREX deep bed filters	1. The 5 I 10.0 E-W steel beams in the N-S trench on the east side were assumed not to be directly loaded.
O2	REDOX sand filter	1. The roof slab thickness was assumed to be 6 in. 2. The roof beam depth was assumed to be 13.5 in. below the bottom face of the slab. 3. Slab thickness above air tunnels was assumed to be 8 in.
O3	241-CX-70	None

3.1 Structure 216-Z-2, Group C1

Overall dimensions of the 216-Z-2 timber crib are 12 x 12 x 14 ft, with 7 ft of soil overburden. The crib frames were constructed of 15.24 x 15.24 cm (6 x 6 in.) timber braces stacked in 27 alternating layers rotated 90° so that the braces are crisscrossed. See Figure 3.1-1 for solid modeling of a single layer and Figure 3.1-2 for solid modeling of a few stacked layers. Figure 3.1-3 and Figure 3.1-4 show general isometric views of the completed solid model.

To prevent shifting during backfill of the excavation, each layer of the timber frame was securely fastened in construction to the next. The top layer of the crib frame was covered with timbers with holes cut to allow vent piping to pass through. Because subsidence has been observed in other structures within Group C1, and the neighbor 216-Z-1 crib already collapsed, degradation was accounted for by increasing the calculated demand stresses by 20%.

Timber beams were meshed with ANSYS SOLID186 elements with an approximate mesh size of 1.5 in. (Figure 3.1-5). All roof, wall, and cross timber members have 9 nodes through the thickness. Layer to layer contact was represented by merged nodes at the corners and where interior cross members meet. The roof is integral with the layer below along the edges, and is in contact with the internal cross members of the layer below using bonded contact. Boundary conditions were simulated with frictionless vertical restraints. All protruding pipes are nonstructural and were not considered. Material properties were assigned and loads applied as described in Appendix A. Variations in timber stiffness due to grain orientation were accounted for using orthotropic properties for the elastic modulus and Poisson's ratio.

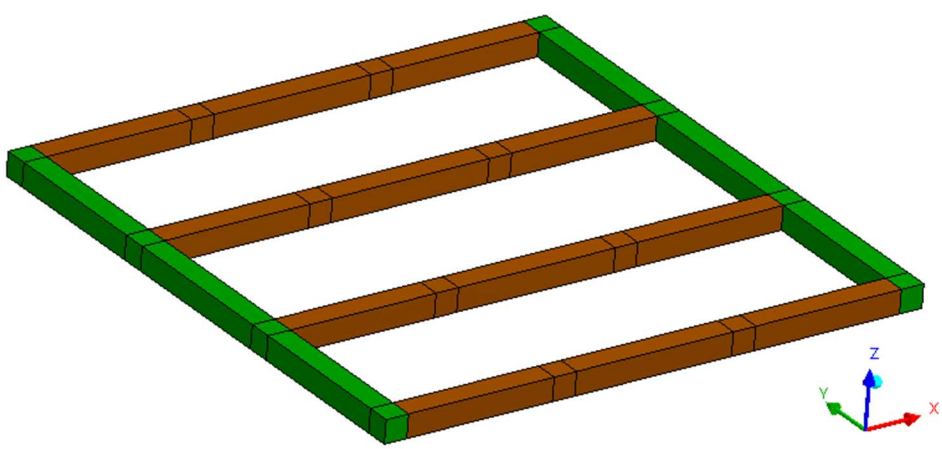

Figure 3.1-1: General View of the ANSYS Solid Model of a Single Layer of 216-Z-2

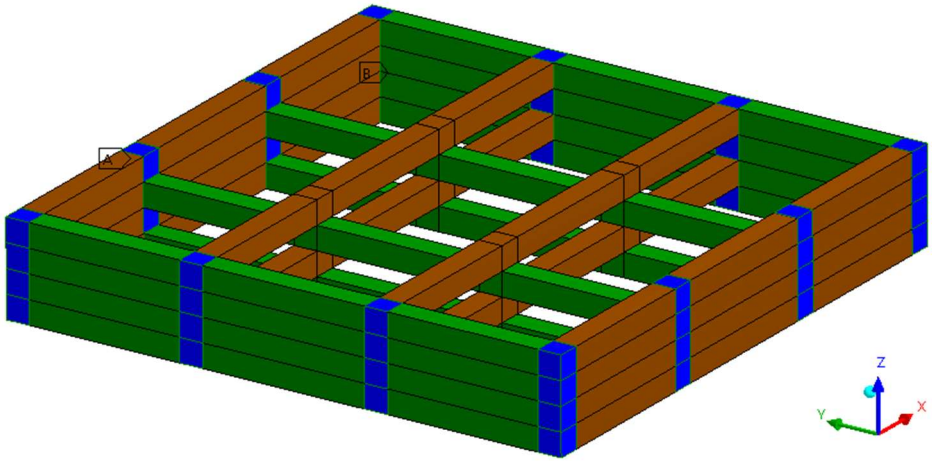

Figure 3.1-2: General View of the ANSYS Solid Model Stacked Layers of 216-Z-2

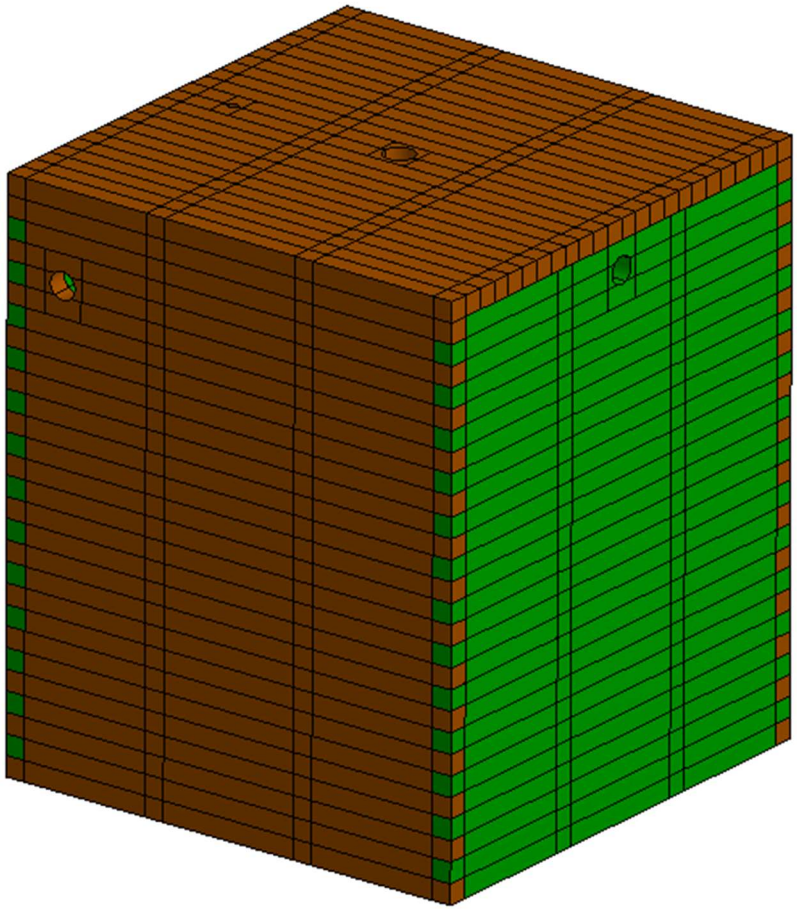

Figure 3.1-3: General View of the ANSYS Solid Model of 216-Z-2

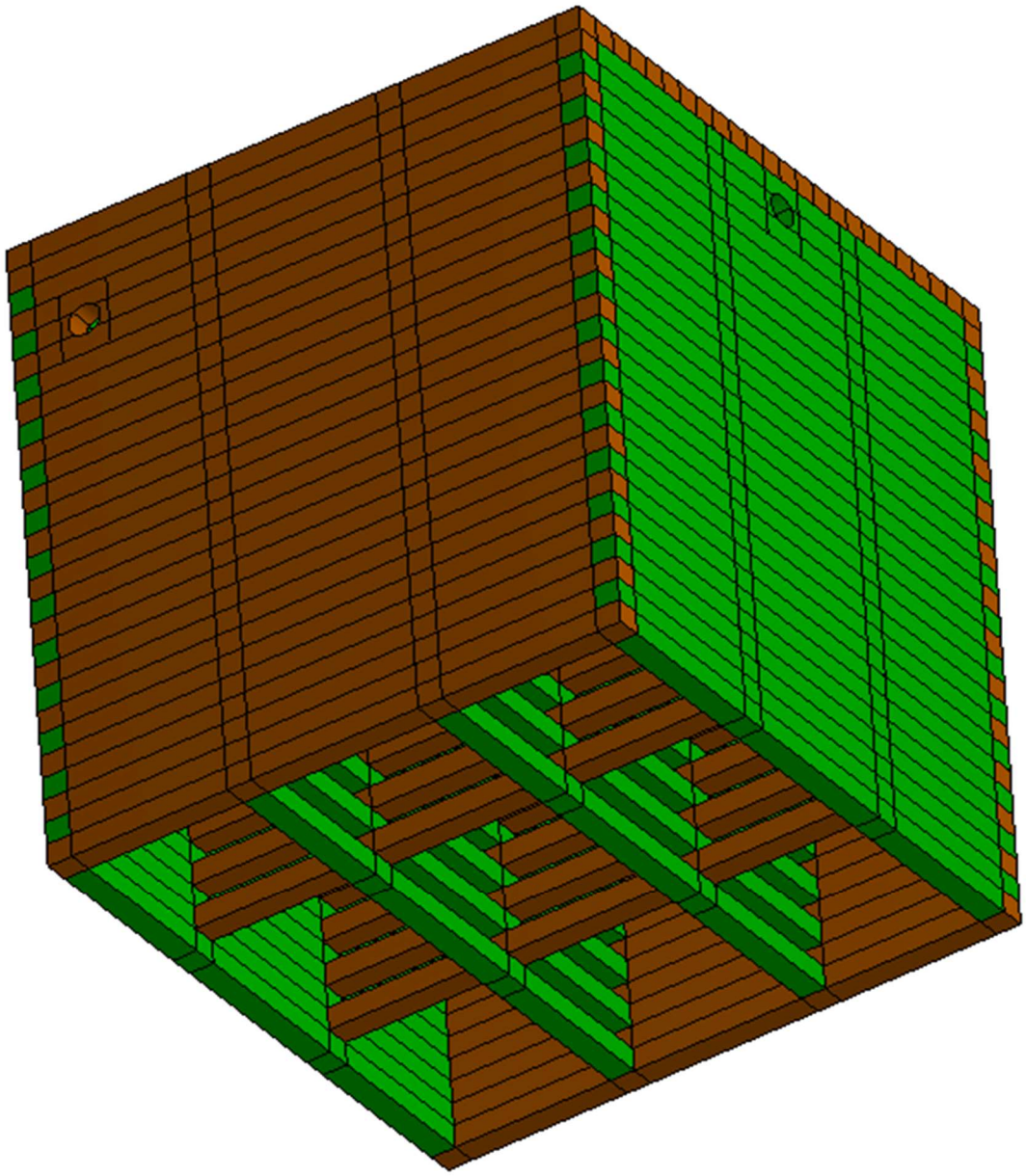

Figure 3.1-4: General View of the ANSYS Solid Model of 216-Z-2 Looking Up

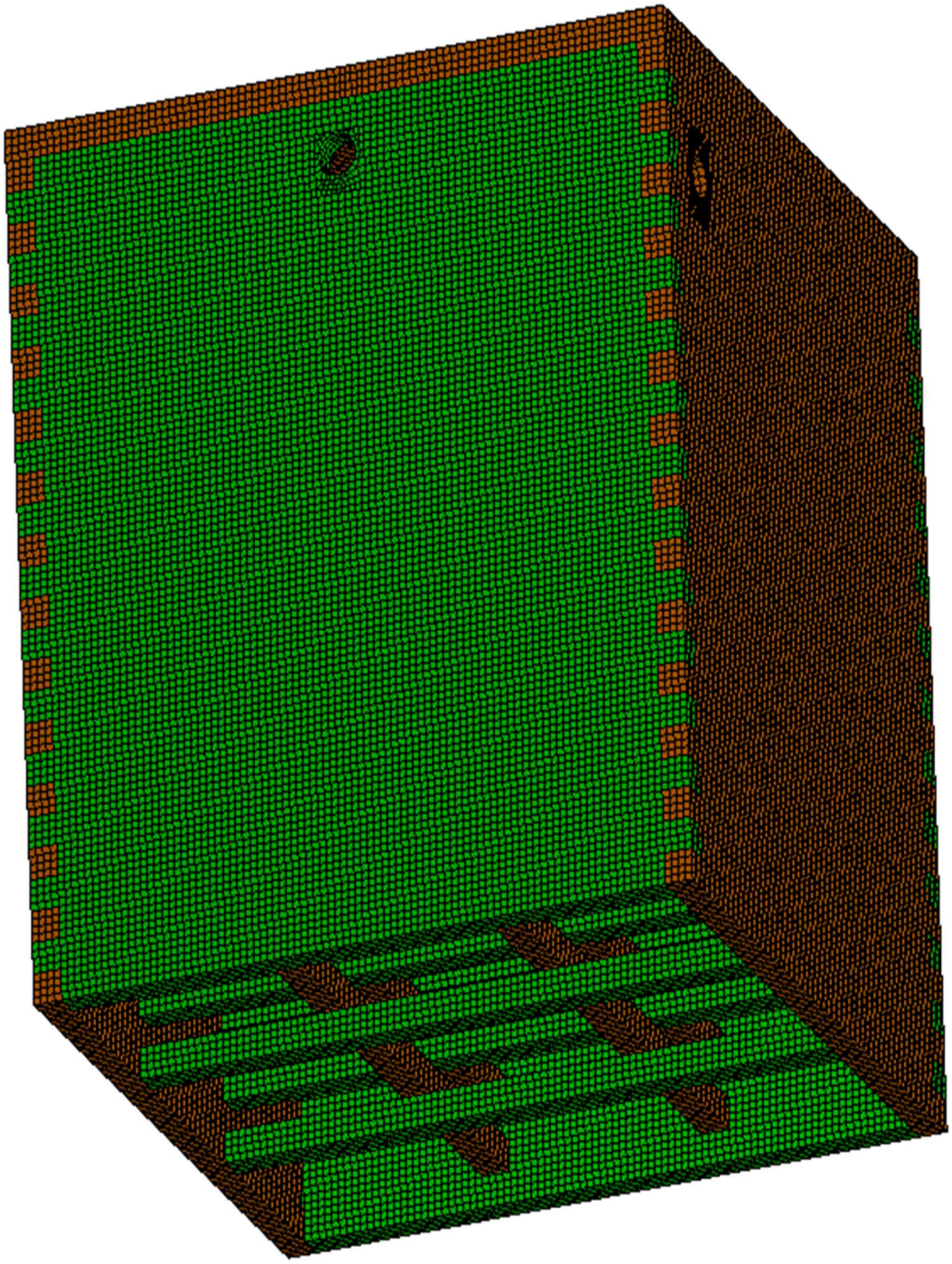

Figure 3.1-5: General View of the ANSYS Finite Element Mesh of 216-Z-2

3.2 Structure 216-B-12, Group C2

Overall dimensions of crib 216-B-12 are 4.9 x 4.9 m (16 x 16 ft) x 3.0 m (10 ft) tall. The crib frames were constructed of 15.24 x 20.32 cm (6 x 8 in.) (Figure 3.2-1) timber (Douglas fir) braces stacked in 15 alternating layers rotated 90° so that the braces are crisscrossed (Figure 3.2-2 through Figure 3.2-4). Each layer of the timber frame was securely fastened to the next to prevent shifting during backfill of the excavation. The top layer of each crib frame was covered with timber containing holes for the vent piping.

The 15 ft of soil overburden was not explicitly modeled, but was accounted for with pressure loading. All timber beams were modeled with SOLID186 elements, with an approximate mesh size of 1.5 in. (Figure 3.2-5). All roof, wall, and cross timber members have at least 9 nodes through the thickness. The outer-wall cross members have 5 nodes through the thickness. Orthotropic material properties were assigned as described in Appendix A. The timber beams were categorized as x-oriented and y-oriented members depending on their direction within the model. Each frame layer was continuously meshed to simulate securely fastened joints.

Between timber layers, the finite element mesh was connected by merging nodes at the intersecting areas for the outer timber. At the intersecting areas of inner timber, sliding with no separation surface-to-surface contact was used. In this way, the structural model was more flexible and the resulting stresses more conservative.

Roof members were meshed independently, as follows: side faces on the members were attached with bonded surface-to-surface contact element pairs, bottom faces of the roof members were bonded with the top frame layer on two sides only, assuming the members were fastened at the ends only, and the roof bears on the mid-span cross members of the layer below were modelled using sliding with no-separation contact, so that they bear, but were still allowed to slide in plane. Boundary conditions were simulated with frictionless vertical restraints.

All protruding pipes are nonstructural members and were not included; however, the penetrations that the pipes are fastened to were kept rigid using ANSYS “remote points” to simulate the bolted steel flanges or concrete cube receiver. The bottom of the structure was fixed such that vertical movement was precluded, but allowed lateral translation and expansion of the base layer. Loading was applied as described in Appendix A of this document - where no waste is present in this crib.

Degradation is expected due to the observed cave-in; however, such degradation is difficult to quantify and incorporate into the model. Consequently, the degradation was accounted for by increasing the calculated demand stresses by 20%.

Figure 3.2-1: General View of the ANSYS Finite Element Solid Model of a Single Layer of 216-B-12

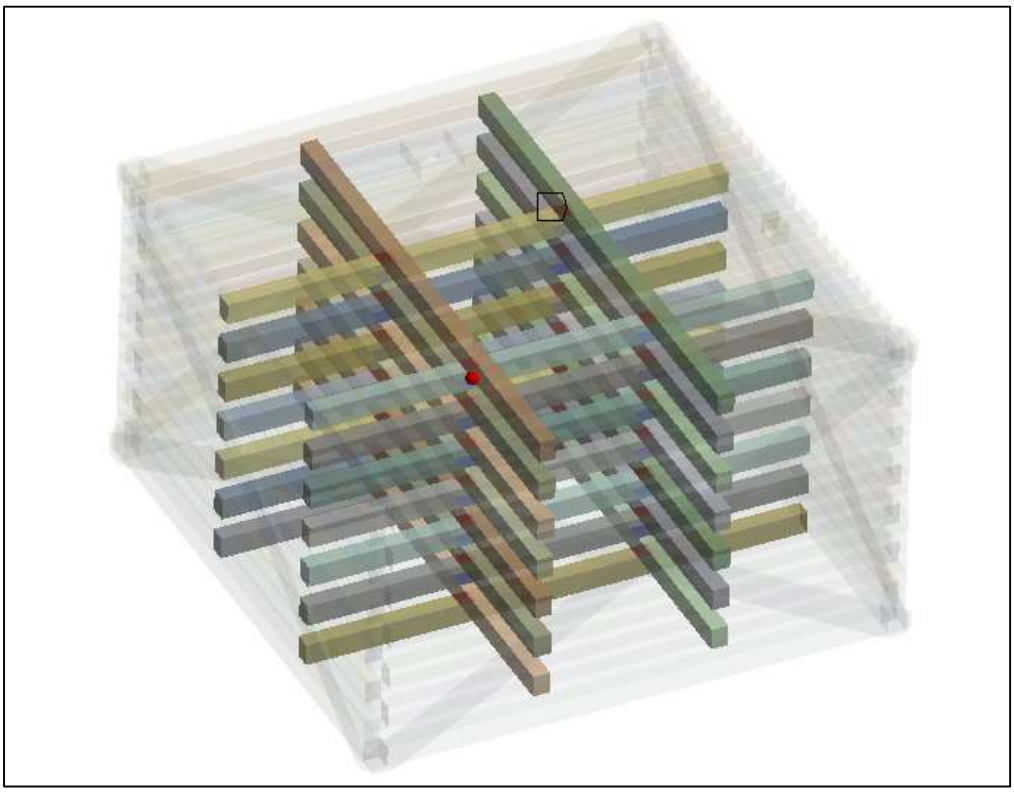

Figure 3.2-2: General View of the ANSYS Finite Element Solid Model of Interior Braces of 216-B-12

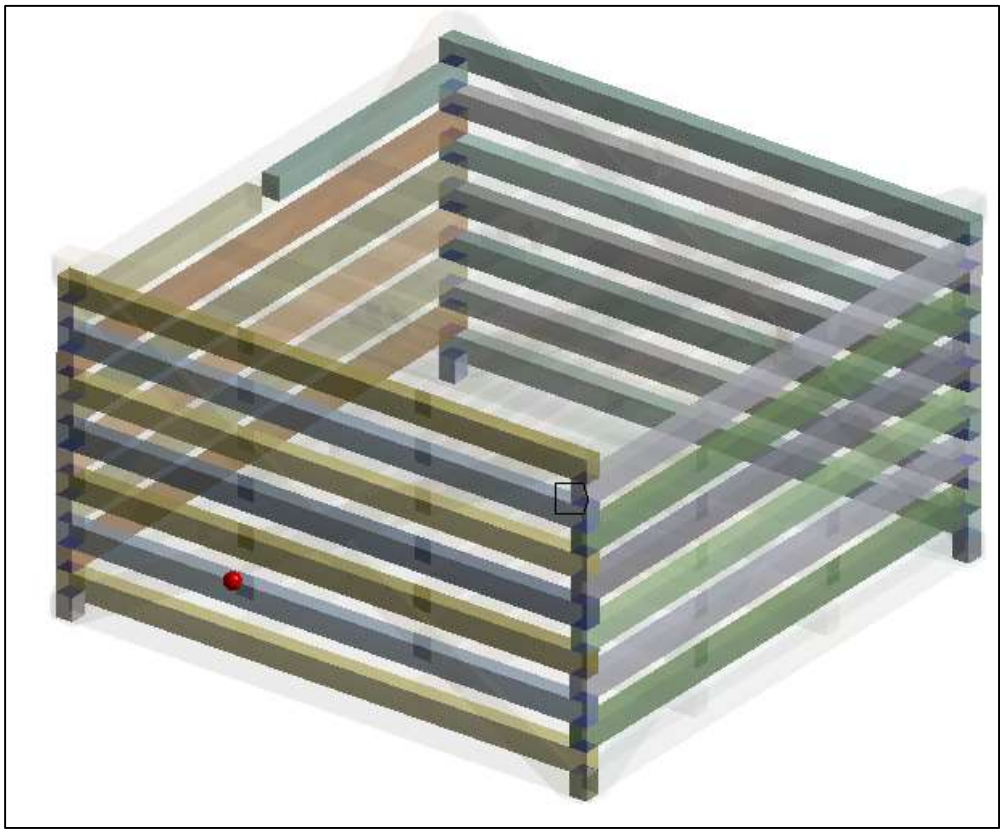

Figure 3.2-3: General View of the ANSYS Finite Element Solid Model of Outer Members of 216-B-12

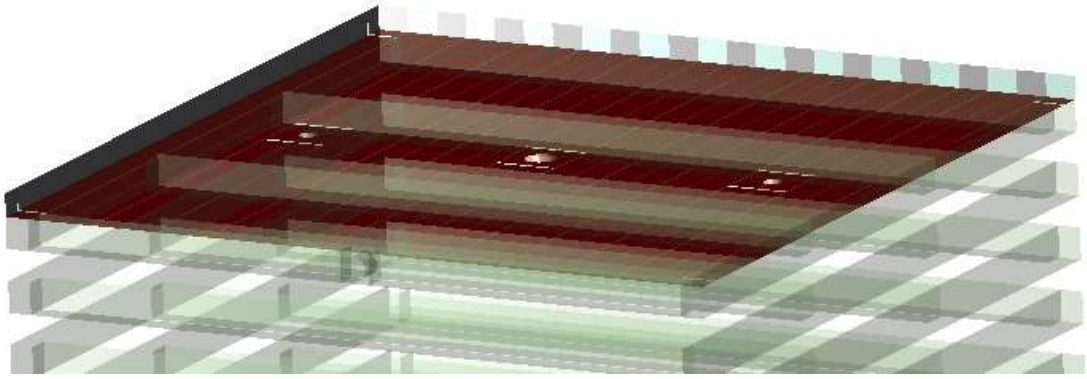

Figure 3.2-4: General View of the ANSYS Finite Element Solid Model of Roof of 216-B-12

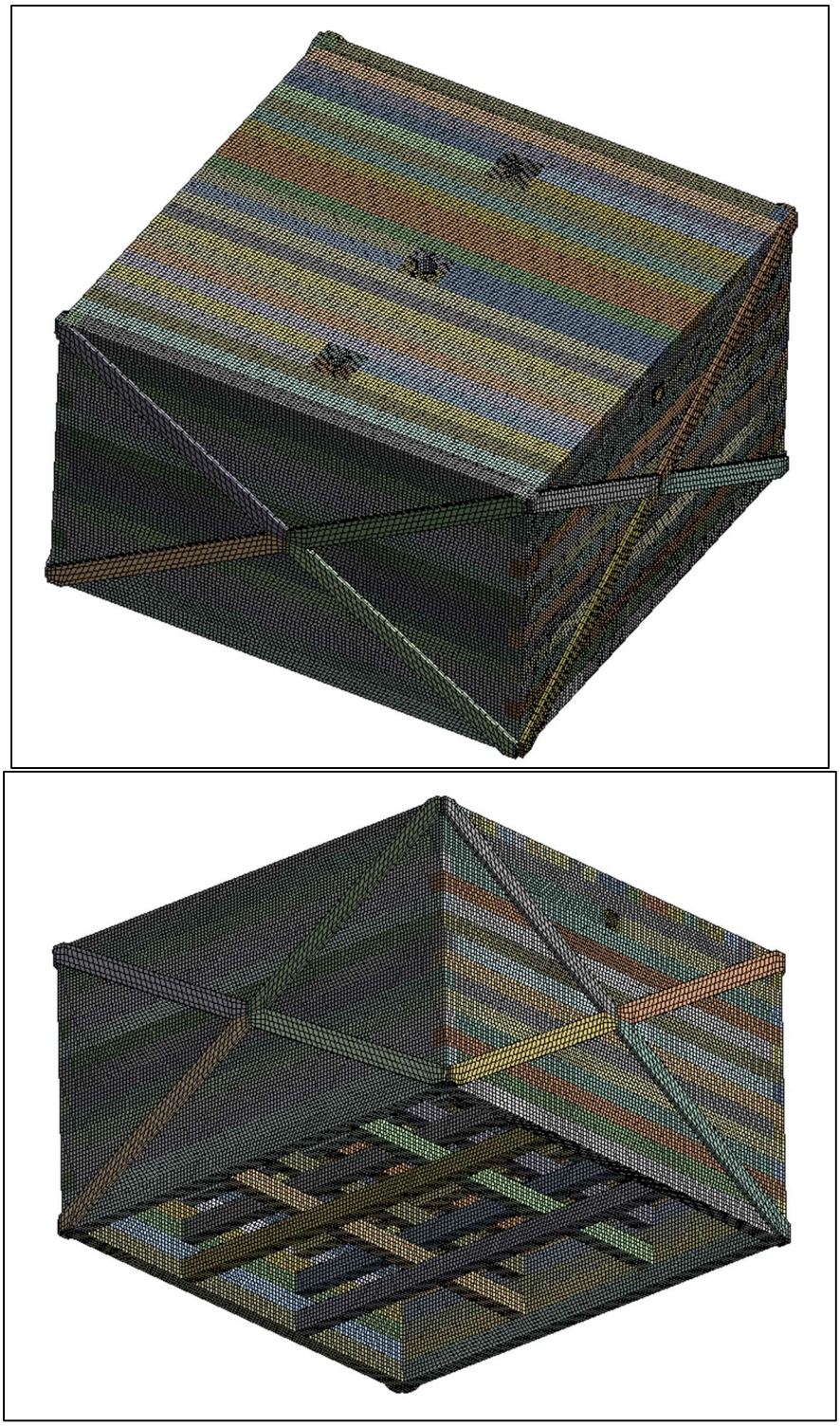

Figure 3.2-5: General View of the ANSYS Finite Element Mesh of 216-B-12

3.3 Structure 216-Z-6, Group C3

Crib 216-Z-6 is approximately 15.24 m (50 ft) long x 1.98 m (6.5 ft) wide x 1.05 m (3.46 ft) tall. The top of the structure is located approximately 2.67 m (8.75 ft) below grade. The top of the crib structure was constructed from 5.1 x 20.3 cm (2 x 8 in.) wooden joists spaced 0.3 m (1 ft) on center. The joists were covered with 5.1 x 25.4 cm (2 x 10 in.) wooden planks. Wood stringers, each 5.1 x 30.5 cm (2 x 12 in.) ran below the crib top for the length of the crib and formed the sides of the structure. Two stringers were laminated together on each side, for a total wall thickness of 10.2 x 61 cm (4 x 24 in.). The bottom of the crib included 10.16 x 10.16 cm (4 x 4 in.) toe blocks spaced approximately 3.05 m (10 ft) on center. Figure 3.3-1 through Figure 3.3-3 include general views of the ANSYS solid model of the individual timber elements.

Six feet of soil overburden on top of the crib roof was included in the analysis. The soil was not explicitly modeled and was accounted for with pressure loading. All timber beams were modeled using SOLID186 elements, with an approximate mesh size of 2 in. (Figure 3.3-4). All roof, cross beam, and end beam timber members have at least 5 nodes through the thickness. Orthotropic material properties were assigned as described in Appendix A. The parts were grouped in to x-oriented and y-oriented members based on the axis of the structural component.

All connections between roof planks, side planks, base planks and cross ties were modeled using bonded surface-to-surface contact with a trim of 0.1 in. to allow beams to flex and thereby generate conservative stresses. Boundary conditions were simulated with frictionless vertical restraints.

All protruding pipes in and out of the trench are nonstructural members and, hence, were not included in the structural model. However, the penetrations (and vent box structures) that the pipes are fastened to were kept rigid using ANSYS “remote points” to simulate the bolted steel flanges. The bottom of the trench was fixed so as to preclude vertical movement, but allow lateral translation and expansion of the base layer.

Degradation is expected due to observed soil overburden cave-in, however, such degradation is difficult to quantify and incorporate into the model. Consequently, the degradation was accounted for by increasing the calculated demand stresses by 20%.

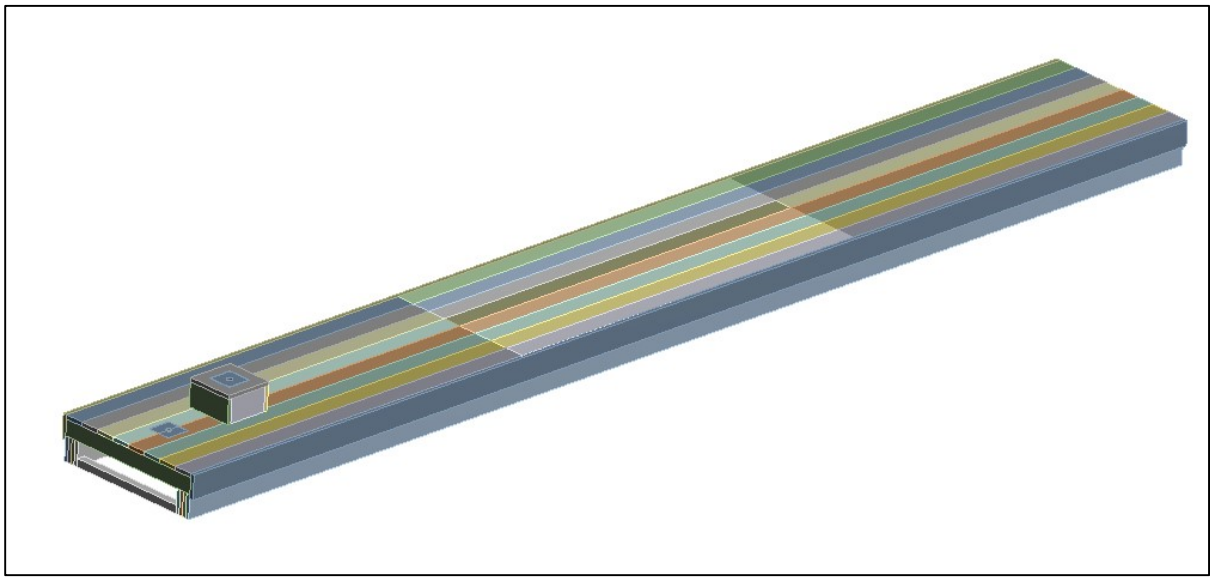

Figure 3.3-1: General View of the ANSYS Finite Element Solid Model of 216-Z-6

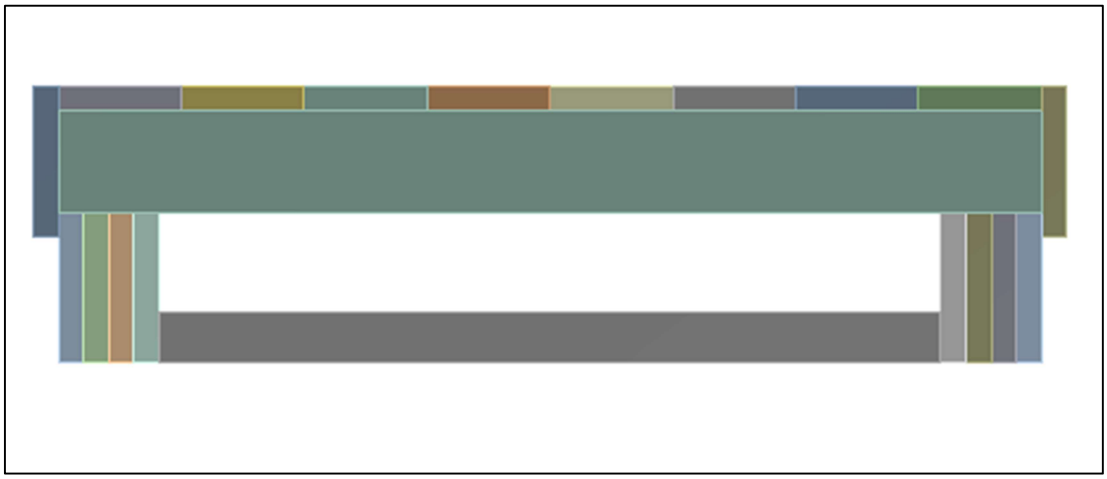

Figure 3.3-2: End View of the ANSYS Finite Element Solid Model of 216-Z-6

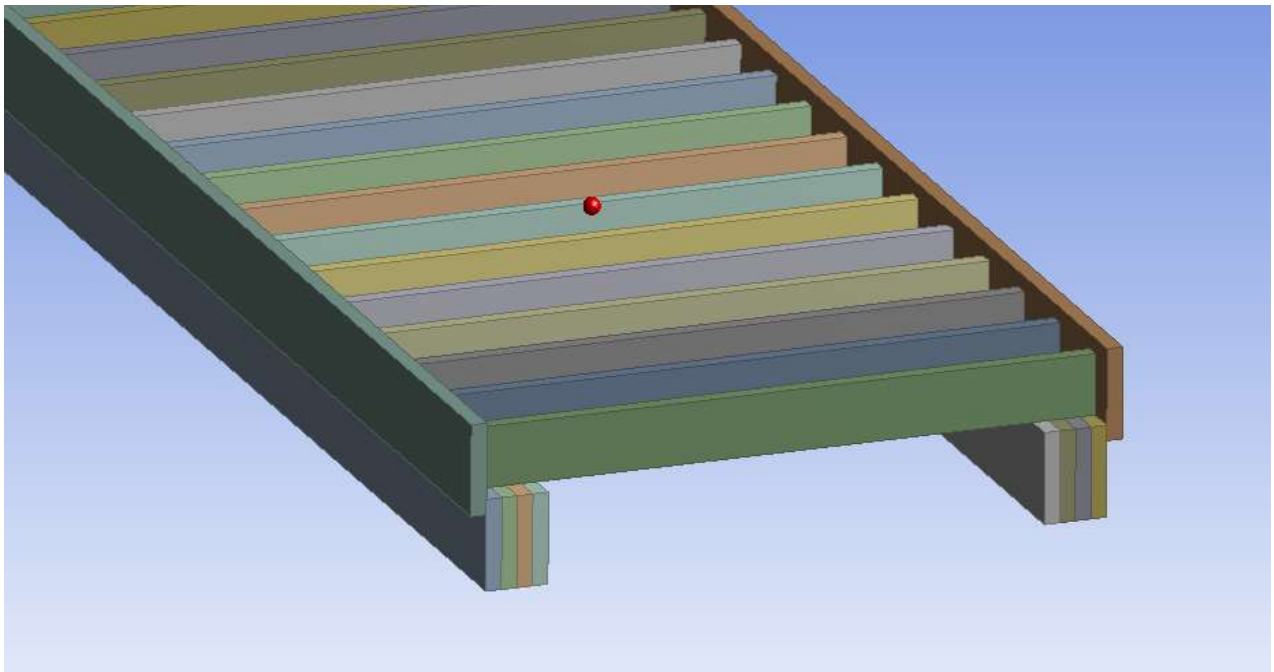

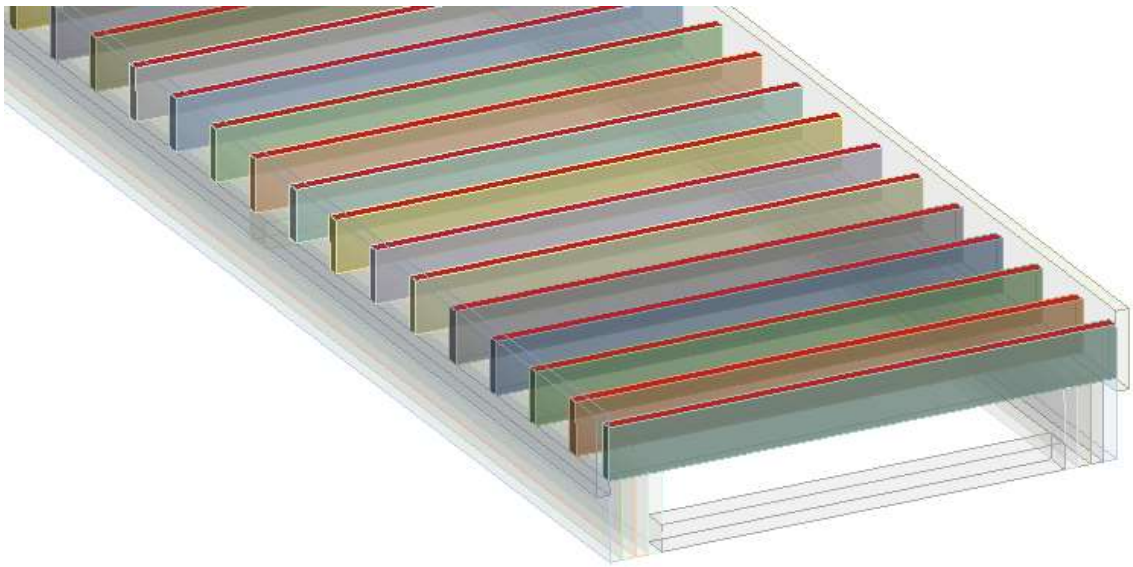

Figure 3.3-3: General View of the ANSYS Finite Element Solid Model Members of 216-Z-6

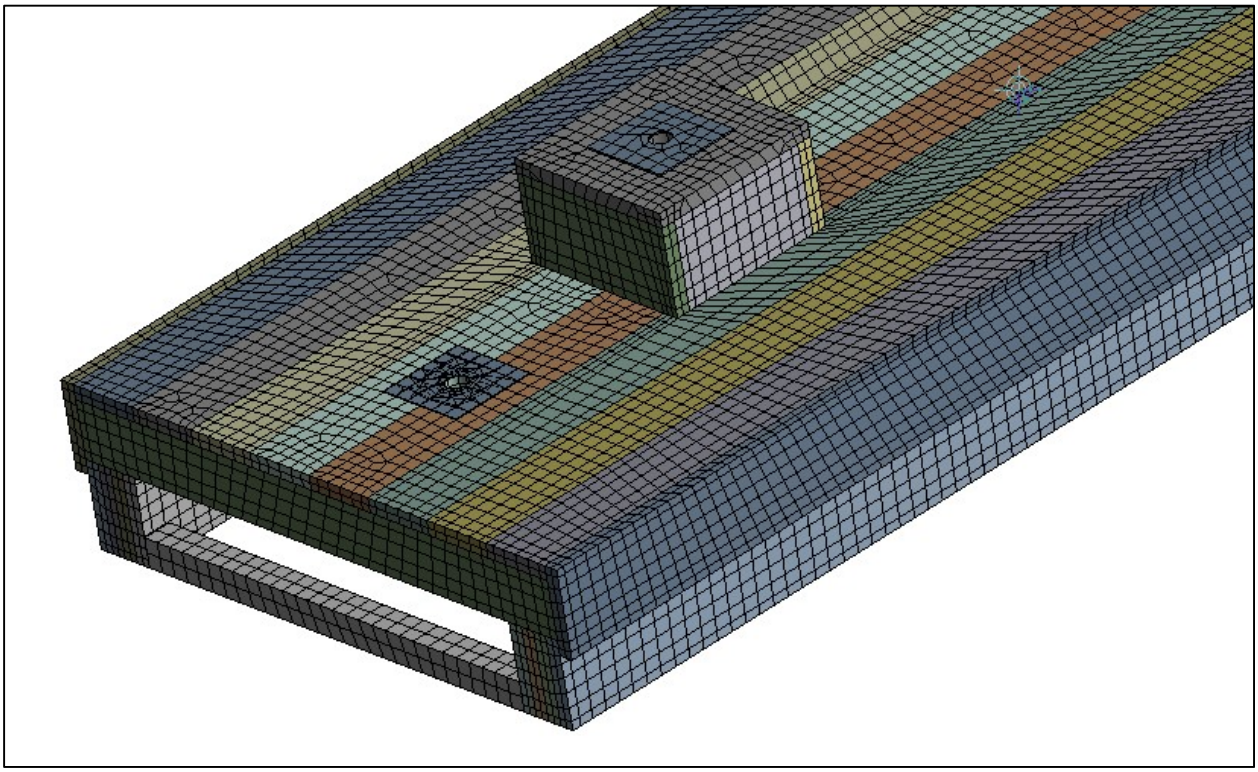

Figure 3.3-4: General View of the ANSYS Finite Element Mesh of 216-Z-6

3.4 Structure 216-Z-7, Group C4

Crib 216-Z-7 consists of two parallel wooden boxes set into two shallow, parallel trenches within a single, terraced excavation. Each crib structure consists of three timber tiers (Figure 3.4-1 and Figure 3.4-2). Vent boxes are located on top of either end of the uppermost tier of trench boxes. The interior, shallow trenches were backfilled with gravel and covered with wooden planks, with the top of the uppermost crib tier sitting flush with the edge of the trench. The uppermost crib tier is the widest, at approximately 2.44 m (8 ft) wide, with the lower two tiers becoming progressively narrower to fit within the shallow trenches. The wooden crib box structures are estimated to be 45.72 m (150 ft) long. There is 6 ft of backfill material above the top of the trench structure. Views of the ANSYS solid model of the individual tier longitudinal members are shown in Figure 3.4-3 and Figure 3.4-4.

All timber beams were modeled using SOLID186 elements, with an approximate mesh size of 3 in. (Figure 3.4-5). All roof, cross beam, and end beam timber members have at least 5 nodes through the thickness. Orthotropic material properties were assigned as described in Appendix A, and are grouped into x-oriented and y-oriented members based on the axis of the member. Between tiers, the beams were connected to the cross members using bonded contact of coincident faces. Boundary conditions were simulated with frictionless vertical restraints.

All protruding pipes in and out of the trench are nonstructural members and, hence, were not included in the structural model. However, the penetrations (and vent box structures) that the pipes are fastened to were kept rigid using ANSYS “remote points” to simulate the bolted steel flanges. The bottom of the trench was fixed so as to preclude vertical movement, but allow lateral translation and expansion of the base layer.

Based on the available information, there is no indication of damage to this structure, therefore, the finite element model represents the as-designed configuration.

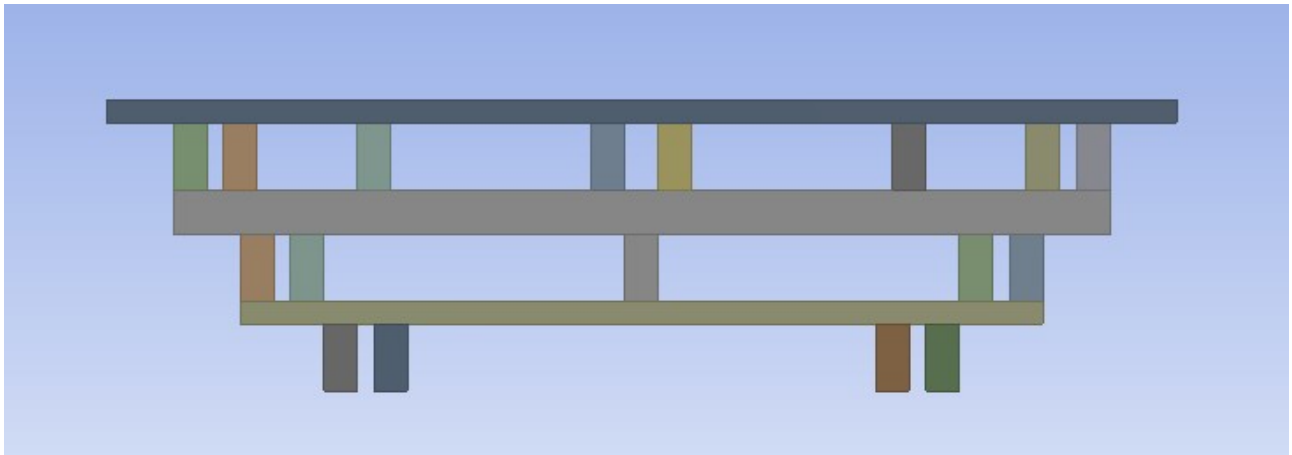

Figure 3.4-1: End View of the ANSYS Solid Model of 216-Z-7

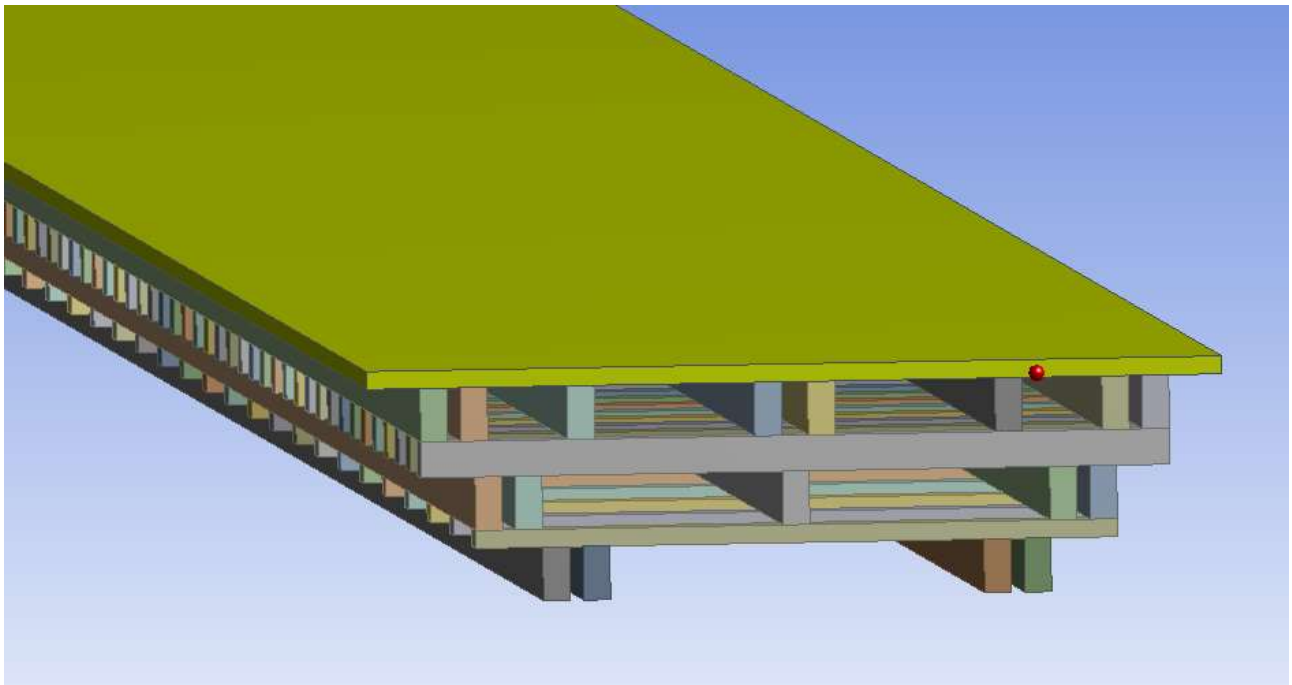

Figure 3.4-2: Isometric View of the ANSYS Solid Model of 216-Z-7

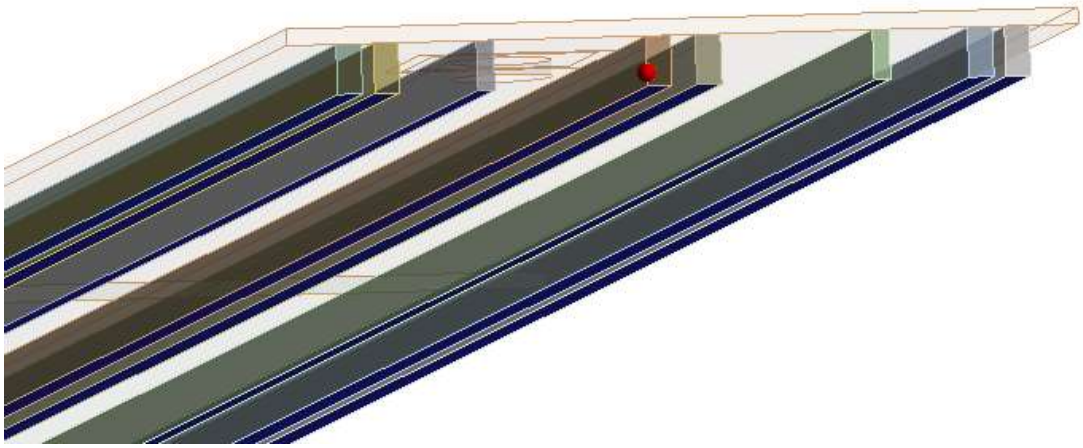

Figure 3.4-3: General View of the ANSYS Solid Model of Top Tier Longitudinal Beams for 216-Z-7

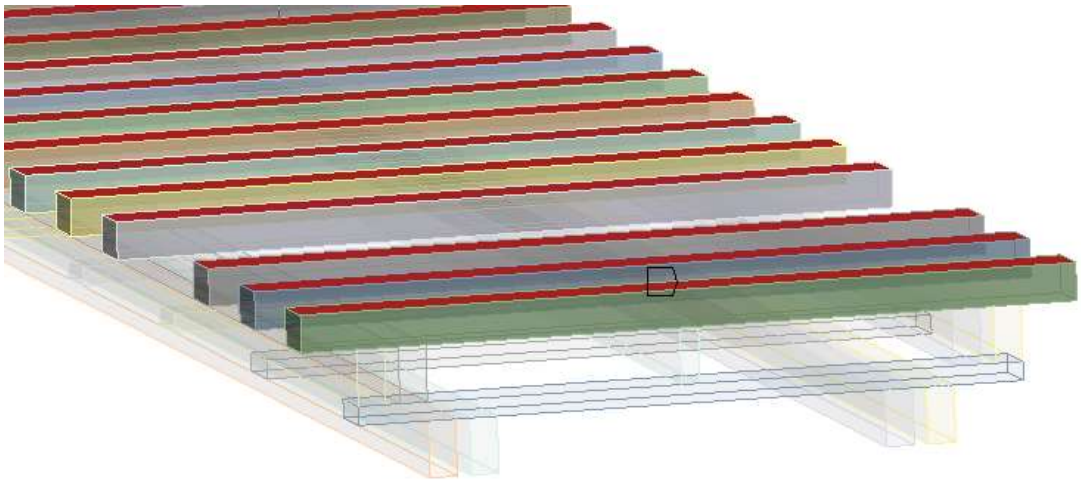

Figure 3.4-4: General View of the ANSYS Solid Model of 1st and 2nd Tiers for 216-Z-7

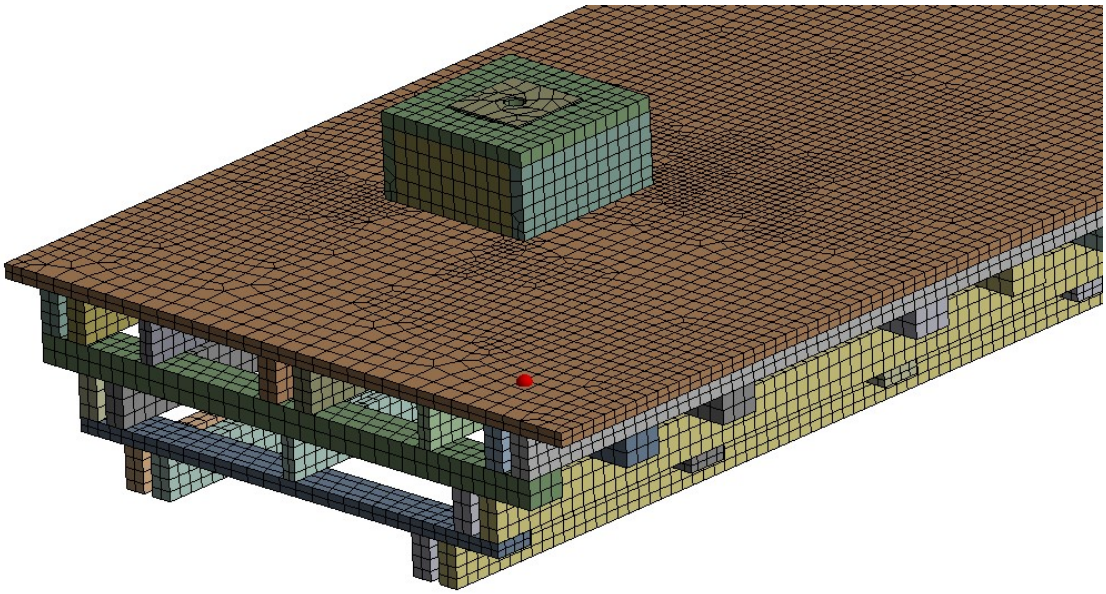

Figure 3.4-5: General View of the ANSYS Mesh for 216-Z-7

3.5 Structure 216-Z-9, Group C5

The 216-Z-9 crib is almost entirely underground, with a reinforced concrete slab roof 22.9 cm (9 in.) thick at grade level. The roof is approximately 36.6 m (120 ft) long x 27.4 m (90 ft) wide. The sides of the structure are slanted and composed of surrounding soil. The underground walls slant inward to a rectangular bottom (60 x 30 ft). The concrete roof is supported by footings around the perimeter and six 7.0 m (23 ft) tall concrete columns located at the corners and long edges of the floor area. The columns have circular cross section 21 in. diameter.

All concrete elements were modeled using SOLID185 and SOLID 186 elements, with an approximate mesh size of 4 in. The roof has 3 nodes through the thickness and the columns have 12 nodes across the diameter. The protective membrane cover below the roof slab was modeled as distributed masses. Material properties were assigned as described in Appendix A. Each structural element was meshed separately and attached to surrounding elements via bonded surface-to-surface contact. Soil surrounding the concrete ledge along the perimeter of the roof was assumed to provide adequate support for vertical and lateral loads. Based on available information, degradation in the roof has been observed; therefore, degradation was simulated by reducing the concrete depth by 1 in.

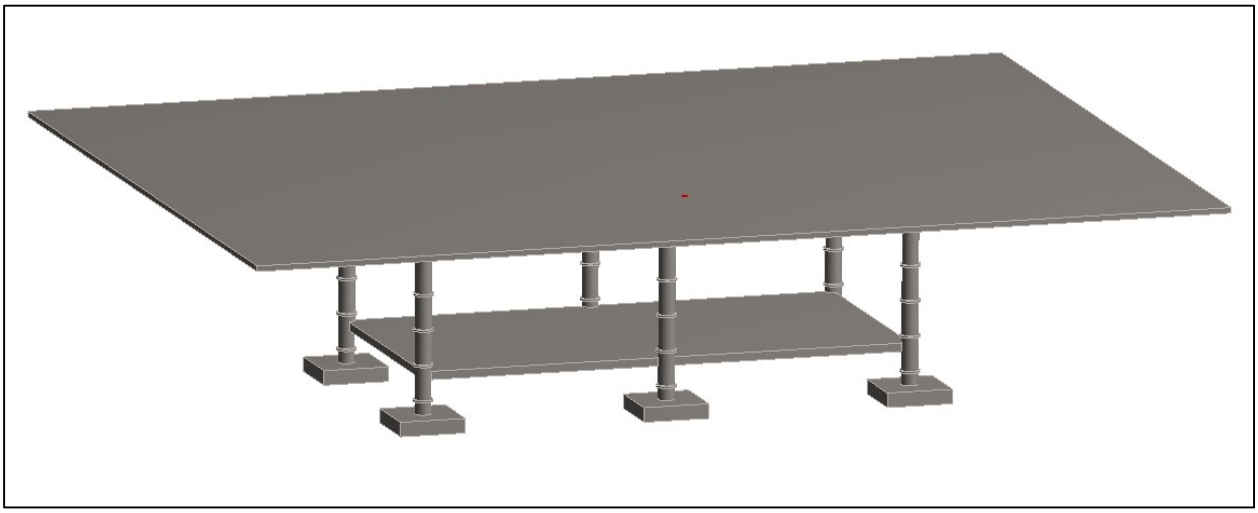

Figure 3.5-1: General View of the ANSYS Solid Model for 216-Z-9

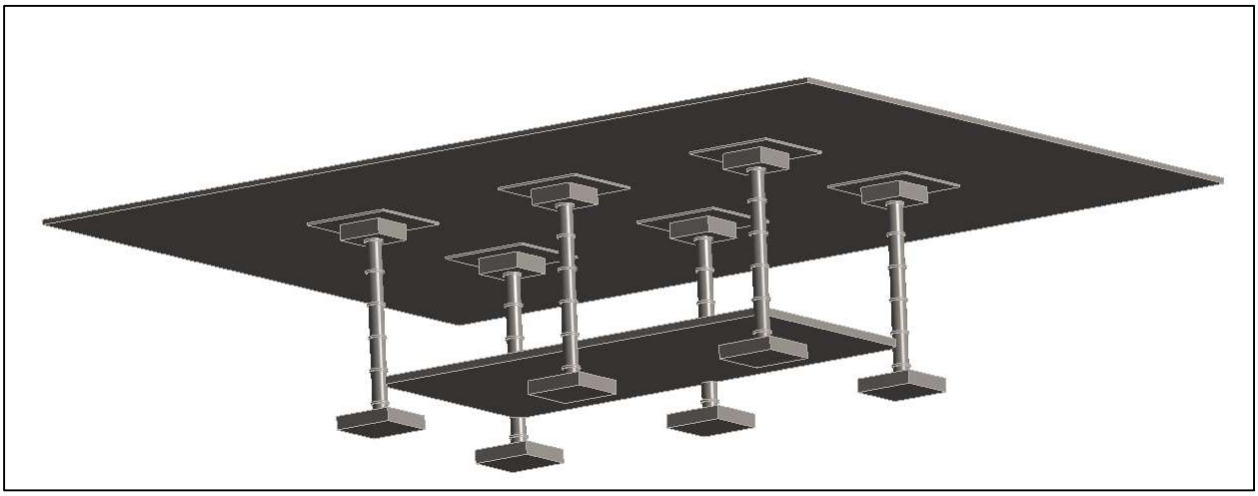

Figure 3.5-2: General View of the ANSYS Solid Model for 216-Z-9

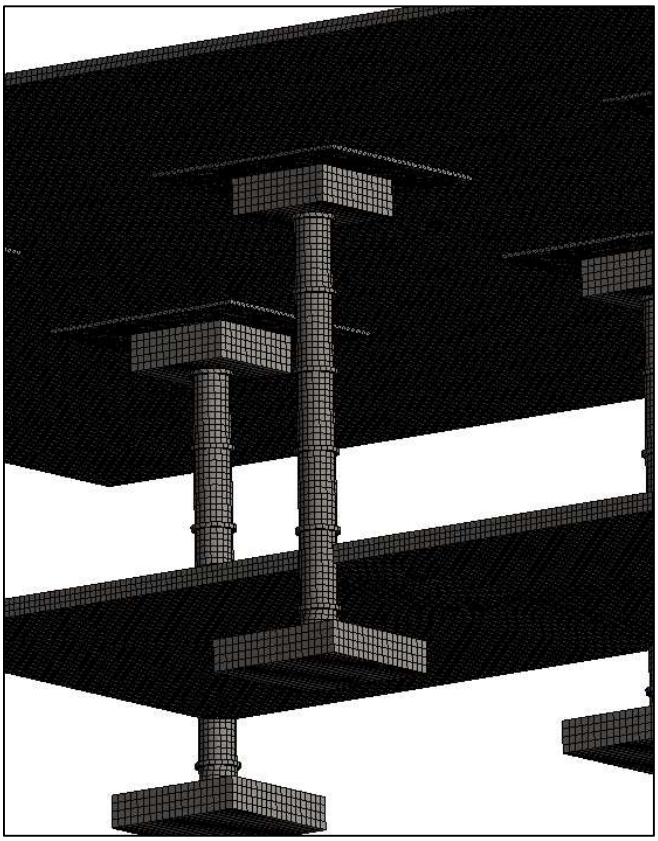

Figure 3.5-3: General View of the ANSYS Solid Model for 216-Z-9

(bottom slab removed in the stress analysis)

3.6 Structure 241-T-361, Group T1

Structure 241-T-361 is a prestressed concrete cylindrical tank (20 ft diameter x 19 ft tall) that contains 10.8 ft of waste, and with 6 ft of soil overburden. There is no available information about the prestressing and other reinforcement in the concrete; therefore, the finite element model for this structure included solid concrete material without prestressing. Furthermore, the finite element results were analyzed based on reinforced concrete design with assumed rebar and without crediting prestressing forces. The 6-in. thick tank walls were modeled using SOLID186 elements, with a mesh size of 2 in. for the walls and dome. The roof, walls, and floor slab have 5 nodes through the thickness. Boundary condition was simulated with frictionless vertical restraints. Protruding pipes were modeled with SHELL281 elements and attached to a concrete dome with bonded surface-to-surface contact element pairs. Figure 3.6-1, Figure 3.6-2, and Figure 3.6-3 illustrate the solid modeling features of the tank. Material properties were assigned and loads applied as described in Appendix A. Based on the available information, there is no indication of damage to this structure. However, due to the harsh environment, degradation was simulated by reducing the concrete thickness and rebar area by 10%.

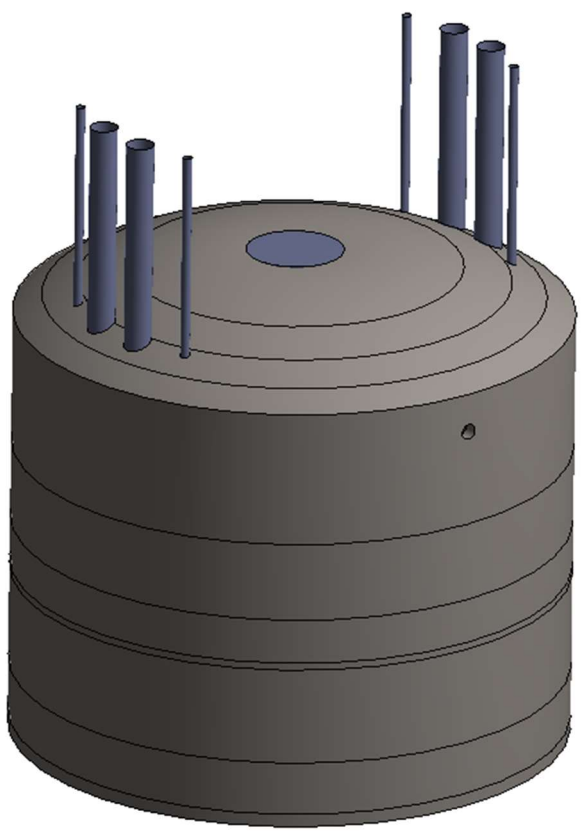

Figure 3.6-1: General View of the ANSYS Solid Model of 241-T-361

Figure 3.6-2: Sectional View of the ANSYS Solid Model of 241-T-361

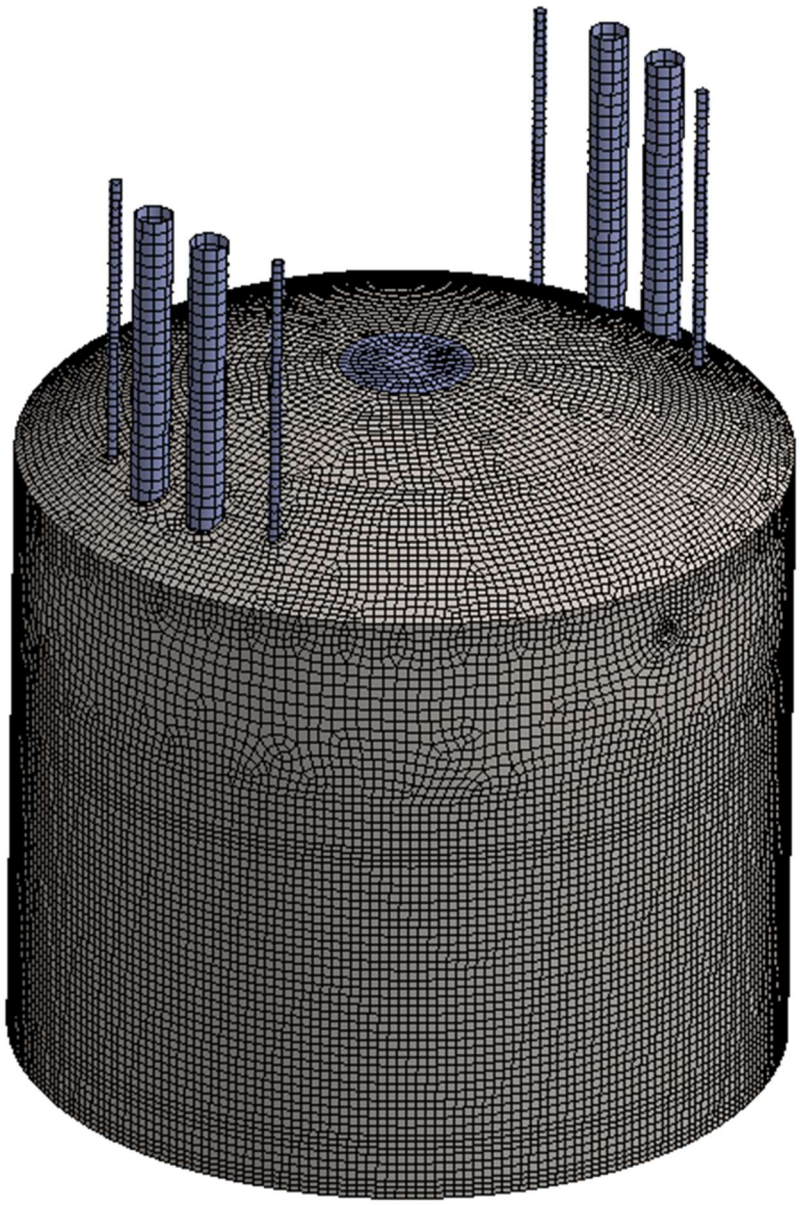

Figure 3.6-3: General View of the ANSYS Finite Element Mesh of 241-T-361

3.7 Structure 241-Z-361, Group T2

The overall dimensions of the 241-Z-361 settling tank are 28 x 15 x 19 ft, with 2 ft of soil overburden. This settling tank contains 8 ft of waste. The tank walls and roof for this tank are 12 in. thick and were modeled using SOLID186 elements having an approximate mesh size of 3 in. The roof, walls, and floor slab have approximately 4, 10, and 7 nodes through the thickness, respectively. Figure 3.7-1, Figure 3.7-2, and Figure 3.7-3 show the solid modeling features of this settling tank. The steel liner was modeled with SHELL281 elements on all internal surfaces above the waste level. Liner shell elements are connected to the concrete solid elements via bonded surface-to-surface contact elements. Stiffener steel angles connected to the liner were not included in the model – this is appropriate since the liner is severely deteriorating and the condition of the angles may be also degraded. All protruding pipes are nonstructural and, thus, not included. Significant openings in the roof were included with protruding pipes modeled using SHELL281 elements. Material properties and loading were applied as described in Appendix A. Boundary conditions were simulated with frictionless vertical restraints.

Based on the available information about the condition of the concrete indicating some level of deterioration, all concrete walls and the roof for this structure were reduced in thickness by 1 in., and rebar area was reduced by 20% to simulate observed degradation.

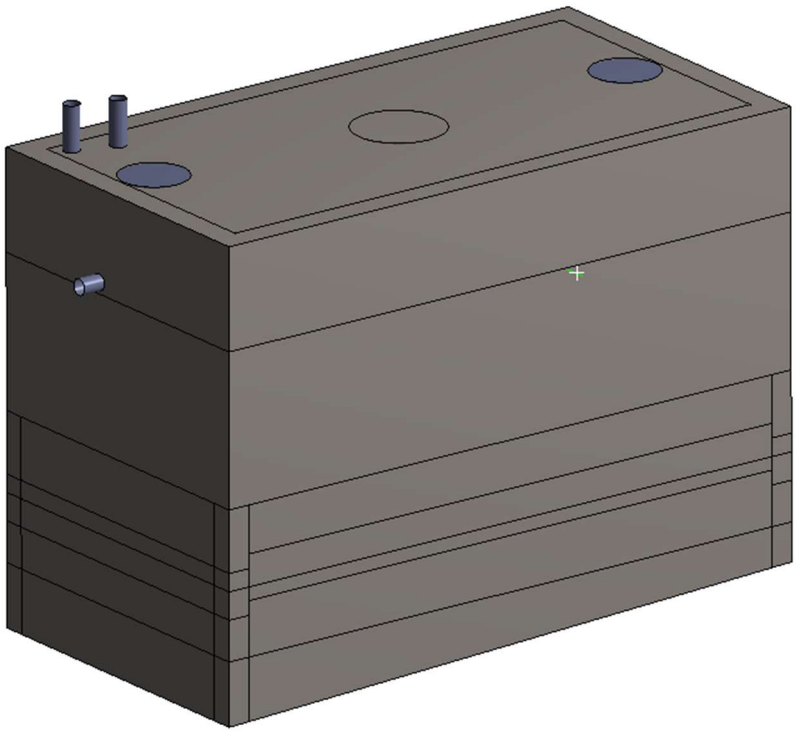

Figure 3.7-1: General View of the ANSYS Solid Model of 241-Z-361

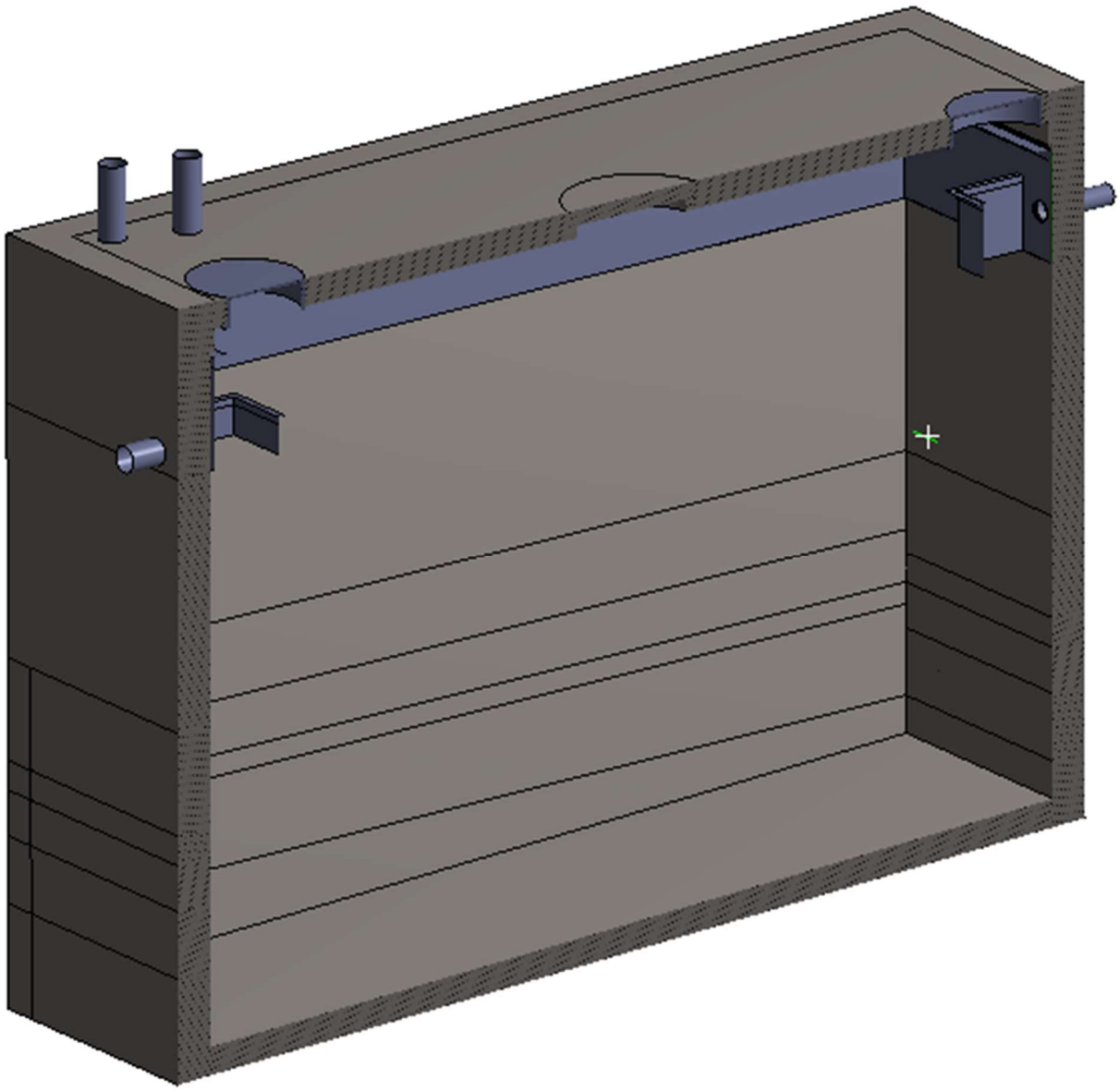

Figure 3.7-2: Sectional Elevation View of the ANSYS Solid Model of 241-Z-361

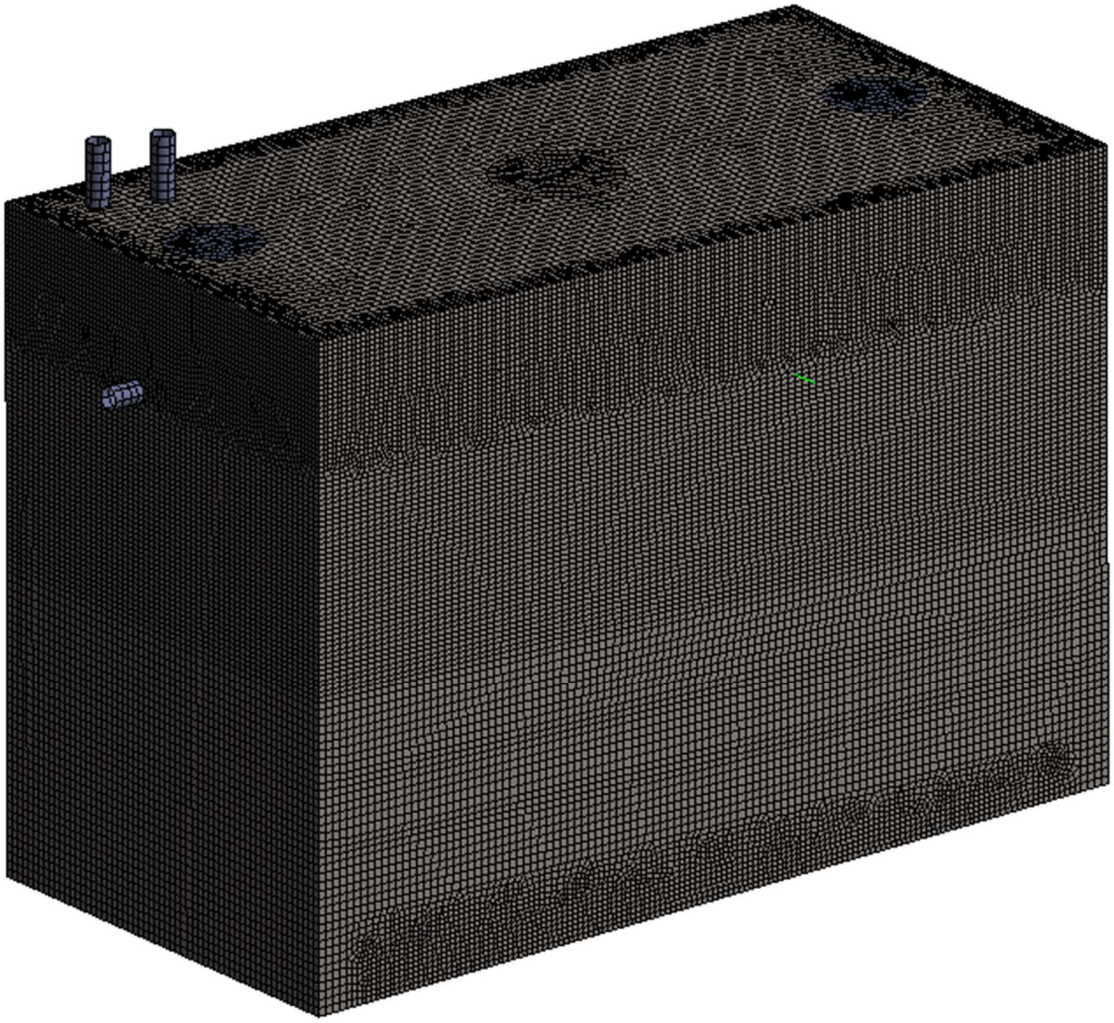

Figure 3.7-3: General View of the ANSYS Finite Element Mesh of 241-Z-361

3.8 Structure 241-Z-8, Group T3

Structure 241-Z-8 is a steel tank, 40 ft long x 8 ft outer diameter, with 5/16 in. thick walls (Figure 3.8-1), and 6 ft of soil overburden. Liquid waste was removed from the 241-Z-8 tank in 1974 - leaving 7 in. (500 gal) of sludge [18]; this level was considered negligible for the structural evaluation compared to the 8 ft diameter (horizontal steel tank).

SHELL281 elements were used to model the tank, with an approximate mesh size of 2 in. (Figure 3.8-2). All shell elements have 3 integration points through the thickness. All protruding pipes were also modeled as thin-walled, steel shells. Material properties were assigned as described in Appendix A. The entire tank and manhole cover were continuously meshed. The tank was restrained along a narrow band at the bottom in the vertical direction. The lower quarter of each tank end was also restrained such that the tank was allowed to move freely in the axial direction. Loading was applied according to the criteria in Appendix A. The soil was not explicitly modeled and is accounted for with pressure loading.

Based on the available information, there is no indication of damage to the tank and, therefore, no degradation was included in the model.

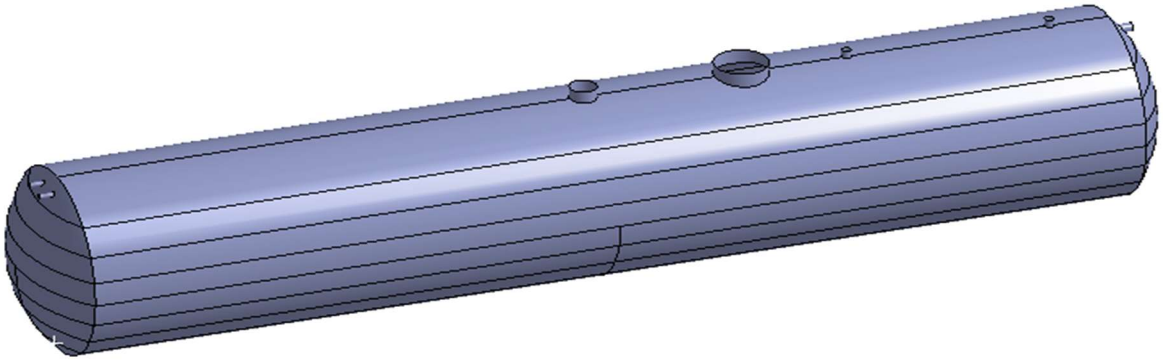

Figure 3.8-1: General View of the ANSYS Finite Element Solid Model of 241-Z-8

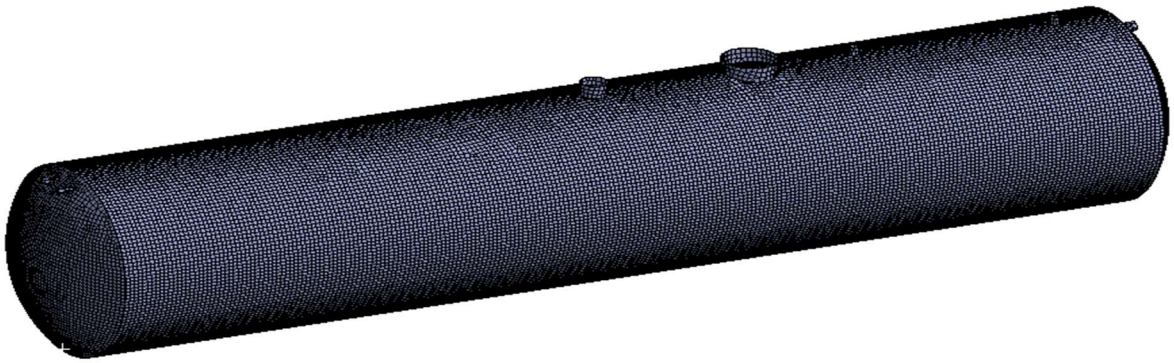

Figure 3.8-2: General View of the ANSYS Finite Element Mesh of 241-Z-8

3.9 Structure PUREX Deep Bed Filters, Group O1

An 8 ft wide x 8 ft high reinforced-concrete exhaust air duct connects the 202-A Building to deep-bed filter 1 (bypassed) and deep-bed filter 2 (active) located in the south yard area and is composed of below-grade concrete exhaust air treatment and discharge equipment. The overall dimensions of deep-bed filter 2 area are 82 x 52 x 13 ft deep. There is 4 ft of overburden on the roof structure and 4 in. of shotcrete to mitigate water intrusion [18]. See Figure 3.9-1 through Figure 3.9-5 for details of the finite element solid model. Appendix B of this document shows results for an additional structural evaluation of the PUREX deep bed filters based on 4 ft of soil overburden and 8 in. of shotcrete (instead of the existing 4 in. of shotcrete).

SOLID185 elements were used (Figure 3.9-6) to model the existing ducts, concrete plugs, walls, floor, and roof slabs (which are at least 6 in. thick). The roof, walls, and floor slab have 4 nodes through the thickness. Steel inspection port covers were modeled using SHELL181 elements and were bonded to the concrete walls. The steel reinforcement angles and I-beams that rest on the southeast trench's concrete ledge (Figure 3.9-5) were modeled as BEAM189 elements, continuously meshed as they are welded. The I-beams do not appear to be directly loaded, as they are only meant to provide lateral stiffness between the open walls (no information is provided as to actual loading on the beams). These beams, angles, and roof slabs used bonded contacts to connect to the ledges. All protruding pipes are nonstructural and, therefore, not included in the structural model. Furthermore, the 4 in. of shotcrete layer over the 4 ft of soil overburden was also included in the model.

Material properties and loading were applied as described in Appendix A, and waste level did not apply to this model. The soil was not explicitly modeled, but was accounted for with pressure loading. The rebar present in the concrete was also not explicitly modeled, however its impact to the structural stability was addressed outside of ANSYS as part of the concrete code evaluation.

Based on the available information, some degradation was present and, thus, simulated by reducing roof slab thickness by 1 in. and rebar cross sectional area by 10% (outside of ANSYS).

The boundary conditions applied to model include:

- Displacement constraint in X and Y at the inlet and outlet ducts, plugged ducts, and filter's middle section, as these were constrained by the attached existing duct (Figure 3.9-7).
- Displacement constraint in Z at the bottom edges of the filter where it rests on soil. The faces were not entirely constrained to allow flexure in the floor slabs (Figure 3.9-8).
- The inlet and outlet ducts were constrained in RotX and RotZ, as they were continuously connected to the attached existing ducts (Figure 3.9-9).

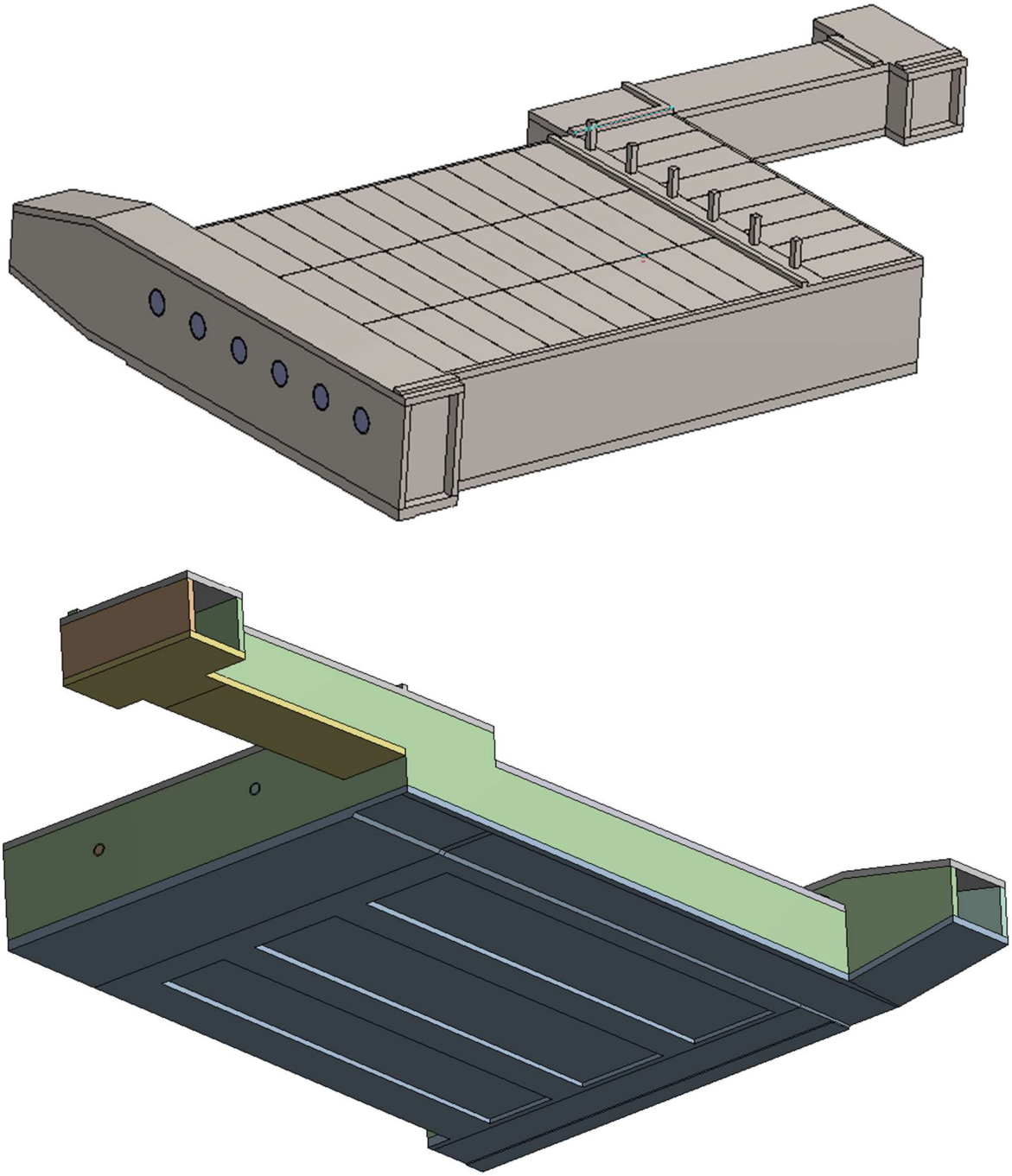

Figure 3.9-1: General View of the ANSYS Finite Element Solid Model of PUREX Filters

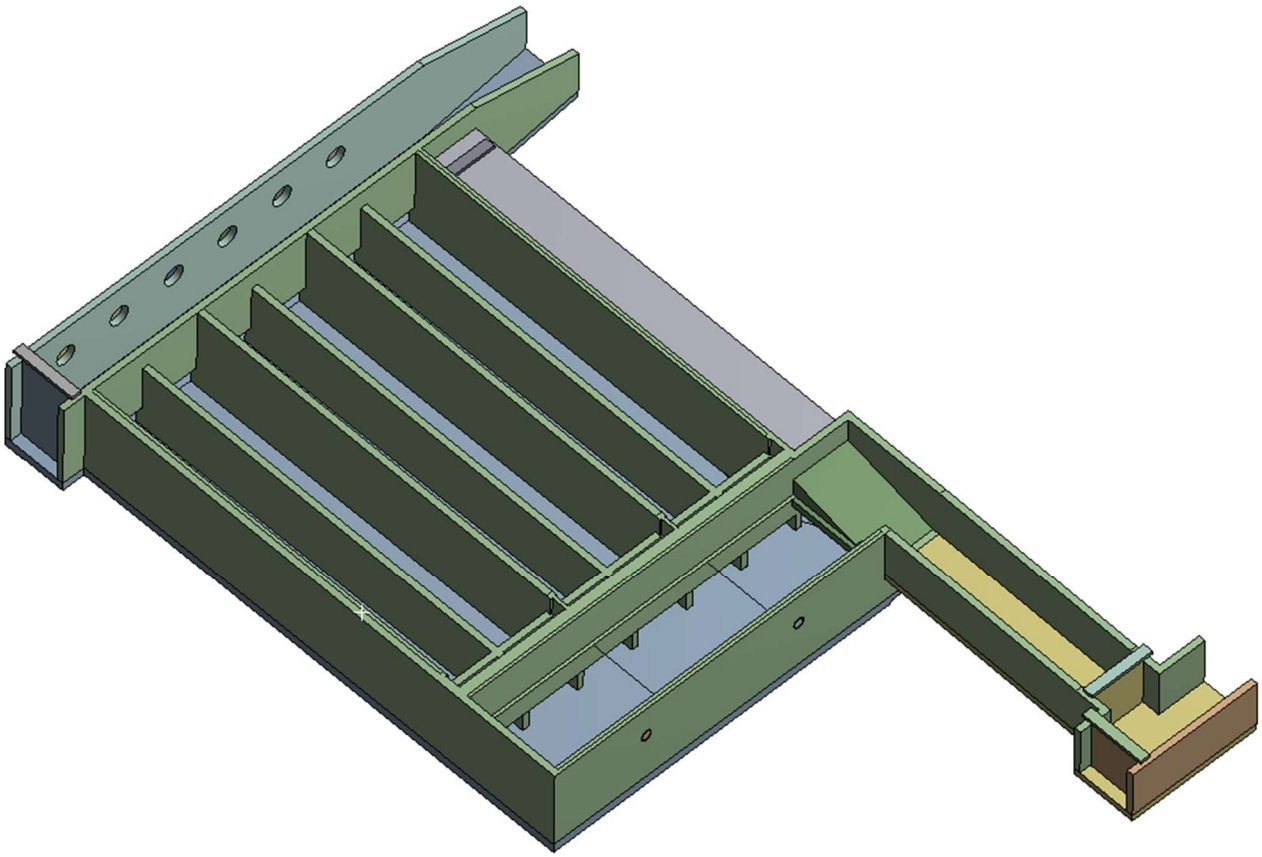

Figure 3.9-2: General View of the ANSYS Finite Element Solid Model of PUREX Filters Without the Top

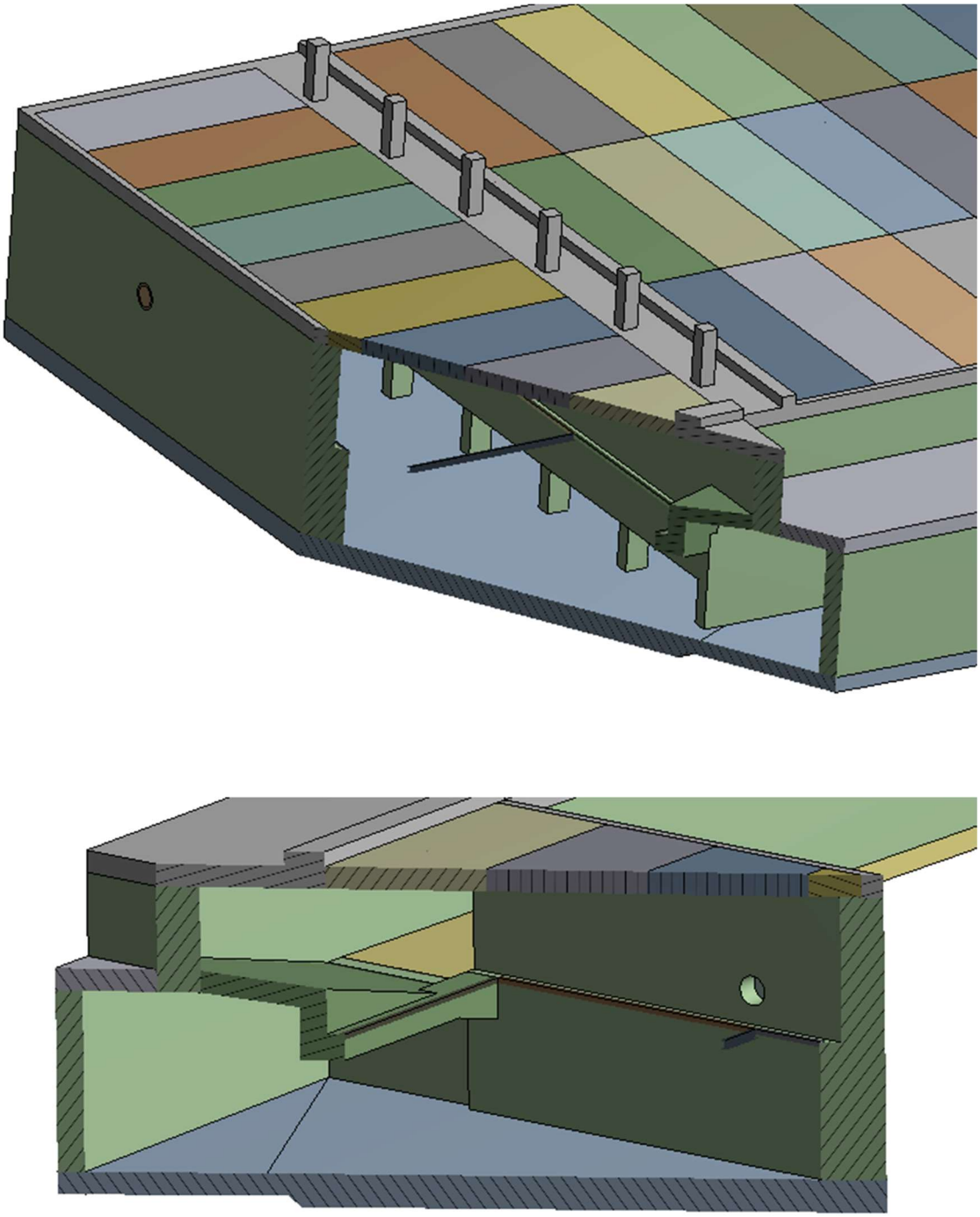

Figure 3.9-3: Sectional View of the ANSYS Finite Element Solid Model of PUREX Filters Outlet

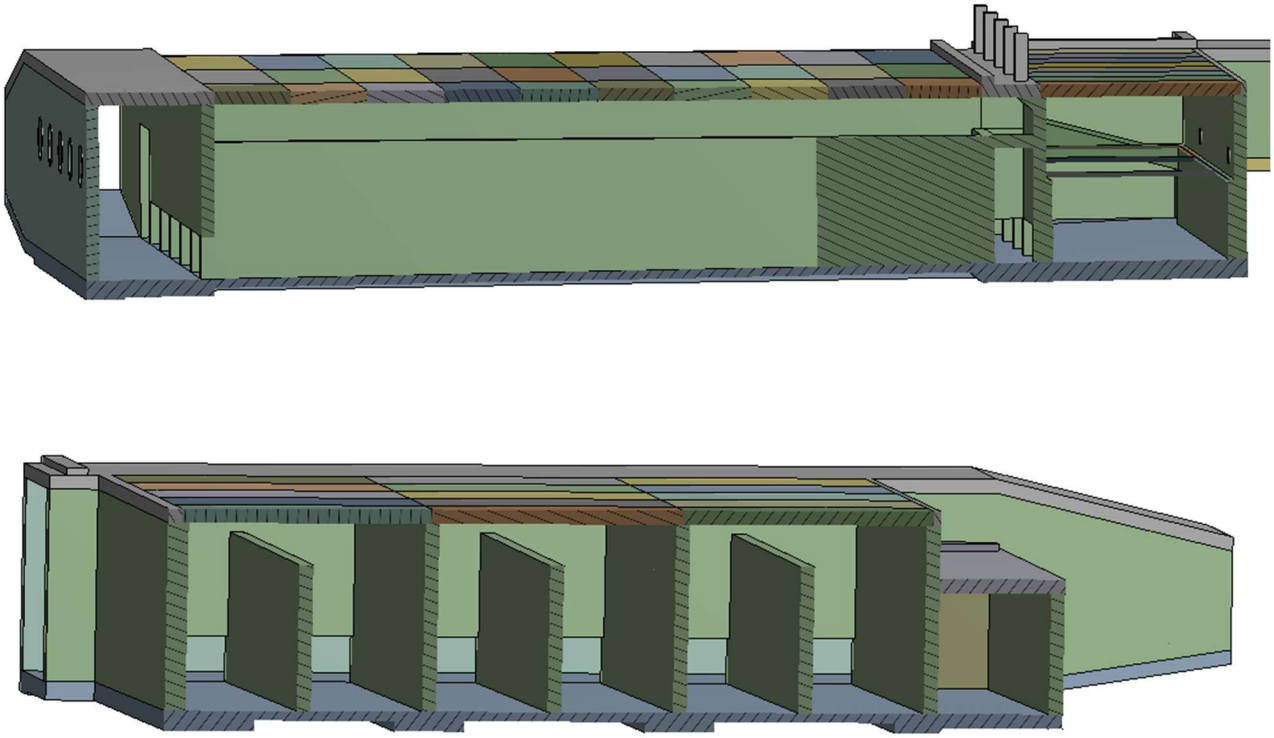

Figure 3.9-4: General Sectional View of the ANSYS Finite Element Solid Model of PUREX Filters

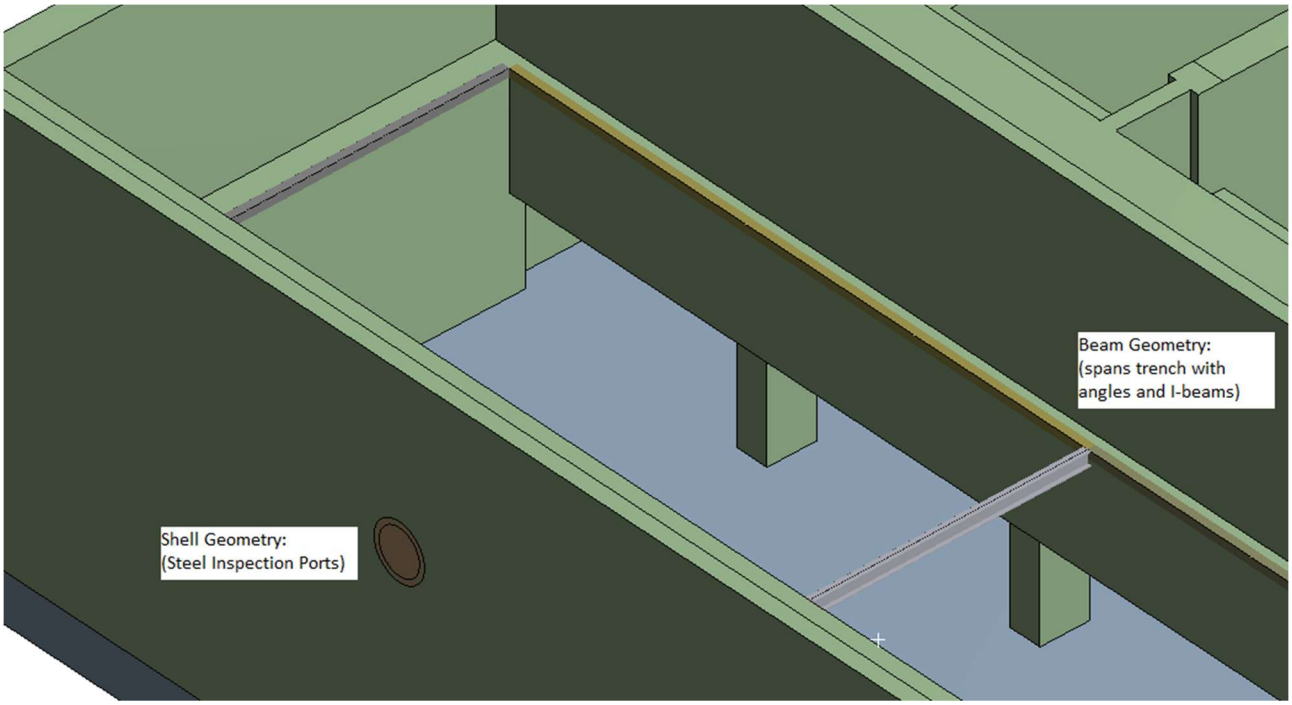

Figure 3.9-5: Top View of the ANSYS Finite Element Solid Model of PUREX Filters Showing One of the Steel Beams

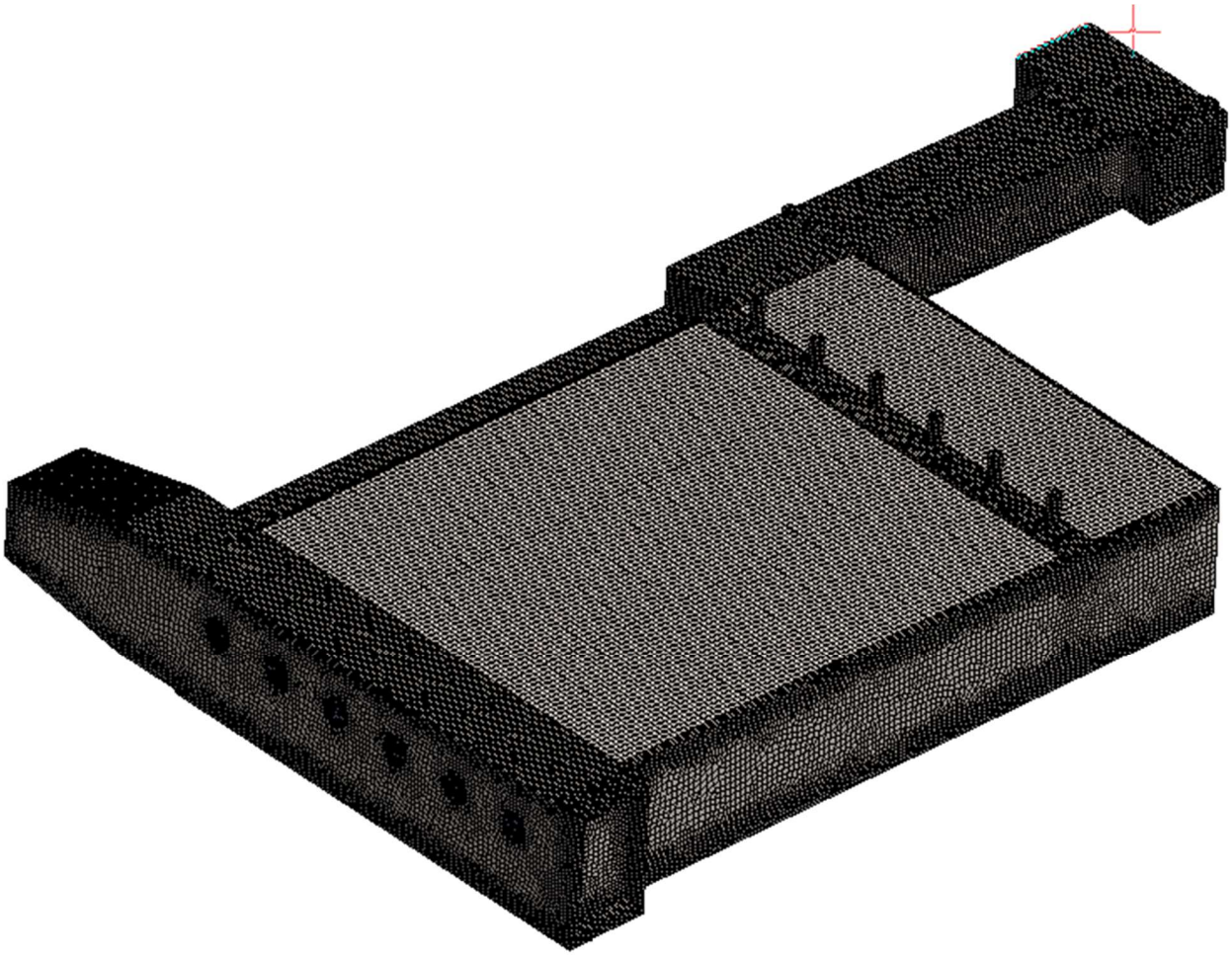

Figure 3.9-6: General View of the ANSYS Finite Element Mesh of PUREX Filters

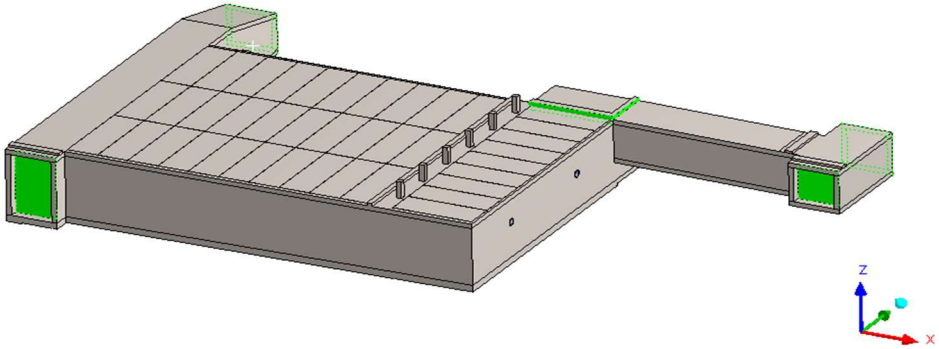

Figure 3.9-7: General View of the ANSYS Boundaries at Inlet/Outlet Ducts of PUREX Filters

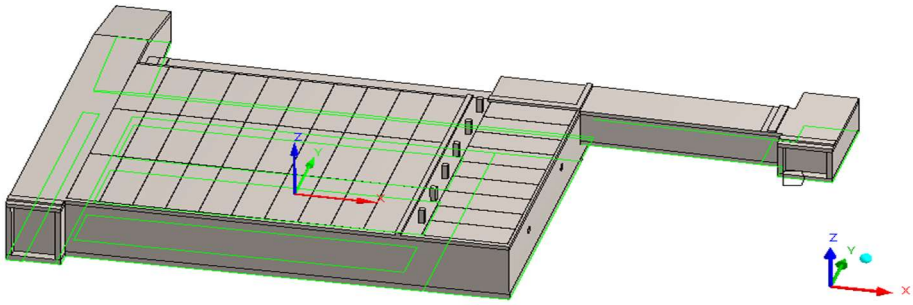

Figure 3.9-8: General View of the ANSYS Boundaries at Base of PUREX Filters

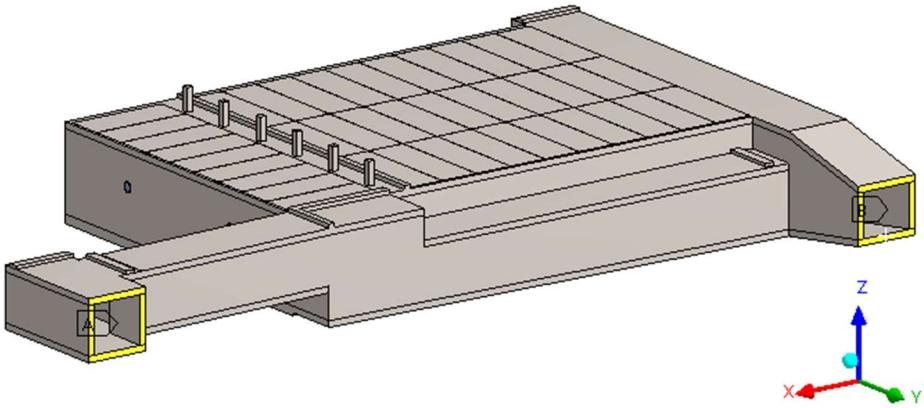

Figure 3.9-9: General View of the ANSYS Boundaries at Inlet/Outlet Ducts of PUREX Filters

3.10 Structure REDOX Sand Filters, Group O2

The REDOX sand filter is a below-grade structure approximately 85 x 85 x 20 ft deep, consisting of approximately 12 ft of sand and 8 ft of air space in a concrete shell. The filter medium decreases in particle size from coarse gravel at the bottom to 30-mesh sand at the top. The roof over the sand filter has been repaired and is in good condition. See Figure 3.10-1 through Figure 3.10-5 for details of the finite element solid model.

SOLID186 elements were used to model the existing ducts, concrete plugs, walls, floor/roof slabs (which are at least 6 in. thick). The model used an approximate mesh size of 5 in., with at least 2 elements through the thickness (Figure 3.10-6 and Figure 3.10-7). The roof, walls, and floor slab have at least 3, 3, and 4 nodes through the thickness, respectively. All protruding pipes are nonstructural and, therefore, not included in the structural model. The filler material was modeled with density, but low stiffness, to contribute to dead weight but not affect the load resisting system.

Material properties and loading were applied as described in Appendix A, and waste level did not apply to this model. The soil was not explicitly modeled and was accounted for with pressure loading.

Analogous to the PUREX deep bed filters degradation from water intrusion, degradation was simulated in the REDOX sand filter by reducing the roof slab thickness by 1 in. and rebar cross sectional area by 10% (outside of ANSYS).

Figure 3.10-1: General View of the ANSYS Finite Element Solid Model of REDOX Filter (top and content sand/gravel removed for clarity)

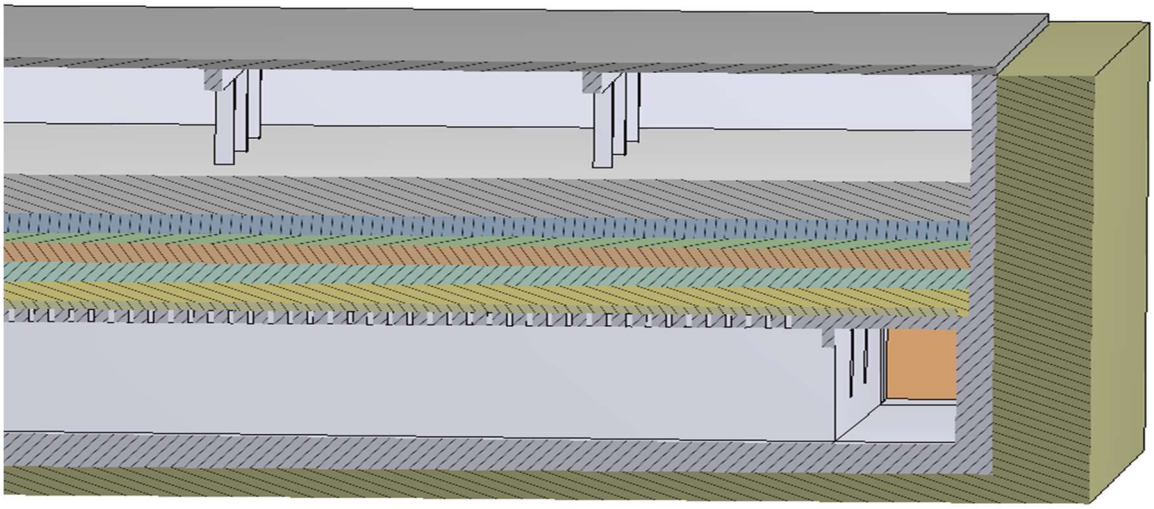

Figure 3.10-2: Section View of ANSYS Finite Element Solid Model of REDOX Filter – West Air Distribution Tunnel

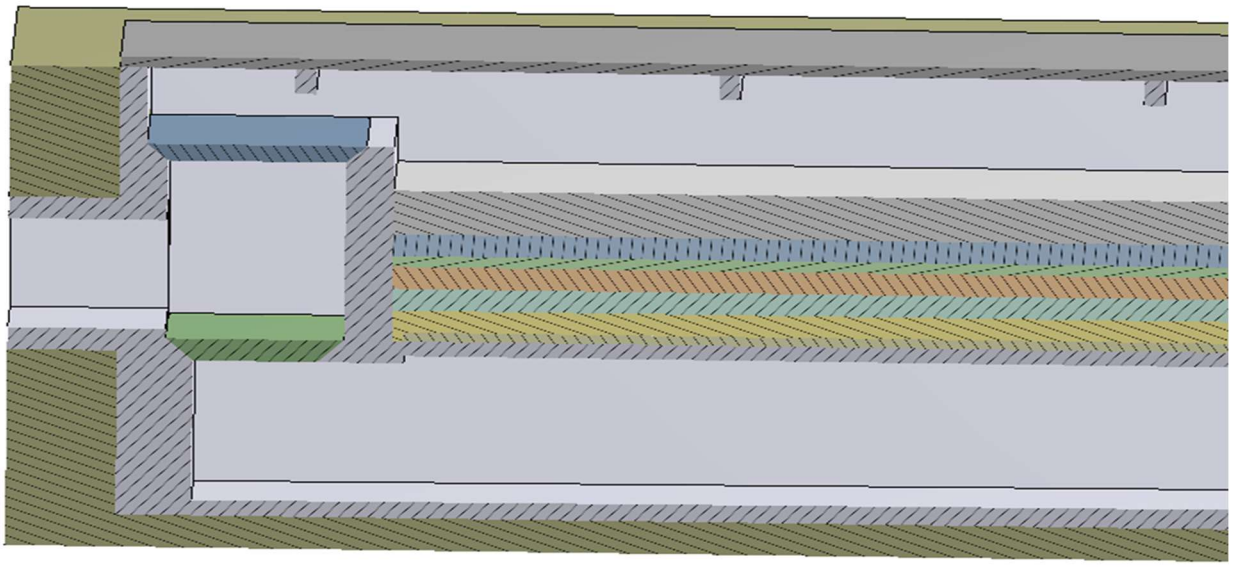

Figure 3.10-3: Section View of ANSYS Finite Element Solid Model of REDOX Filter – East Air Distribution Tunnel and Outlet

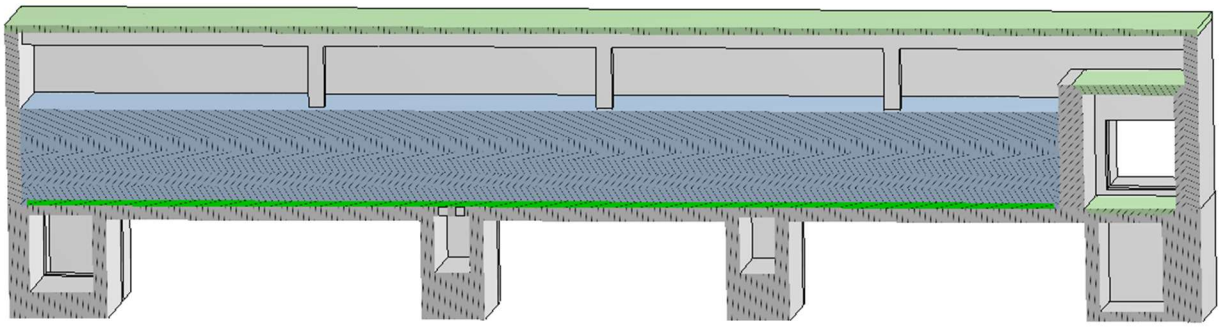

Figure 3.10-4: Section View of ANSYS Finite Element Solid Model of REDOX Filter – North End Across Air Distribution Tunnels

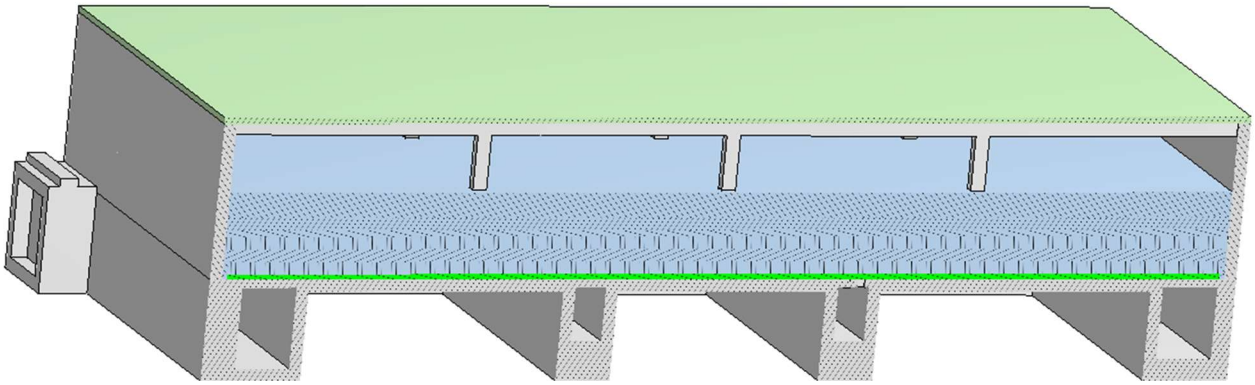

Figure 3.10-5: Section View of ANSYS Finite Element Solid Model of REDOX Filter – South End Across Air Distribution Tunnels

Figure 3.10-6: General and Sectional Views of ANSYS Finite Element Mesh of REDOX Filter

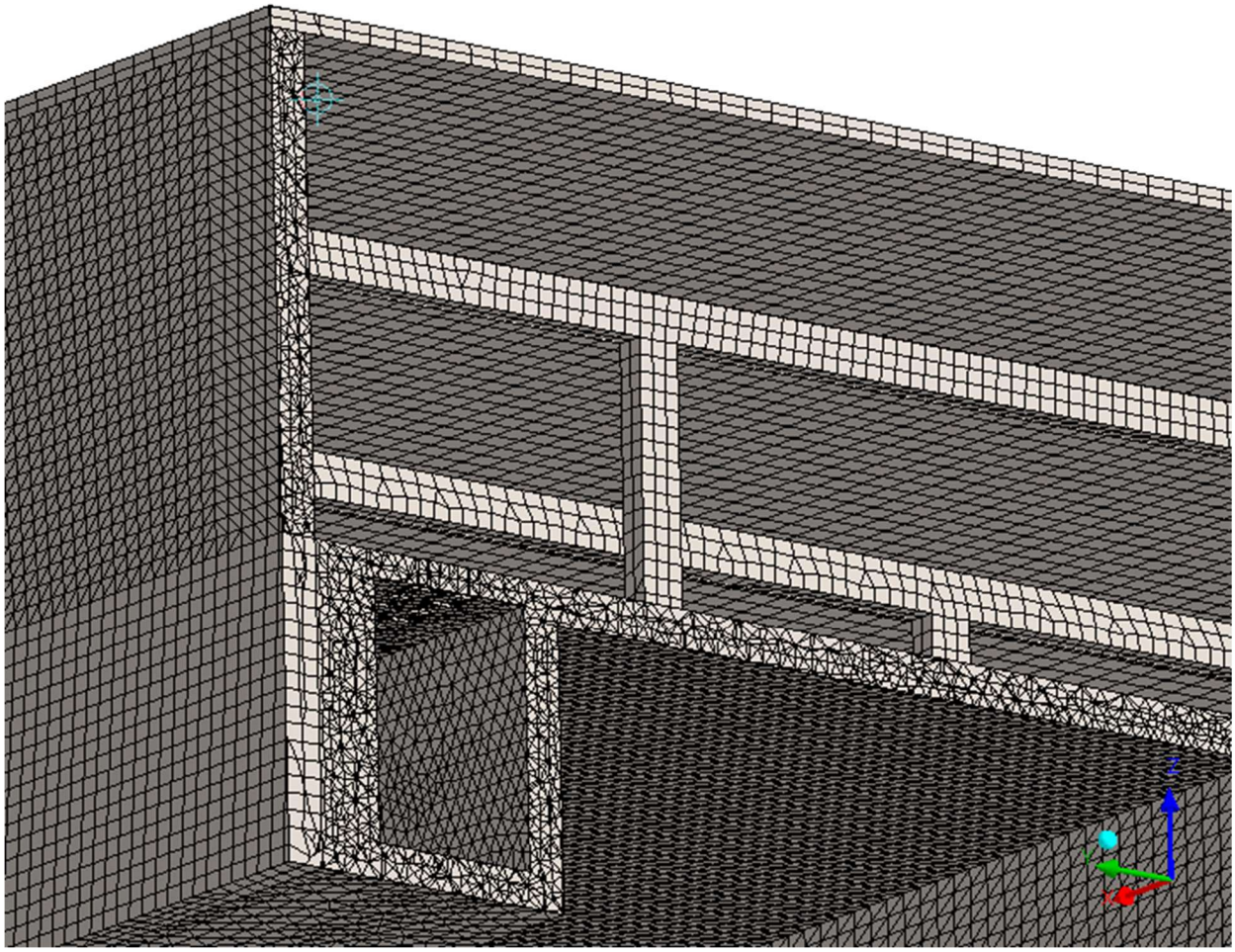

Figure 3.10-7: Partial Sectional View of ANSYS Finite Element Mesh of REDOX Filter

3.11 Structure 241-CX-70, Group O3

The 241-CX-70 cylindrical tank is a vertical, below grade, 4.6 m (15 ft) tall reinforced concrete tank with an inside diameter of 6.1 m (20 ft). The tank has a 6.4 mm (0.25 in.) thick stainless steel plate liner. The sides are 0.33 m (13 in.) thick and the top is 0.3 m (1 ft) thick. The bottom thickness varies from 0.6 m (2 ft) at the edges to 0.2 m (8 in.) at the center (Figure 3.11-1 and Figure 3.11-2). The tank top is approximately 3.4 m (11 ft) below grade.

All concrete components, including the tank lid and housings surrounding the pipe inlets, were modeled using SOLID186 elements, with an approximate mesh size of 3.5 in. (Figure 3.11-3 and Figure 3.11-4). The roof, walls, and floor slab have approximately 8, 8, and 15 nodes through the thickness, respectively. All protruding pipes were modeled as steel, meshed with quad/tri elements and were connected to the concrete dome using bonded surface-to-surface contact. Material properties were assigned as designated in Appendix A. The entire tank was continuously meshed. Masses were included at the bottom face of the roof slab to simulate weight of miscellaneous attachments. Boundary conditions were simulated with frictionless vertical restraints.

The concrete was modeled as a solid linear elastic material, and cracking was not simulated in the finite element analysis; therefore, rebar and stainless steel stiffeners within the concrete lid were not modeled. Excluding the stiffeners in the analysis is conservative and adequate since the condition of the stiffeners cannot be verified.

Loading was applied to the model as described in Appendix A. The soil above and around the tank was not explicitly modeled, but accounted for with pressure loading on the top and side surfaces of the tank. Based on the available information, there is no indication of damage to the tank and, therefore, no degradation was included in the model [27].

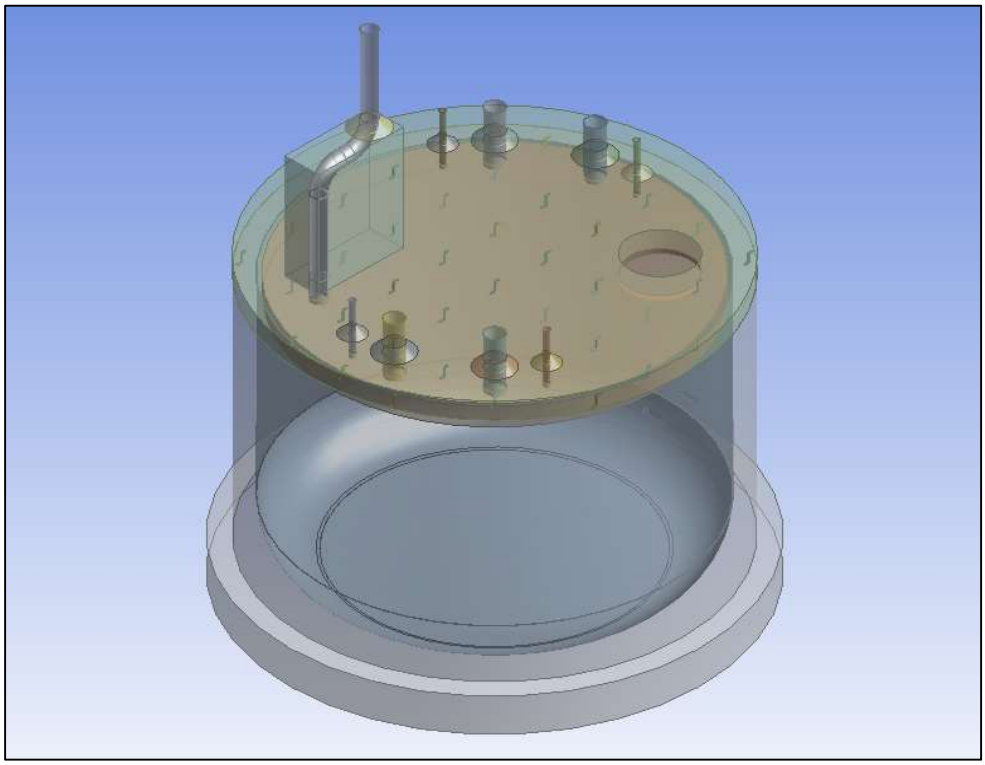

Figure 3.11-1: General View of ANSYS Finite Element Solid Model of 241-CX-70

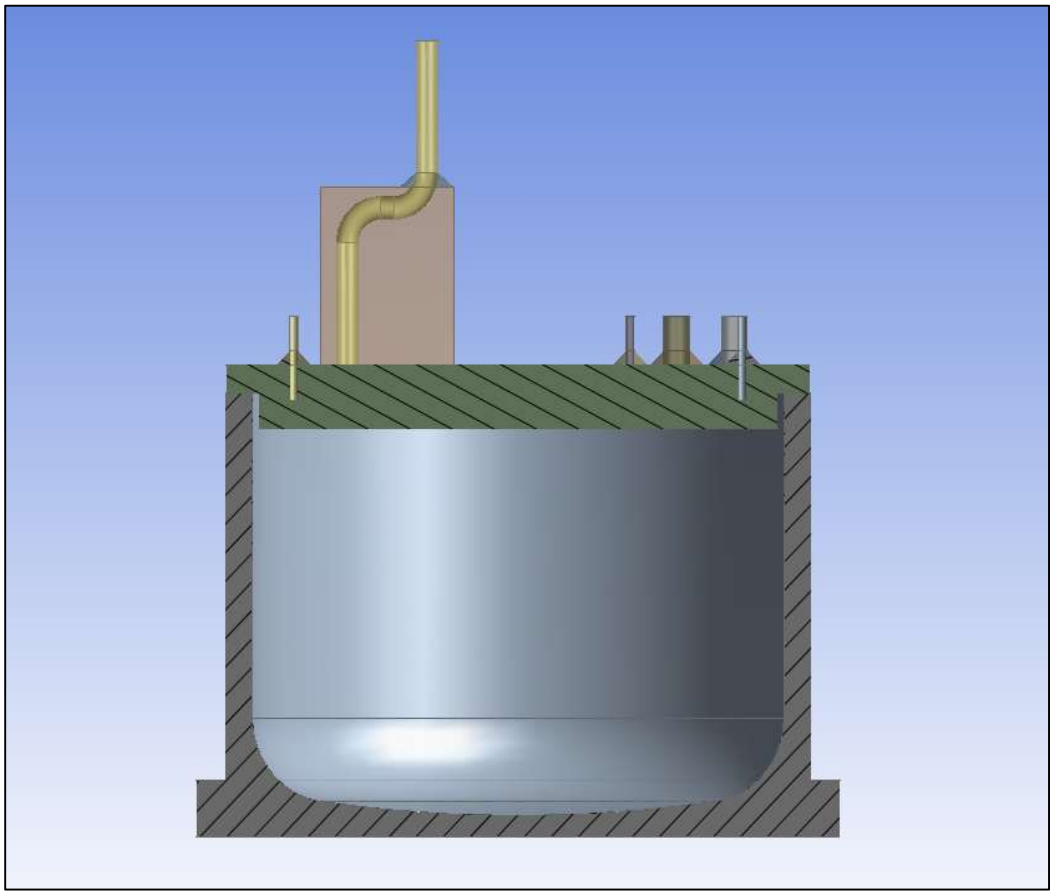

Figure 3.11-2: Sectional View of ANSYS Finite Element Solid Model of 241-CX-70

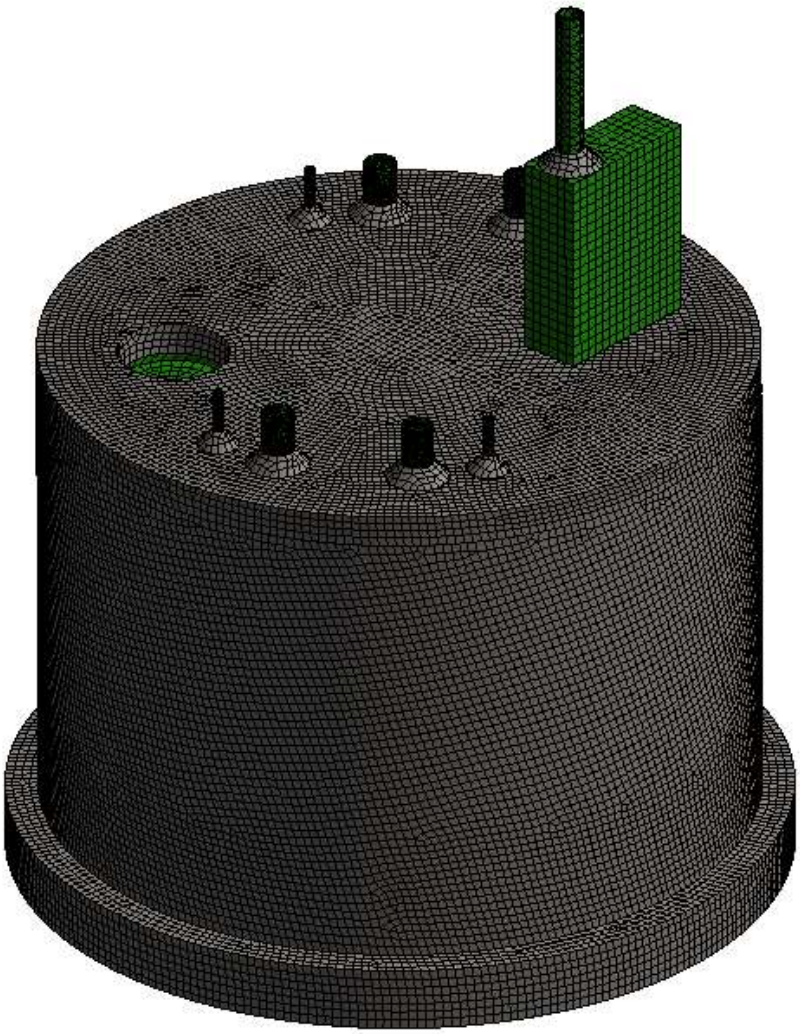

Figure 3.11-3: View of ANSYS Finite Element Mesh of 241-CX-70

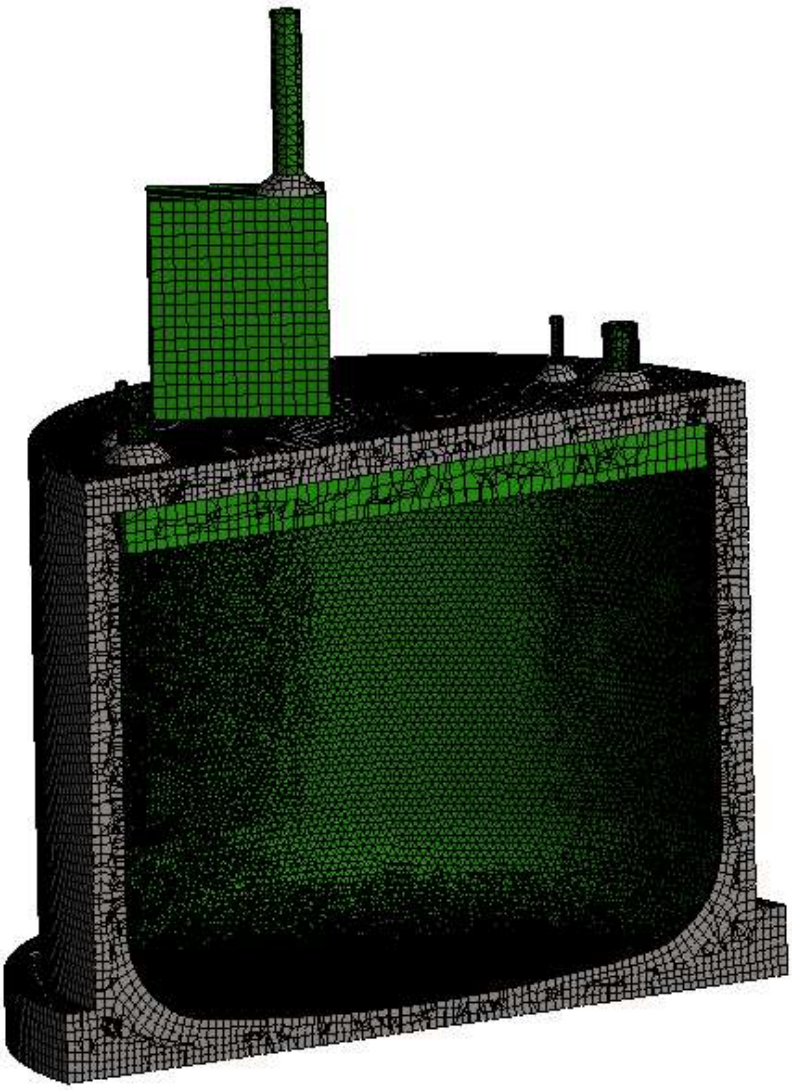

Figure 3.11-4: Sectional View of ANSYS Finite Element Mesh of 241-CX-70

4. EVALUATION OF FINITE ELEMENT RESULTS

Finite element analyses of the selected structures, shown in Table 2-1, were performed for the loading and load combinations identified in Appendix A of this report. Resulting stresses and member forces and moments are reported and evaluated against strength limits to assess margin to failure in accordance with methods consistent with ACI [4 5], ASCE/SEI 41 [11], ASCE 7 [24], IBC [3], and AISC [6] codes and standards, and the Wood Handbook [12]. Certain assumptions were made due to lack of design information for some structures (Table 3-2). Observed degradation was simulated by reduction in member sizes or an increase in the factors to calculated demand. The analyses were performed for the two load combinations identified in Appendix A. The results presented are generally for Load Combination 1[11] - the more critical of the two load combinations (see Appendix A of this document).

Note, units in subsequent figures are in. for deflection (or displacement), psi for stress, in.-lb for moment, and lb for force. Explanation is provided below for legends in the subsequent ANSYS contour plot figures (included in the figures as applicable).

Legend Item	Explanation
Type	ANSYS generated description of type of result in the plot
Load Multiplier	Buckling eigenvalue (factor applied to analyzed load to determine the buckling load).
Unit	Unit of the result values shown in the contour colored legends
Coordinate System	This is an identifier of the coordinate system for the results shown. Included only for directional results.
Time	User selected value that identifies the load combination. In all analyses herein, a value of 9 refers to load combination 1 and value of 10 refer to load combination 2. Load combinations 1 and 2 are defined in Section 4 of Appendix A.
Custom	
MAX	Maximum algebraic value of the result, only shown if contour values are user defined.
MIN	Minimum algebraic value of the result, only shown if contour values are user defined.
Date and time stamp	Date and time the figure was created in ANSYS.
Text Preceding “Type”	User-defined figure name for additional clarification

[11] Load Combinations 1 and 2 in Appendix A are defined in the ANSYS analysis as load cases 9 and 10, respectively.

For concrete structures, ANSYS calculated stresses were integrated for selected representative slice (strip) of elements along the critical locations in the roof and walls to obtain the demand axial and shear forces and bending moments. The integrated results are compared to design strength values calculated based on the ACI 318 Code. The integrated axial and shear forces and bending moments are presented in 2-D graphs along the length of the selected strip of elements. The selected elements for the integration are shown on translucent views of the finite element models.

The “Distance” axis in the 2-D graph represents the distance along the length of the strip of elements. A X, Y, and Z coordinate triad is shown to indicate the origin (distance “0”) and direction of the element strip. The selected strip of elements runs through the critical (high-stress) regions in walls and slabs identified in the stress contour plots - as well as the wall-roof (or floor-slab) intersections. However, the integrated results at those intersecting locations are not used in the Code evaluations as they are not applicable to either the walls, roofs, or floor slabs. Dashed lines are shown on the 2-D graphs to indicate the boundaries of such intersections. Also, depending on the selected mesh of the finite element model, the selected strip of elements may have irregular shape (due to refined meshing). The irregular shape causes indications (dips/humps) in the 2-D graphs. The selection of the peak values from the 2-D graphs for Code evaluation was based on smoothing of the graphs to eliminate such dips and humps.

Appendix C of this document provides additional information on the finite element modeling results that was requested for the review comment record (RCR) comment resolutions.

4.1 Structure 216-Z-2, Group C1

Results for timber structure 216-Z-2 include total deformation contours (Figure 4.1-1), stress contour plots of axial stresses (Figure 4.1-2), and shear stresses (Figure 4.1-3). A maximum displacement of 0.47 in. occurs at the center of the roof. The stress plots are presented such that the focus is on the areas of peak stress. As shown, the maximum axial stress due to axial forces and bending moments on the 6 in. timber logs is 2,521 psi in compression. The maximum shear stress of 1,372 psi is localized at geometric discontinuities (see lower plot in Figure 4.1-3) and the general max shear stress is 548 psi (see upper plot in Figure 4.1-3).

Evaluation of these peak stresses with the material strength for Douglas Fir timber with 12% moisture content is given below. The factored combined stresses include a 20% increase to simulate possible degradation.

Stress Component	Demand	Limit/Capacity (1)	Demand/Capacity (2)
Axial	2,521 psi	6,230 psi	0.49 < 1.0
Shear	548 psi	1,130 psi	0.58 < 1.0

(1) Obtained from Wood Handbook [12] for Douglas Fir, 12% moisture.

(2) Note that the 20% increase in demand stresses as described in Section 3.1 (and Appendix A) is applied in the stress ratios.

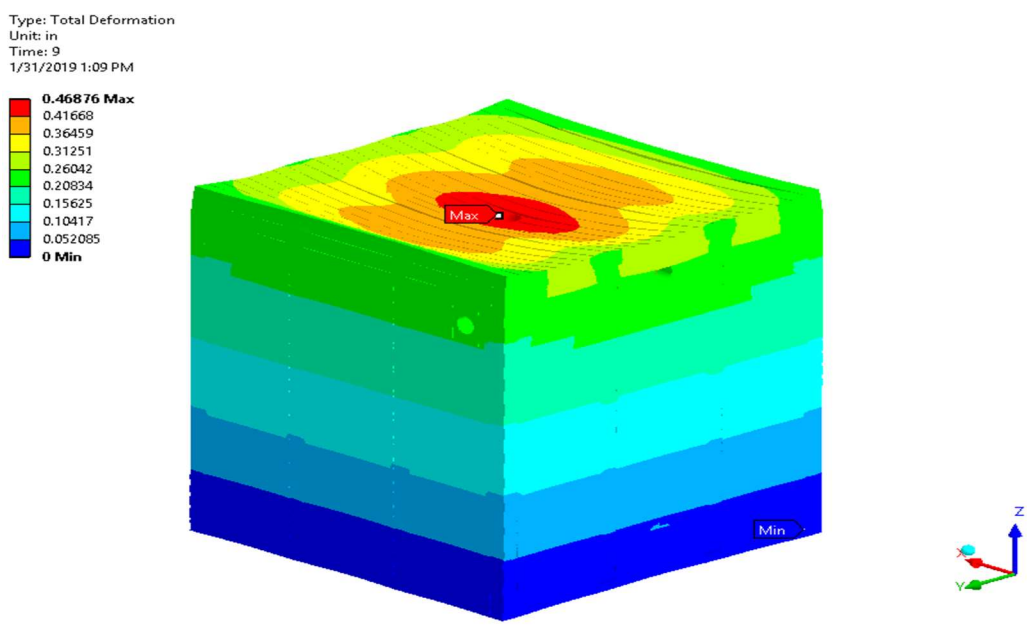

Figure 4.1-1: Contour Plot Total Displacements (in.) for 216-Z-2

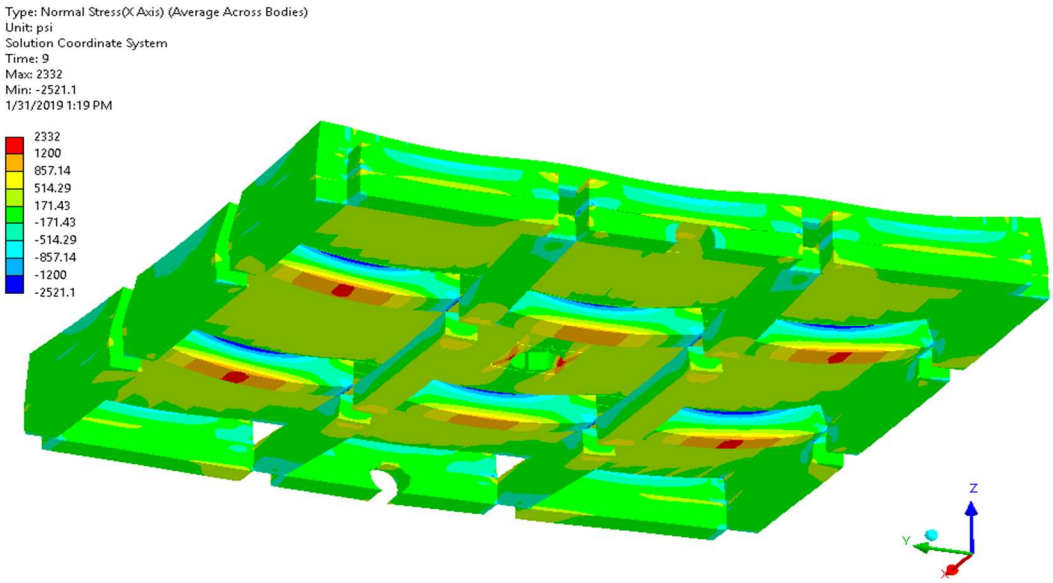

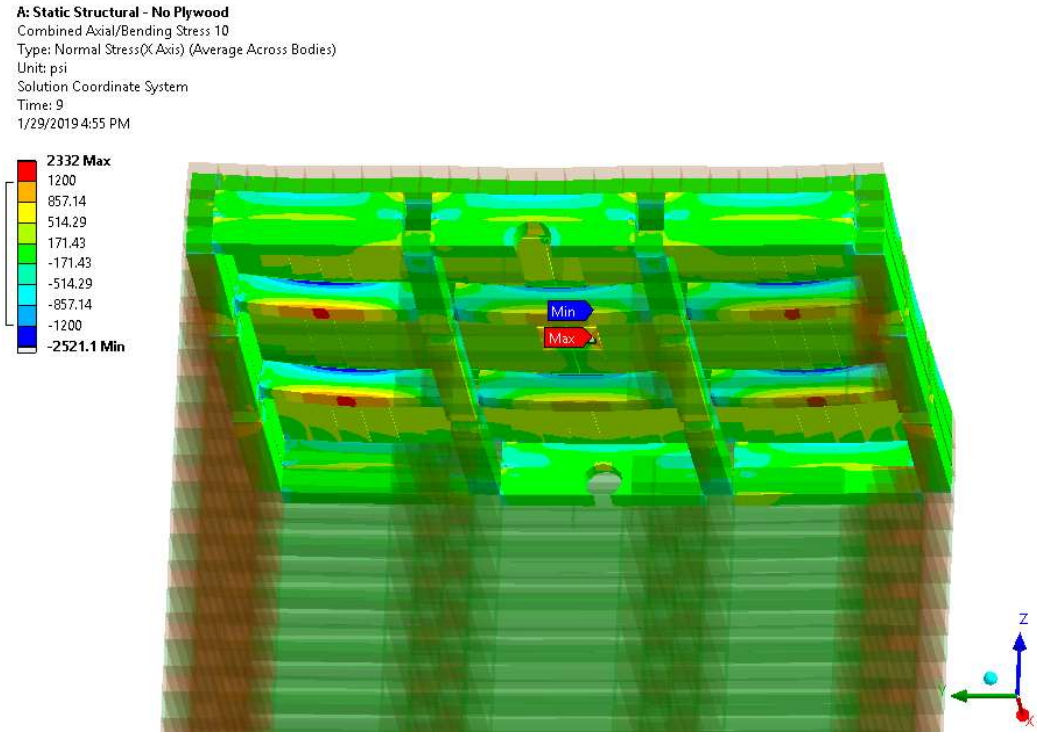

Figure 4.1-2: Contour Plots of Axial Stresses (psi) for 216-Z-2 Roof – Bottom Figure With Translucent View of Whole Model

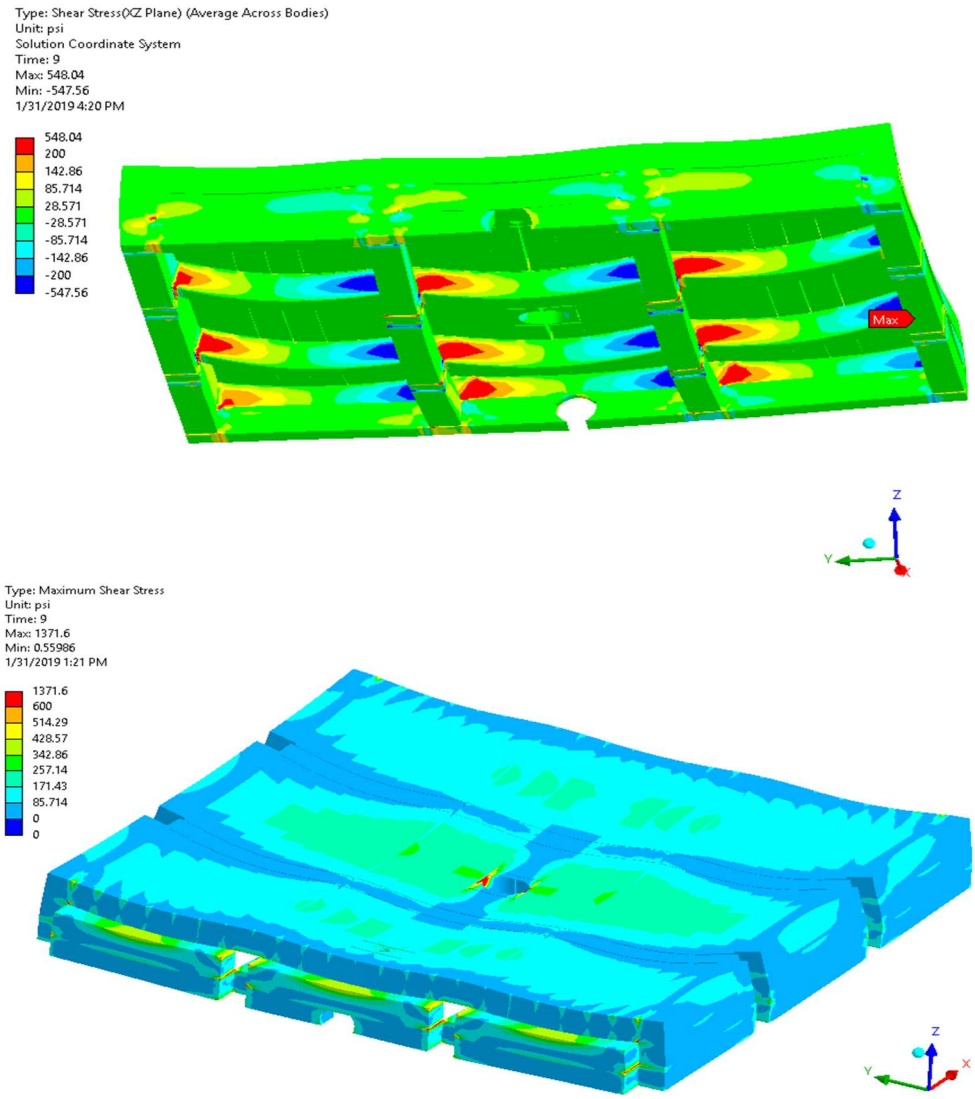

Figure 4.1-3: Contour Plots of Shear Stresses (psi) for 216-Z-2 Roof – Upper figure is for the main shear stress component XZ, the Bottom figure is for the resultant shear stress (the peak value in this figure is localized stress)

4.2 Structure 216-B-12, Group C2

Results for timber structure 216-B-12 include total deformation contours (Figure 4.2-1), stress contour plots of axial/bending stresses (Figure 4.2-2), and shear stresses (Figure 4.2-3). A maximum displacement of 1.6 in. occurs at the center of the roof. The stress plots are presented such that the focus is on the areas of peak stress. As shown, the maximum axial stress due to axial forces and bending moments in the timber is 6,568 psi in compression. The maximum shear stress is 3,511 psi. It is likely that averaging would result in lower member stresses, however, the stress level is considered to be very high, thus, negating any benefit from averaging.

Evaluation of these peak stresses with material strength for Douglas Fir timber with 12% moisture content is given below.

Stress Component	Demand	Limit/Capacity (1)	Demand/Capacity (2)
Axial	6,568 psi	6,230 psi	1.27 > 1.0 NG
Shear	3,511 psi	1,130 psi	3.73 >> 1.0 NG

(1) Obtained from Wood Handbook for Douglas Fir, 12% moisture.

(2) Note that the 20% increase in demand stresses as described in Section 3.2 (and Appendix A) is applied in the stress ratios

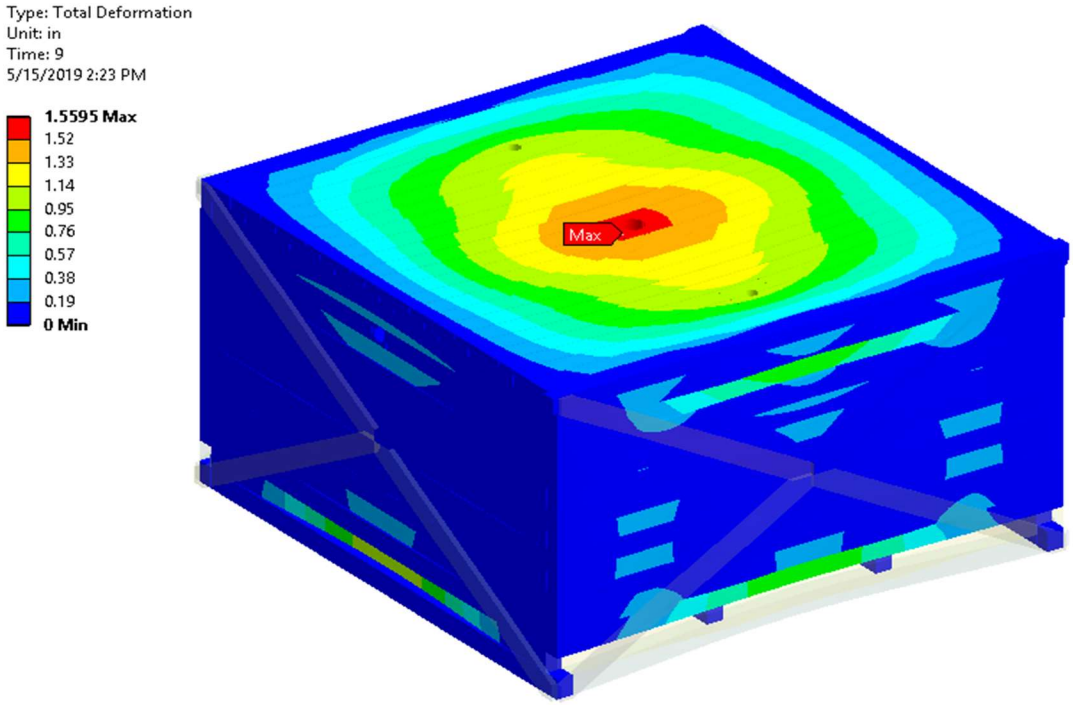

Figure 4.2-1: Contour Plots of Deflections (in.) for 216-B-12

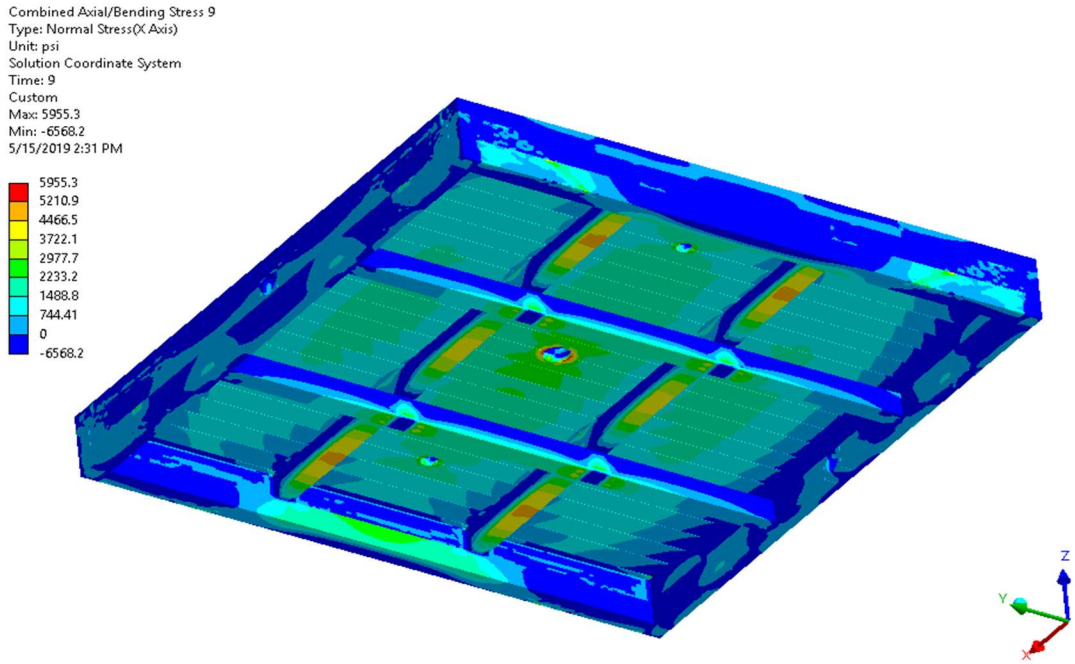

Figure 4.2-2: Contour Plots of Bending Stress (psi) for 216-B-12 Roof

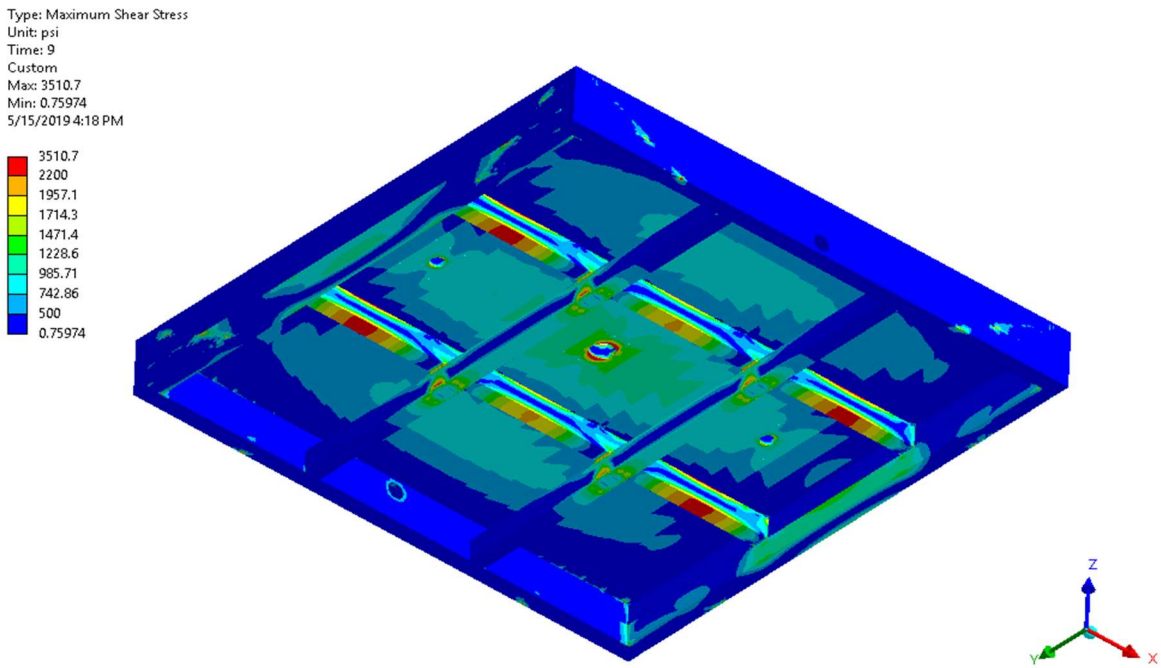

Figure 4.2-3: Contour Plots of Shear Stress (psi) for 216-B-12 Roof

4.3 Structure 216-Z-6, Group C3

Results for timber structure 216-Z-6 include total deformation contours (Figure 4.3-1), stress contour plots of axial/bending stresses (Figure 4.3-2) and shear stresses (Figure 4.3-3). The maximum displacement of 0.11 in. occurs at the center of the roof. The stress plots are presented such that the focus is on the areas of peak stress. As shown, the maximum axial stress due to axial forces and bending moments in the timber is 1,961 psi in tension. The maximum shear stress is 1,064 psi.

Evaluation of these peak stresses with material strength for Douglas Fir timber with 12% moisture content is given below.

Stress Component	Demand	Limit/Capacity(1)	Demand/Capacity(2)
Axial	1,961 psi	6,230 psi	0.38
Shear	1,064psi	1,130 psi	1.13 (3)

(1) Obtained from Wood Handbook for Douglas Fir, 12% moisture.

(2) Includes 20% increase in the demand stress to simulate degradation.

(3) This stress interaction ratio (IR) is based on maximum stress in a cross section. With the assumed increase in the demand, the maximum shear strength of the timber is exceeded indicating potential for failure.

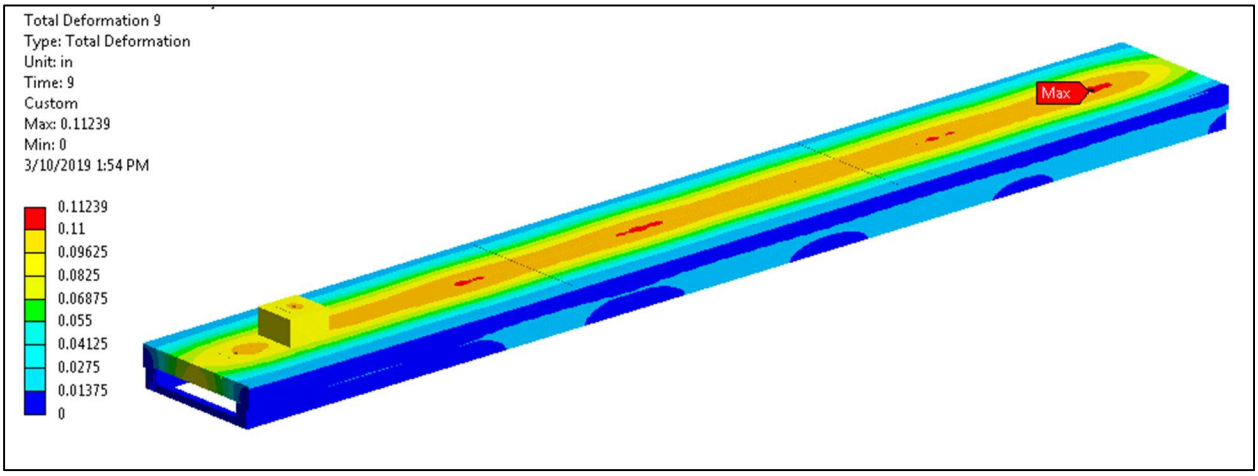

Figure 4.3-1: Contour Plots of Deflections (in.) for 216-Z-6

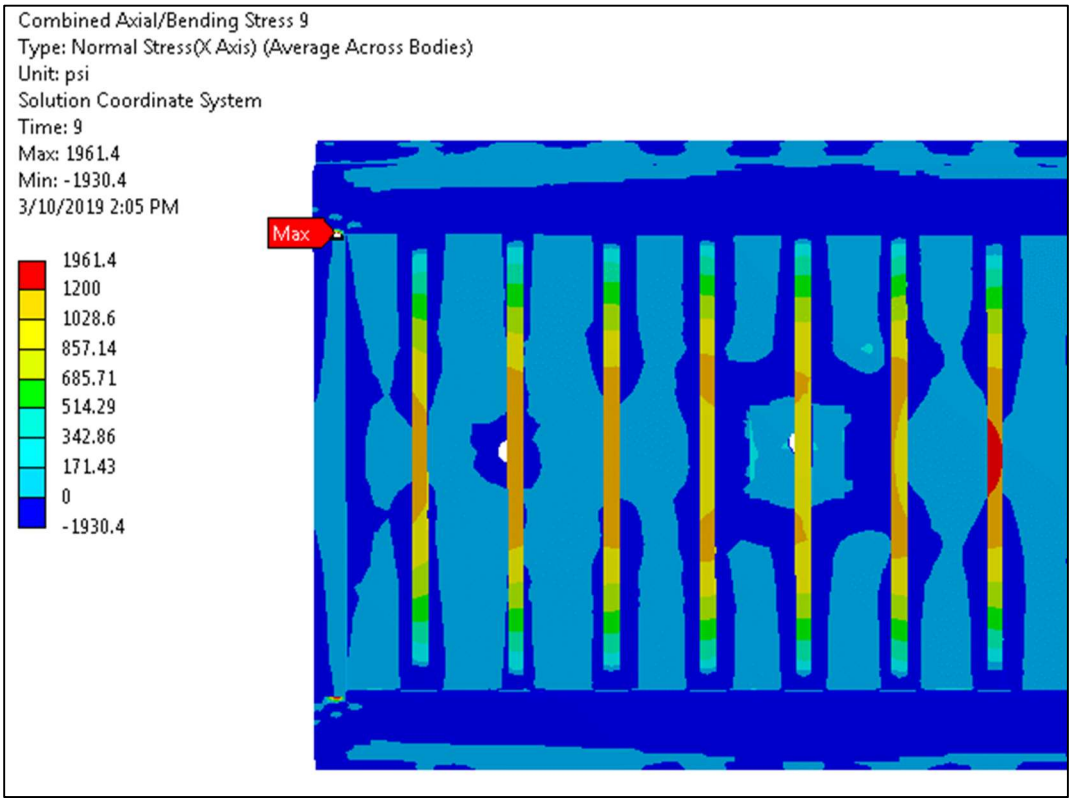

Figure 4.3-2: Contour Plots of Bending Stress (psi) for 216-Z-6 – Plan View Looking Up

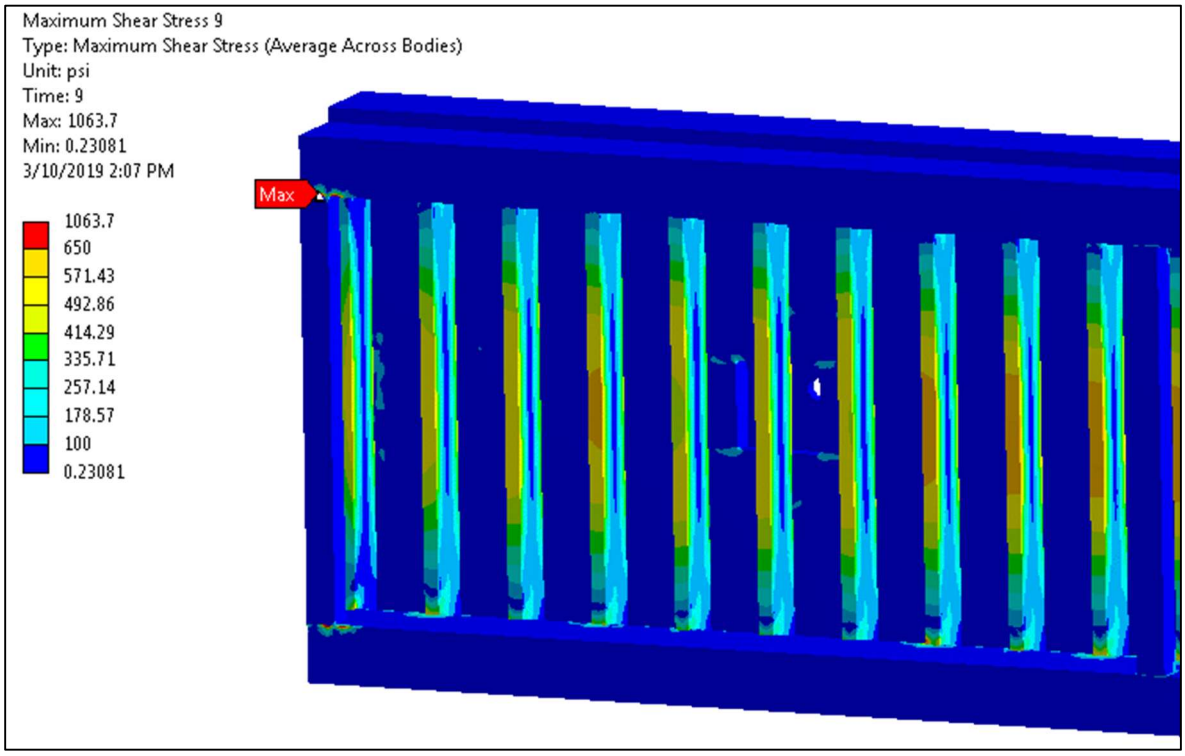

Figure 4.3-3: Contour Plots of Shear Stress (psi) for 216-Z-6 – Plan View Looking Up

4.4 Structure 216-Z-7, Group C4

Results for timber structure 216-Z-7 include total deformation contours (Figure 4.4-1), stress contour plots of axial/bending stresses (Figure 4.4-2) and shear stresses (Figure 4.4-3). A maximum displacement of 0.27 in. occurs at the center of the roof. The stress plots are presented such that the focus is on the areas of peak stress. As shown, the maximum axial stress due to axial forces and bending moments in the timber is 5,717 psi in compression. The maximum shear stress is 2,837 psi. This maximum shear stress is highly localized as shown in Figure 4.4-4. By inspection of the contours, an average shear stress over the cross section is reasonably represented by the 975-1,300 psi contour band. The average shear stress in the timber cross section is thus taken as (975+1,300)/2 = 1,138 psi.

Evaluation of these stresses with material strength for Douglas Fir timber with 12% moisture content is given below. No degradation is included with this structure.

Stress Component	Demand	Limit/Capacity (1)	Demand/Capacity
Axial	5,717 psi	6,230 psi	0.92 < 1.0
Shear	1,138 psi	1,130 psi	1.007 ≈ 1.0

(1) Obtained from Wood Handbook for Douglas Fir, 12% moisture.

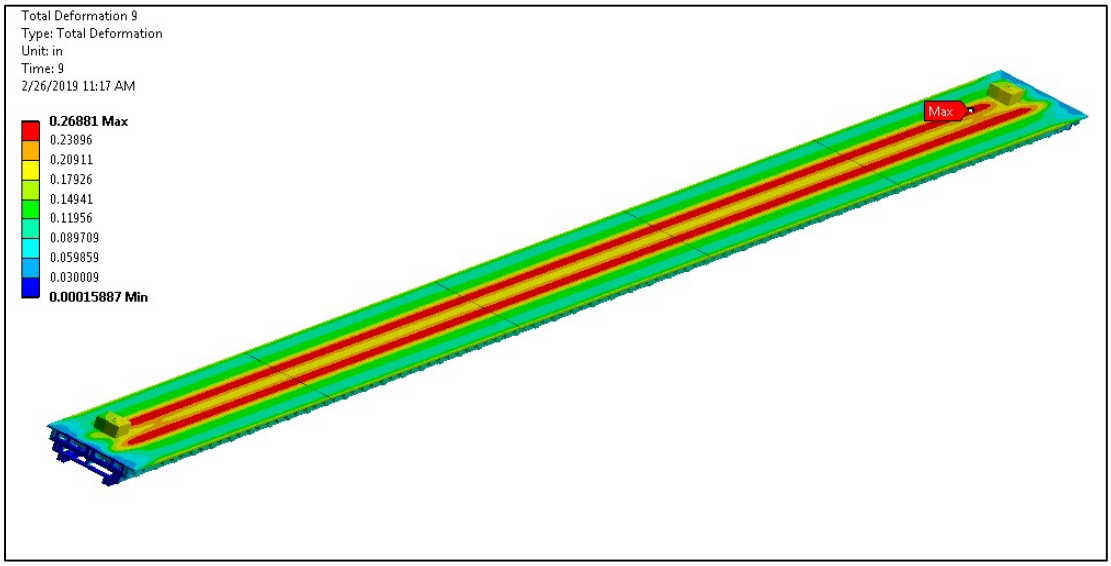

Figure 4.4-1: Contour Plots of Deflections (in.) for 216-Z-7

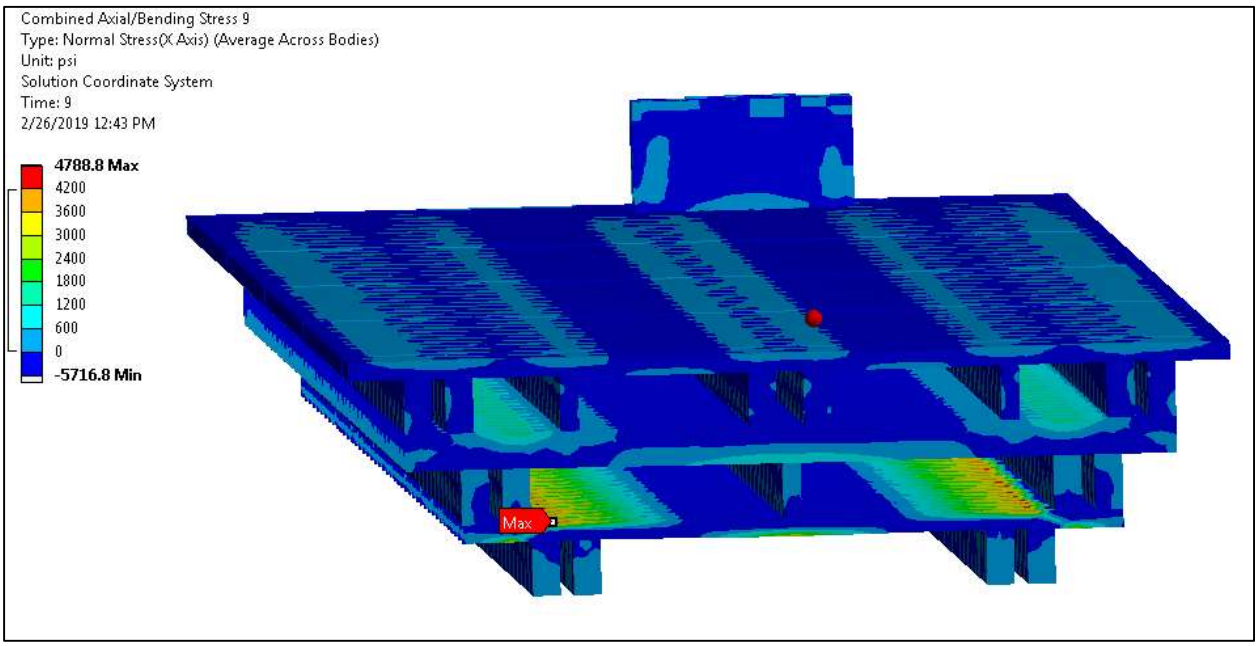

Figure 4.4-2: Contour Plots of Bending Stress (psi) for 216-Z-7

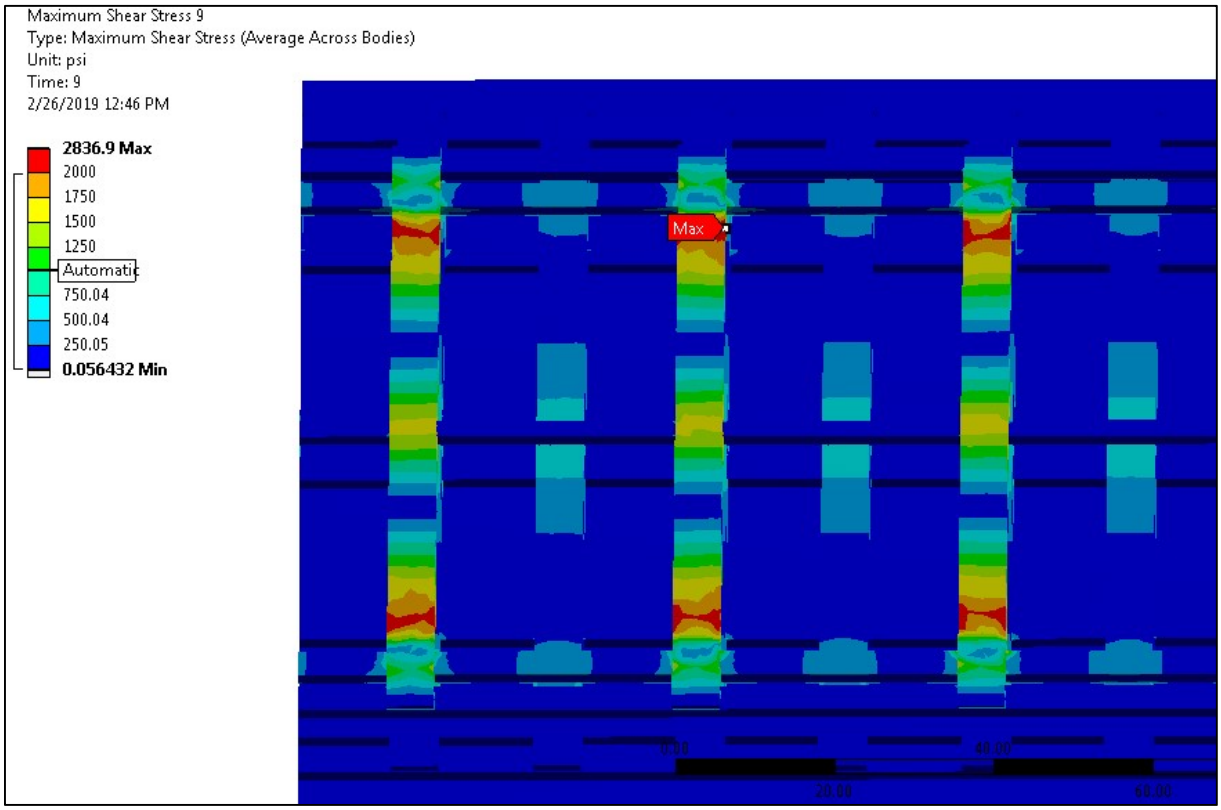

Figure 4.4-3: Contour Plots of Shear Stress (psi) for 216-Z-7 – Plan View Showing Cross Members

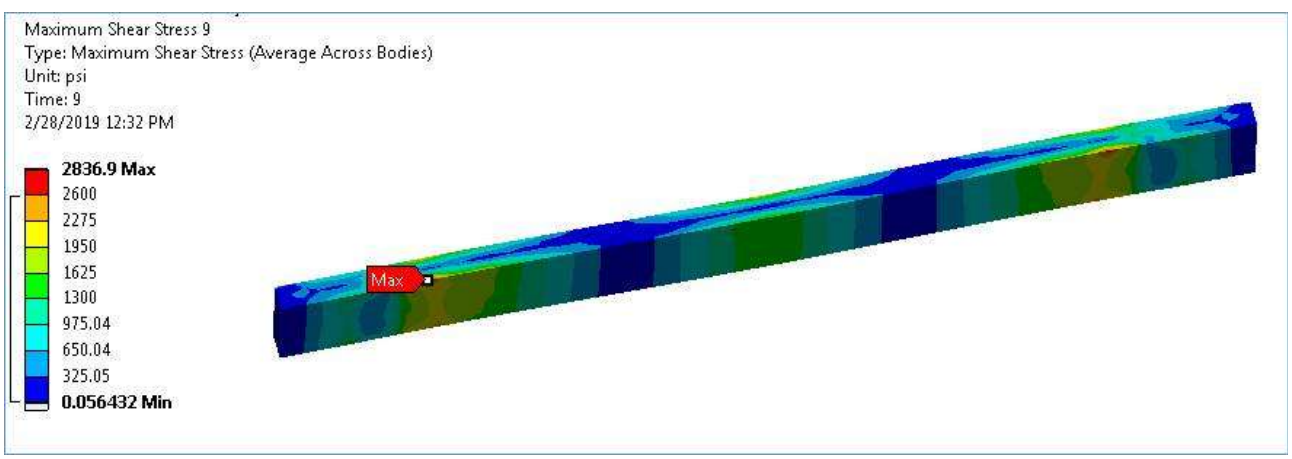

Figure 4.4-4: Contour Plots of Shear Stress (psi) at Maximum Shear for 216-Z-7

4.5 Structure 216-Z-9, Group C5

Since the slab design for 216-Z-9 does not include beams, the evaluation was performed using methods for flat slab design. Analysis of flat slabs consists of analysis of column strips and middle strips based on design drawings that include details of the slab reinforcement. Results from the finite element analysis were used to analyze the more critical of the column strip and middle strip per Chapter 13 of ACI 318 [4].

Deformation contours are shown in Figure 4.5-1 and Figure 4.5-2 with a maximum vertical displacement of 0.4 in. at the roof between the column line and perimeter ledge due to load combination 1. Maximum tensile stresses are shown in Figure 4.5-3 and maximum compression in Figure 4.5-4. Contours of the axial compression in the columns are shown in Figure 4.5-5. Graphs of the integrated forces and moments in the slab and column are in Figure 4.5-6 through Figure 4.5-15.

The cross section of the slab is 9 in. deep but was modeled as 8 in. to simulate observed degradation. The slab reinforcement is shown in the crib structural drawings. All bars are No. 5 (5/8 in. diameter). The number of bars is summarized below.

	Bottom face Outer span	Top face over column or column strip	Bottom face Inner span
North-South Direction – Middle Strip	19	17	16
North-South Direction – Column Strip	25	37	20
East-West Direction – Middle Strip	19	17	16
East-West Direction – Column Strip	25	37	20

Per drawings, the middle and column strips are 15 ft wide. The drawings specify rebar clearance of 0.75 in. for the top and 1 in. for bottom. The concrete section capacity for a 12 in. wide section in the outer span of a middle strip was obtained as follows:

As = 0.31 in.^{2} x 19 x 1/15 rebar cross sectional area for 12 in. wide concrete section (19/15 rebar x size 0.625-in. rebar area)

As' = 0 no compression reinforcement (not considered)

b = 12 in. 12 in. wide section

d = 9 in. – 1 in. – 0.5 in./2 = 7.75 in. tensile rebar depth (1 in. clear cover)

fc = 3,000 psi compressive strength of concrete

fy = 40,000 psi yield strength of reinforcing steel

Bending Moment Capacity of Roof Slab

ϕMn = 0.9 x As fy { d – As fy / (2 x 0.85 fc b) }

= 0.9 x 0.31*19/15 x 40,000 {7.75 – 0.31*19/15 x 40,000 / (2 x 0.85 x 3,000 x 12)}

= 105,926 in.-lb bending capacity for 12 in. wide section

Similar calculations were performed for other locations in the slab excluding the enlarged sections over the columns, the results of which are summarized below. In all cases, the bottom rebar is in tension and the rebar depth is 7.75 in.

	Bending Moment Capacity in.-lb	Bending Moment Demand in.-lb
Middle strip - outer	105,926	210,000
Middle strip - inner	89,683	76,000
Column strip – outer	137,869	160,000
Column strip - inner	111,300	100,000

As shown above, the bending moment capacity is less than the demand moment for the outer middle strip and outer column strip. As such, the slab section is not adequate for bending moment.

Shear Capacity of Roof Slab

Reduced shear stress capacity of the concrete section using ACI 349 [5] Eq. 11-3:

$\phi\tau n = 0.75 \times 2 \times \sqrt{fc} = 82$ psi

$\phi Vn = 82$ psi x 12 in. x 7.75 in. = 7,626 lb

By comparison with the demand shear diagrams, the shear capacity exceeds the demand shear. Therefore, the slab is acceptable for shear.

Bending Capacity of Columns

The columns are 21 in. diameter and contain 10 #5 rebar (0.625 in. diameter) with 1.5 in. clear cover. Axial and bending moment demands in the column from the finite element figures are:

Pu_column = 234,000 lb (compression)

Mu_column = 1.2×10^6 in.-lb

$\phi Pn = 0.7 \times 0.8\ (0.85 \times fc \times (Ag - As) + fy\ As)$

$= 0.7 \times 0.8\ (0.85 \times 3000\ (\pi\ 21^2/4 - 0.31 \times 10) + 40{,}000 \times (0.31 \times 10))$

= 559,616 lb

Bending capacity of the circular section without axial compression was calculated per [26]. Using Eq. 11 therein and employing Figure 9 therein:

C = cover = 1.5 in.

R = radius of section = 21 in./2

C/R = 0.14

Using the parameter ω defined following Eq. 7 in [26]:

$\omega = As\ fy / (\pi R^2\ fc) = (0.31\ \text{in.}^2 \times 10)\ 40{,}000 / (\pi\ (21\ \text{in.} / 2)^2\ 3{,}000) = 0.12$

From Figure 9 in the reference, the k factor can be taken as 1.0

$Mn = k\ As\ fy\ r = k\ (0.31\ \text{in.}^2 \times 10)\ 40{,}000\ \text{psi} \times 21\ \text{in.} / 2 = 1.3 \times 10^6$ in.-lb

$\phi Mn = 0.9 \times Mn = 1.172 \times 10^6$ in.-lb

Using linear axial compression/bending interaction:

$Pu/\phi Pn + Mu/\phi Mn = 1.44 > 1.0$ The columns are thus not acceptable.

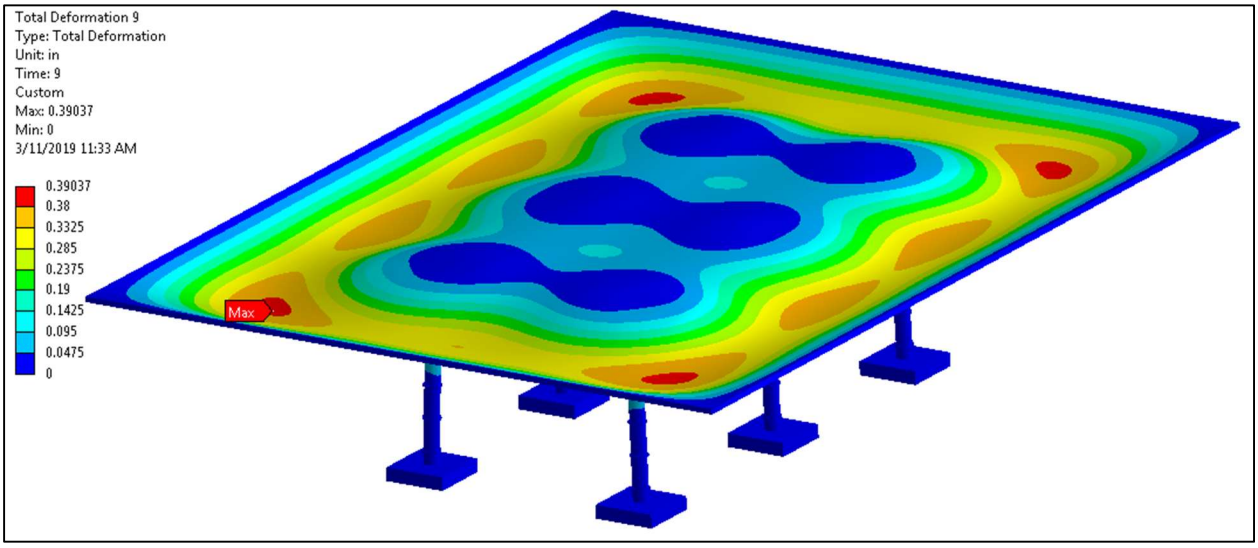

Figure 4.5-1: Contour Plots of Load Combination 1 Deformations (in.) for 216-Z-9

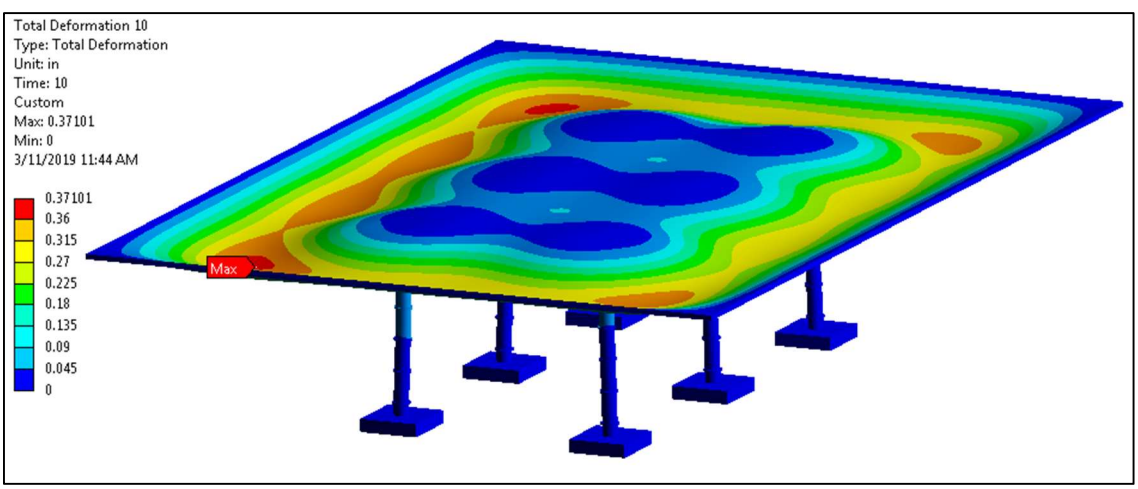

Figure 4.5-2: Contour Plots of Load Combination 2 Deformations (in.) for 216-Z-9

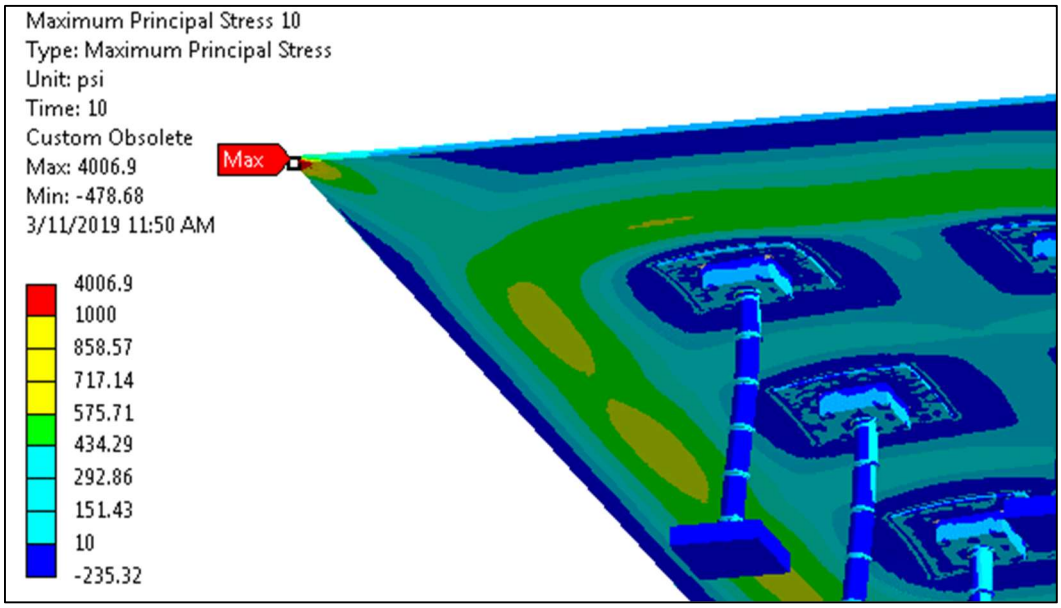

Figure 4.5-3: Contour Plots of Maximum Principal Stress (psi, max tension) for 216-Z-9

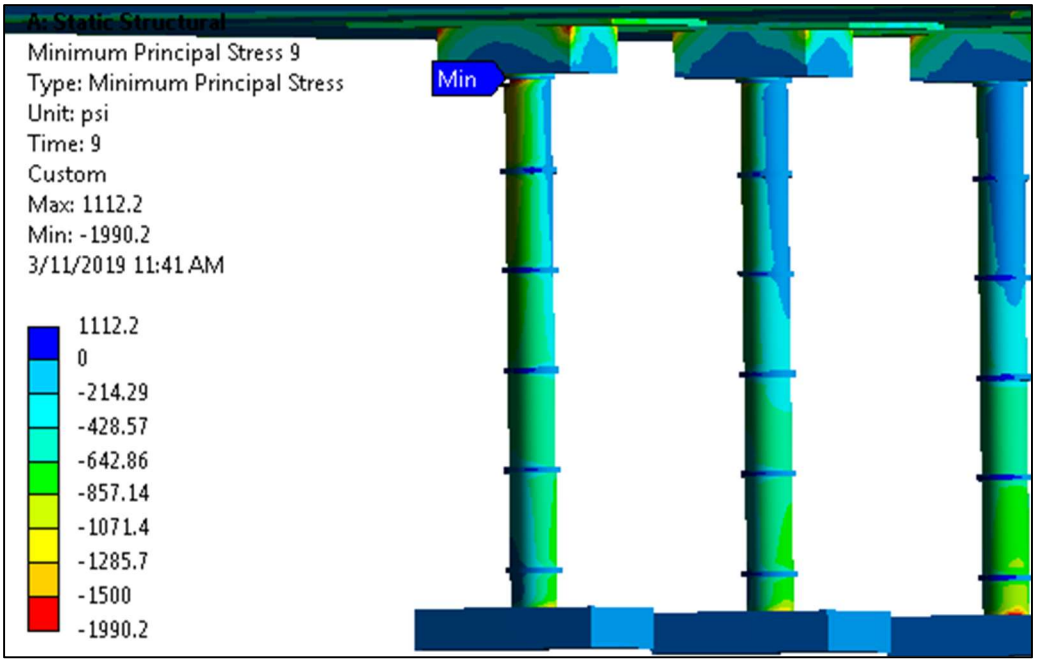

Figure 4.5-4: Contour Plots of Minimum Principal Stress (psi, max compression) for 216-Z-9

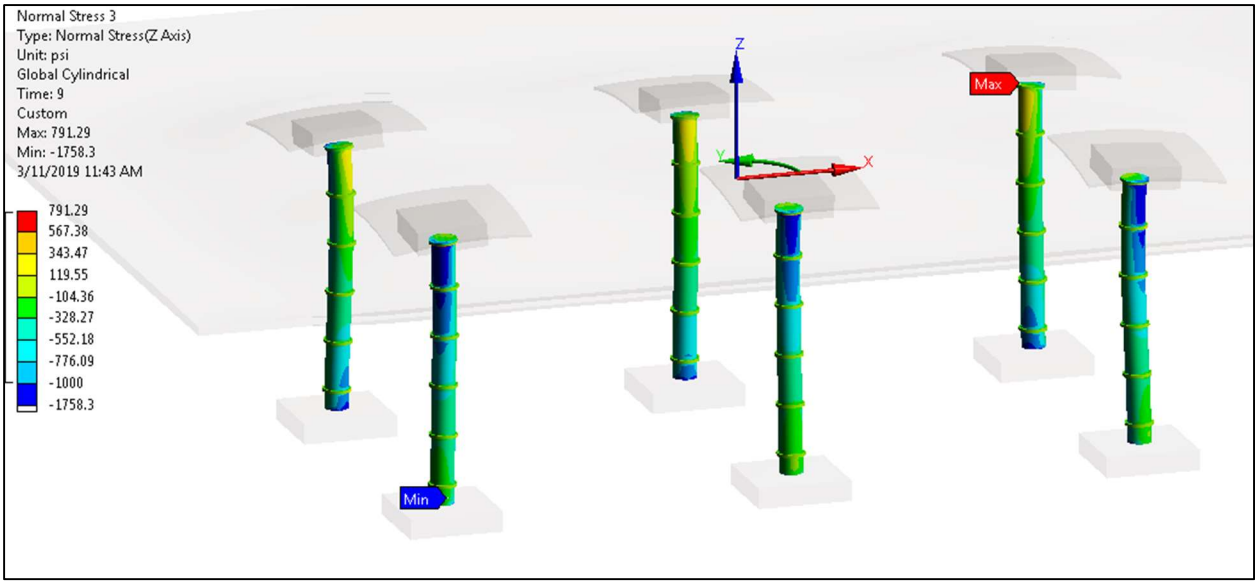

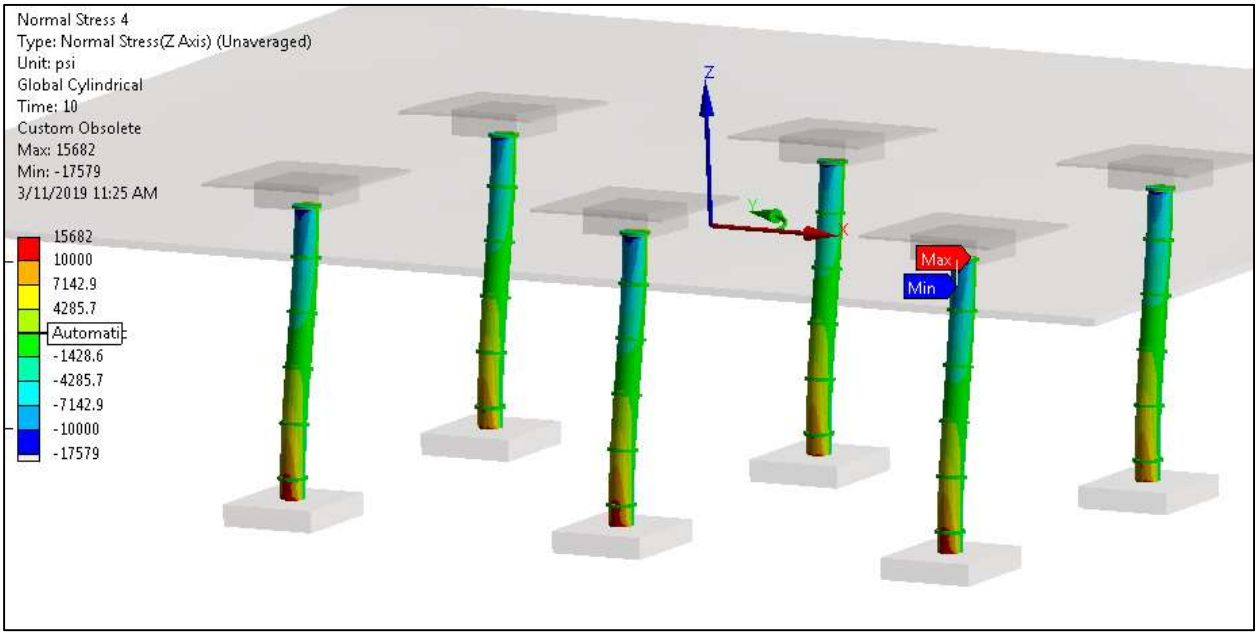

Figure 4.5-5: Contour Plots of Column Axial Stress (psi) for 216-Z-9 (Load combination 1 top and Load combination 2 bottom)

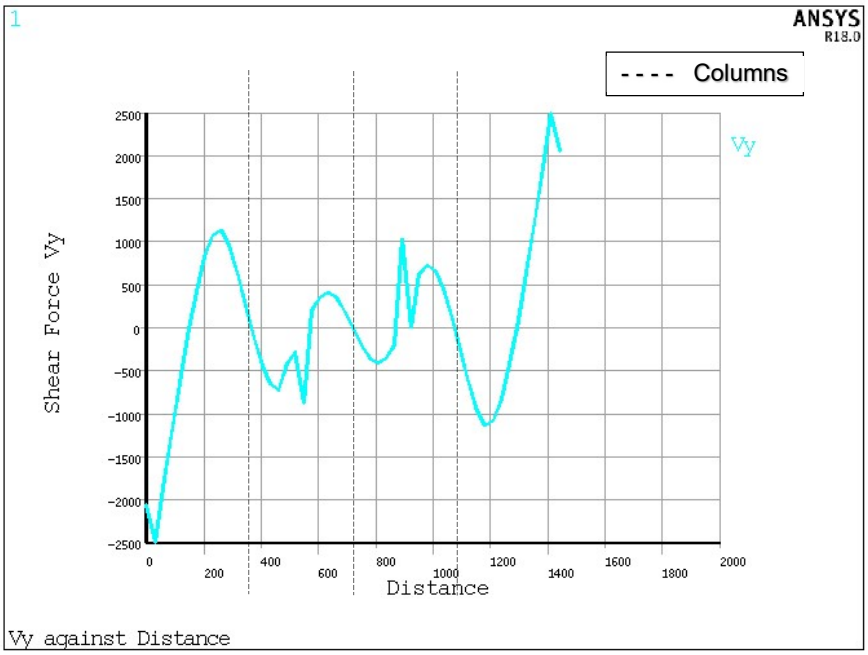

Figure 4.5-6: Graph of Integrated Roof Shear Force (lb) for 216-Z-9 - N/S Middle Strip

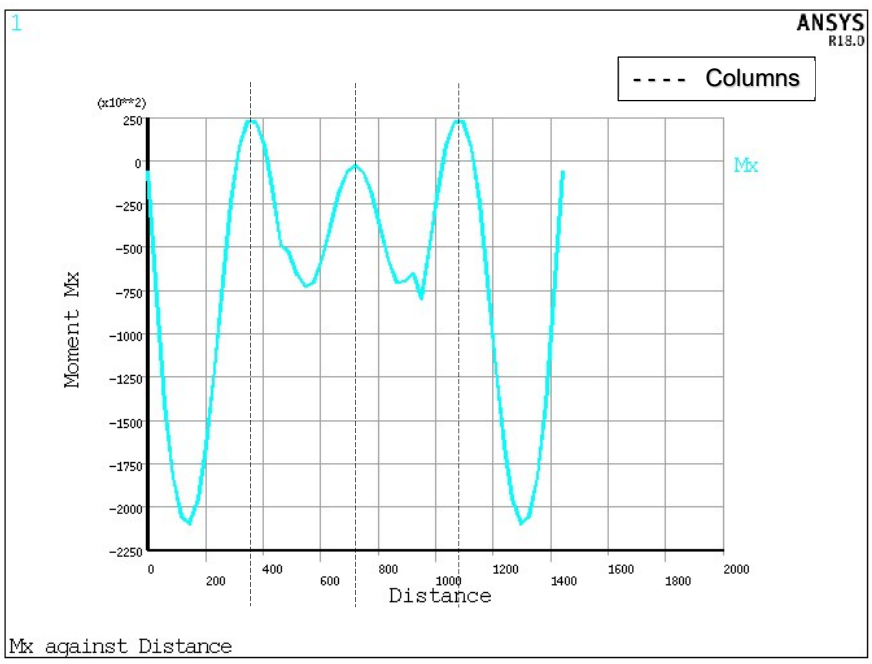

Figure 4.5-7: Graph of Integrated Roof Bending Moment (in.-lb) for 216-Z-9 – N/S Middle Strip

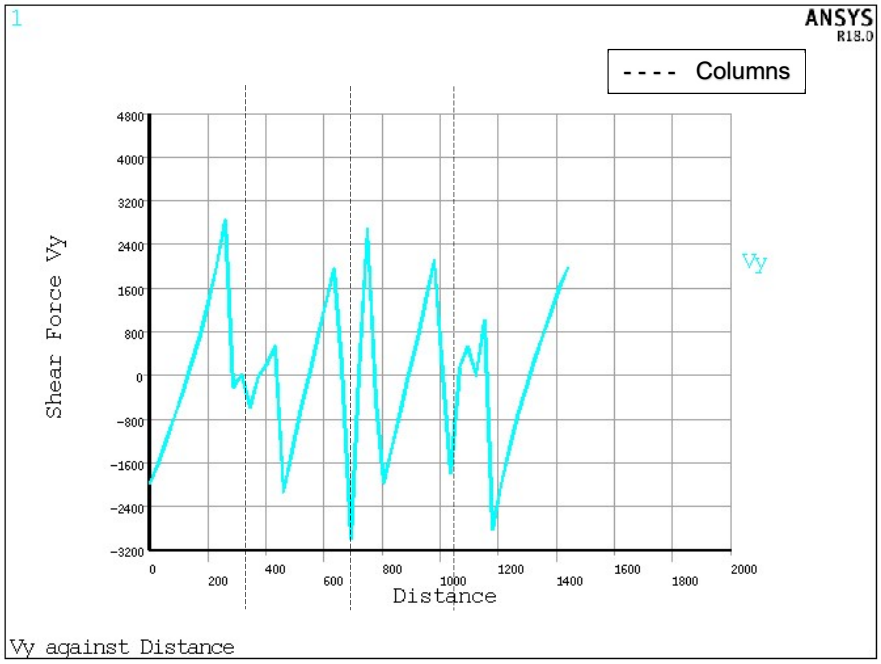

Figure 4.5-8: Graph of Integrated Roof Shear Force (lb) for 216-Z-9 - N/S Column Strip

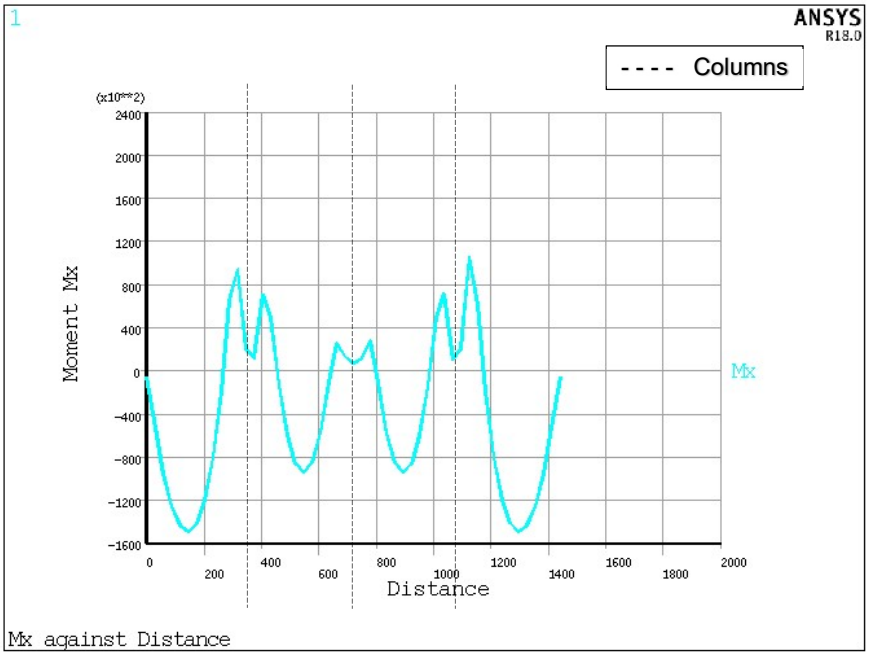

Figure 4.5-9: Graph of Integrated Roof Bending Moment (in.-lb) for 216-Z-9 – N/S Column Strip

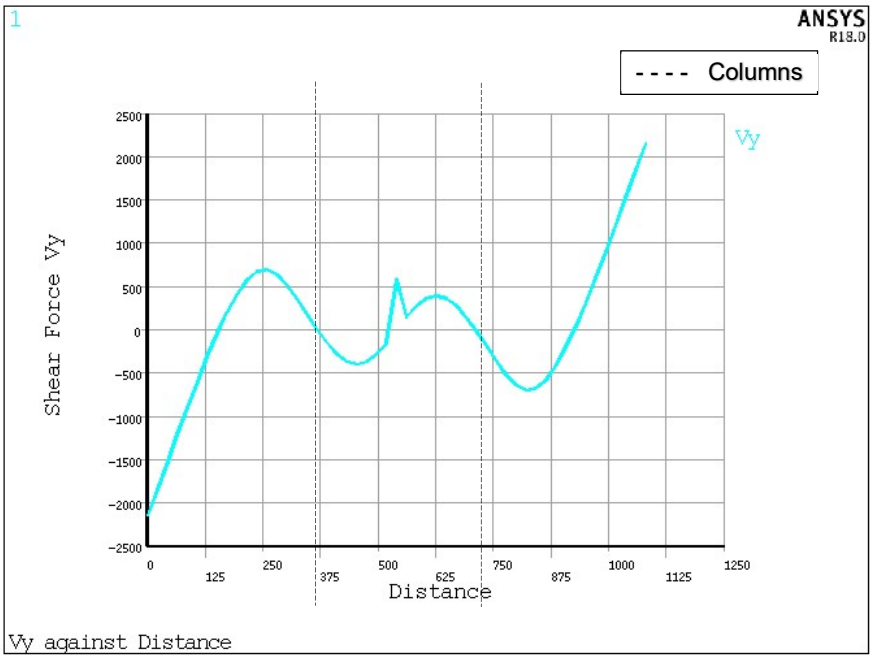

Figure 4.5-10: Graph of Integrated Roof Shear Force (lb) for 216-Z-9 – E/W Middle Strip

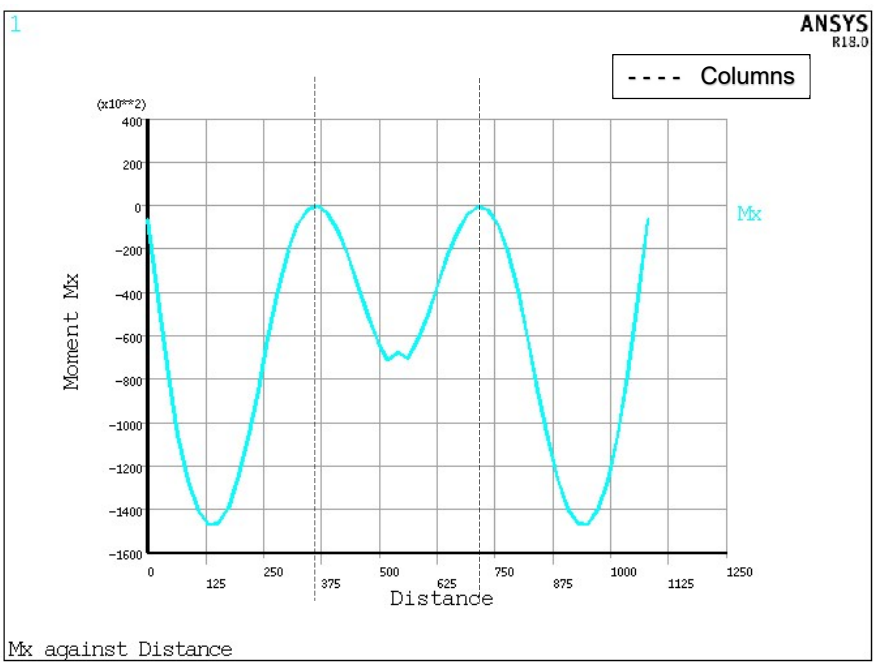

Figure 4.5-11: Graph of Integrated Roof Bending Moment (in.-lb) for 216-Z-9 – E/W Middle Strip

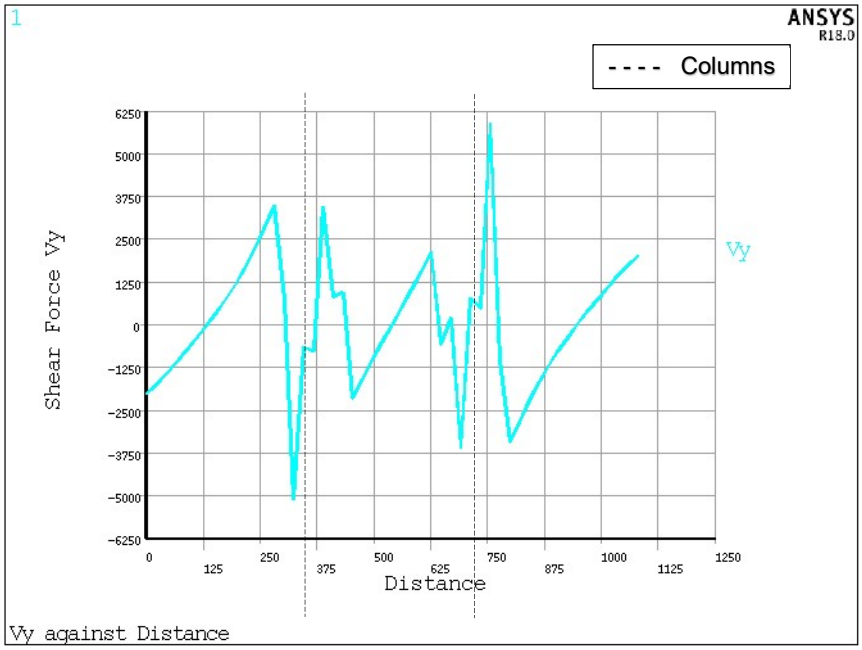

Figure 4.5-12: Graph of Integrated Roof Shear Force (lb) for 216-Z-9 – E/W Column Strip

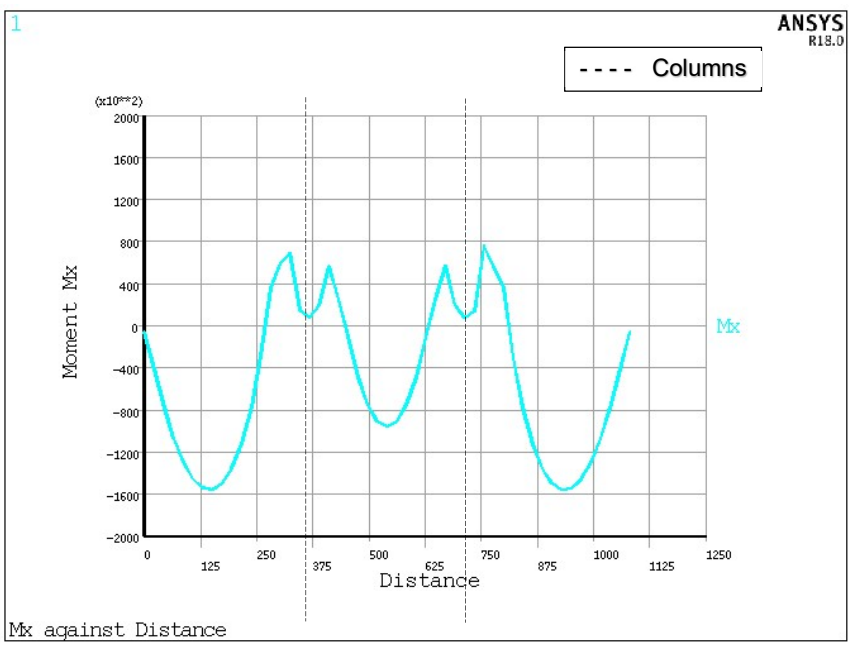

Figure 4.5-13: Graph of Integrated Roof Bending Moment (in.-lb) for 216-Z-9 – E/W Column Strip

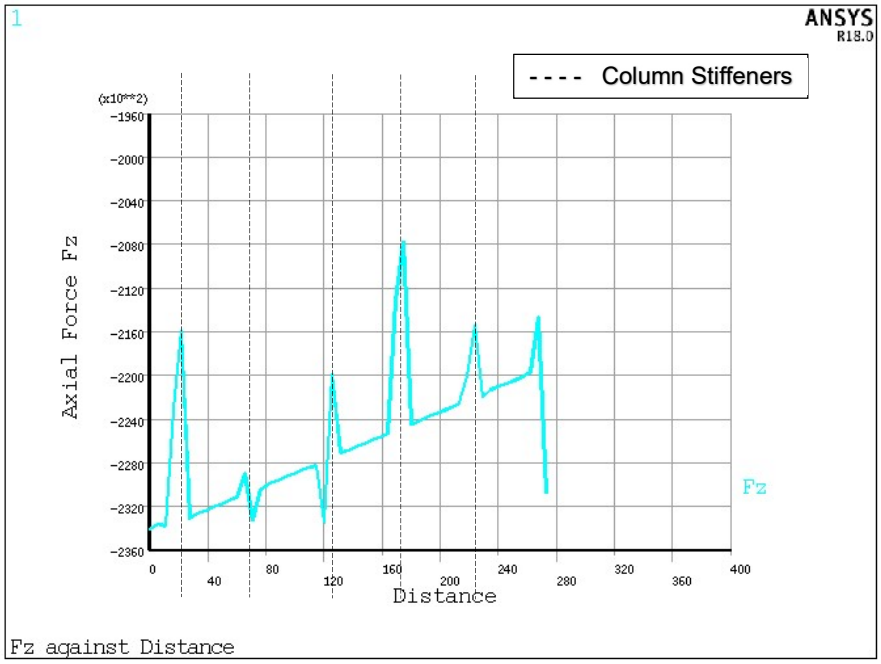

Figure 4.5-14: Graph of Integrated Column Axial Force (lb) for 216-Z-9

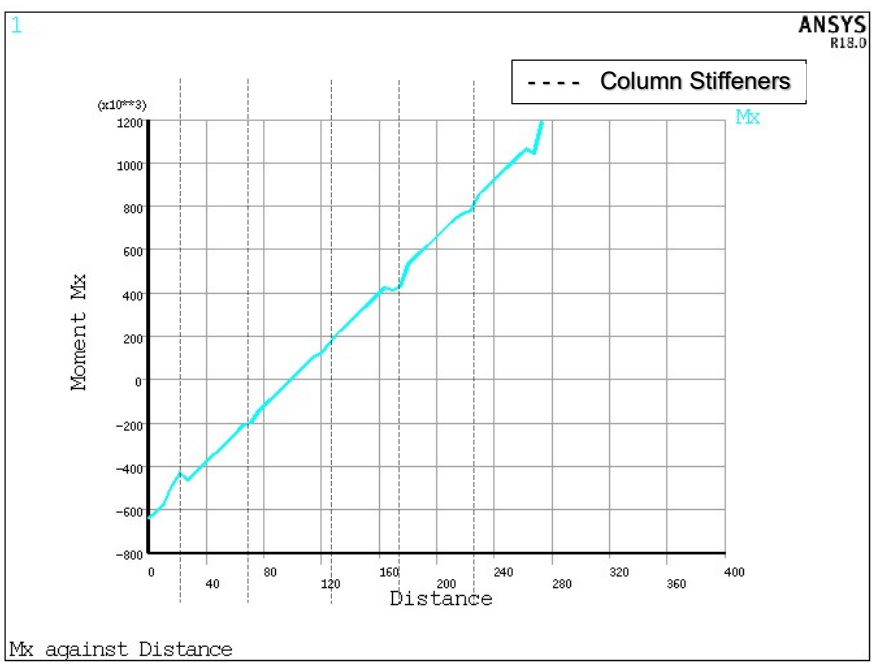

Figure 4.5-15: Graph of Integrated Bending Moment (in.-lb) for 216-Z-9

4.6 Structure 241-T-361, Group T1

Degradation was considered in the tank analysis by reducing the concrete thickness in the finite element modeling and concrete evaluation. Rebar area was also reduced by 10% in the concrete evaluation. Deformation contours for 241-T-361 are shown in Figure 4.6-1, with a maximum displacement of 0.034 in. at the center of the dome for load combination 1. Stress levels are controlled by load combination 1. Vertical axial wall stresses are shown in Figure 4.6-2. The maximum axial stress is 455 psi tension and -1007 psi compression. Maximum shear stress is 623 psi (Figure 4.1-3). Hoop stresses (Figure 4.6-4) indicate maximum hoop tension of 532 psi and maximum compression of -334 psi. Concrete section forces and moments were obtained by integration of stresses over a 12 in. wide strip (5.4 in. thick), which are shown in Figure 4.6-5 through Figure 4.6-7 for the wall and Figure 4.6-8 through Figure 4.6-10 for the roof. These results are summarized below.

	Wall	**Roof**
Bending Moment (in.-lb)	55,000	71,000
Axial Force (lb)	+4,800 / -9,000	+4,000 / -22,000
Shear Force (lb)	4,000	6,350

All results are based on analysis of concrete without application of prestressing. An average concrete stress was obtained by application of the above forces and moments on the 12 in. x 5.4 in. cross section, as follows:

Average axial stress = axial force / (5.4 in. x 12 in.) + moment / (12 in. x 5.4 in.^{2} / 6)

Average shear stress = shear force / (5.4 in. x 12 in.)

The resulting average stresses are as follows:

Average Stress Type	**Wall**	**Roof**
Axial (psi)	+1,017 / -1,082	+1,451 / -1,728
Shear (psi)	61	98

From the above, the axial force stresses in the roof are less than 20% of the combined axial and bending stresses. Therefore, the flexure margin was evaluated based on bending alone and interaction with axial was not considered. The evaluation was simplified by not considering prestressing forces and calculating capacity based on regular reinforcement.

Bending Moment Capacity

It was assumed that the reinforcement is No. 5 (rebar cross section area = 0.31 in.^{2}) every 6 in. on both faces, and that the rebar cover is 1 in. to center of rebar. Then, this reinforcement was verified to be below the balance reinforcement condition required to ensure that capacity is controlled by ductile yielding of the steel, and that it is above the minimum reinforcement area in ACI 318 as shown below.

fc = 3,000 psi

fy = 40,000 psi

b = 12 in. section width

d = 5.4 in. – 1 in. = 4.4 in. depth to center of tension rebar

Balance reinforcement ratio = ρ_b = 0.85 x β x fc x 87,000 / fy / (fy + 87,000) = 0.037 (see equation B-1 in ACI 318-08 which is derived based on Figure R10.3.3 therein where β=0.85 for 3,000 psi concrete)

As = 2 x 0.31 in.^{2} x 0.9 = 0.558 in.^{2} every 12 in.

ρ = As / b d = 0.558 / (12 x 4.4) ratio of steel area to concrete area, see notations in Chapter 2 of ACI 318-08.

= 0.011 < 0.75 ρ_b per ACI 318-08, R10.3.5

Thus, ductile failure is guaranteed. The minimum reinforcement areas of ACI 318-08, Section 10.5.1, are also met:

As_{min} = maximum (3$\sqrt{fc}$ /fy b d & 200 b d / fy)

= maximum (3 $\sqrt{3,000}$ / 40,000 x 4.4 in x 12 in., 200 x 4.4 in. x 12 in. / 40,000)

= 0.264 in.^{2}

Thus, the assumed reinforcement is within the ACI Code limits.

The bending moment capacity of the section is given by (not considering compression rebar):

ϕMn = 0.9 x As fy { d – As fy / (2 x 0.85 fc b) } See [25, page 12-6]

= 0.9 x 0.558 x 40,000 {4.4 – 0.558 x 40,000 / (2 x 0.85 x 3,000 x 12)}

= 81,061 in.-lb

This moment capacity exceeds the demand moments for the wall and roof.

Shear capacity

Reduced shear stress capacity of the concrete section using ACI equation 11-3:

$\phi\tau n = 0.75 \times 2 \times \sqrt{fc} = 82$ psi

For the roof section with maximum axial compression, Nu, of 22,000 lb using ACI Eq. 11-4:

$\phi\tau n = 0.75\ (1 + Nu / (2000 \times Ag))\ 2 \times \sqrt{fc}$

$= 0.75\ (1 + 22{,}000 / (2000 \times 12 \times 6))\ 2 \times \sqrt{3000} = 96$ psi

The shear stress capacity is approximately 2% below the demand value for the roof of 98 psi. This is a small difference and considering the Code reduction factor applied to the strength and the load increase factors applied in the load combinations, failure due to shear overstress is not considered likely. Thus, the maximum tabulated shear stresses are considered acceptable.

Prestressing and reinforcement information for this tank are not available, and the time of construction of the tank preceded the creation of the Prestressing Concrete Institute (PCI) and the development of recognized prestressing codes. However, the evaluation above is conservative by not considering prestressing forces.

Stability of the tank against buckling was verified by performing Eigen value buckling analysis. The buckling analysis determines the load multiplier at which buckling instability would occur. The calculated first buckling mode is shown in Figure 4.6-11. The lowest buckling load multiplier is 205, that is, the postulated combined loads are less than 200th of the critical buckling load. Therefore, there is significant margin for stability.

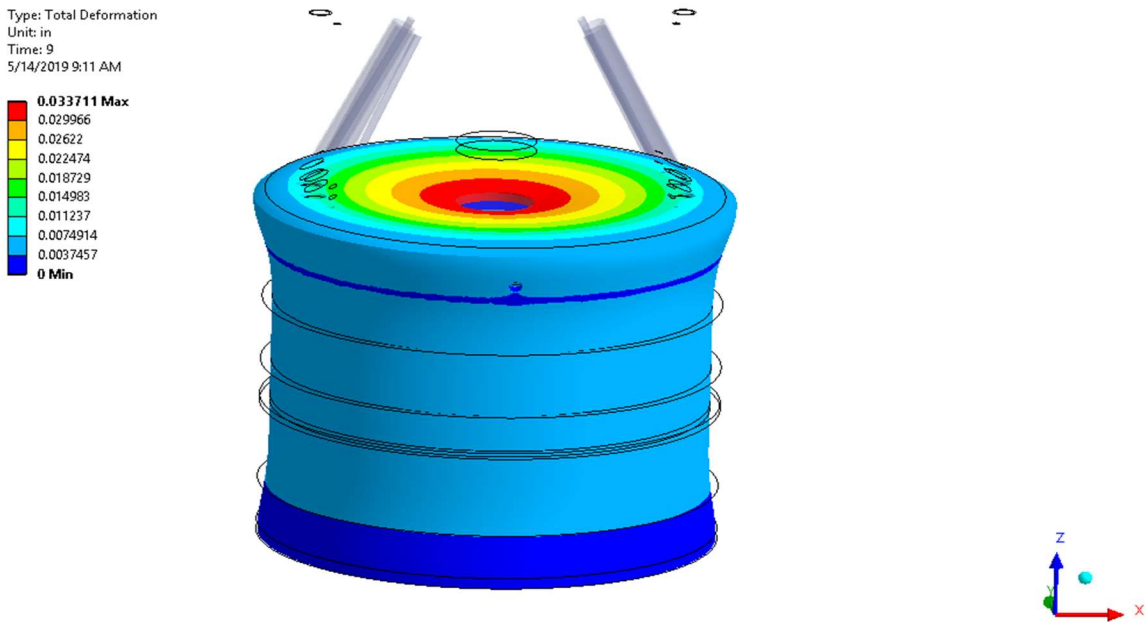

Figure 4.6-1: Contour Plot of Deformations (in.) for 241-T-361

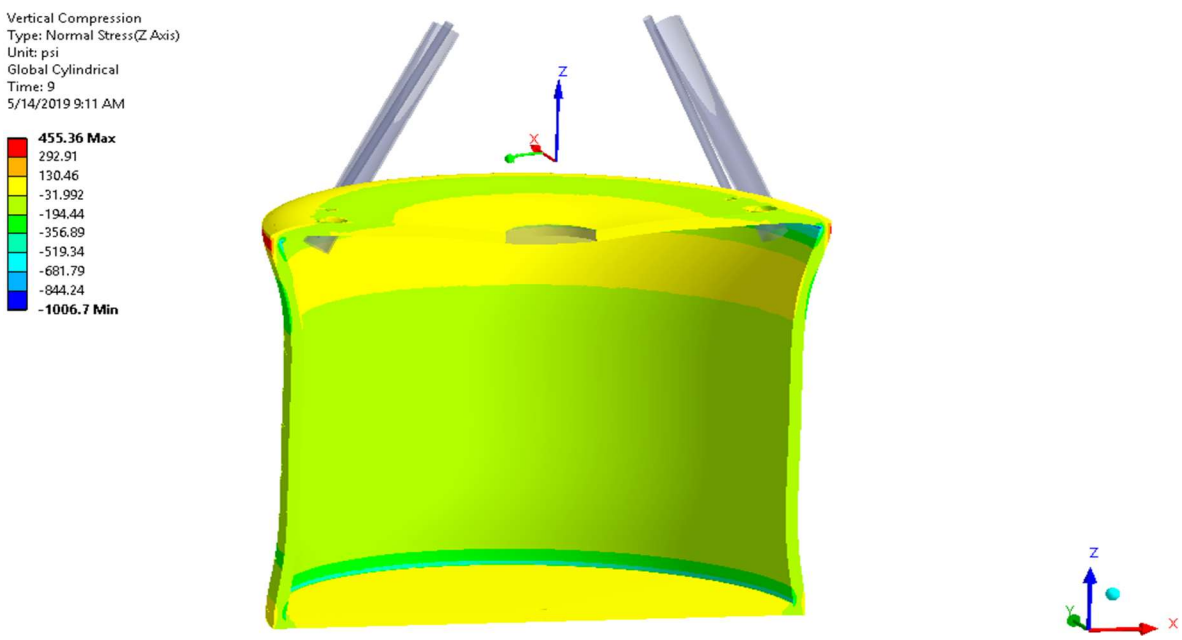

Figure 4.6-2: Contour Plot of Vertical Axial Stress (psi) for 241-T-361 – Sectional View

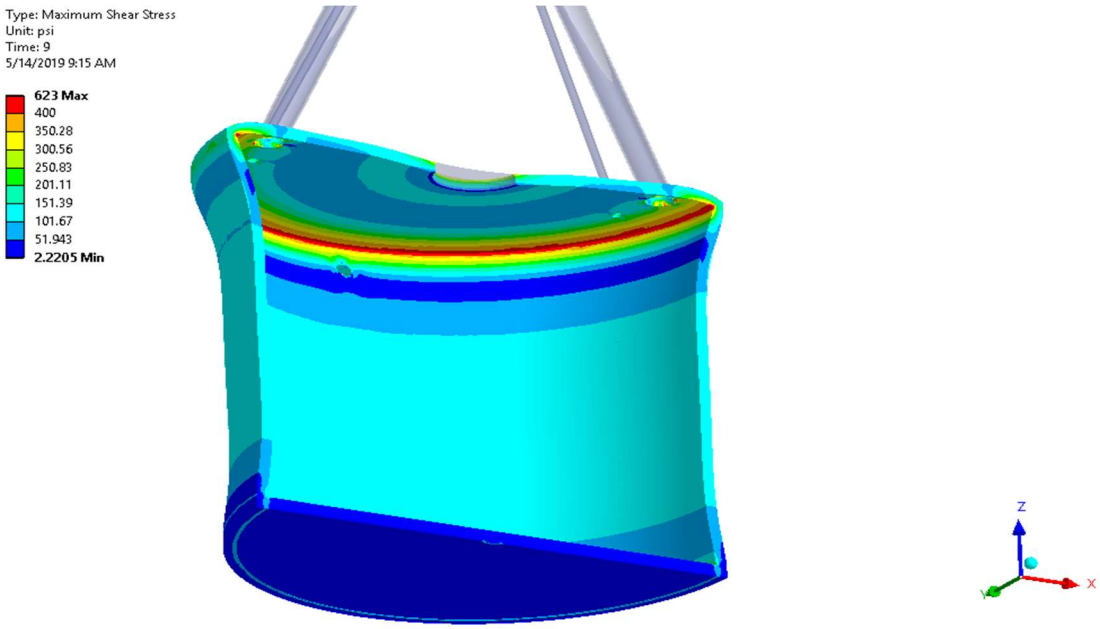

Figure 4.6-3: Contour Plot of Maximum Shear Stress (psi) for 241-T-361 – Sectional View

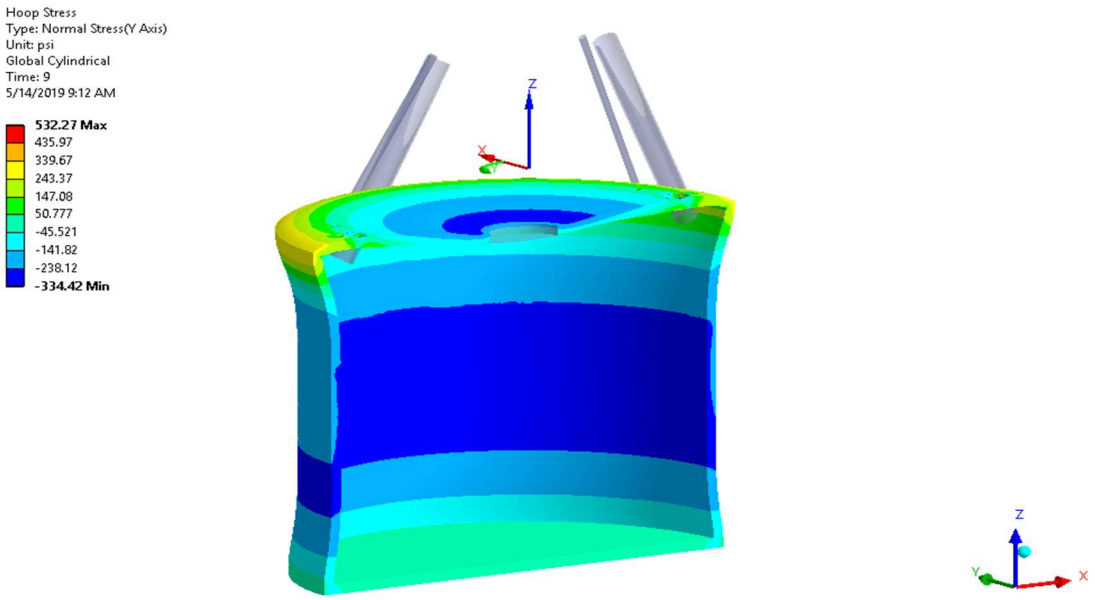

Figure 4.6-4: Contour Plot of Hoop Stress (psi) for 241-T-361 – Sectional View

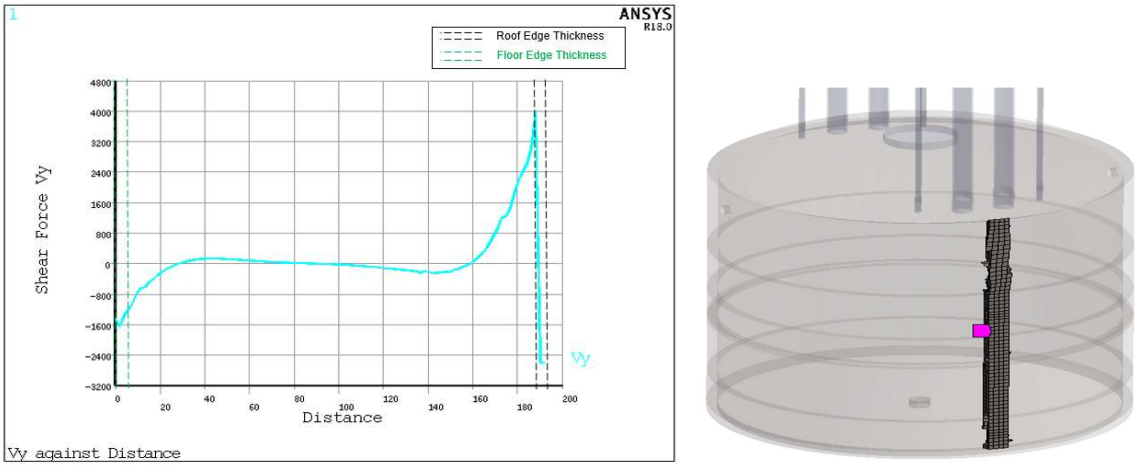

Figure 4.6-5: Graph of Integrated Wall Radial Shear Force (lb) for 241-T-361

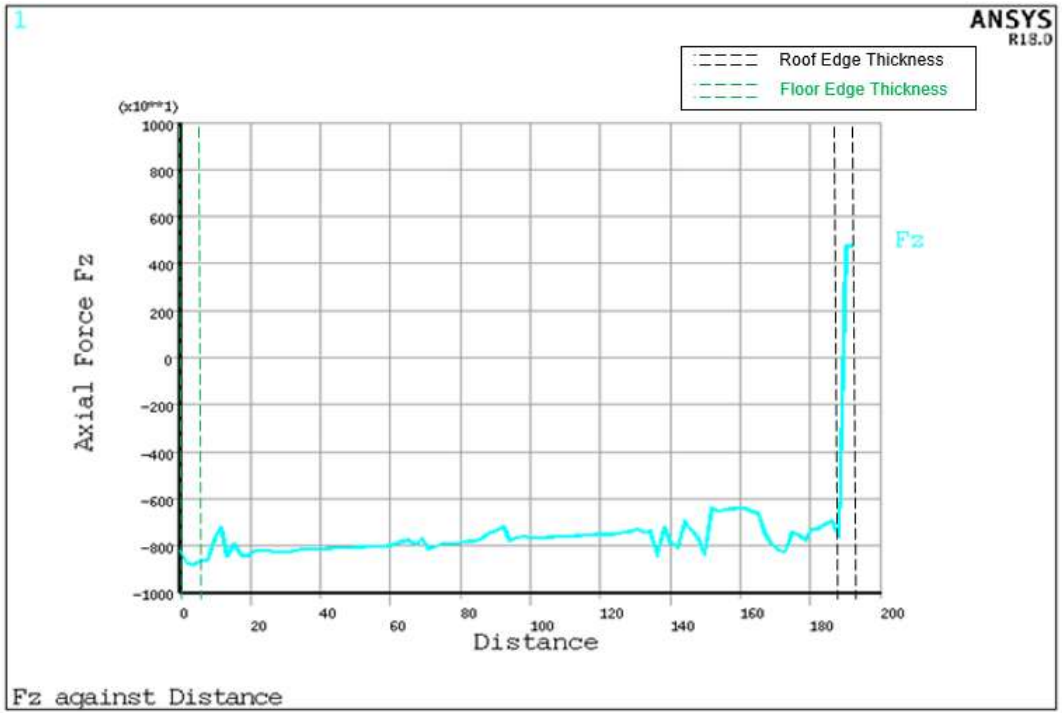

Figure 4.6-6: Graph of Integrated Wall Vertical Force (lb) for 241-T-361

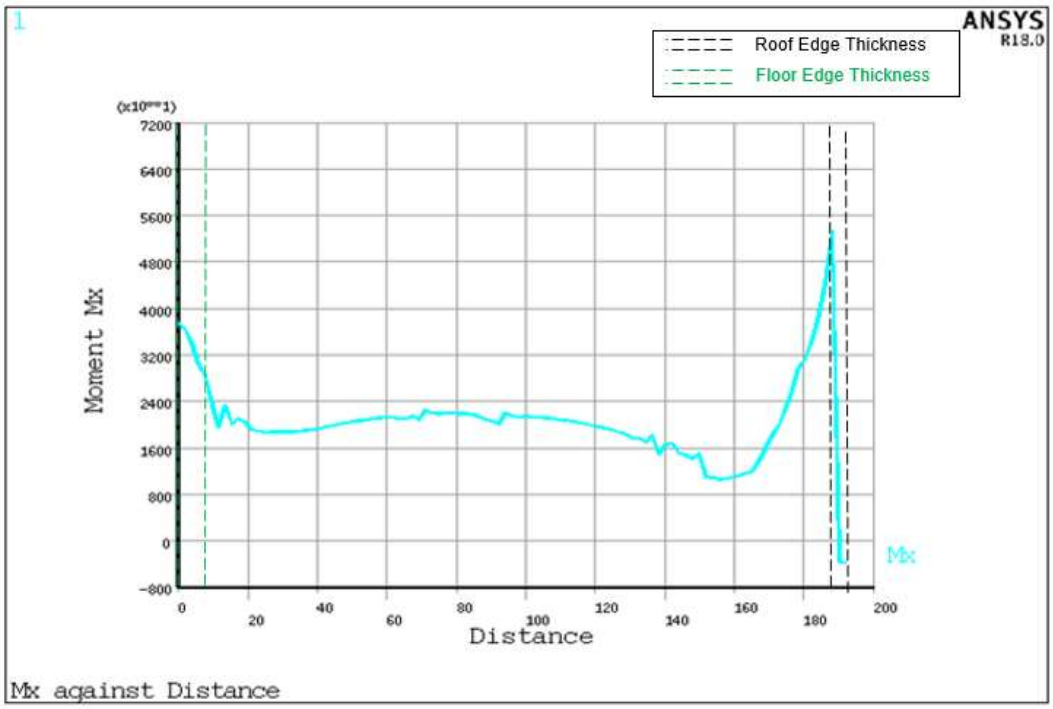

Figure 4.6-7: Graph of Integrated Wall Bending Moment (in.-lb) for 241-T-361

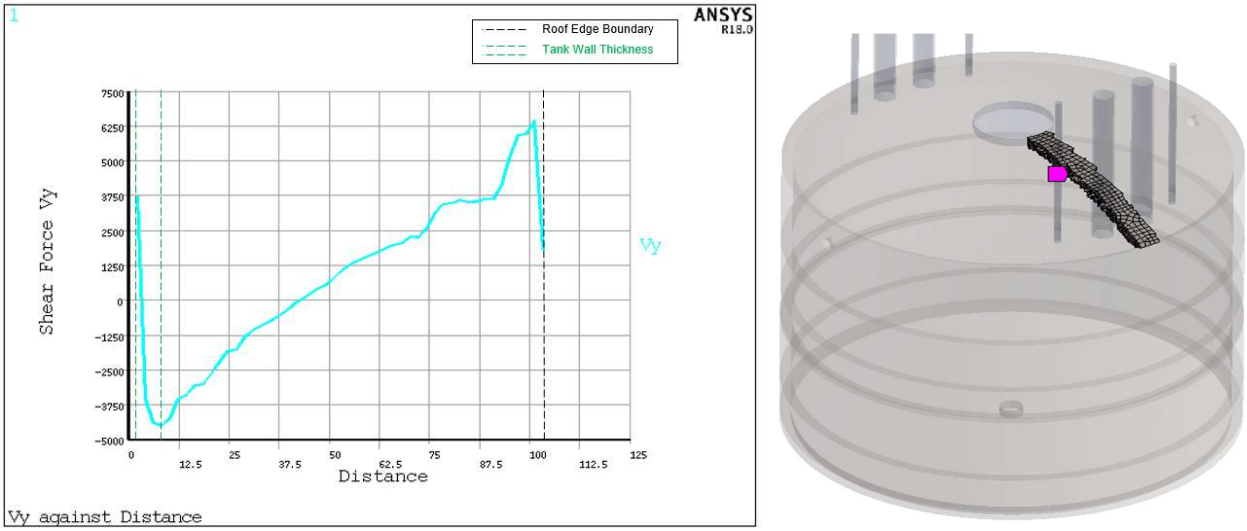

Figure 4.6-8: Graph of Integrated Roof Shear Force (lb) for 241-T-361

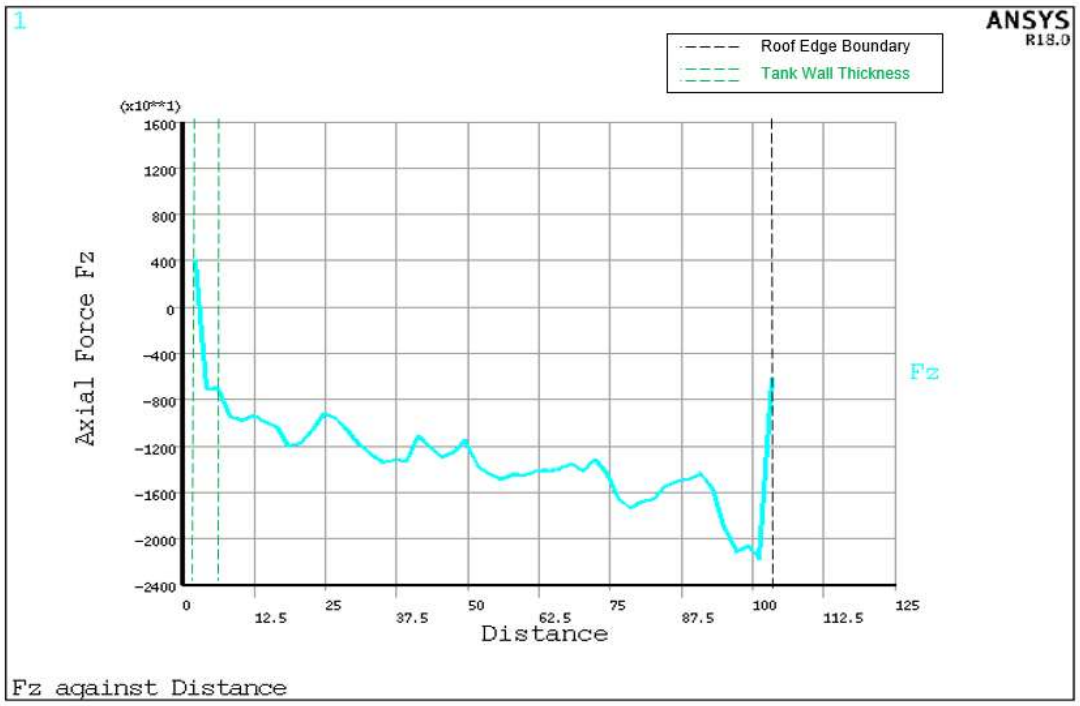

Figure 4.6-9: Graph of Integrated Roof Axial Force (lb) for 241-T-361

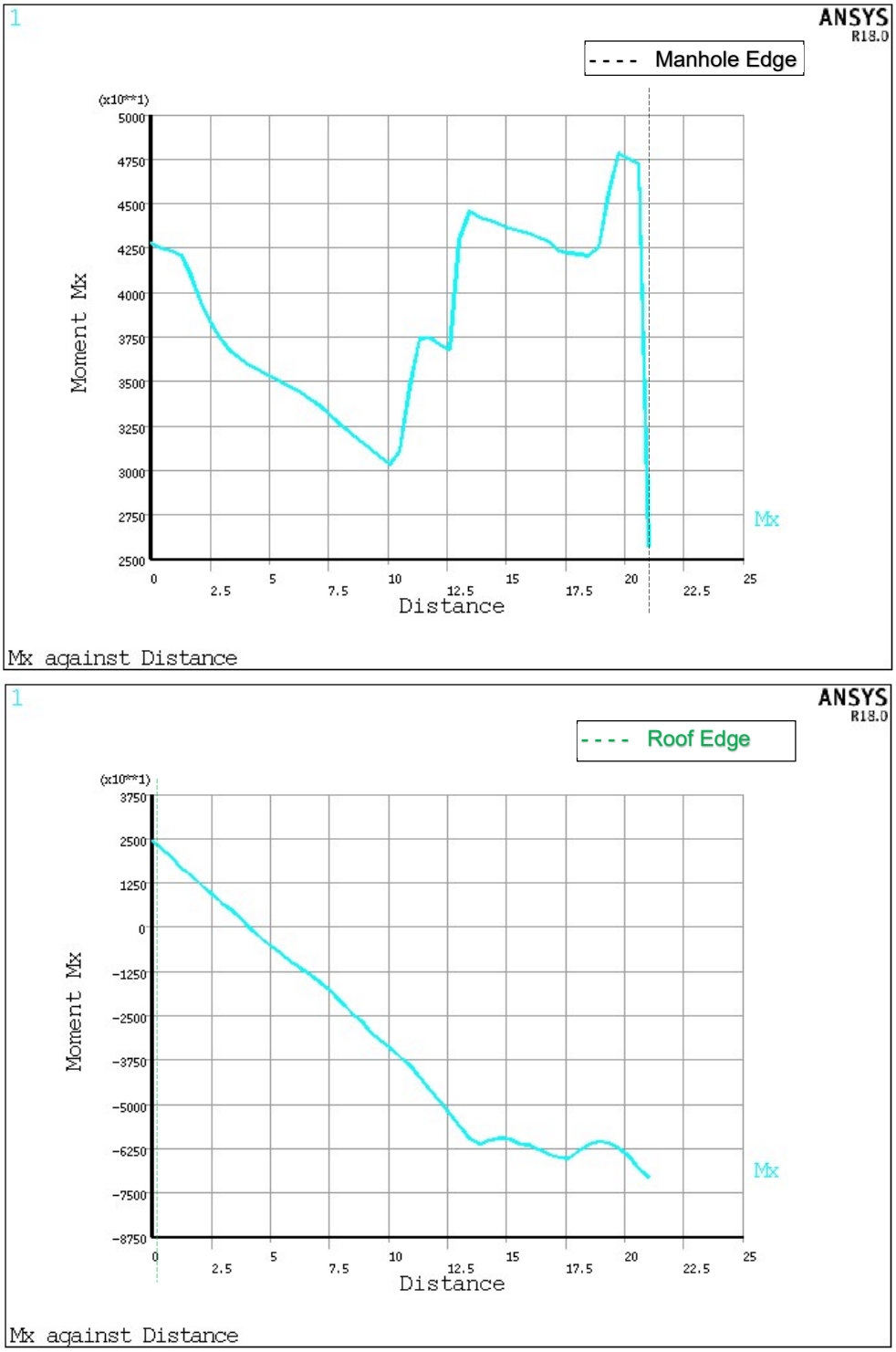

Figure 4.6-10: Graph of Integrated Roof Bending Moment (in.-lb) for 241-T-361
(top graph at center of roof, bottom graph at edge of roof)

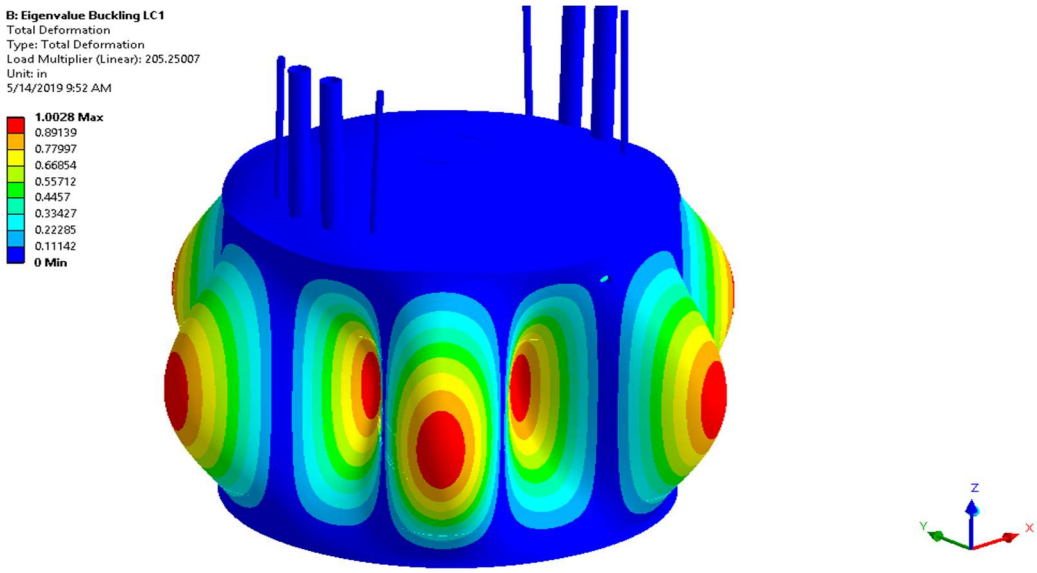

Figure 4.6-11: Contour Plot of Normalized Deformations (in.) at First Buckling Mode for 241-T-361

4.7 Structure 241-Z-361, Group T2

Deformation contours for 241-Z-361 are shown in Figure 4.7-1 with a maximum displacement of 0.085 in. near the geometric center of the long (vertical) walls of the tank for load combination 1 (the controlling load combination). Vertical axial wall stresses are shown in Figure 4.7-2. The maximum axial stress is 1,159 psi tension and -1863 psi compression. Both extreme values occur on the lower end of the long wall. Integration of the wall stresses gives section shear forces, axial forces, and bending moments, which are shown in Figure 4.7-3 through Figure 4.7-5 for a 12 in. wide wall strip and in Figure 4.7-6 through Figure 4.7-8 for a 14 in. wide roof strip.

	Wall (12 in. wide)	**Roof (14 in. wide)**
Bending Moment (in.-lb)	450,000 Figure 4.7-5 near zero distance	200,000 Figure 4.7-8 near zero distance
Axial Force (lb)	+10,000 / -12,000 Figure 4.7-4 near zero distance for negative value and near 214 in. distance for positive value	-9,750 Figure 4.7-7 near 25 in. distance
Shear Force (lb)	14,000 Figure 4.7-3: Graph of Integrated Long Wall Shear Force (lb) for 241-Z-361 near zero distance	4,800 Figure 4.7-6 near zero distance

An average concrete stress was obtained by application of the above forces and moments on the 12 in. (14 in. for the roof) x 11 in. deep cross section as follows:

Average axial stress = axial force / (12 in. x 11 in.) + moment / (12 in. x 11 in.^{2} / 6)

Average shear stress = shear force / (12 in. x 11 in.)

The resulting average stresses are given below.

Average Stress Type	Wall (12 in. wide)	Roof (14 in. wide)
Axial (psi)	+1,935 / -1,950	+645 / -772
Shear (psi)	106	31

The wall strip was evaluated since the tabulated results above indicate it is more limiting than the roof. Bending capacity of the roof strip is also calculated for reference.

The cross section of wall is 11 in.[12] deep and the main vertical rebar are No. 8 every 12 in. on both faces per the design drawings. It was assumed that the concrete cover is 2.0 in. based on ACI 318-08, Section 7.7.1 (assuming external concrete surfaces are protected from soil) and assuming the cover is similar to that on the outside face of the short walls as shown on the design drawings. The following concrete section capacity for the wall was obtained:

As = 0.79 in.^{2} x 0.8 — cross sectional area of 1-in. rebar reduced by 20% to account for rebar corrosion and strength reduction due to concrete cracking in the roof

As' = As — Similar reinforcement on both sides

d = 11 in. – 2.0 in. = 9.0 in. — tensile rebar depth

b = 12 in. — web width

fc = 3,000 psi — compressive strength of concrete

fy = 40,000 psi — yield strength of reinforcing steel

Axial compression capacity with no bending (using strength reduction factor (ϕ) of 0.7 per ACI 349-08, Section 9.3.2.2):

<u>Wall axial compression capacity (ACI 349 equation 10-1)</u>

$$\phi Pn = 0.7 \times 0.80 \{0.85 \times fc (A_{cross} - As - As') + fy (As + As')\}$$

$$= 0.7 \times 0.80 \{0.85 \times 3{,}000 (11 \times 12 - 0.79 \times 0.8 - 0.79 \times 0.8) + 40{,}000 (0.79 \times 0.8 + 0.79 \times 0.8)\}$$

$$= 215{,}005 \text{ lb}$$

[12] The reduction of wall thickness is from the inside face due to presence of waste material.

Wall bending moment capacity

ϕMn = 0.9 x As fy { d – As fy / (2 x 0.85 fc b) } see [25] page 12-6

= 0.9 x 0.79 x 0.8 x 40,000 {9.0 – 0.79x0.8 x 40,000 / (2 x 0.85 x 3,000 x 12)}

= 195,370 in.-lb

The above moment capacity is less than the demand moment and therefore the section is not adequate for bending.

The contribution of the compression rebar to pure bending is small and not considered.

Shear capacity

Reduced shear stress capacity of the concrete section using ACI Eq. 11-3:

$\phi\tau n = 0.75 \times 2 \times \sqrt{fc} = 82$ psi

With maximum compression of 12,000 lb using ACI Eq. 11-4:

$\phi\tau n = 0.75\ (1 + Nu / (2000 \times Ag))\ 2 \times \sqrt{fc}$

$= 0.75\ (1 + 12{,}000 / (2000 \times 12 \times 11))\ 2 \times \sqrt{3000} = 86$ psi

This shear stress limit is less than the demand stress and, as such, the wall section is not adequate for shear.

By comparison, the calculated pure bending capacity is significantly less than the demand bending moment. This indicates potential local bending failure at the bottom of the long wall. However, this failure is likely limited in extent since the contour plots indicate the high stresses to be confined to about the middle third of the wall. This failure will also relax the rigidity of the wall boundary condition at the bottom and increase the stresses near the middle of the height. Additional analysis should be performed to determine if progressive failure would occur at that location.

The design parameters for the roof slab are as follows:

As = 0.79 in.^{2} x 0.8	cross sectional area of 1-in. rebar reduced by 20% to account for rebar corrosion and strength reduction due to concrete cracking in the roof
As' = As	Similar reinforcement on both sides

d = 12 in. – 1.0 in. = 11.0 in.	tensile rebar depth (concrete cover is shown in the drawing to be 3/4 in. The loss of 1 in. of roof concrete on the inside face effectively remove the cover and is assumed not to affect contribution of the rebar in the strength.
b = 14 in.	roof strip width

Roof bending moment capacity

The roof section is 14 in. wide by 11 in. deep. The main reinforcement is at the bottom face in the short direction of the roof. The design drawing shows variations in the size of those main rebar with 1 in. every 12 in. being the lower bound.

ϕMn = 0.9 x As fy { d – As fy / (2 x 0.85 fc b) } see [25] page 12-6

= 0.9 x 0.79 x 0.8 x 40,000 {11.0 – 0.79x0.8 x 40,000 / (2 x 0.85 x 3,000 x 14)}

= 242,216 in.-lb

This calculated bending capacity for the roof slab envelops the demand of 200,000 in.-lb calculated by the finite element analysis.

The demand shear stress in the roof of 31 ksi is also well within the design shear of 82 ksi calculated above. Thus, the roof slab is adequate for bending and shear stresses.

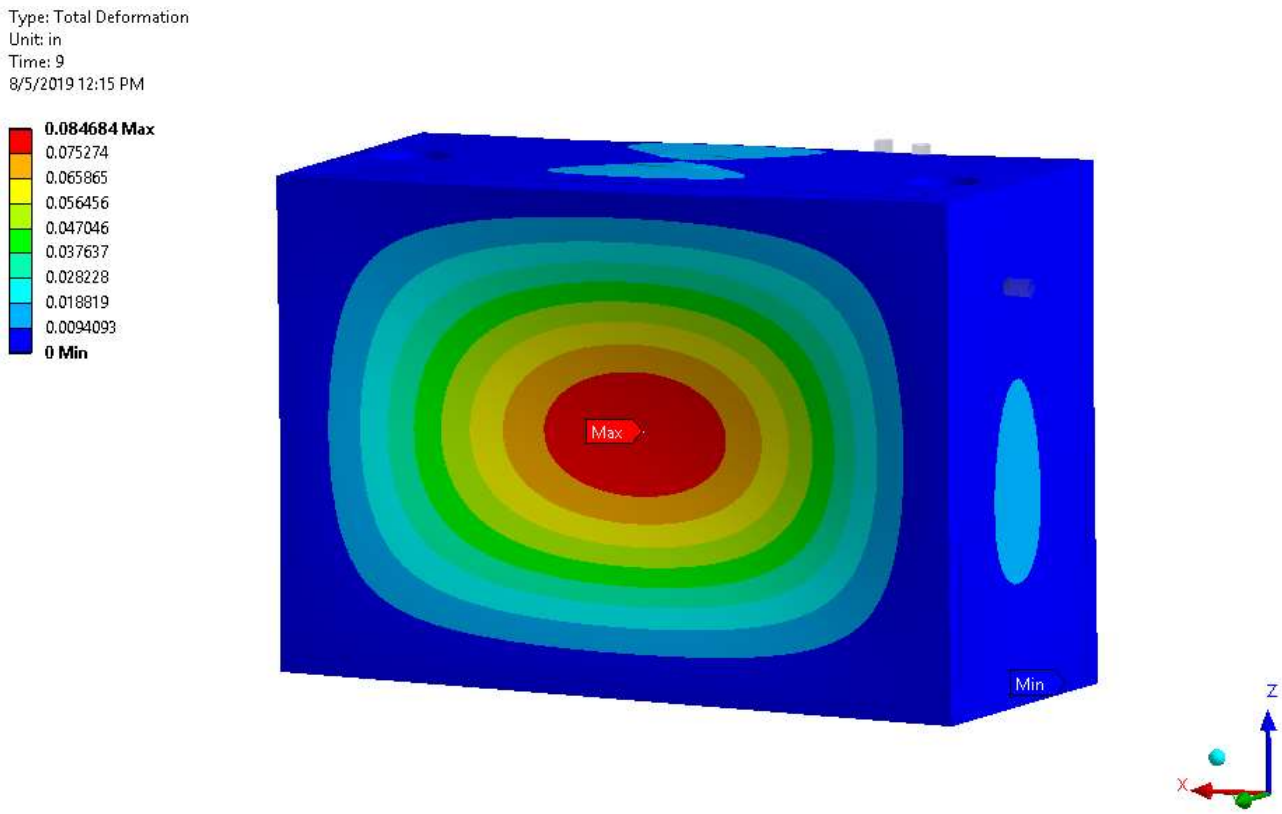

Figure 4.7-1: Contour Plots of Deformations (in.) for 241-Z-361

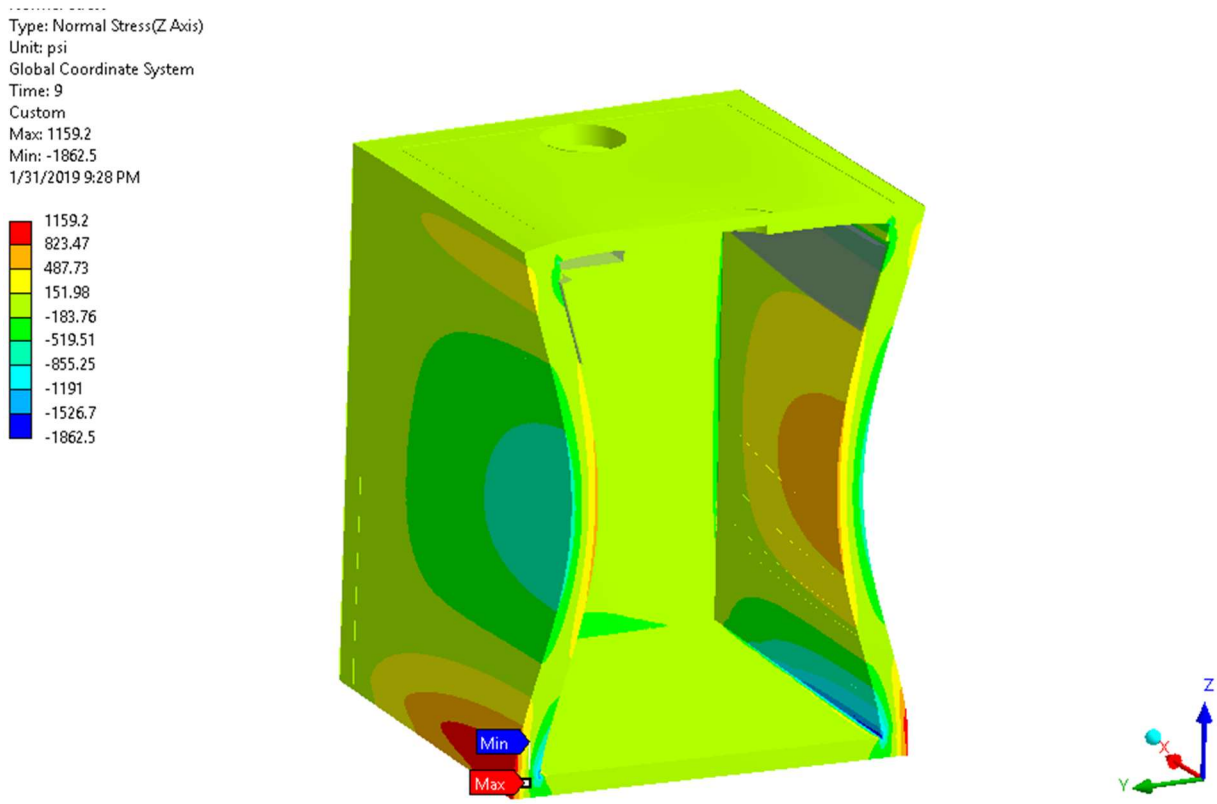

Figure 4.7-2: Contour Plots of Vertical Axial Stress (psi) for 241-Z-361 – Sectional View

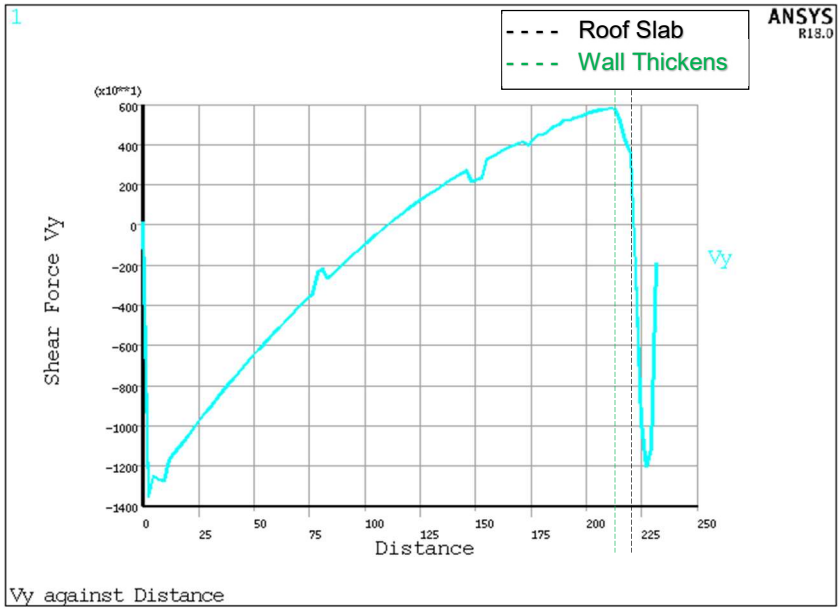

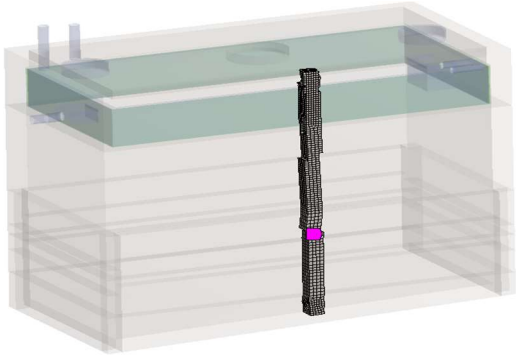

Figure 4.7-3: Graph of Integrated Long Wall Shear Force (lb) for 241-Z-361

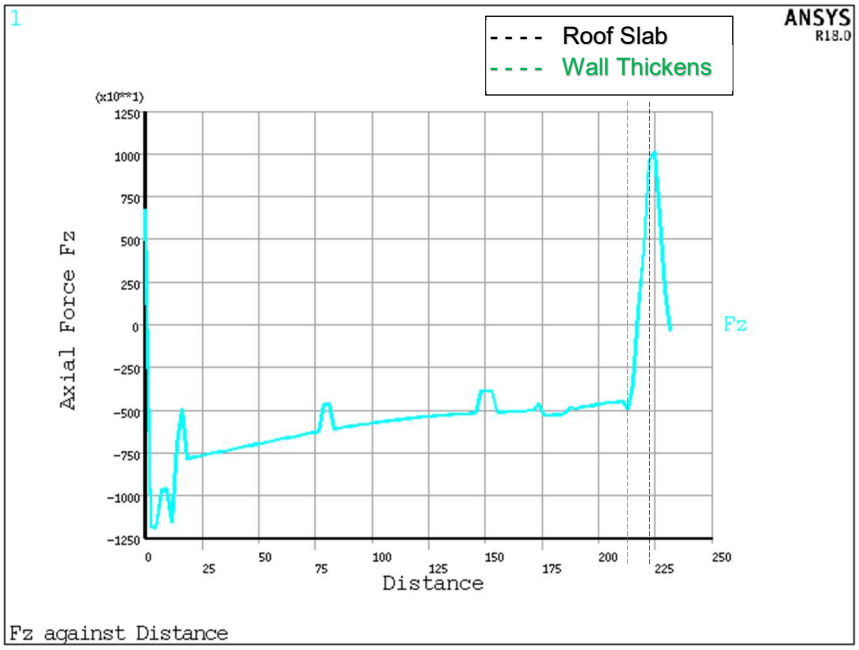

Figure 4.7-4: Graph of Integrated Long Wall Axial Force (lb) for 241-Z-361

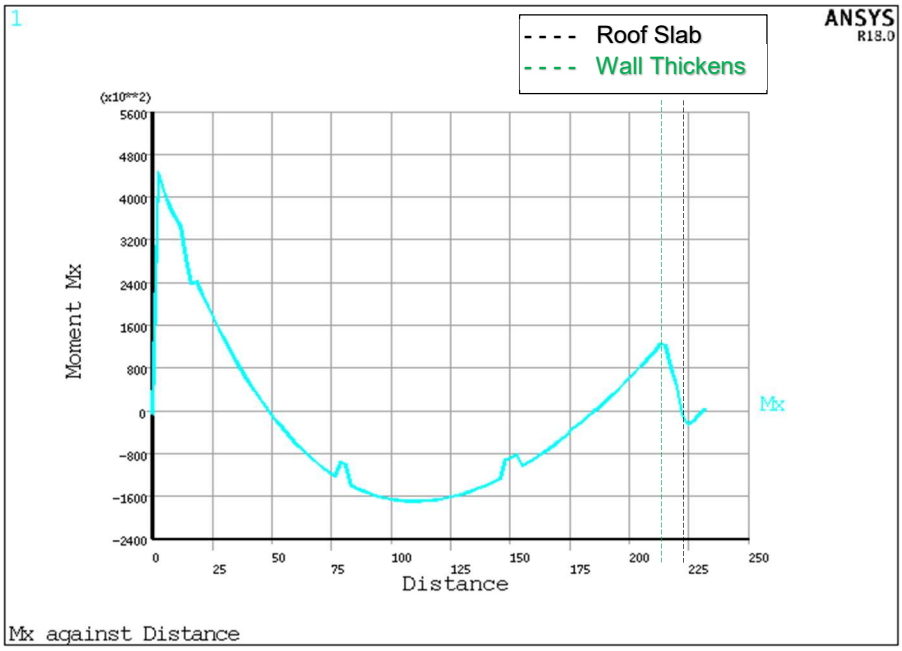

Figure 4.7-5: Graph of Integrated Long Wall Bending Moment (in.-lb) for 241-Z-361

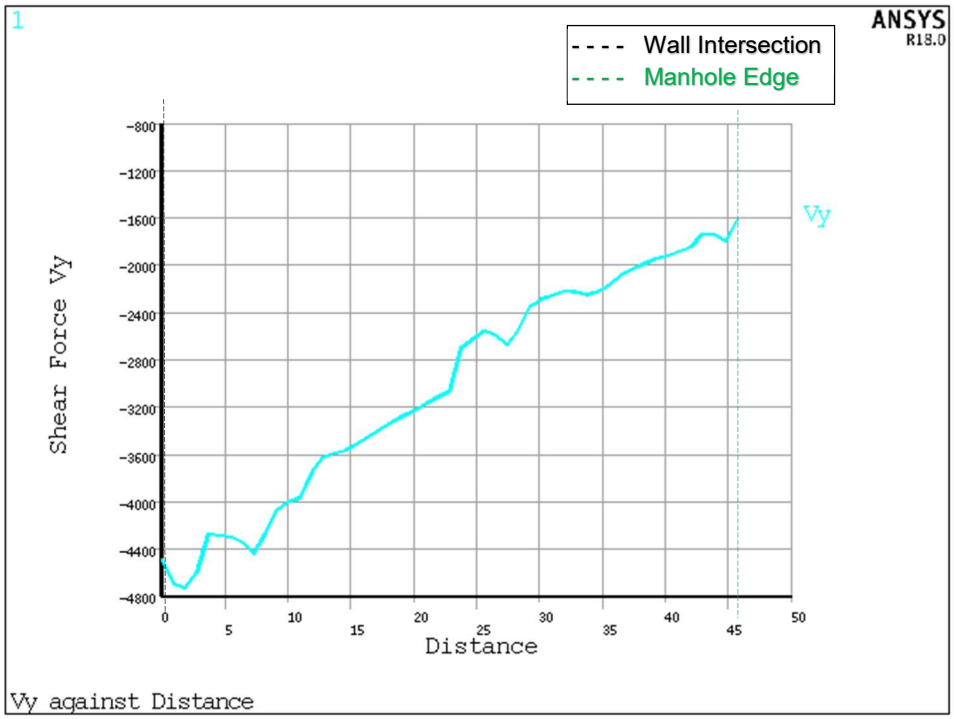

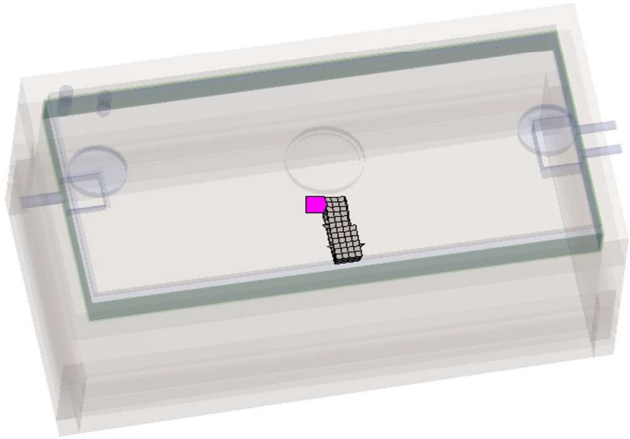

Figure 4.7-6: Graph of Integrated Roof Shear Force (lb) for 241-Z-361

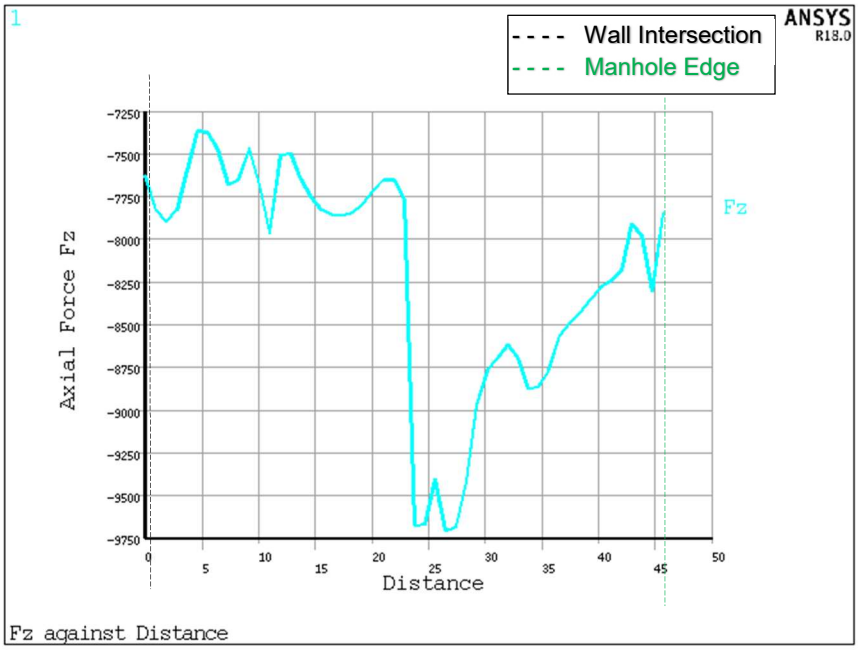

Figure 4.7-7: Graph of Integrated Roof Axial Force (lb) for 241-Z-361

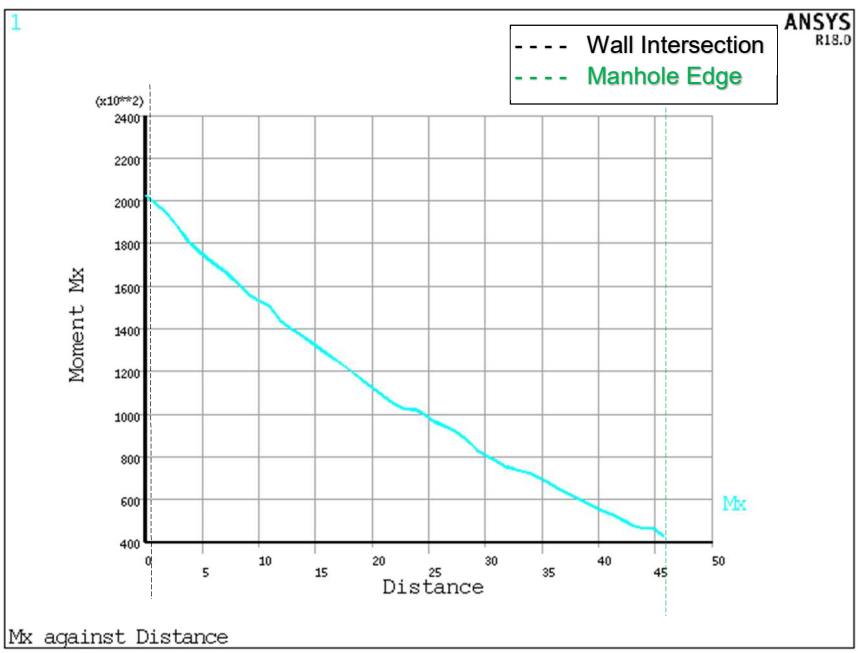

Figure 4.7-8: Graph of Integrated Roof Bending Moment (in.-lb) for 241-Z-361

4.8 Structure 241-Z-8, Group T3

The tank 241-Z-8 drawing specifies the tank material as steel or wrought iron. Accordingly, a lower bound tank yield strength of 24 ksi was conservatively used in the evaluation.

Deformation contours are shown in Figure 4.8-1, with a maximum displacement of 1.04 in. at the center. Hoop stresses are shown in Figure 4.8-2. To obtain the general hoop stress, local peak stresses that are attributed to the assumed boundary conditions or geometric discontinuity were excluded. A maximum hoop stress of 24 ksi is representative and is dominated by bending based on the wave form of the hoop stress around the circumference. Shear stresses are included in Figure 4.8-3. Maximum shear stress was taken as 18 ksi. Since the waste level in the tank is negligible, the Specification for Structural Steel Buildings [6] provides strength-based stress limits were used to assess the likelihood of failure as follows:

- Axial stress = 0.9 x yield stress (Chapter D of the specification)
- Shear stress = 0.9 x 0.6 x yield stress (Chapter G of the specification)

The stress comparison is shown below:

Stress Component	Demand (psi)	Limit (psi)	IR
Axial (hoop)	24,000	0.9 x 24,000	1.11
Shear	18,000	0.9 x 0.6 x 24,000	1.39

The above exceedance of the stress limits does not necessarily indicate collapse of the tank. Rather, the exceedance is small and indicates plastic deformation and not necessarily tear out or cracking. Thus, it is expected that some yielding occurs and that available ductility in the steel will provide margin against failure.

Figure 4.8-4 shows the first buckling mode of the tank. The corresponding buckling load is 1.13 times the factored loads. Thus, there is margin against buckling of the tank as well.

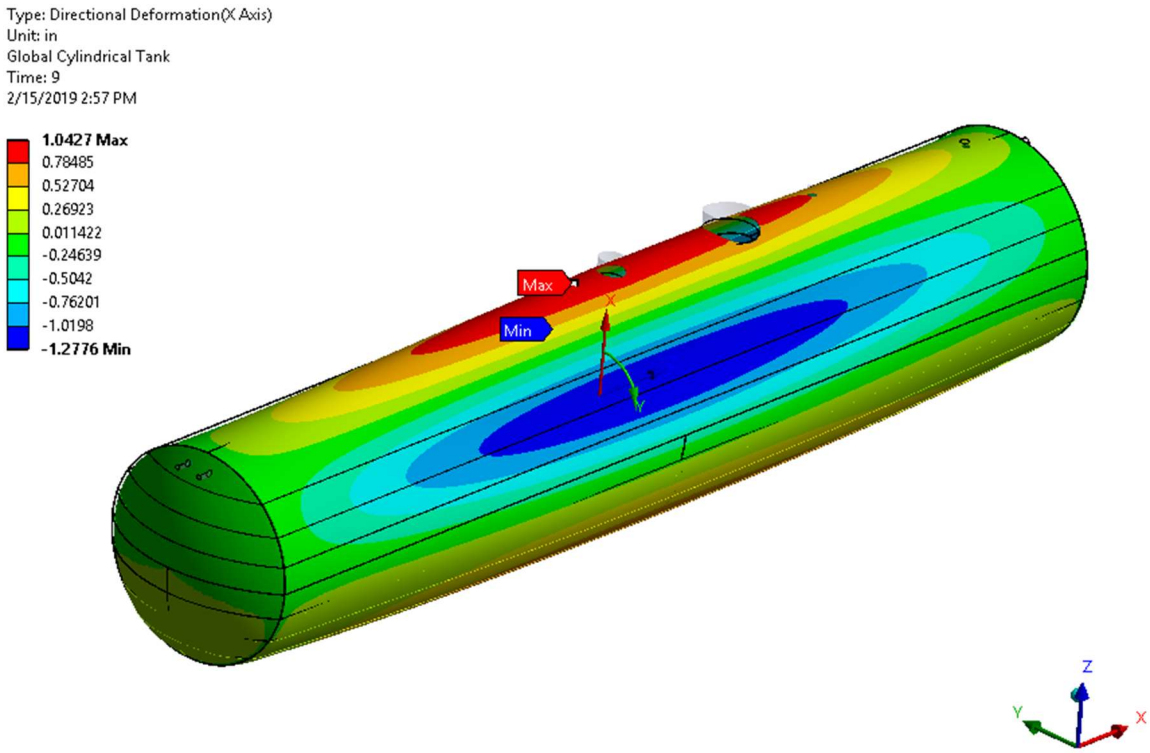

Figure 4.8-1: Contour Plot of Deformations (in.) for 241-Z-8

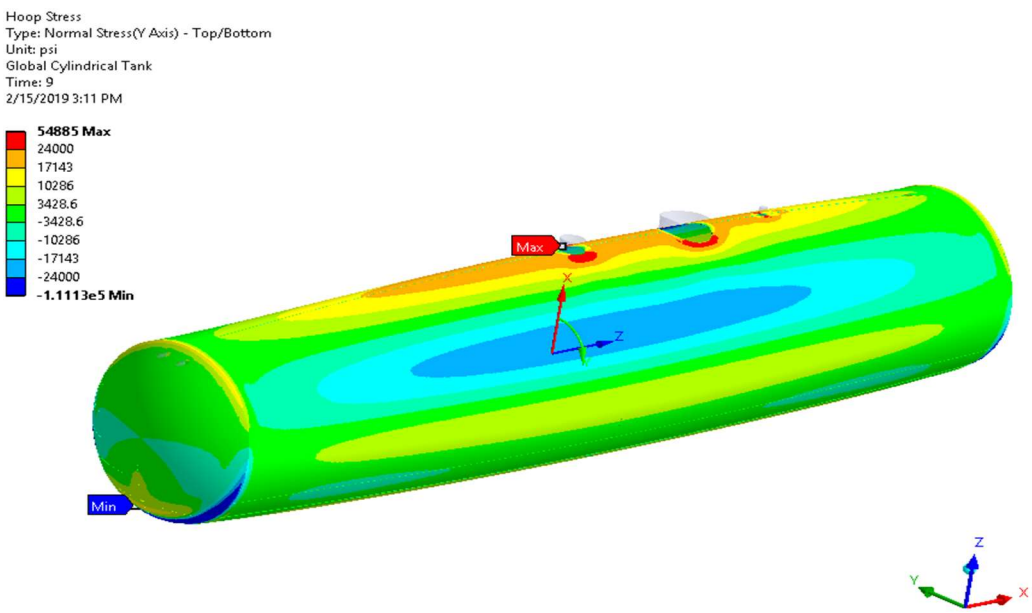

Figure 4.8-2: Contour Plot of Hoop Stress (psi) for 241-Z-8

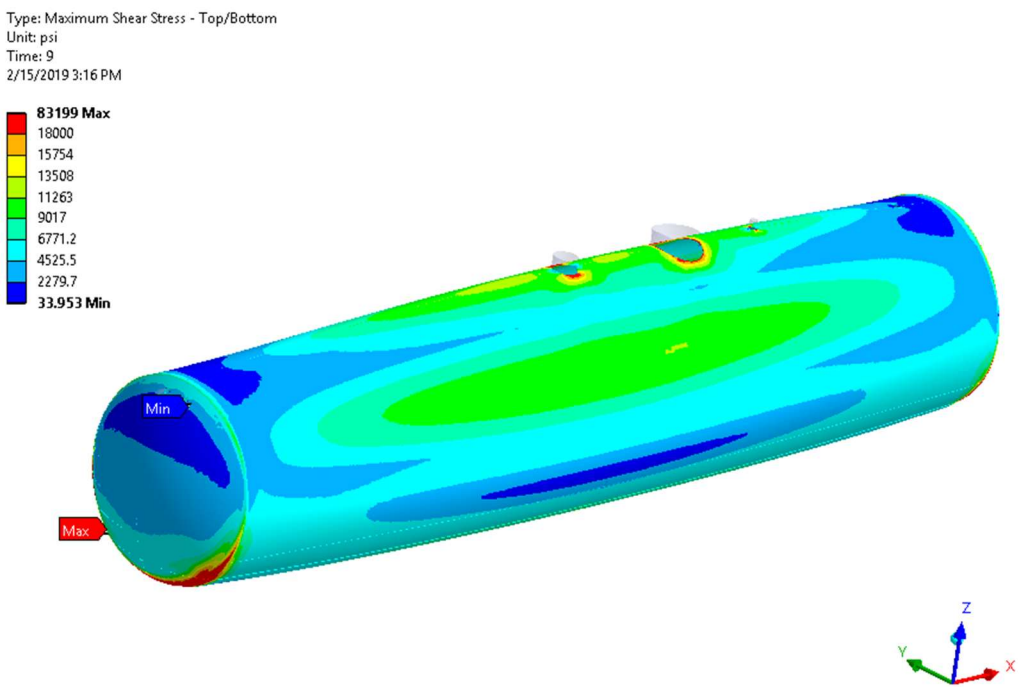

Figure 4.8-3: Contour Plot of Shear Stress (psi) for 241-Z-8

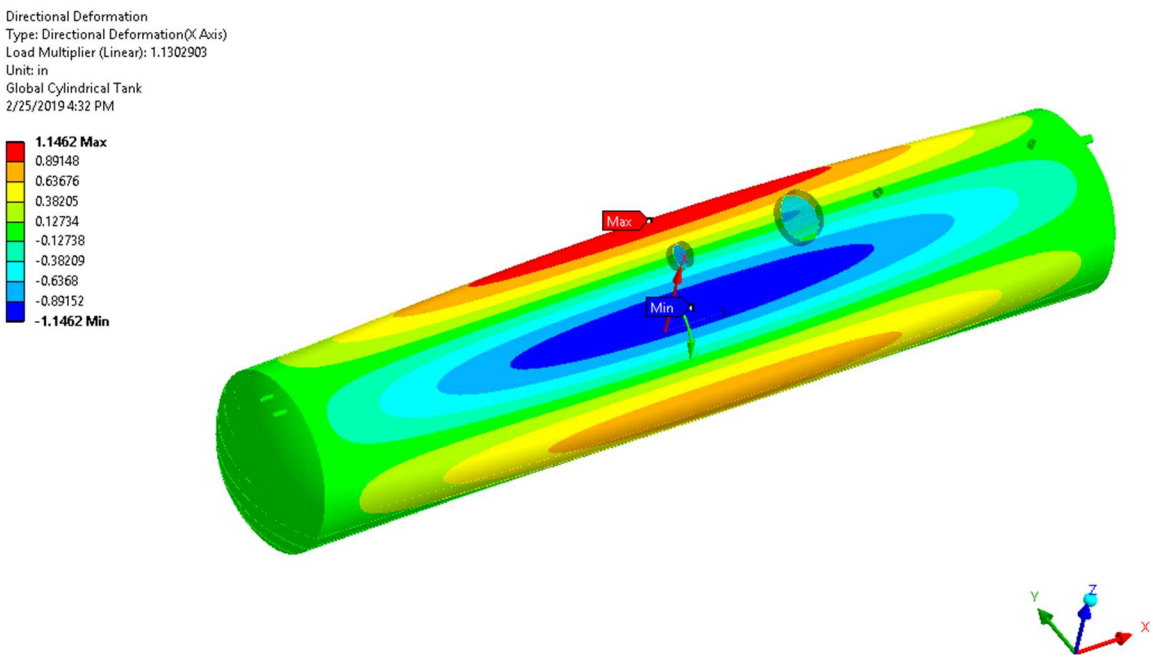

Figure 4.8-4: Contour Plot of Deformations (in.) at First Buckling Mode for 241-Z-8

4.9 Structure PUREX Filters, Group O1

Detailed structural drawings for the PUREX filters were used to obtain concrete geometry and rebar information. The roof slab was reduced 1 in. in the modeling and in the concrete evaluation to account for degraded conditions. Similarly, the rebar cross sectional area was reduced by 10%.

Deformation of the structure is shown in Figure 4.9-1, which indicates a maximum deflection of 0.08 in. Contour plots of maximum tension and compression stresses are given in Figure 4.9-2 and Figure 4.9-3. Contour plots of shear stress are shown in Figure 4.9-4. The resulting stresses were integrated over concrete sections to obtain section shear force, axial force, and bending moment, which are shown in Figure 4.9-5 through Figure 4.9-8. Figure 4.9-9 shows loading on the steel beam. The following table summarizes the maximum demand forces and moments on critical sections of the structure.

Building Component	Size	Shear Force (lb)	Axial Force (lb)	Bending Moment (in.-lb)
Roof slab	16 in. x 11 in. deep	9,000 (1)	-12,000	290,000
Steel Beam	5 I 10	105	--	3,372

(1) Per Figure 4.9-6, the maximum shear force of 27,000 lb occurs at the slab terminal supports and does need not be considered for the slab evaluation. Similarly, high shear forces occurring within the intermediate walls do not need to be considered.

<u>Roof Slab</u>

Cross section = 16 in. wide x 11 in. deep

Assume rebar are No. 6 @ 6 in. top (smaller of top and bottom rebar is used)

Area of #6 rebar = 0.44 in.^{2} (to be reduced by 10%)

Rebar depth = 11 in. (assuming 1 in. clear cover so that rebar becomes exposed with 1 in. loss of thickness)

<u>Axial compression capacity</u>

Axial compression capacity with no bending (using strength reduction factor of 0.7):

$\phi Pn = 0.7 \times 0.8\ (0.85\ fc\ (A_{cross} - As) + fy\ (As))$

= 0.7 x 0.8 (0.85 x 3,000 (16x11 – 0.44x16/6x0.9) + 40,000 (0.44x16/6x0.9))

= 273,500 lb >> 12,000 lb

The axial compression capacity is significantly larger than the demand axial compression.

Bending Moment Capacity

ϕMn = 0.9 x As fy {d – As fy / (2 x 0.85 fc b)}

= 0.9 x (0.44x16/6x0.9) x 40,000 x

{11.0 – (0.44x16/6x0.9) x 40,000 / (2 x 0.85 x 3,000 x 16)}

= 398,497,006 in.-lb >> 290,000 in.-lb

Shear Capacity

Reduced shear stress capacity of the concrete section using ACI Eq. 11-3:

$\phi\tau$n = 0.75 x 2 x $\sqrt{}$fc = 82 psi

ϕVn = 82 psi x 16 x 8 = 14,460 lb > 9,000 lb

Thus, the roof slab is acceptable. The loads on the steel beam are acceptable by inspection based on the magnitude and size of the 5 x 10 I-beam section.

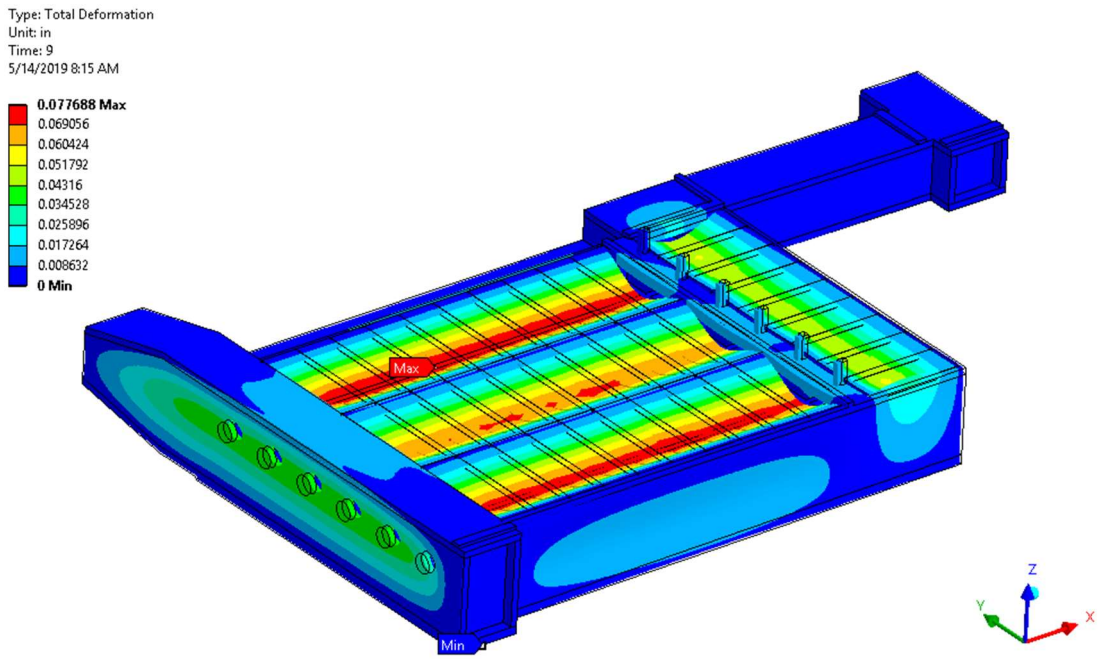

Figure 4.9-1: Contour Plot of Deformations (in.) for PUREX Filters

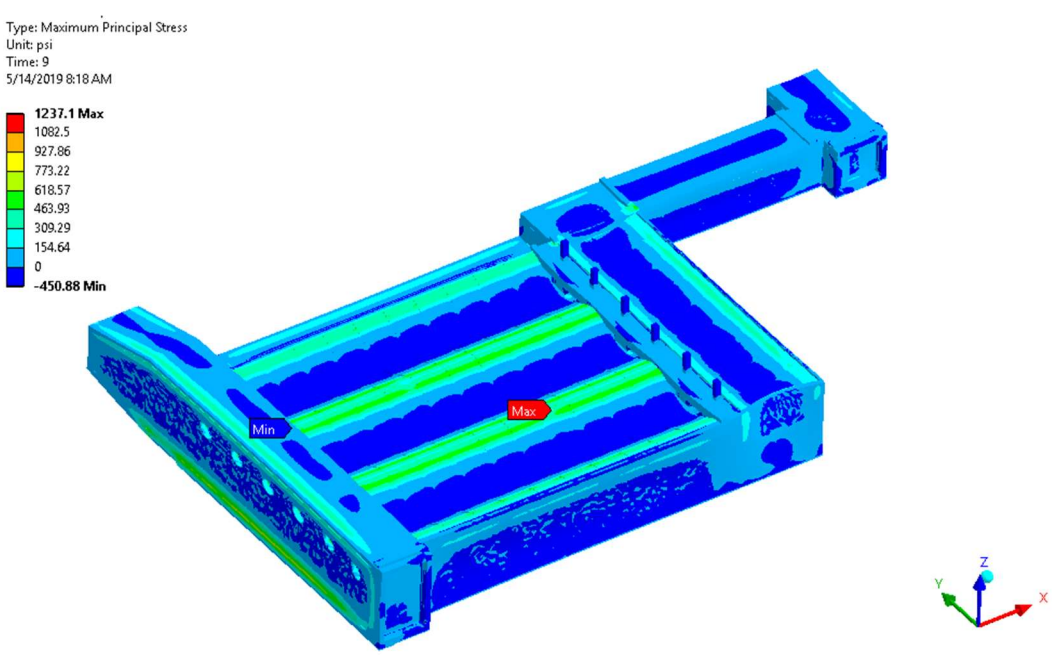

Figure 4.9-2: Contour Plots of Maximum Principal Stress (psi) for PUREX Filters

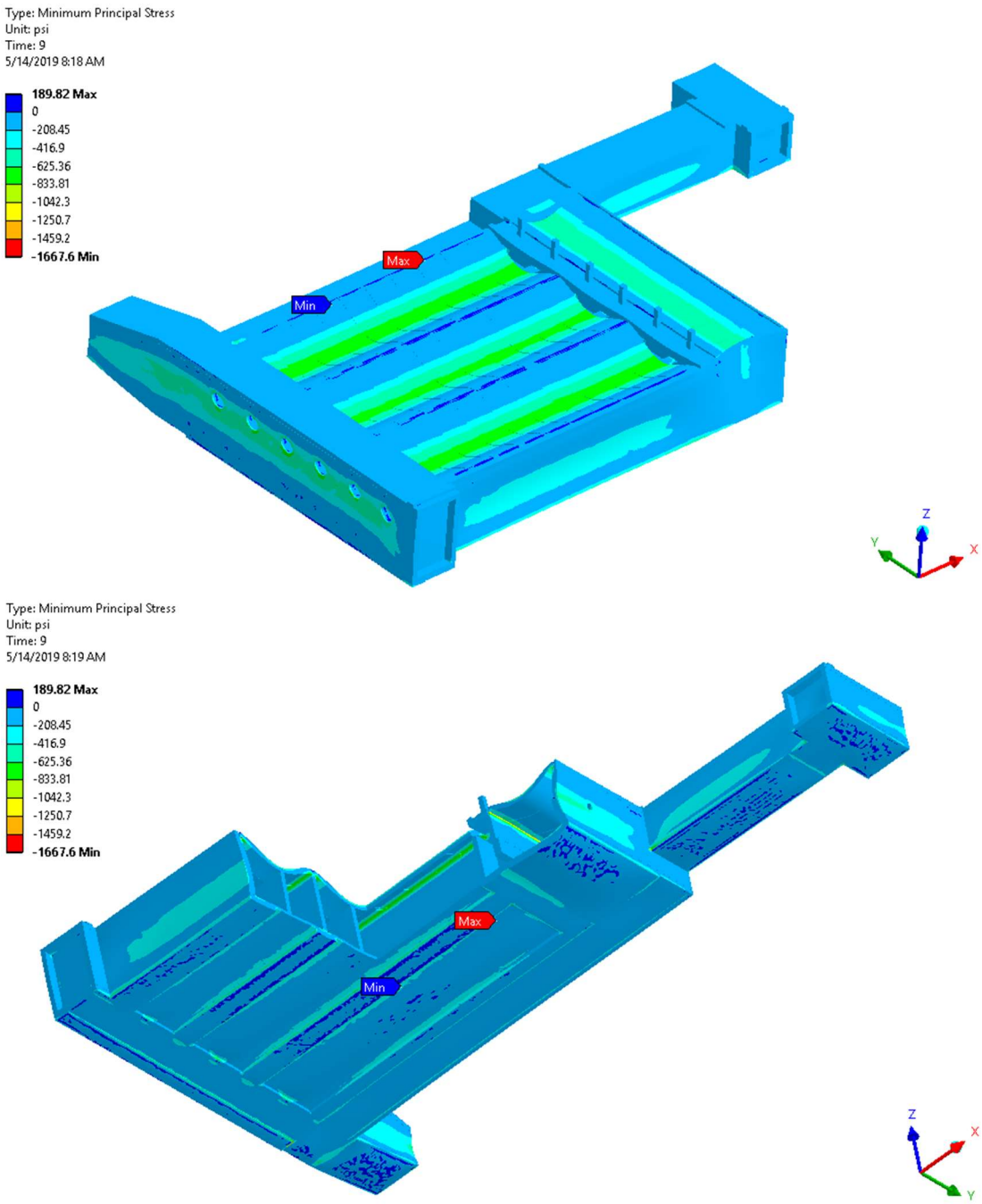

Figure 4.9-3: Contour Plots of Minimum Principal Stress (psi) for PUREX Filters – Sectional View

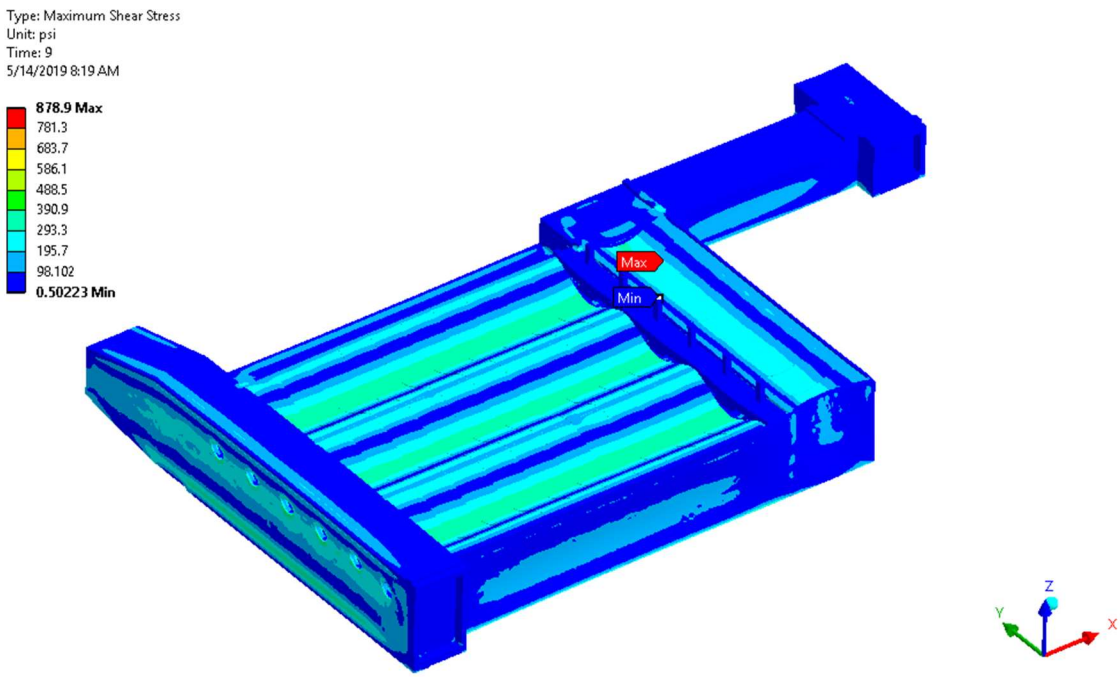

Figure 4.9-4: Contour Plots of Shear Stress (psi) for PUREX Filters

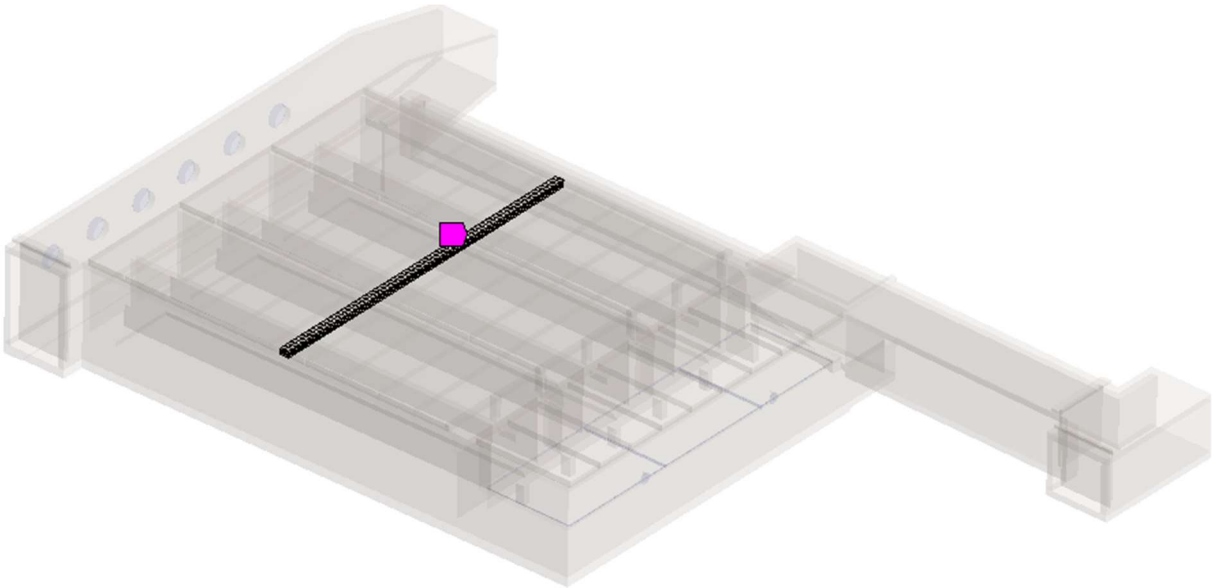

Figure 4.9-5: Roof Slab Strip for PUREX Filters

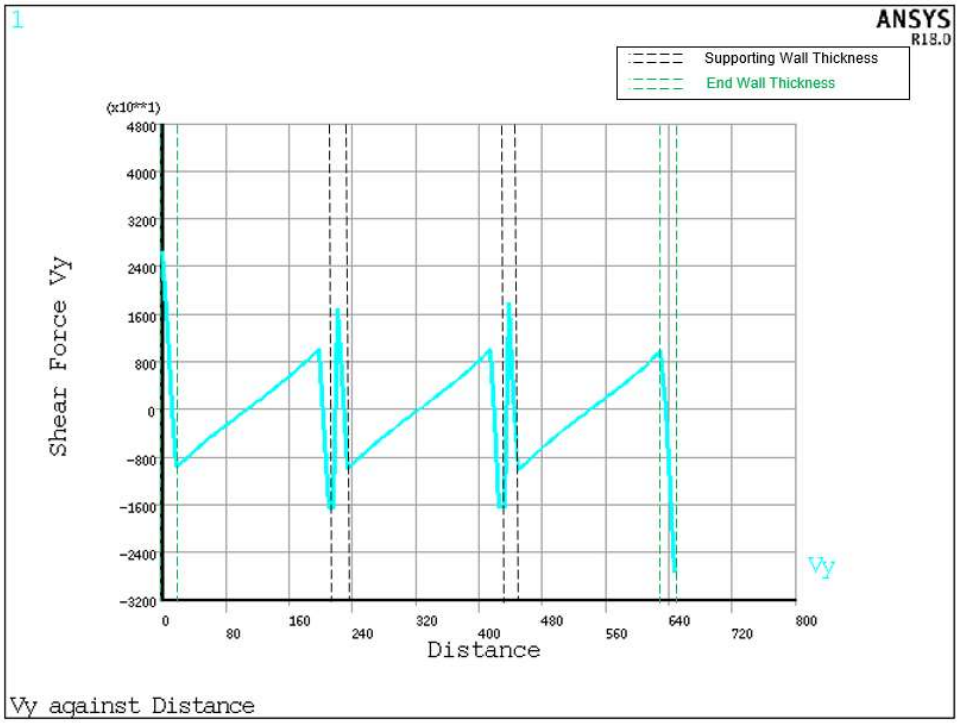

Figure 4.9-6: Roof Slab Strip Shear Force (lb) Diagram for PUREX Filters

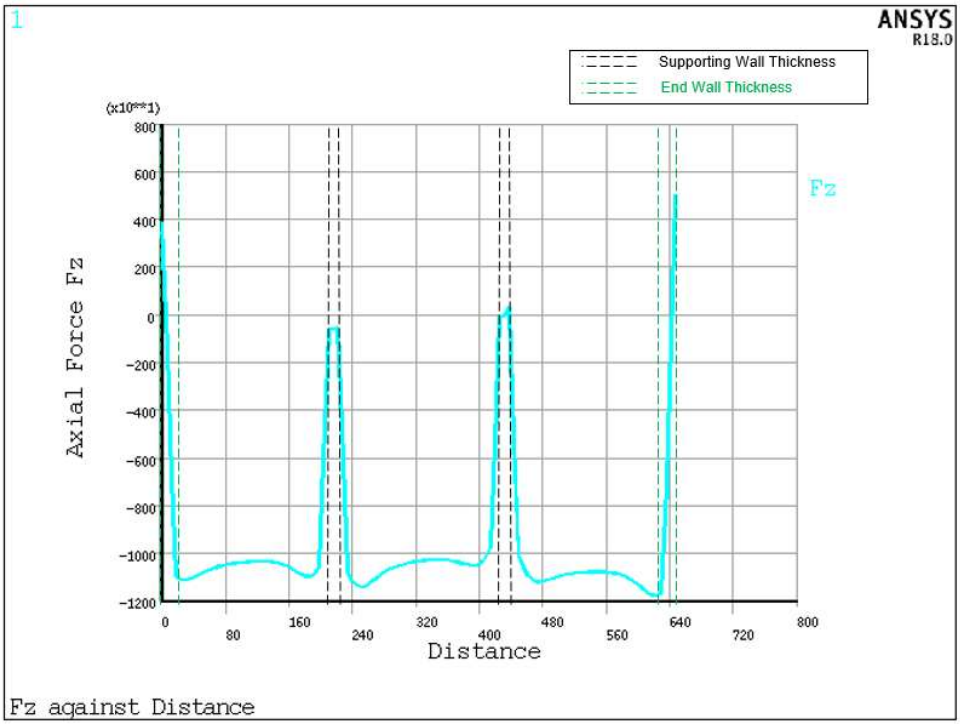

Figure 4.9-7: Roof Slab Strip Axial Force (lb) Diagram for PUREX Filters

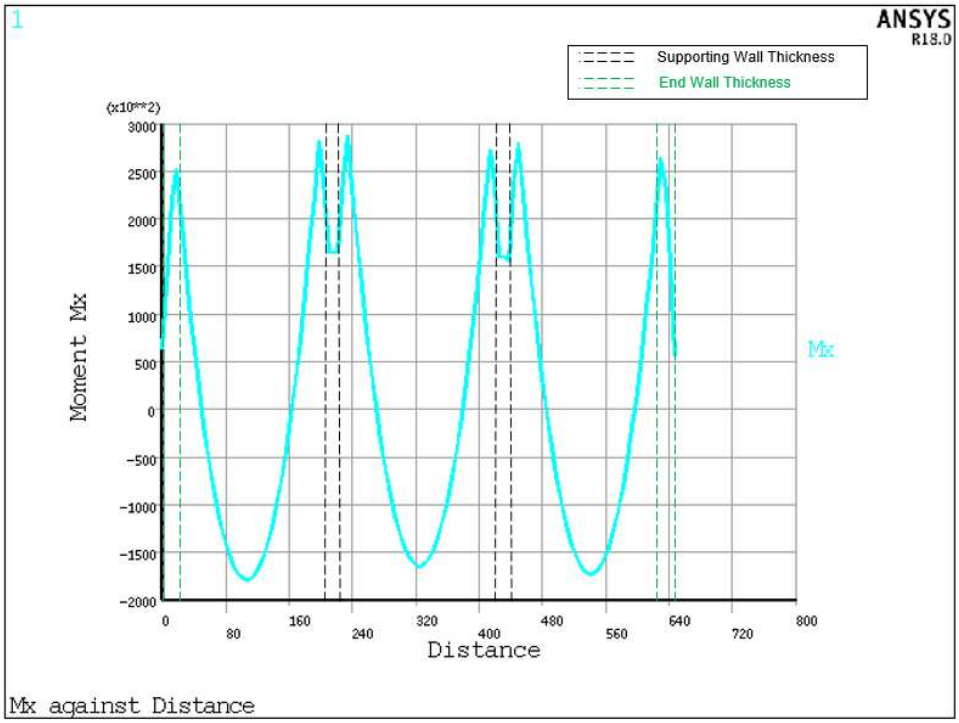

Figure 4.9-8: Roof Slab Strip Moment (in.-lb) Diagram for PUREX Filters

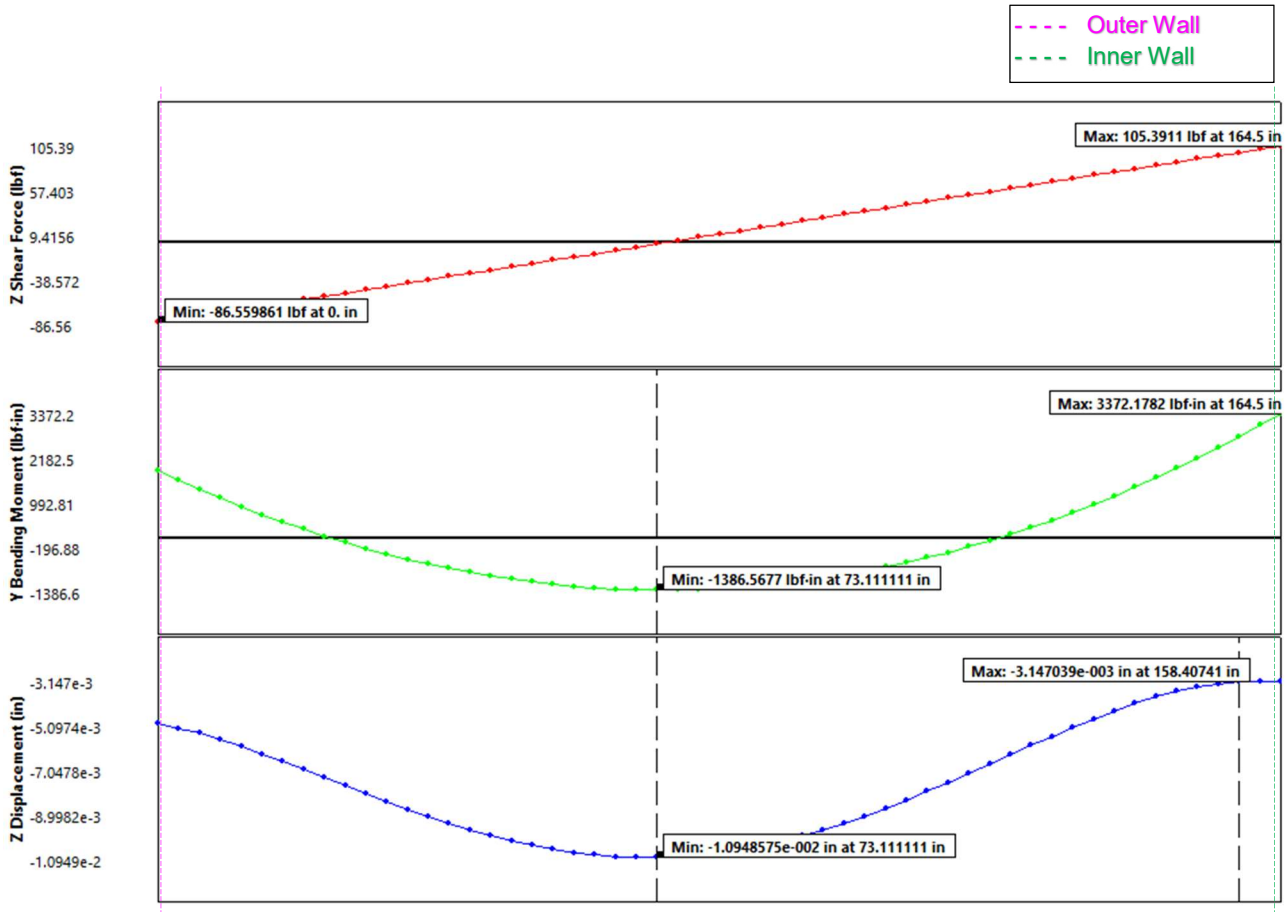

Figure 4.9-9: Steel Beam Action Diagrams for PUREX Filters

4.10 Structure REDOX Filter, Group O2

Structural detailed drawings for the REDOX filter do not show the size/thickness of the concrete slabs and beams and no information was provided about the reinforcement. Consequently, concrete member sizes were approximated from the drawings. An assumption was made regarding the amount of reinforcement in the slabs, beams, and columns. The reinforcement was assumed such that balanced reinforcement is not exceeded in accordance with general practice in design of concrete structures. The following table lists the filter material layer weights on top of the floor slab:

	Thickness (in.)	Density (lb/ft^3)	Pressure (psi)
Floor slab	8	150	0.694
Clay tiles	5	125	0.362
Type A	12	100	0.694
Type B	12	105	0.729
Type C	12	110	0.764
Type E	6	115	0.399
Type F	12	120	0.833
Type G	24	125	1.736
Total			6.212

The above layers are described in the design drawings and are incorporated into the finite element modeling so that the total floor pressure calculated in the table is applied on the slab.

Deformation of the structure is shown in Figure 4.10-1, which indicates a maximum deflection of 0.23 in. Contour plots of maximum tension and compression stresses are given in Figure 4.10-2 through Figure 4.10-8. Contour plots of shear stress are in Figure 4.10-9. The resulting stresses were integrated over concrete sections to obtain section shear force, axial force, and bending moment. Those results are shown in Figure 4.10-10 through Figure 4.10-25. The following table summarizes the maximum demand forces and moments on various sections of the structure.

Building Component	Size	Shear Force (lb)	Axial Force (lb)	Bending Moment (in.-lb)
Roof slab	9 in. x 6 in. deep	3,400	-3,800	44,000
Wall	12 in. x 12 in.	4,400	12,000	200,000
Roof beam	9 in. x 24 in.	23,000	+31,000/-76,000	900,000
Column	9 in. x 13.5 in.	Maximum tension = 1,550 psi Maximum compression = 2,183 psi Excluding local concentrated stresses resulting from sharp corners		

Roof Slab

Cross section = 9 in. wide x 6 in. deep

Assume rebar are size 0.5 in. every 6 in., Area of 0.5 in. rebar = 0.31 in.^{2}

1 in. reduction in slab depth and 10% reduction in slab rebar area was applied in the ACI Code qualification to simulate possible degradation. The 1 in. concrete depth reduction was applied to all internal surfaces. Note that at the section of the maximum moment in the roof slab, the tension side rebar cover and the 1 in. concrete loss are on opposite sides and therefore are additive.

Rebar depth = 6 in. – 1 in. – 1 in. – 0.5/2 in.= 3.75 in.

(assuming 1 in. clear rebar cover)

Axial compression capacity

Axial compression capacity with no bending (using strength reduction factor of 0.7):

ϕPn = 0.7 x 0.8 (0.85 fc (A_{cross} – As) + fy (As))

= 0.7 x 0.8 (0.85 x 3,000 (9x3.75 – 0.31x9/6x0.9) + 40,000 (0.31*9/6*0.9))

= 56,972 lb >> 3,800 lb

The axial compression capacity is significantly larger than the demand axial compression.

Bending moment capacity

$\phi Mn = 0.9 \times As\ fy \{d - As\ fy / (2 \times 0.85\ fc\ b)\}$

$= 0.9 \times (0.31 \times 9/6 \times 0.9) \times 40{,}000 \{3.75 - (0.31 \times 9/6 \times 0.9) \times 40{,}000/(2 \times 0.85 \times 3{,}000 \times 9)\}$

$= 51{,}003$ in.-lb >> 44,000 in.-lb

This moment capacity is greater than the demand moment.

Shear capacity

Reduced shear stress capacity of the concrete section using ACI Eq. 11-3:

$\phi\tau n = 0.75 \times 2 \times \sqrt{fc} = 82$ psi

Per Figure 4.10-11 and Figure 4.10-13, the bending moment is negligible at the section of maximum shear force. As such, rebar depth, d, is obtained by considering the 1 in. loss and concrete cover are overlapped.

$\phi Vn = 82$ psi $\times 9 \times 4.75 = 3{,}506$ lb > 3,400 lb

This shear capacity exceeds the demand shear.

Thus, the concrete roof slab is adequate for the postulated loads.

Floor Slab Above the Air Tunnels

The floor slab was assumed to be 8 in. thick. It is considered acceptable based on comparison to the evaluation of the roof slab, however, it was evaluated for bending and shear to demonstrate acceptance for the filter material it is supporting. The moment and shear in the slab was calculated based on the floor loads tabulated above using the longest span of 4.5 ft. The single span over the air tunnel was assumed to be pinned-fixed to maximize the demand bending and shear. The demand was calculated for the controlling load Combination 1 for a 12 in. wide strip.

Mu (demand moment) = 1.4×6.212 psi $\times 12$ in. $\times (4.5\ ft)^2 \times 12\ in.^2/ ft^2/ 8 = 38{,}042$ in.-lb

Vu (demand shear) = 1.4×6.212 psi $\times 12$ in. $\times 5 \times 4.5$ ft / 8 = 3,522 lb

Cross section = 12 in. wide x 8 in. deep

Assume rebar are size 0.5 in. every 6 in., Area of 0.5 in. rebar = 0.31 in.^{2}

1 in. reduction in slab depth and 10% reduction in slab rebar area was applied in the ACI Code qualification to simulate possible degradation.

Rebar depth = 8 in. – 1 in. – 1 in. – 0.5/2 in.= 5.75 in.

(assuming 1 in. clear rebar cover)

<u>Bending moment capacity</u>

ϕMn = 0.9 x As fy {d – As fy / (2 x 0.85 fc b) }

= 0.9 x (0.31x12/6x0.9) x 40,000 {5.75 – (0.31x12/6x0.9) x 40,000/(2 x 0.85 x 3,000 x 12)}

= 108,180 in.-lb >> 38,042 in.-lb

This moment capacity is greater than the demand moment.

<u>Shear capacity</u>

Reduced shear stress capacity of the concrete section using ACI Eq. 11-3:

$\phi\tau$n = 0.75 x 2 x $\sqrt{}$fc = 82 psi

ϕVn = 82 psi x 12 x 5.75 = 5,669 lb > 3,522 lb

This shear capacity exceeds the demand shear.

Thus, the concrete floor slab over the air tunnels is adequate for the postulated loads.

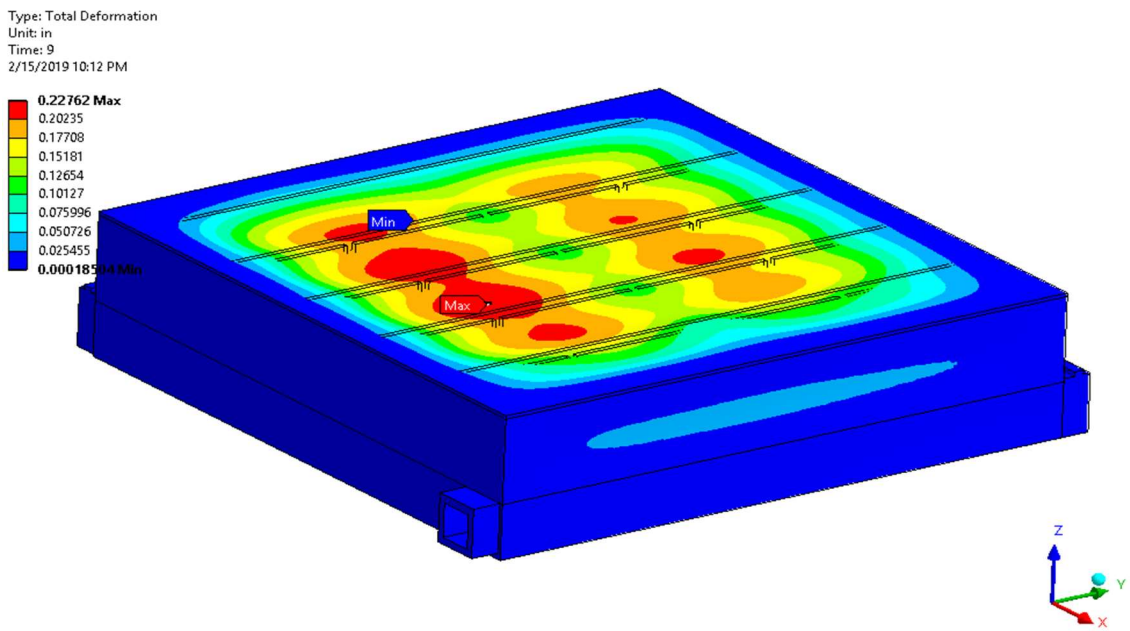

Figure 4.10-1: Contour Plots of Deformations (in.) for REDOX Filter - Overall

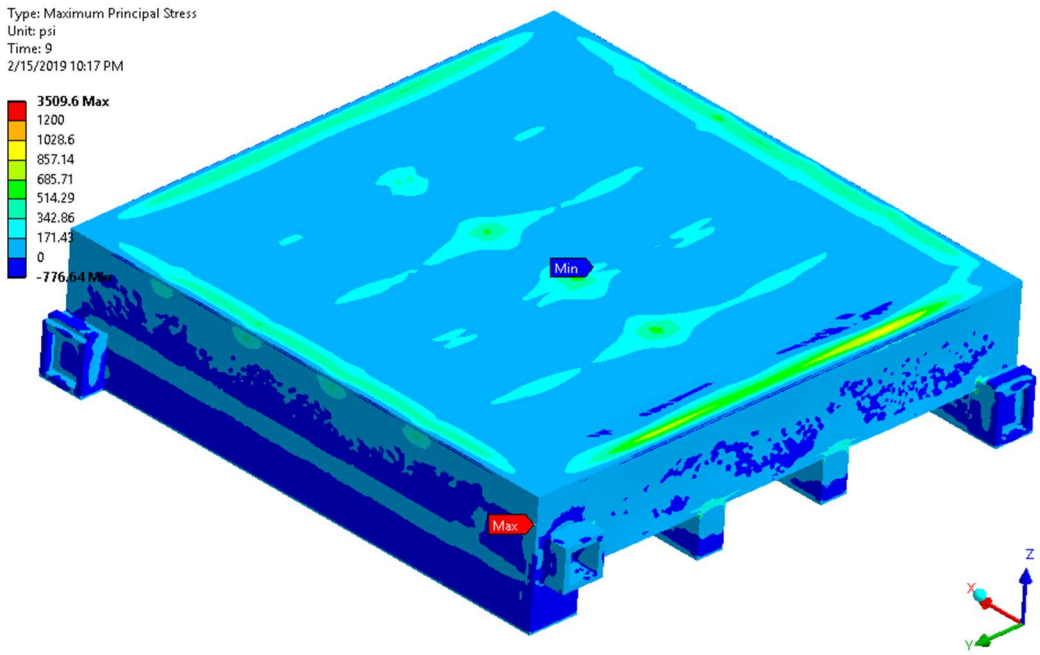

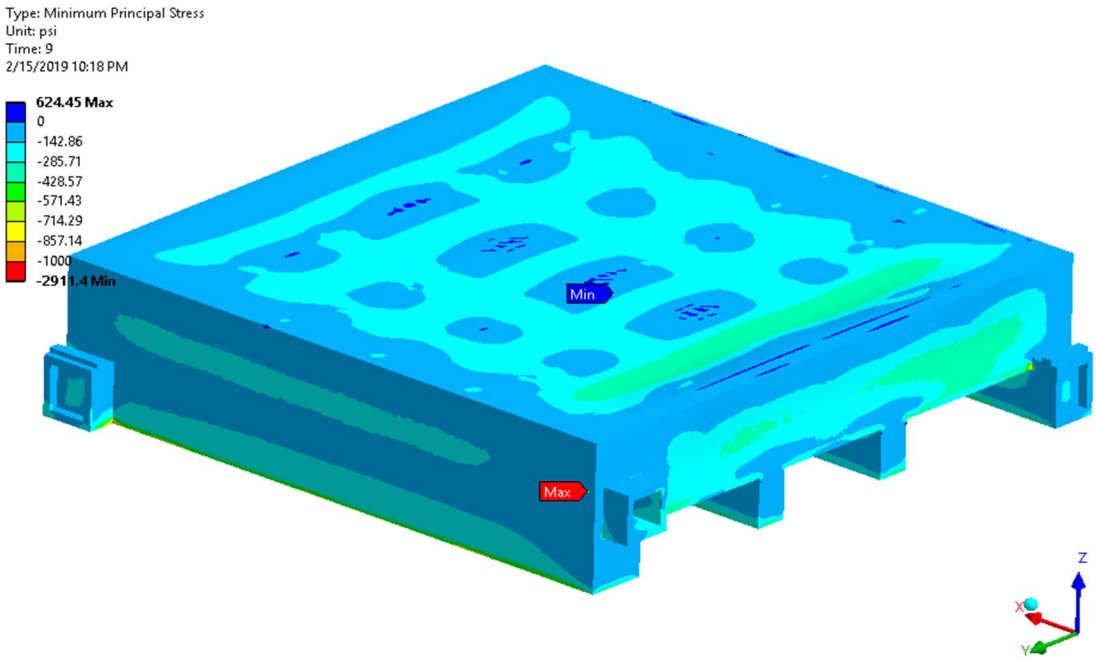

Figure 4.10-2: Contour Plots of Maximum and Minimum Principal Stresses (psi) for REDOX Filter - Overall

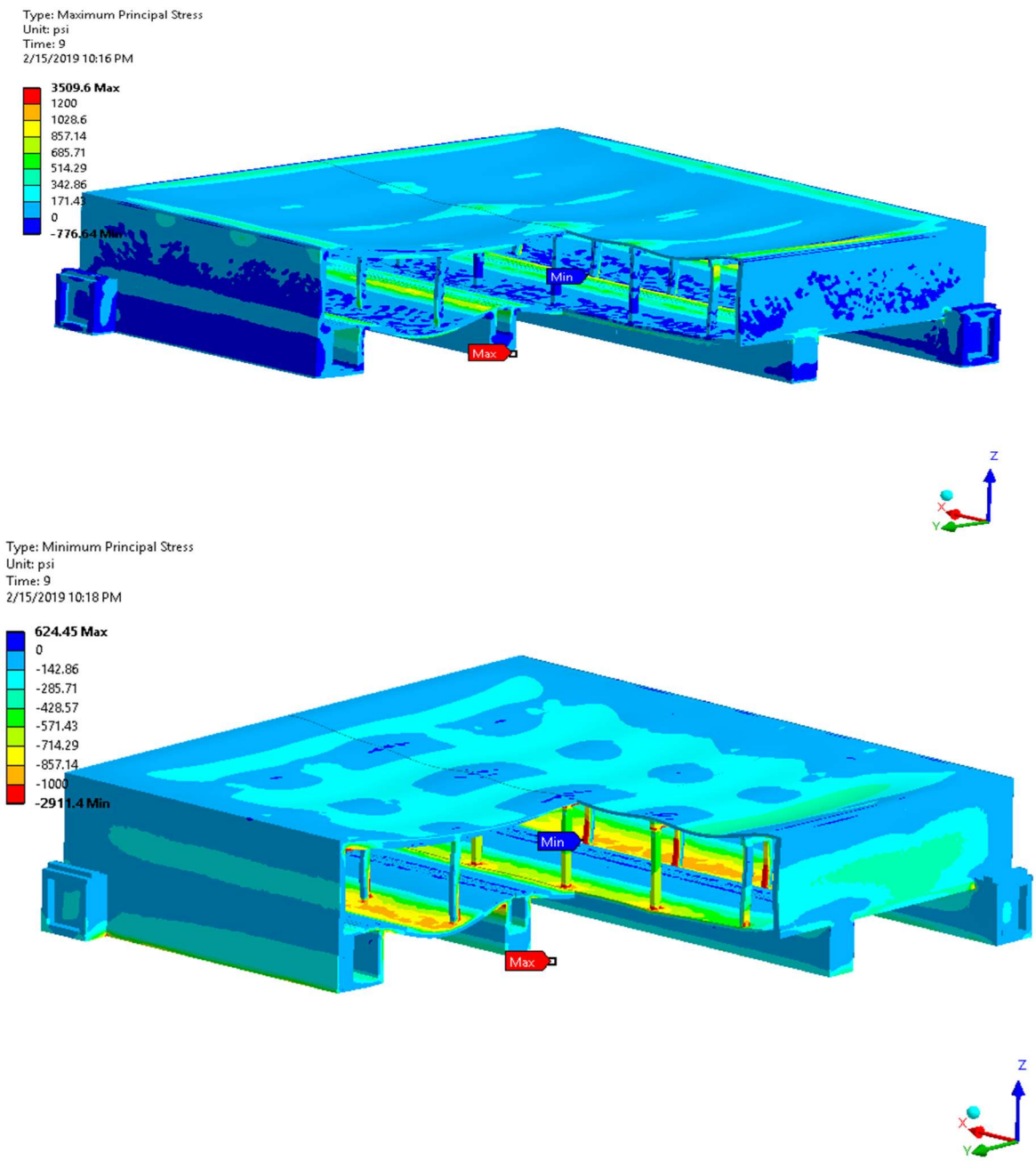

Figure 4.10-3: Contour Plots of Maximum and Minimum Principal Stresses (psi) for REDOX Filter – Overall Sectional View

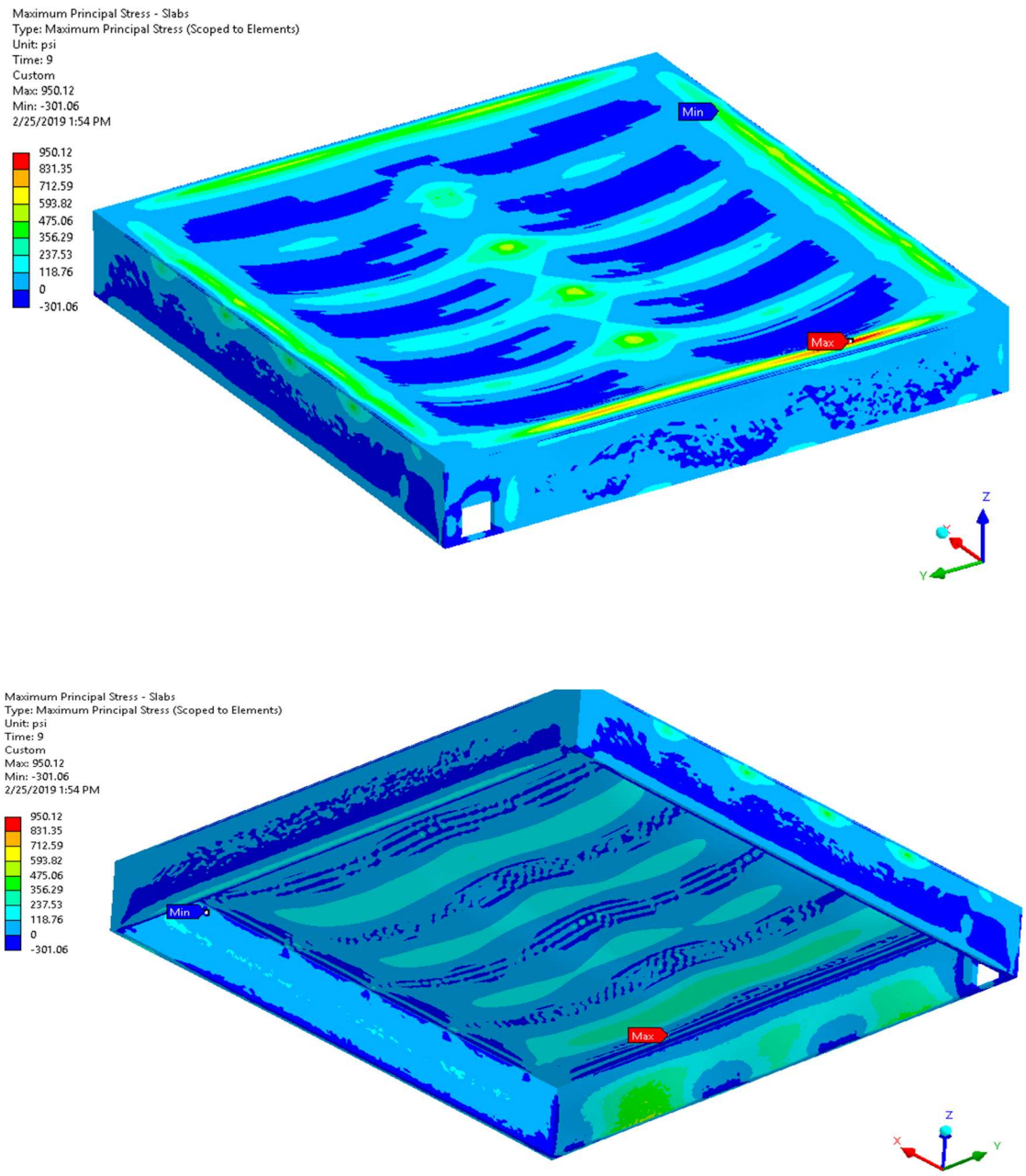

Figure 4.10-4: Contour Plots of Maximum Principal Stresses (psi) for REDOX Filter – Roof Slab Top View Looking Down, Bottom View Looking Up

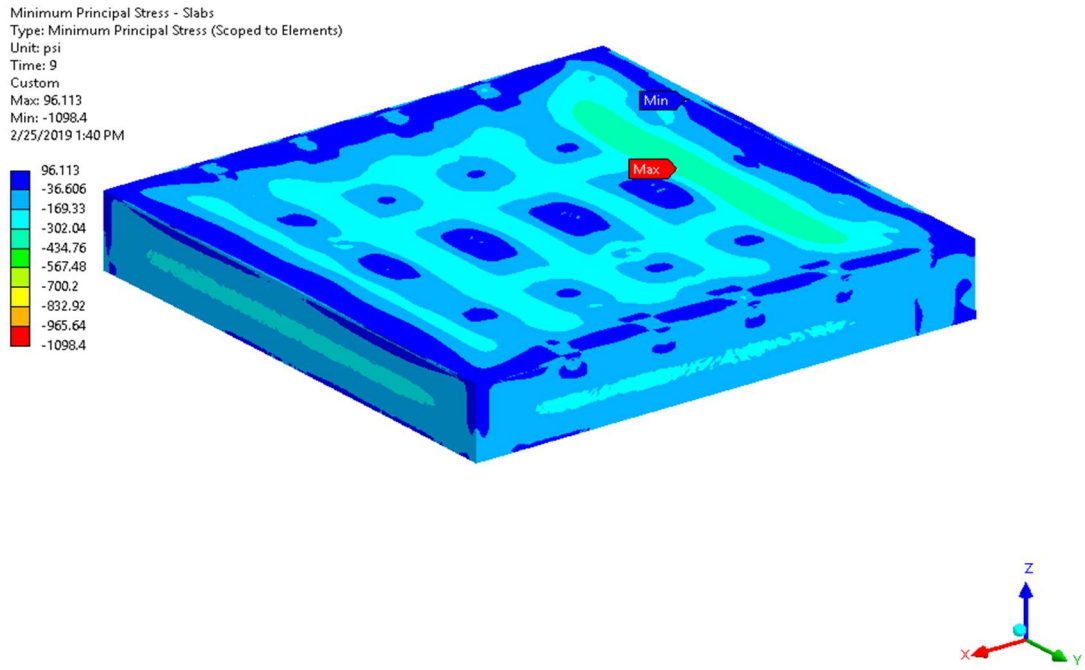

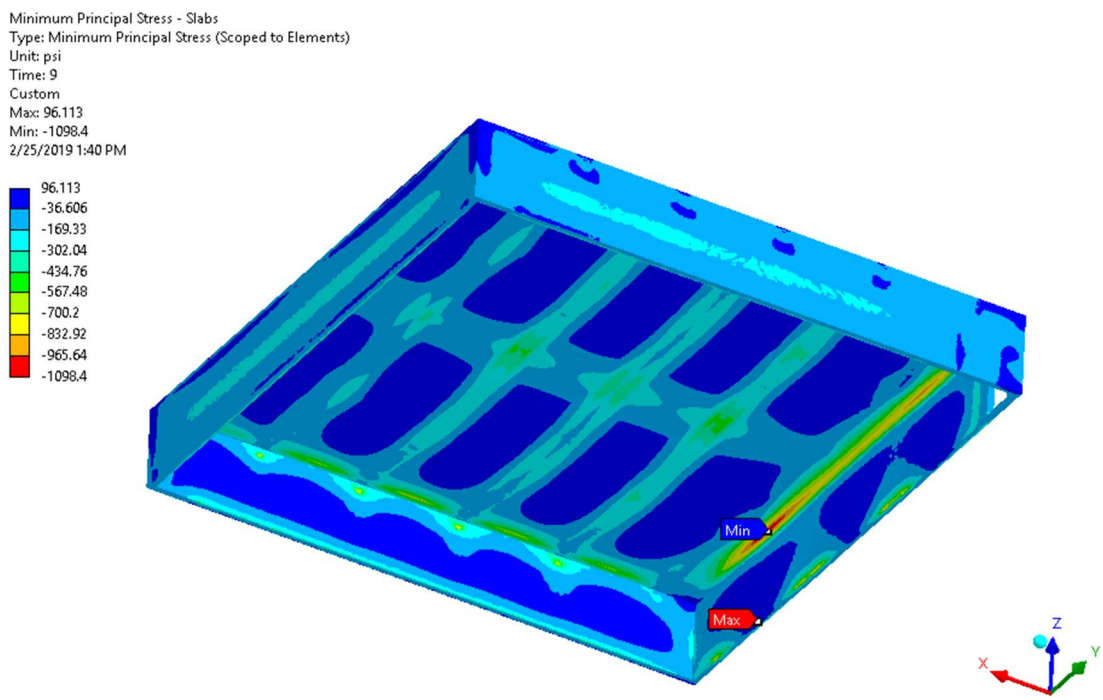

Figure 4.10-5: Contour Plots of Minimum Principal Stresses (psi) for REDOX Filter – Roof Slab Top View Looking Down, Bottom View Looking Up

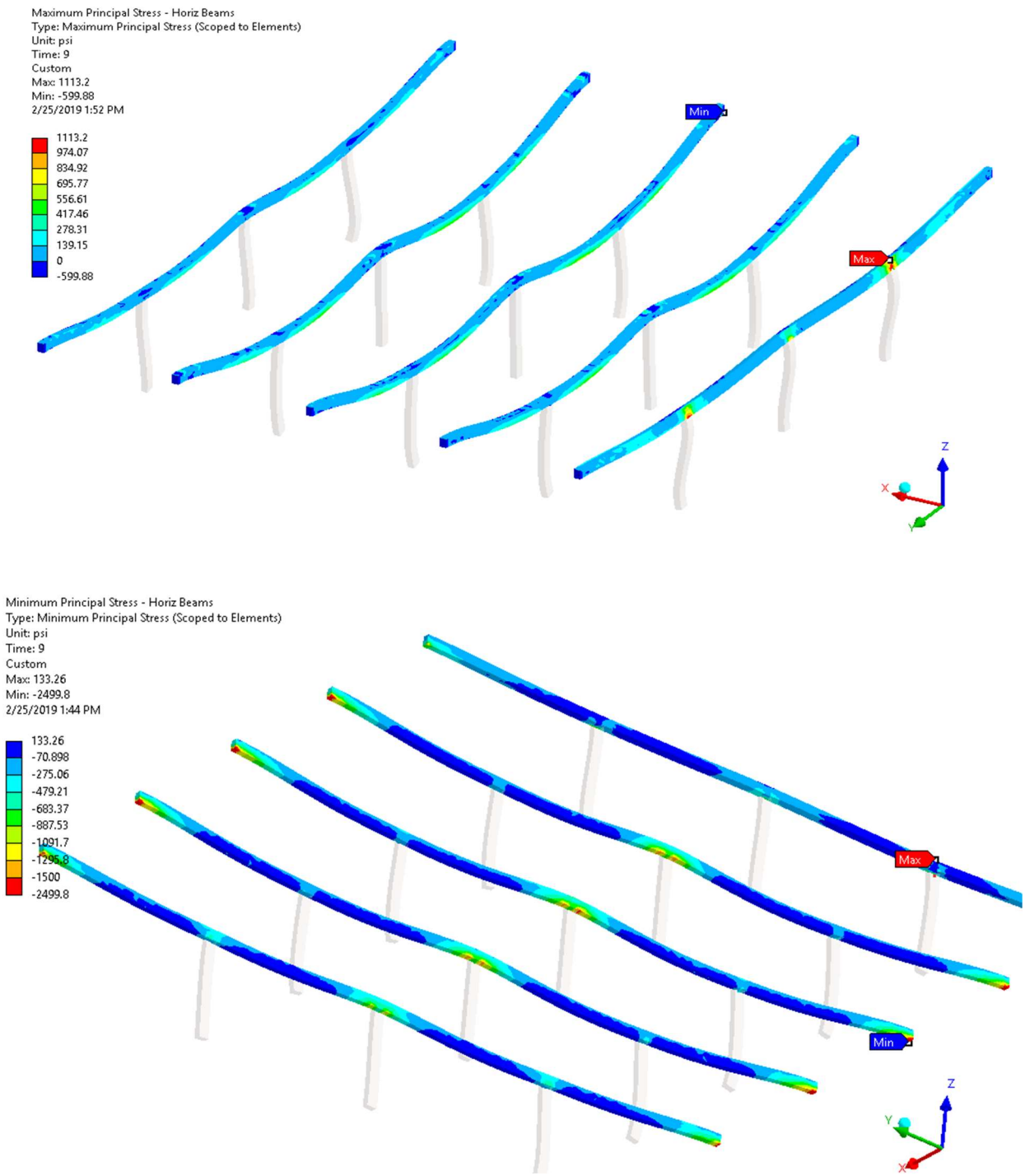

Figure 4.10-6: Contour Plots of Maximum and Minimum Principal Stresses (psi) for REDOX Filter – Roof Beams

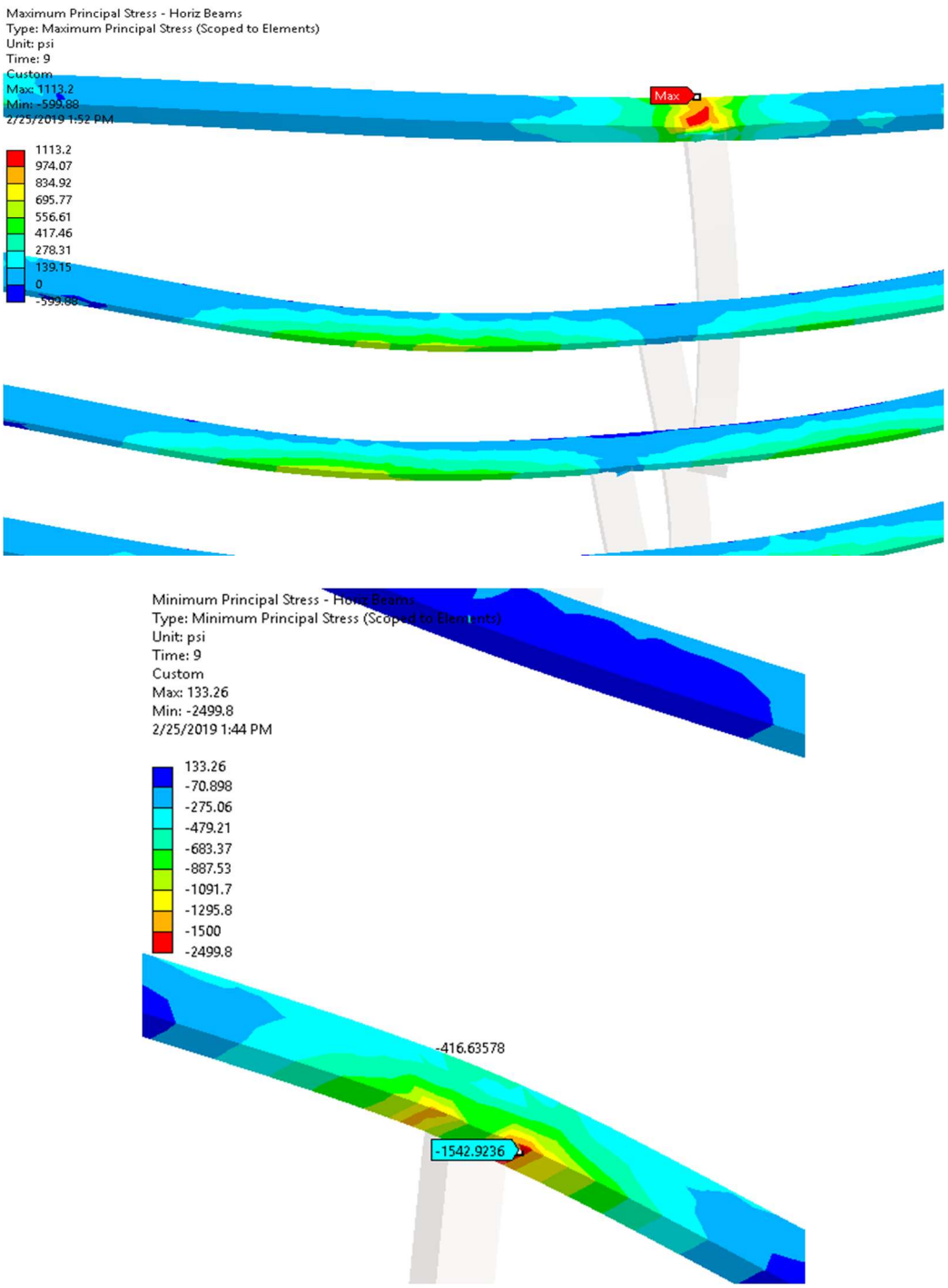

Figure 4.10-7: Contour Plots of Maximum and Minimum Principal Stresses (psi) for REDOX Filter – Roof Beams Close-up

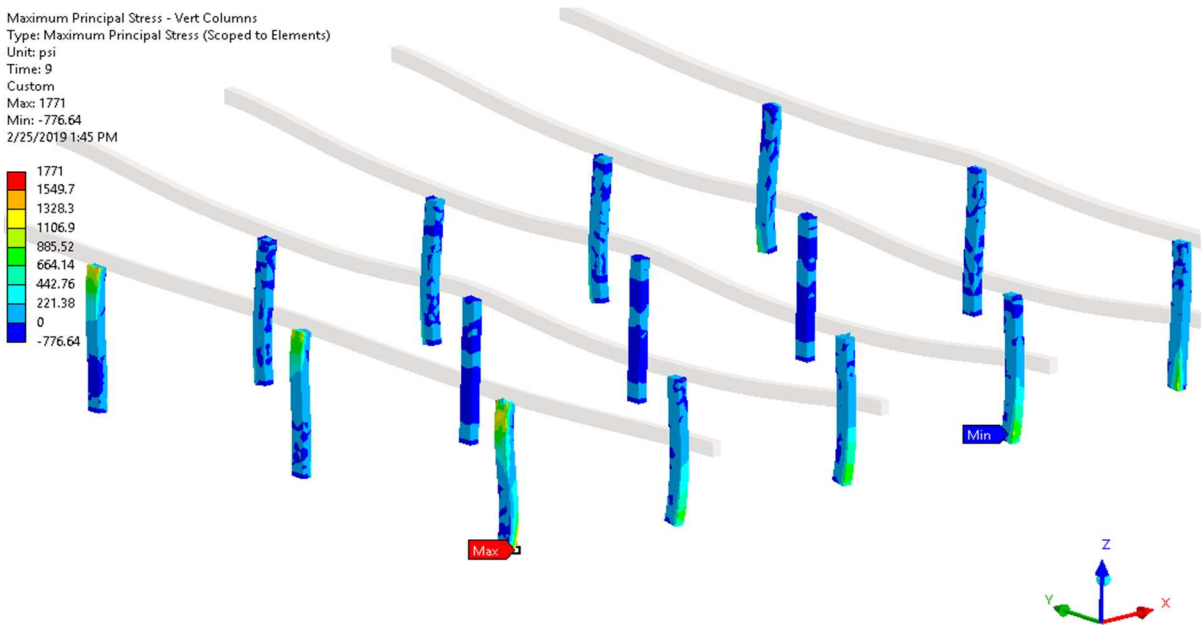

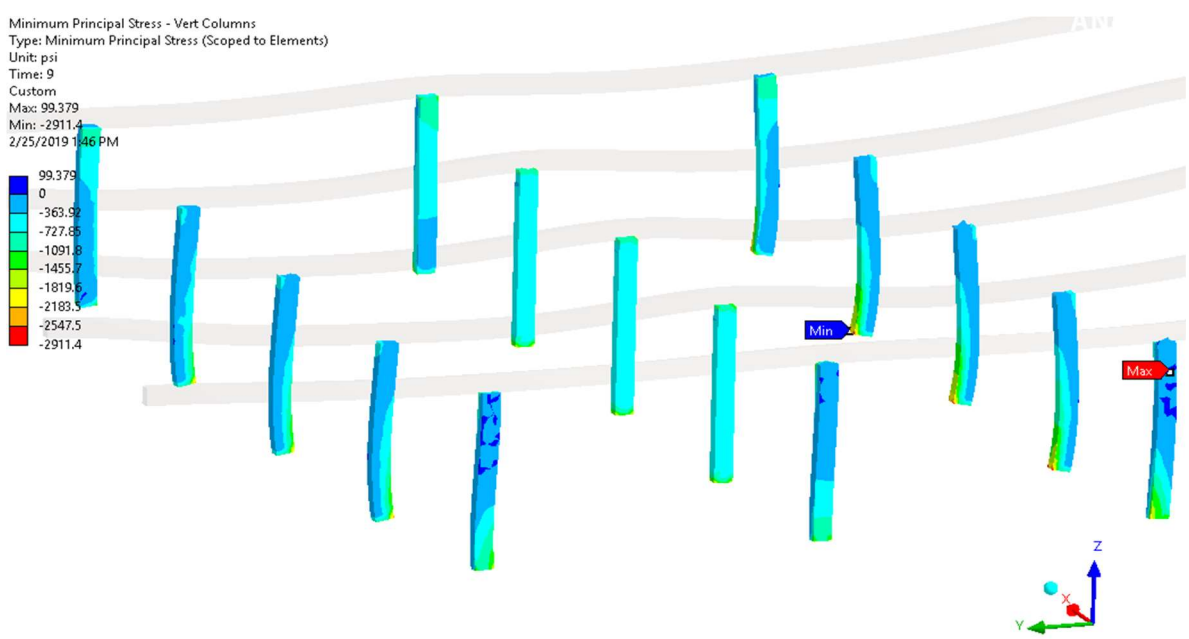

Figure 4.10-8: Contour Plots of Maximum and Minimum Principal Stresses (psi) for REDOX Filter – Columns

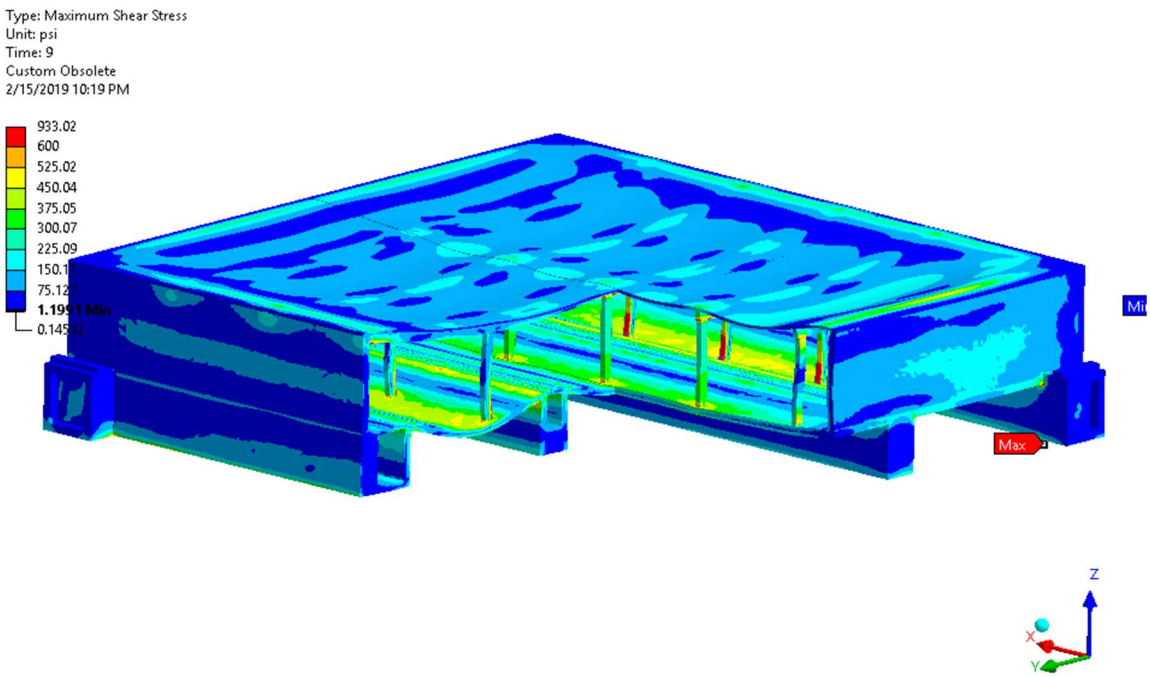

Figure 4.10-9: Contour Plots of Shear Stresses (psi) for REDOX Filter – Overall Sectional View

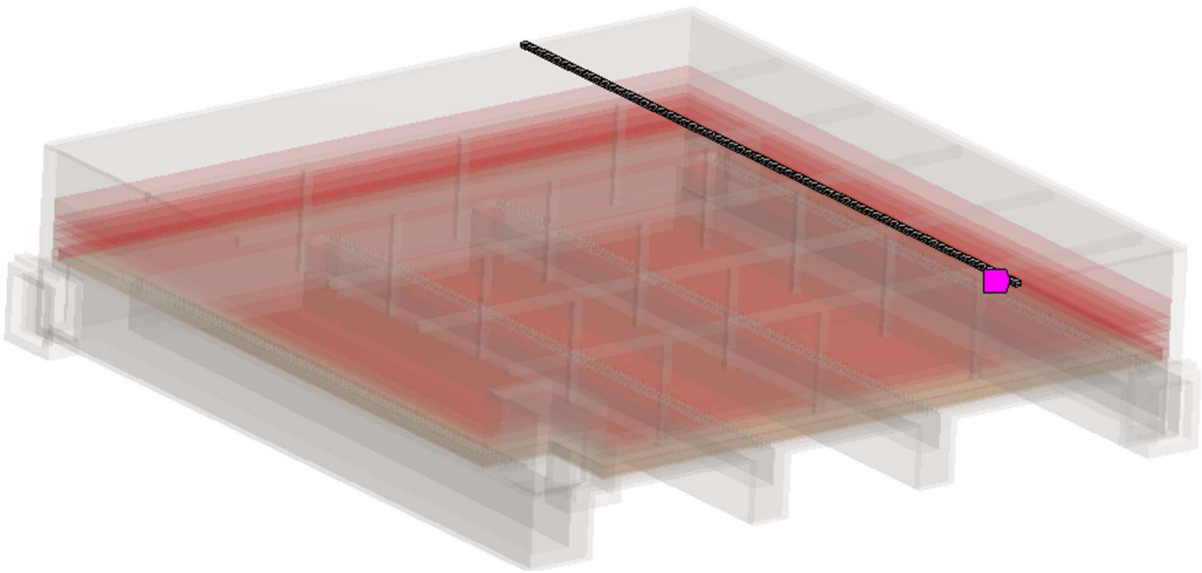

(9 in. wide slice of elements)

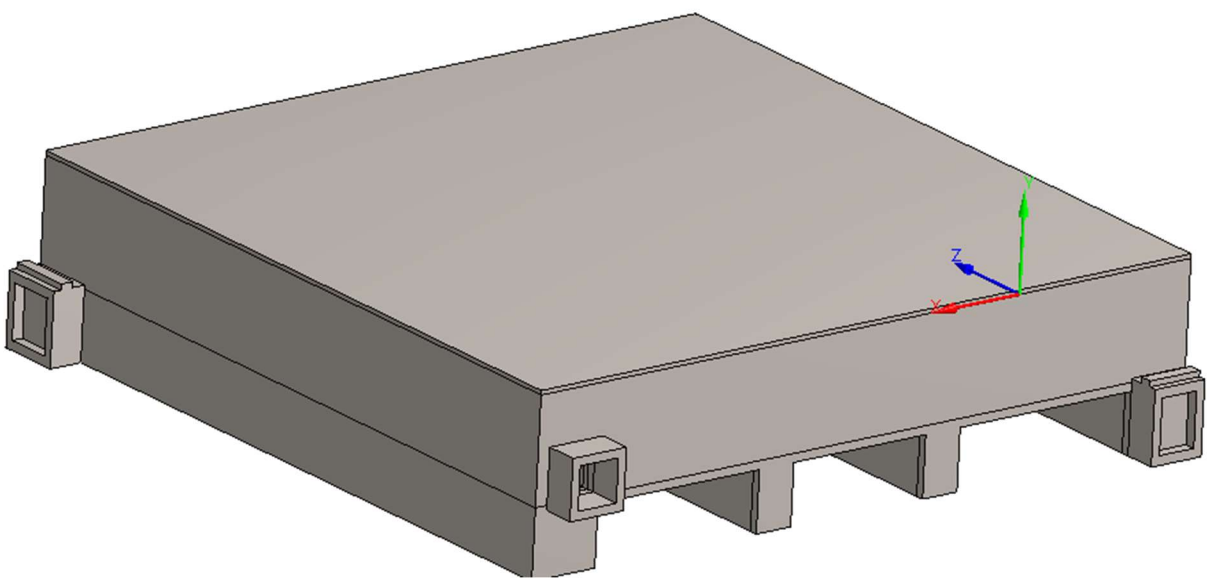

Figure 4.10-10: Strip Location and Coordinates for Integrated Stresses for REDOX Filter – Roof Slab

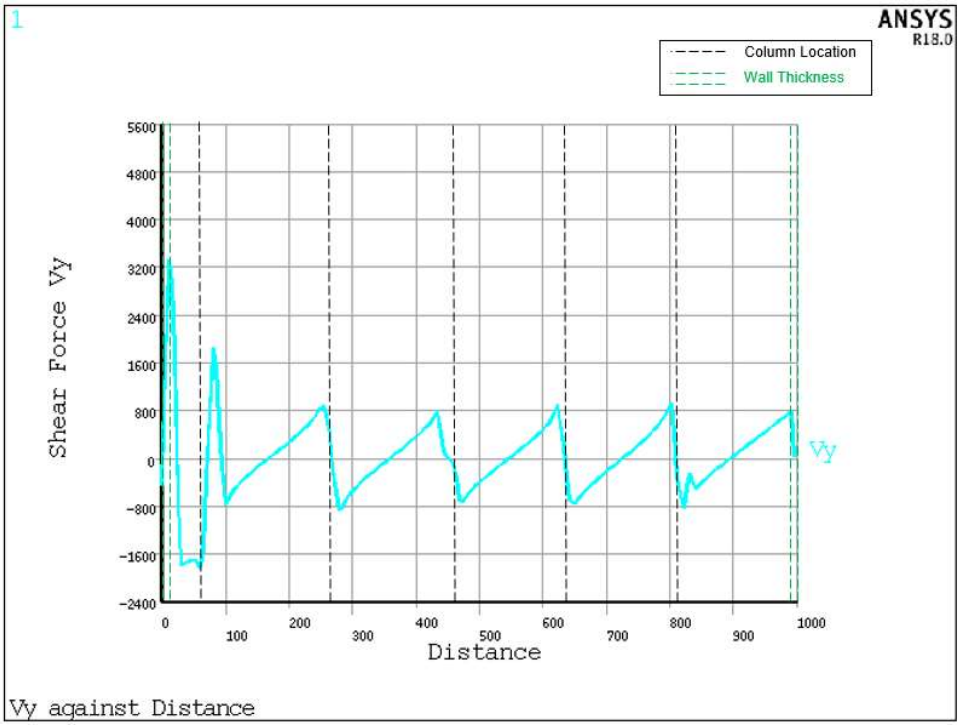

Figure 4.10-11: Graph of Integrated Shear Force (lb) for REDOX Filter – Roof Slab

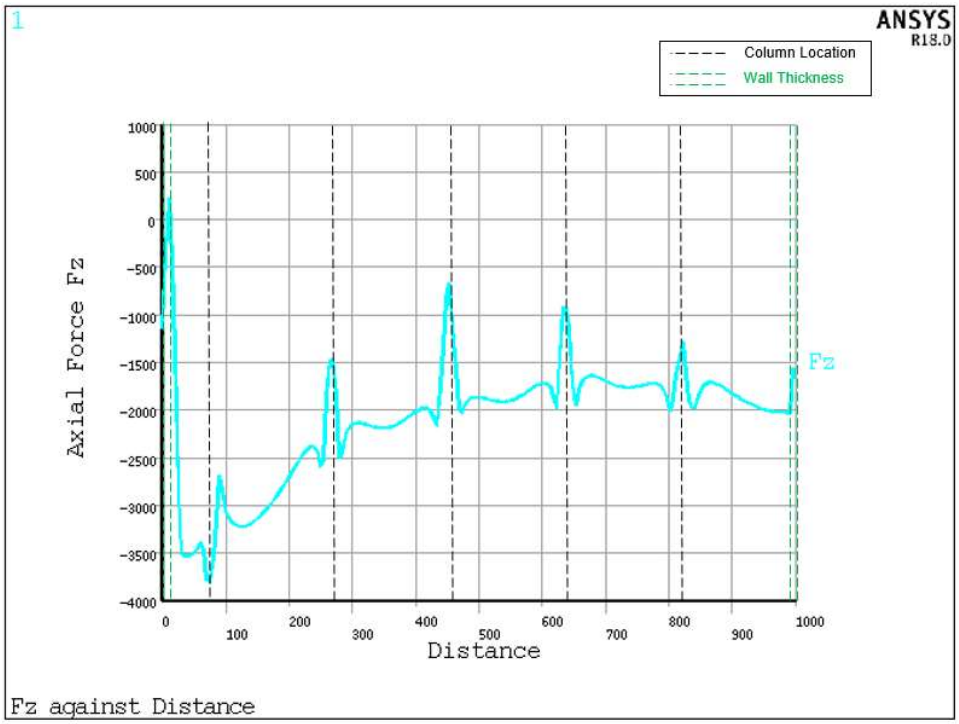

Figure 4.10-12: Graph of Integrated Axial Force (lb) for REDOX Filter – Roof Slab

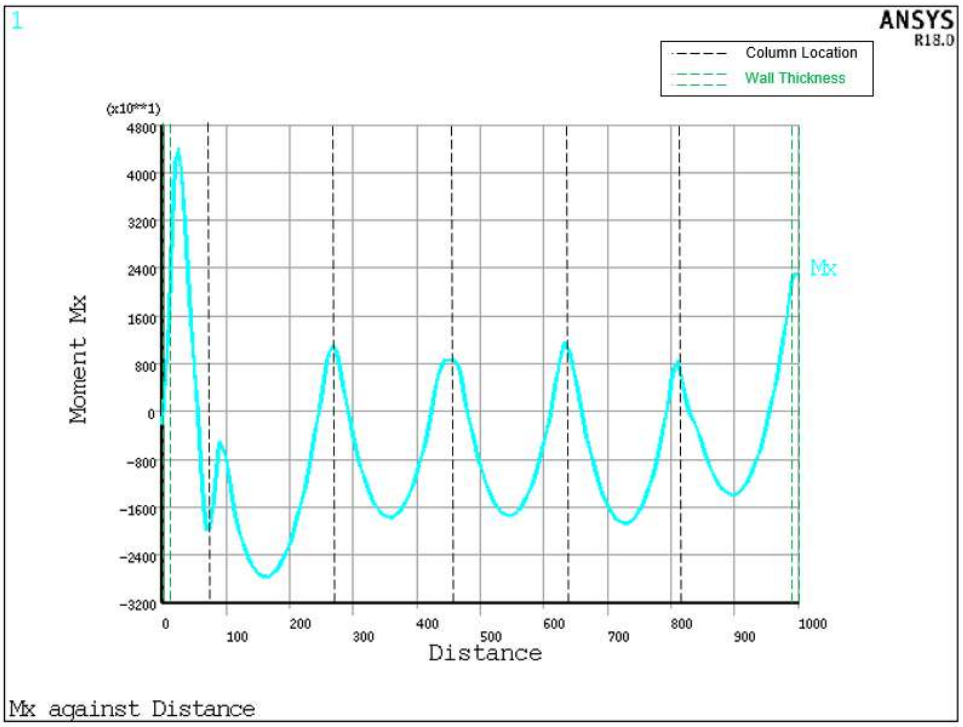

Figure 4.10-13: Graph of Integrated Bending Moment (in.-lb) for REDOX Filter – Roof Slab

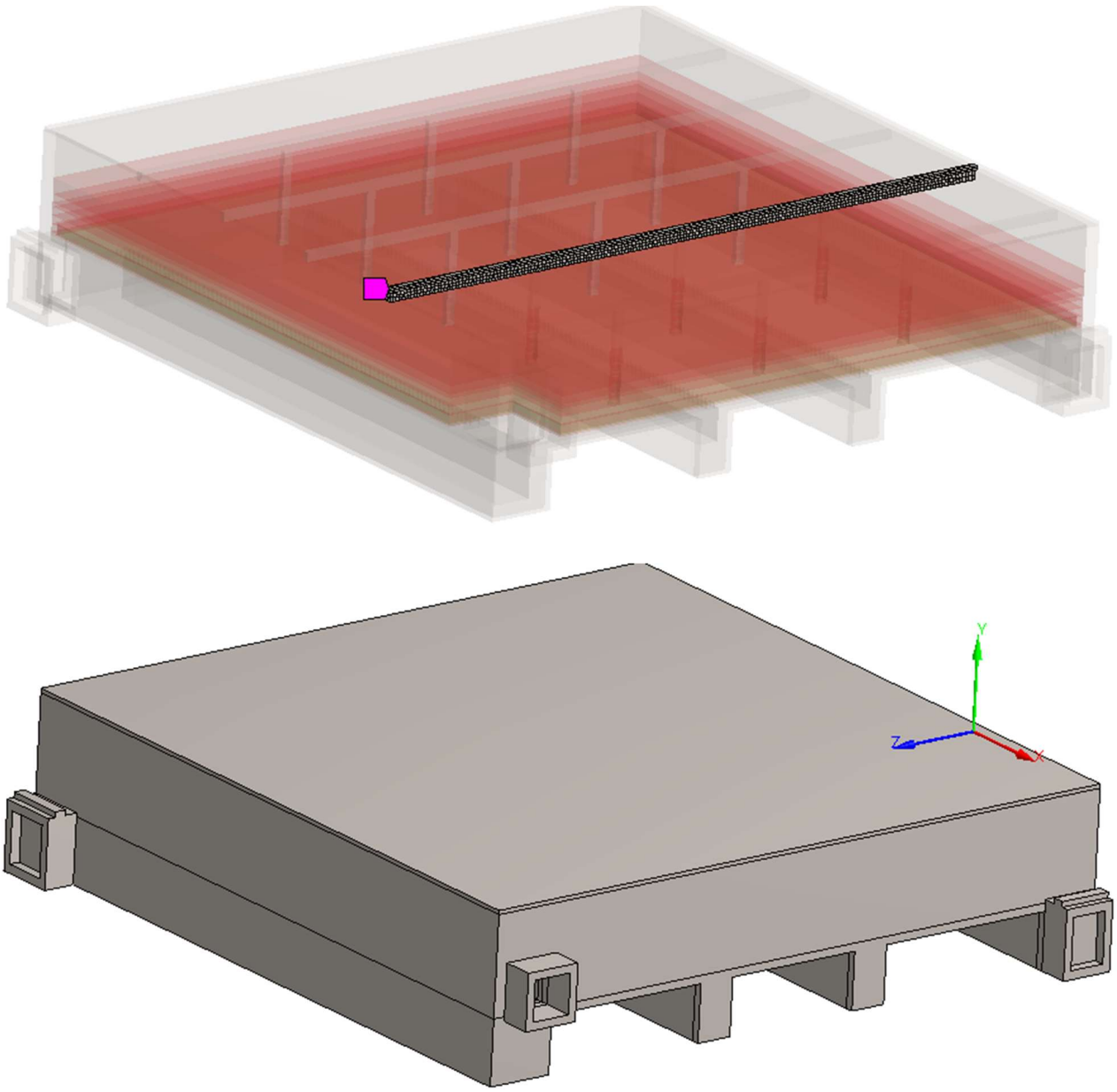

Figure 4.10-14: Strip Location and Coordinates for Integrated Stresses for REDOX Filter – Roof Beam

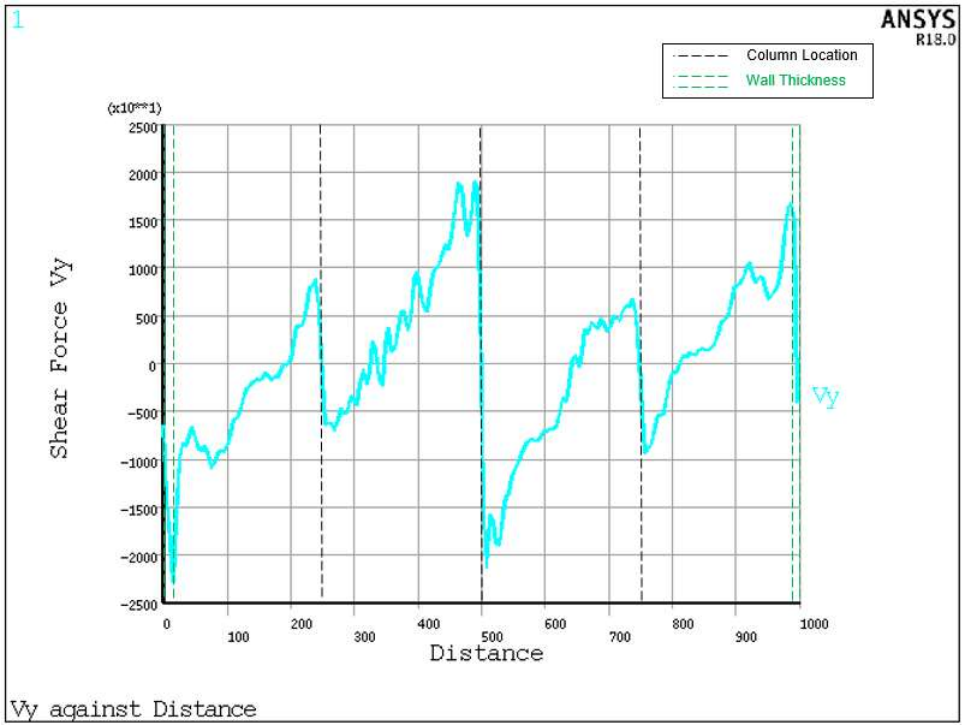

Figure 4.10-15: Graph of Integrated Shear Force (lb) for REDOX Filter – Roof Beam

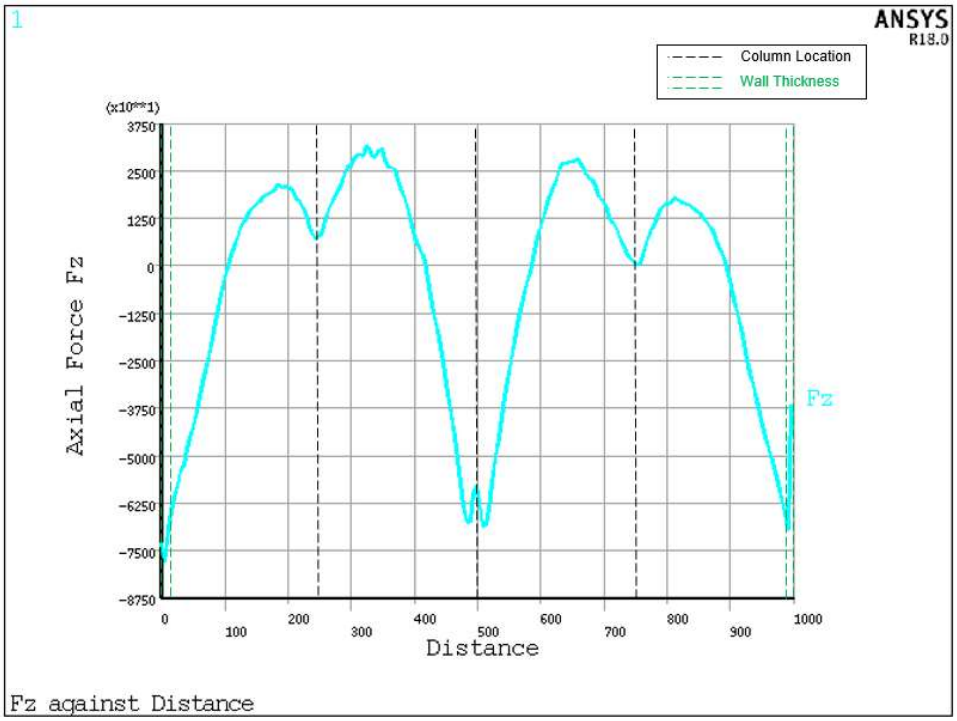

Figure 4.10-16: Graph of Integrated Axial Force (lb) for REDOX Filter – Roof Beam

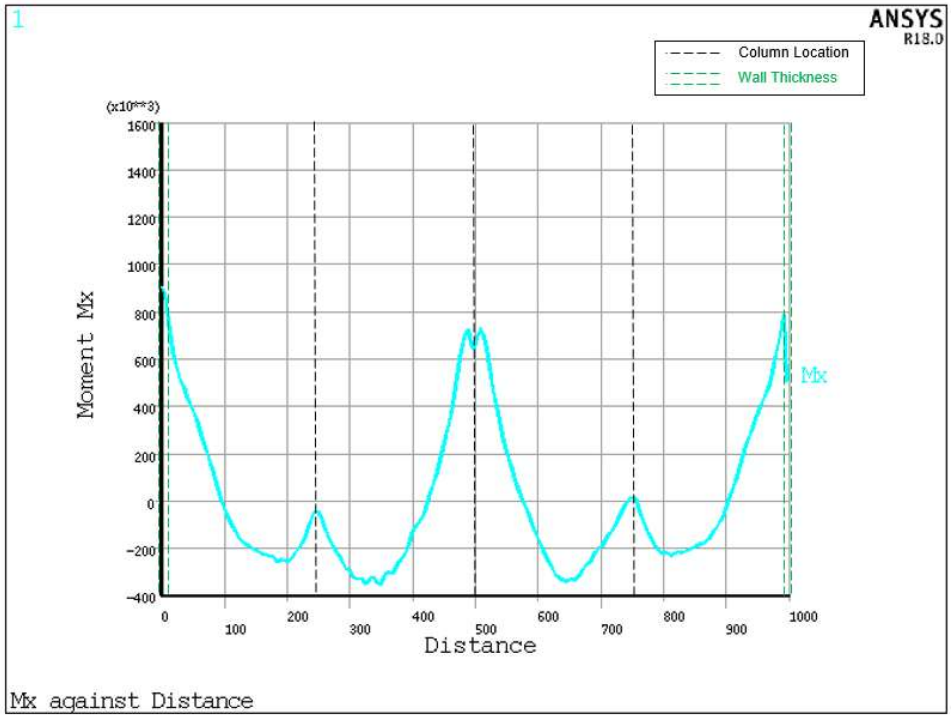

Figure 4.10-17: Graph of Integrated Bending Moment (in.-lb) for REDOX Filter – Roof Beam

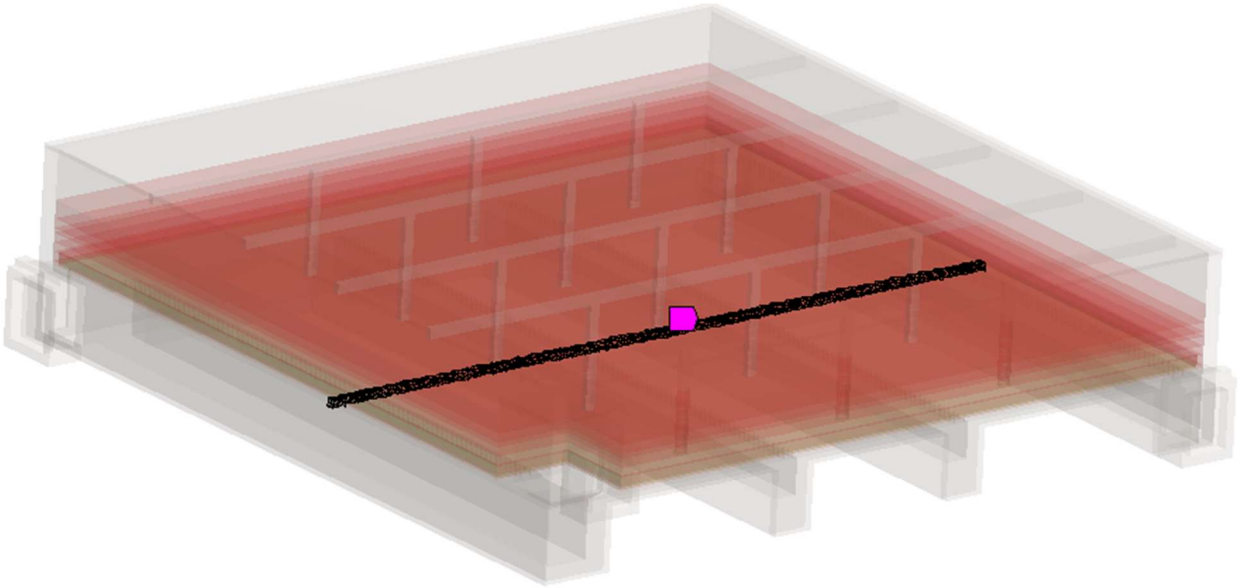

(1 ft wide slice of elements)

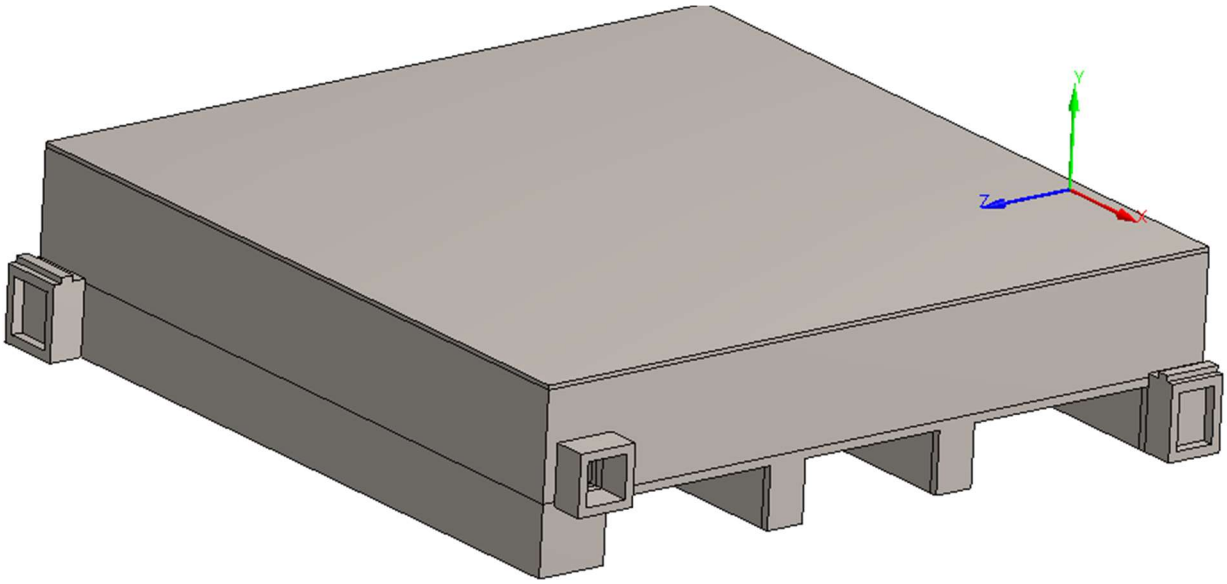

Figure 4.10-18: Strip Location and Coordinates for Integrated Stresses for REDOX Filter – Floor Slab

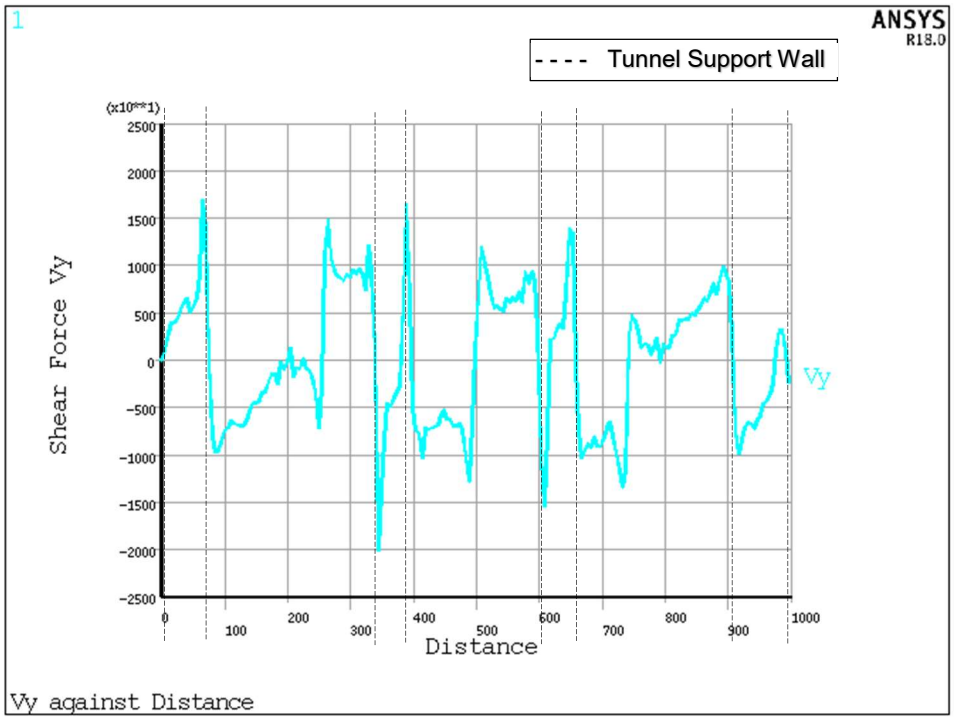

Figure 4.10-19: Graph of Integrated Shear Force (lb) for REDOX Filter – Floor Slab

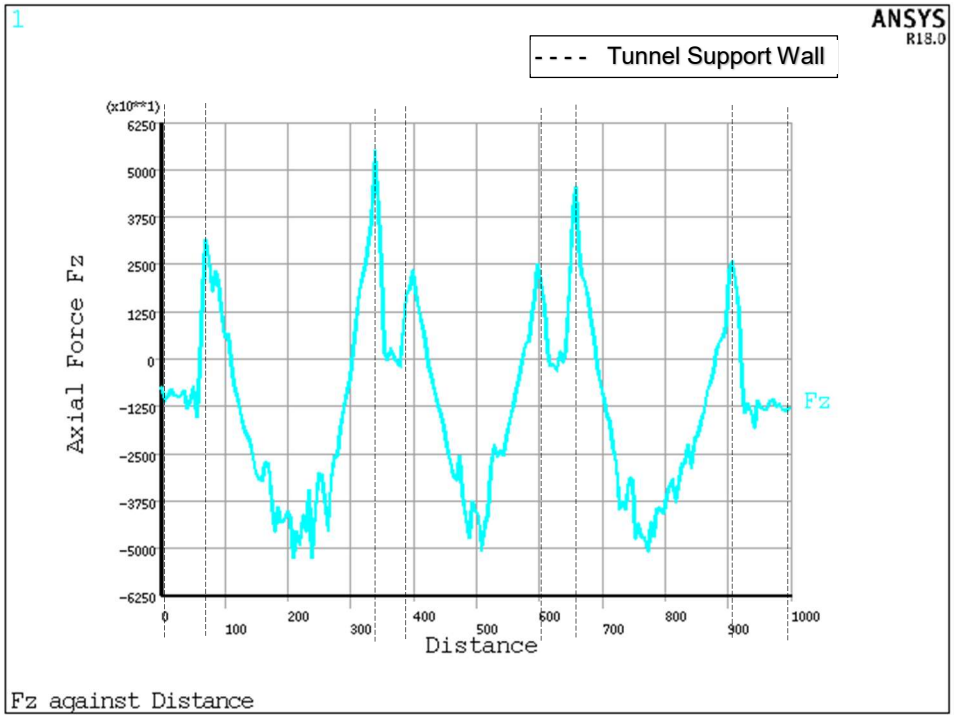

Figure 4.10-20: Graph of Integrated Axial Force (lb) for REDOX Filter – Floor Slab

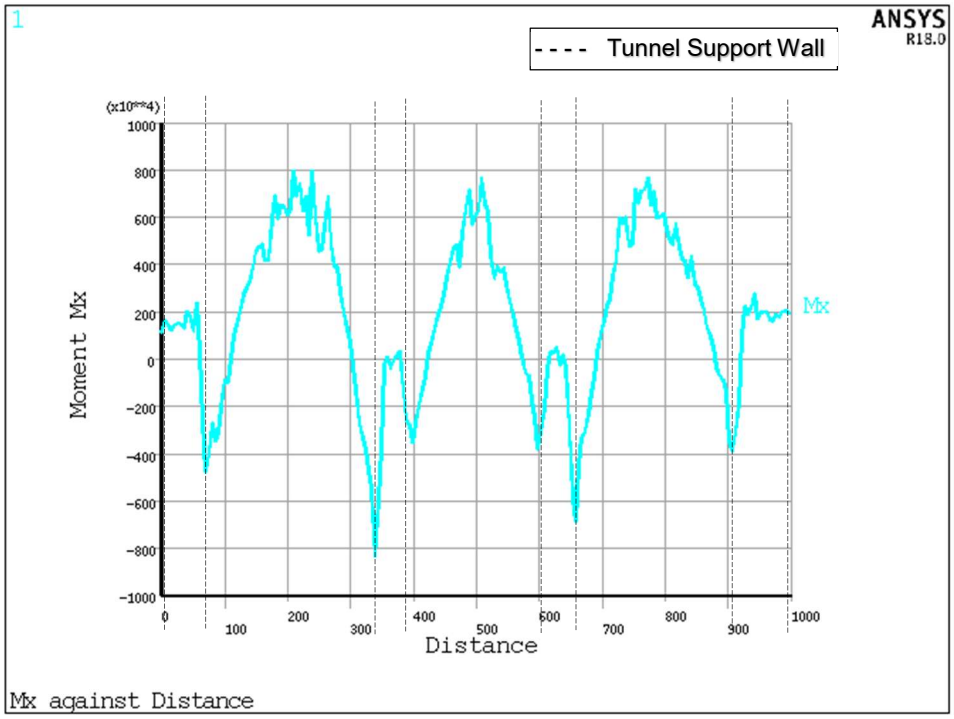

Figure 4.10-21: Graph of Integrated Bending Moment (in.-lb) for REDOX Filter – Floor Slab

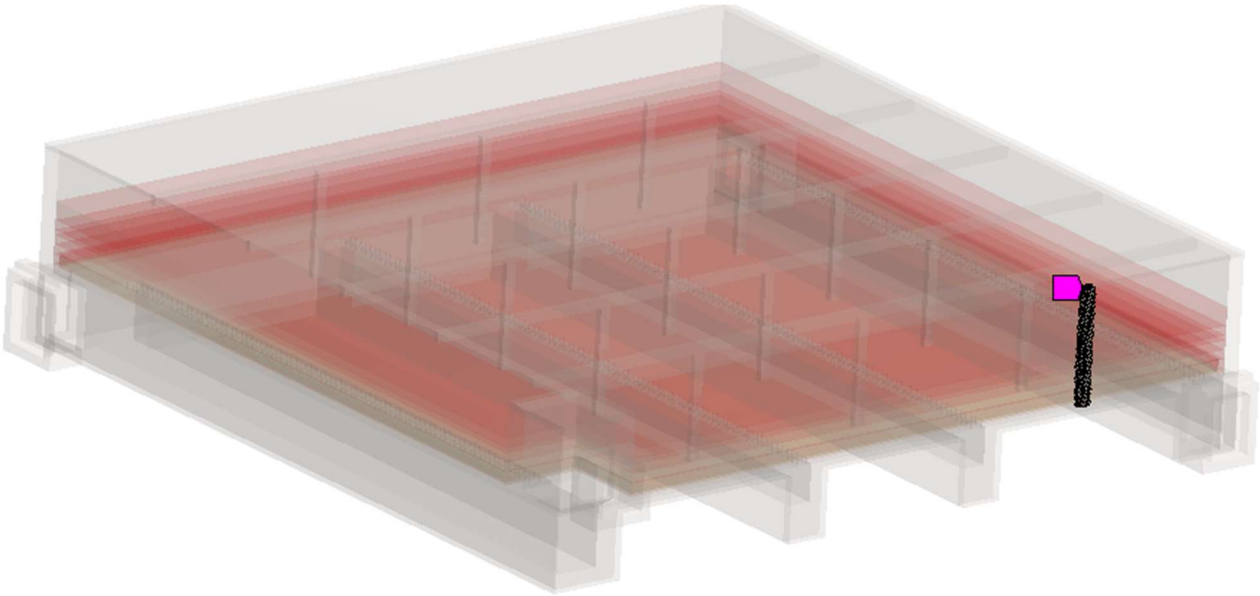

(1 ft wide slice of elements)

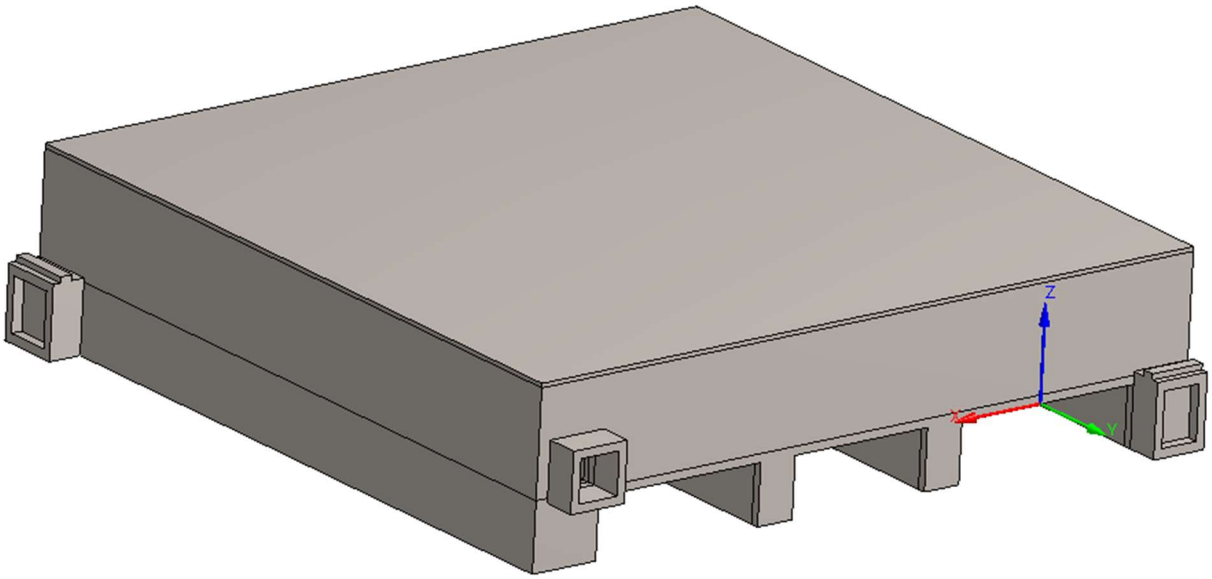

Figure 4.10-22: Strip Location and Coordinates for Integrated Stresses for REDOX Filter – Wall

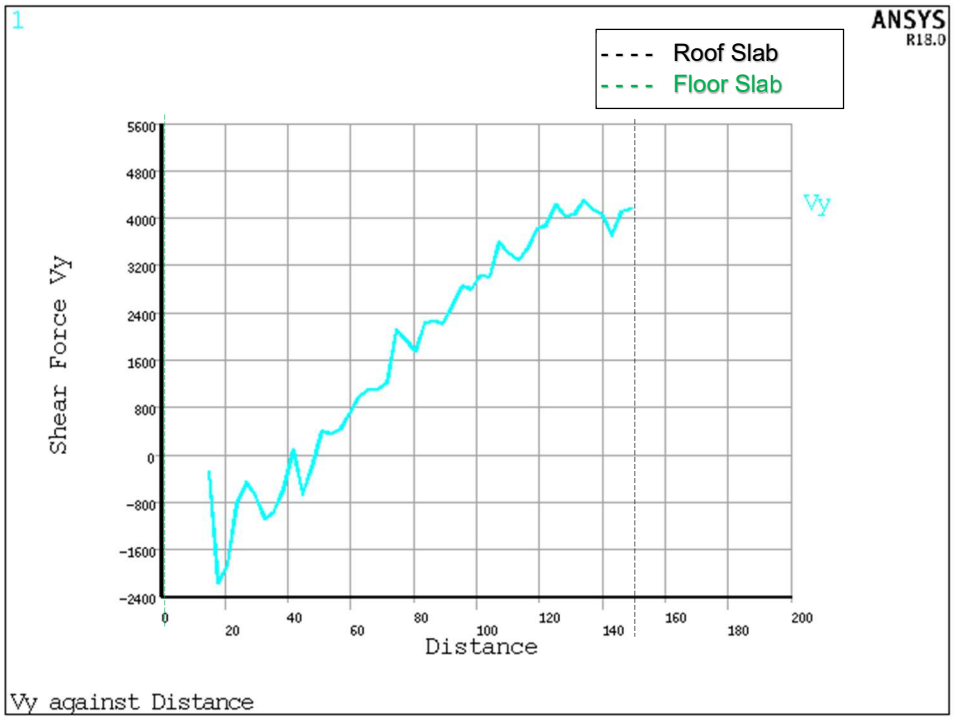

Figure 4.10-23: Graph of Integrated Shear Force (lb) for REDOX Filter – Wall

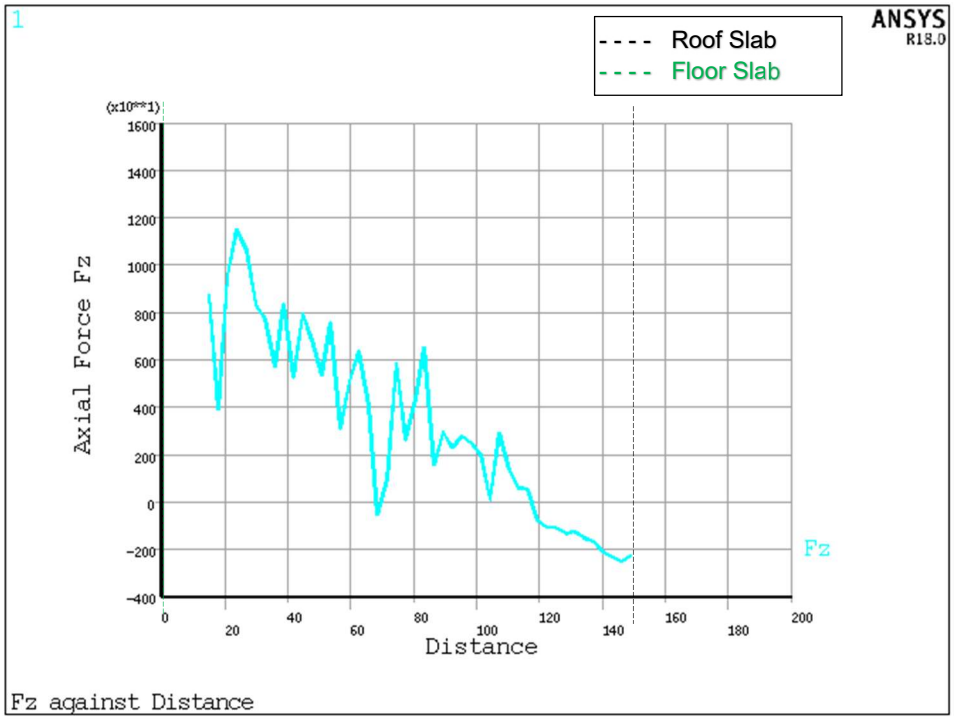

Figure 4.10-24: Graph of Integrated Axial Force (lb) for REDOX Filter – Wall

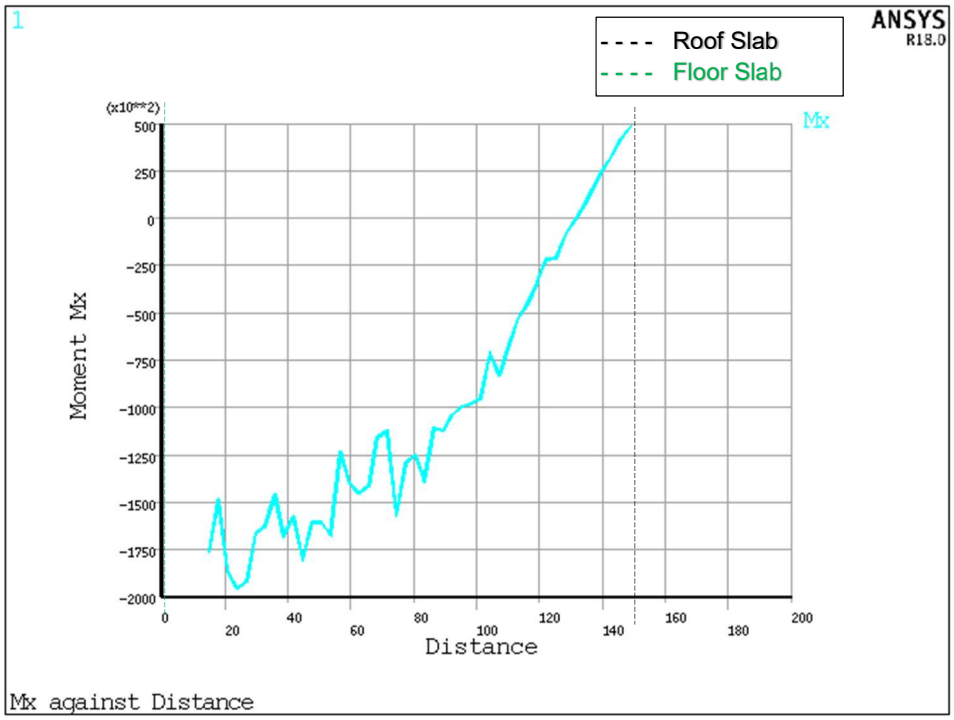

Figure 4.10-25: Graph of Integrated Bending Moment (in.-lb) for REDOX Filter – Wall

4.11 Structure 241-CX-70, Group O3

Detailed structural drawings for 241-CX-70 were used to obtain concrete geometry and rebar information.

Deformation of the structure is shown in Figure 4.11-1, which indicates a maximum deflection of 0.12 in. at the center of the roof. Contour plots of maximum tension and compression stresses are given in Figure 4.11-2 and Figure 4.11-3. Contour plots of shear stress are in Figure 4.11-4. Contour plots of the hoop stresses are in Figure 4.11-5. Graphs of shear force, axial force, and bending moments along the most critical 12 in. wide strip (of the roof and the vertical wall) are included in Figure 4.11-6 through Figure 4.11-13. The following table summarizes the maximum demand stresses and integrated forces and moments for the roof and walls.

	Rebar	Steel Area per 12 in. width (in.^{2})	Thickness x Cover	Max Tension (psi)	Max Compression (psi)
Roof radial @ center	#8@6	1.57	12 in. x 2 in.	1,454	1,000
Roof radial @ wall	#4@16	0.15	12 in. x 2 in.	1,454	2,712
Wall vertical At roof	#6@12	0.44	13 in. x 2 in.	727	800
Wall hoop Inside face (3)	#5@11	0.2	13 in. x 2.75 in.	--	412
Wall hoop Outside face (3)	#5@11	0.34	13 in. x 2.75 in.	--	412

(1) Wall maximum vertical stresses occur at the roof junction and are enveloped
(2) Cover was taken to be from concrete face to edge of rebar
(3) Rebar are total of 19 over the 16 ft - 3 in. (195 in.) height of the wall. Thus, the spacing is 195 in. / 18 = 10.8 in., use 11 in.

The section axial and bending capacities are per standard ACI Code equations below, respectively:

$\phi Pn = 0.7 \times 0.85 (0.85 \times fc (A_{cross} - As) + fy (As))$

$\phi Mn = 0.9 \times As\ fy \{d - As\ fy / (2 \times 0.85\ fc\ b)\}$

Where:

fc = 3,000 psi compressive strength of concrete

fy = 40,000 psi yield strength of reinforcing steel

b = 12 in. section width

As = rebar cross-sectional area

d = thickness (depth) – cover – half rebar size

A_{cross} = thickness x 12 in. (for standard 12 in. wide strip)

The results of the calculation are summarized in the following table.

	Demand Bending Moment (in.-lb)	**Demand Axial Force (lb)**	**Moment Capacity (in.-lb)**	**Axial Capacity (lb)**
Roof radial @ center	250,000	-	479,156	-
Roof radial @ wall (1)	360,000	-	51,179	-
Wall vertical @ roof	400,000	-	164,391	-
Wall hoop inside face	-	64,270(2)	-	229,787
Wall hoop outside face	-	64,270(2)	-	229,787

(1) Note that there is extra rebar from the wall reinforcement that extend into the top face of the roof slab. This rebar, however, does not extend far enough to provide the required moment resistance in the slab section at the wall junction. This is evident by review of the extent of the roof positive moment (Figure 4.11-9) relative to the wall rebar extended length of 3 ft and 3 in. per [2, H-2-4321-1 & H-2-4322-1].

(2) Demand axial in the wall (hoop) is taken as the maximum compression hoop stress listed in the previous table times the wall hoop strip sectional area (12 x 13 in.).

These results show the bending moment capacity is significantly exceeded at the roof wall junction. This is indicative of potential local failure at the roof/wall junction. Additional analysis would be required to assess the extent of such failure.

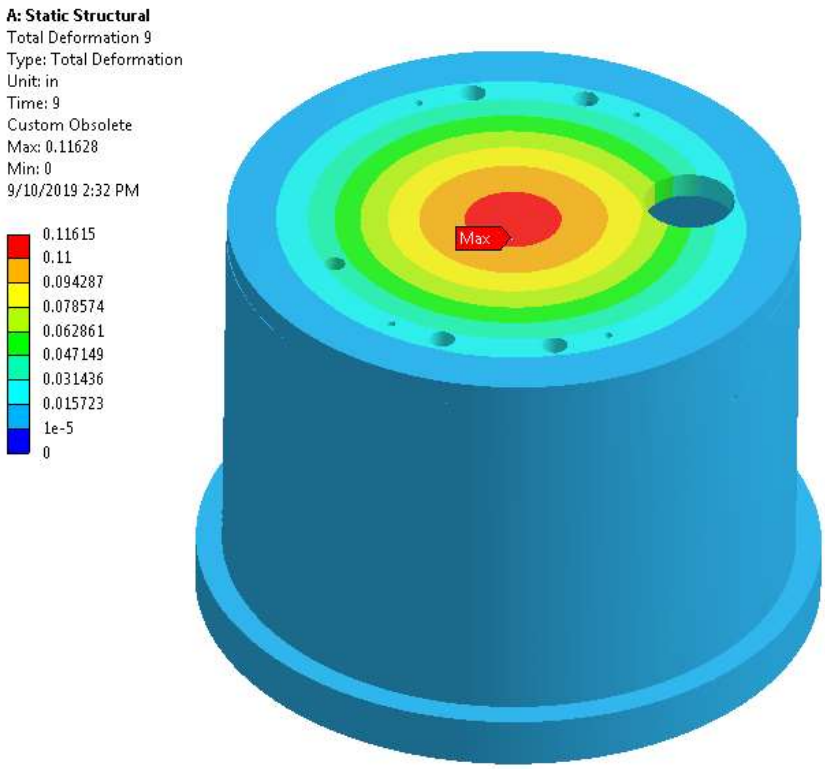

Figure 4.11-1: Contour Plot of Deformations (in.) for 241-CX-70

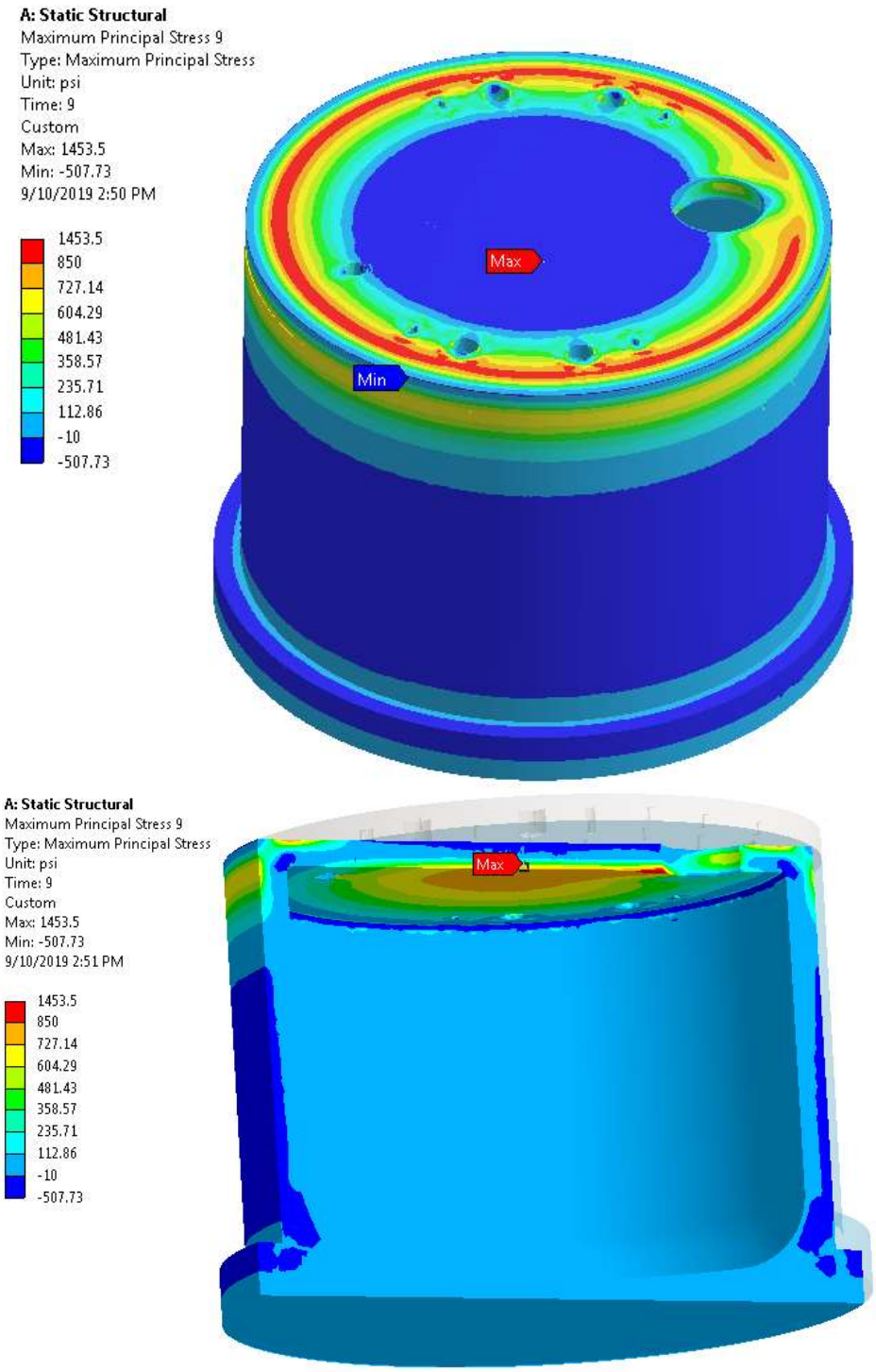

Figure 4.11-2: Contour Plots of Maximum Principal Stresses (psi) for 241-CX-70 – Top Full View, Bottom Sectional View

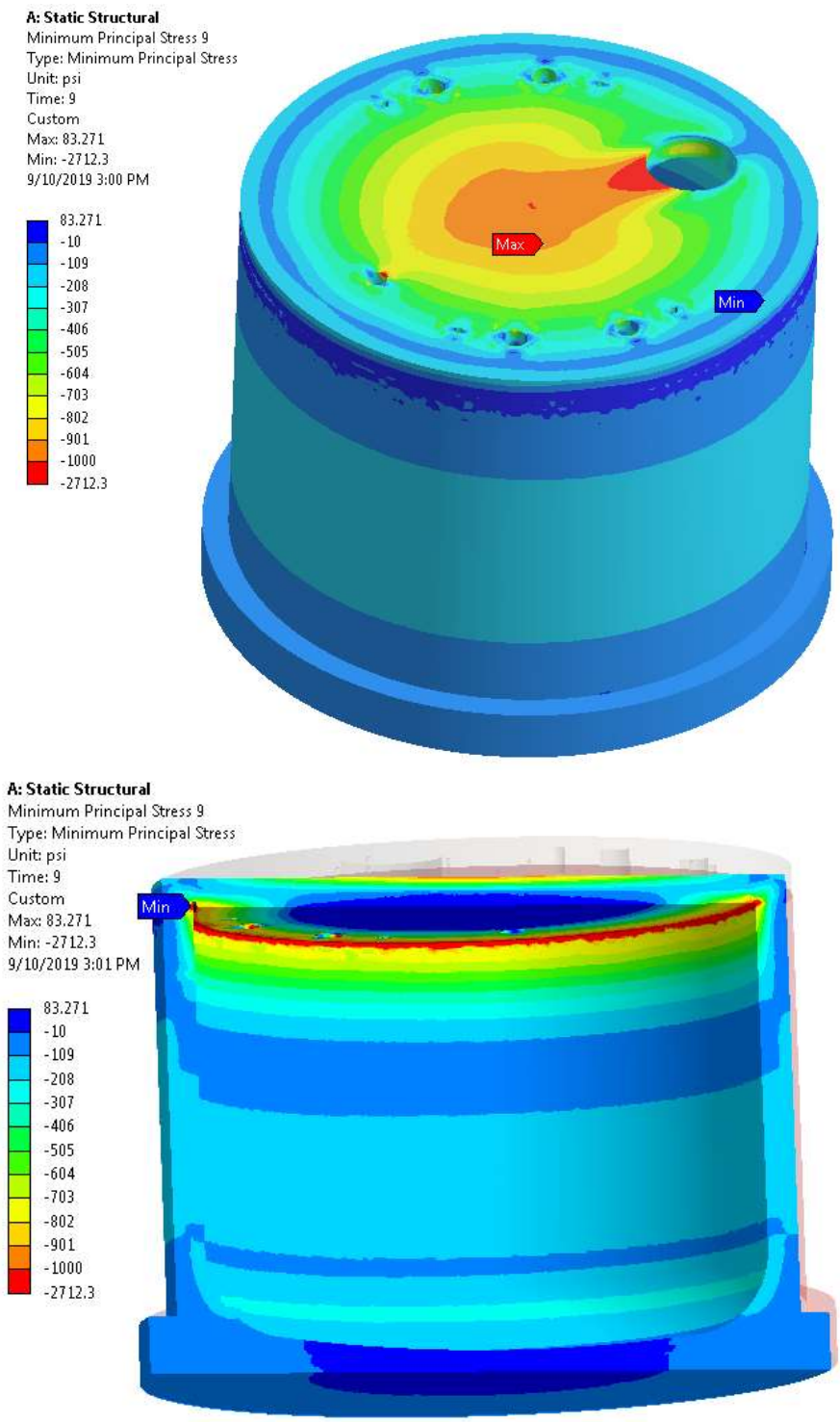

Figure 4.11-3: Contour Plots of Minimum Principal Stresses (psi) for 241-CX-70– Top Full View, Bottom Sectional View

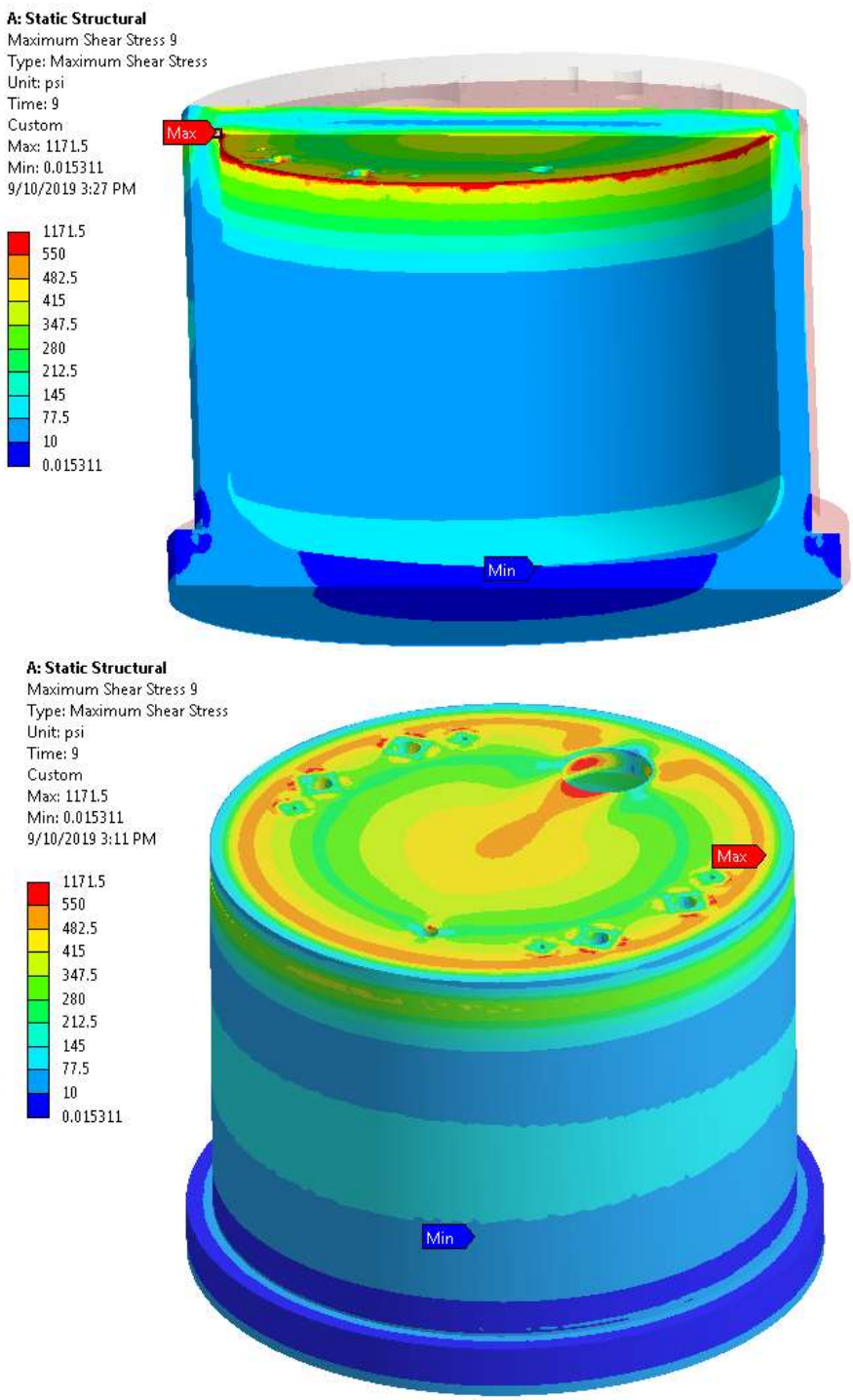

Figure 4.11-4: Contour Plots of Shear Stresses (psi) for 241-CX-70– Top Full View, Bottom Sectional View

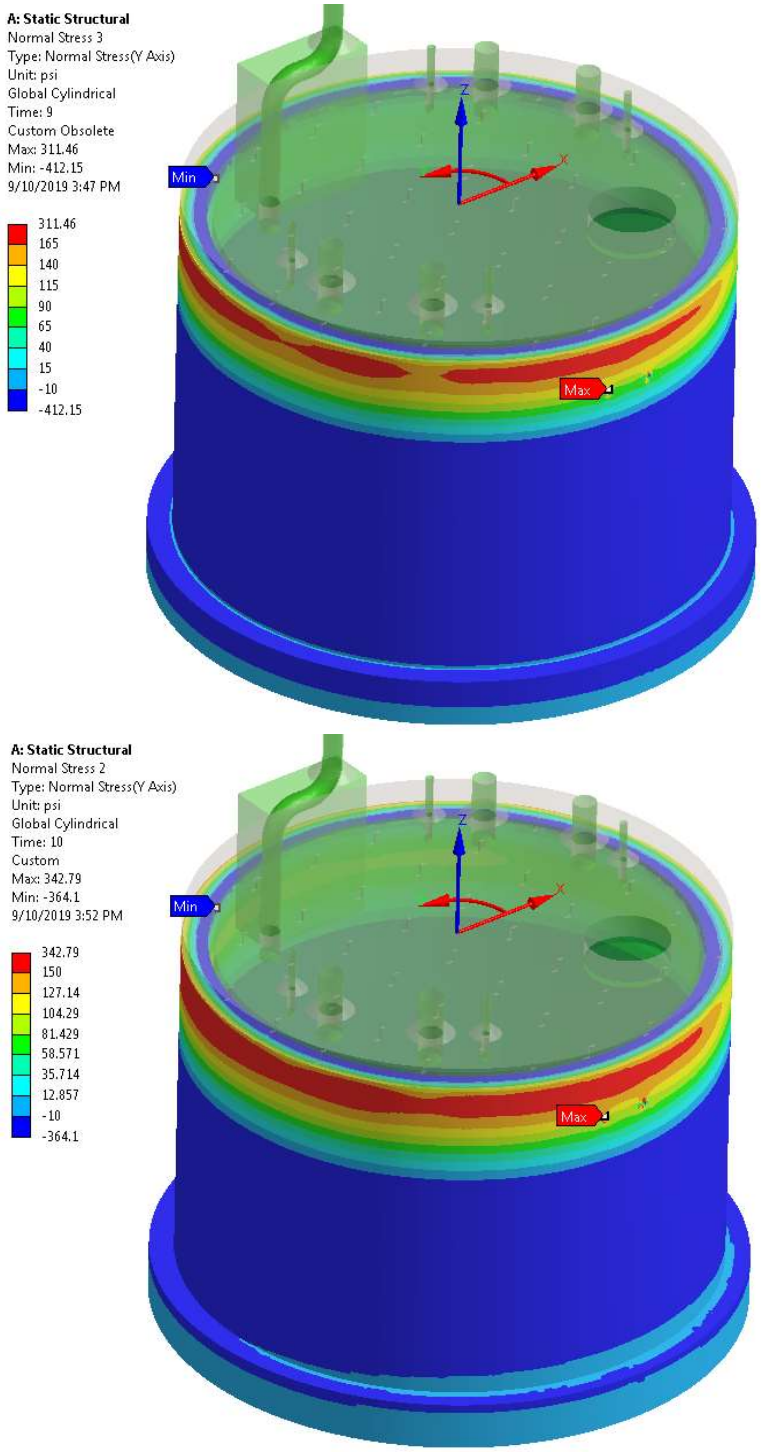

Figure 4.11-5: Contour Plots of Hoop Stresses (psi) for 241-CX-70

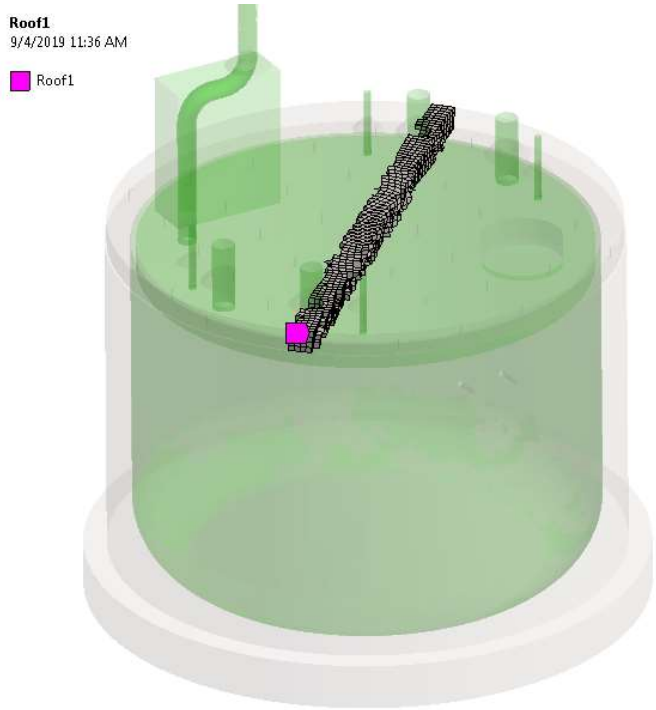

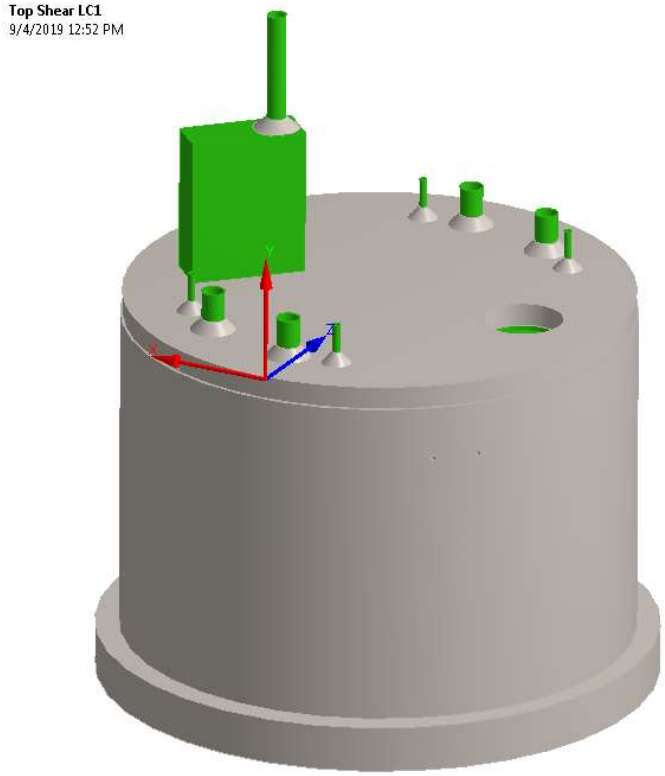

Figure 4.11-6: Roof Strip for Integrated Stresses for 241-CX-70

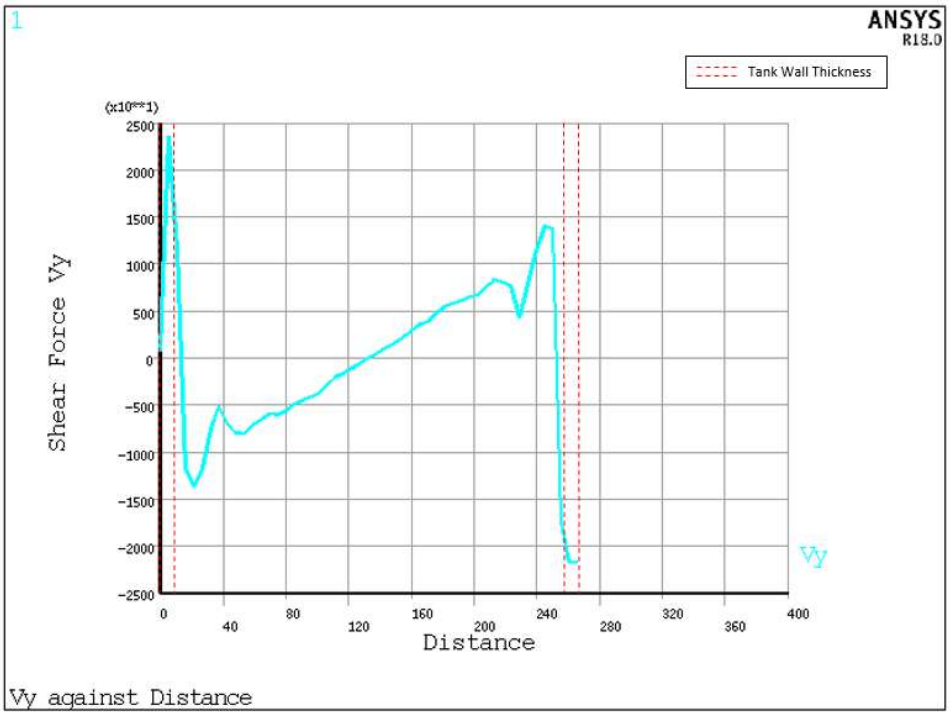

Figure 4.11-7: Graph of Integrated Roof Shear Force (lb) for 241-CX-70

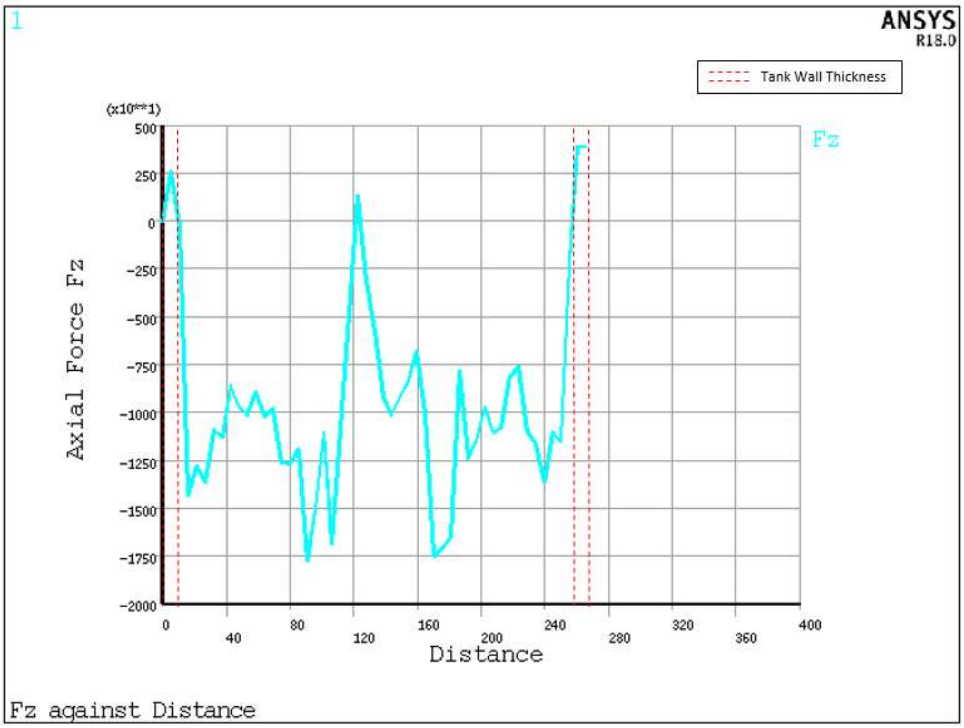

Figure 4.11-8: Graph of Integrated Roof Axial Force (lb) for 241-CX-70

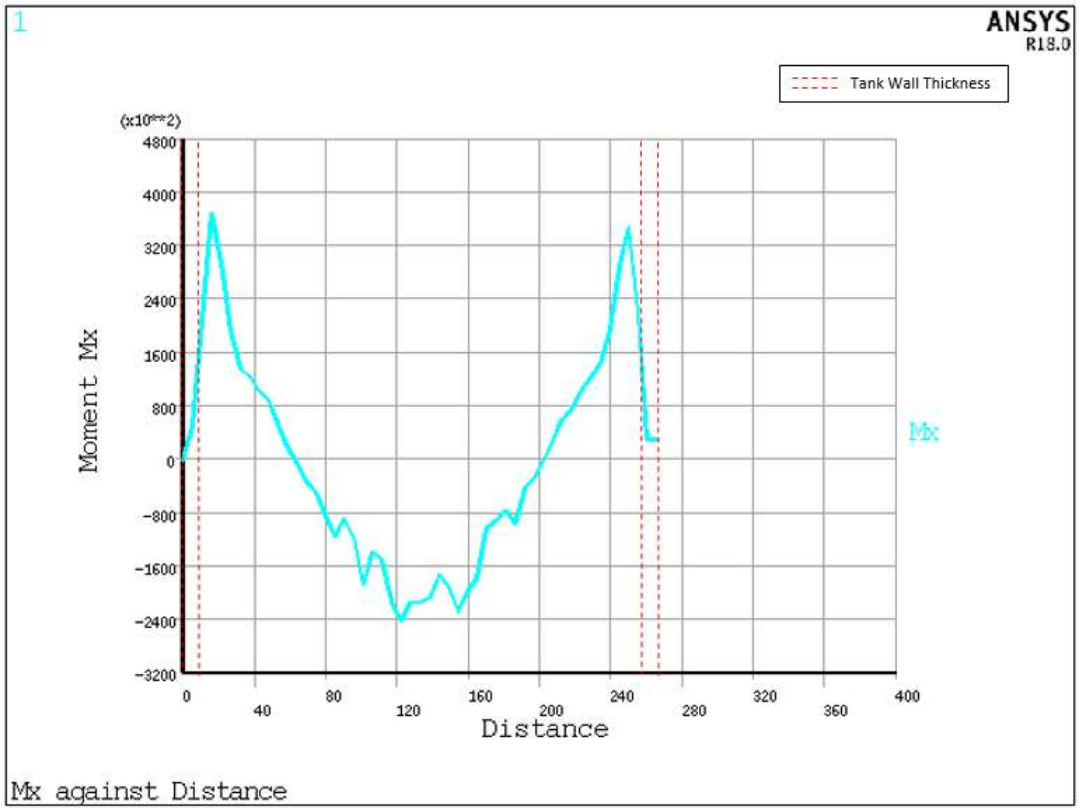

Figure 4.11-9: Graph of Integrated Roof Bending Moment (in.-lb) for 241-CX-70

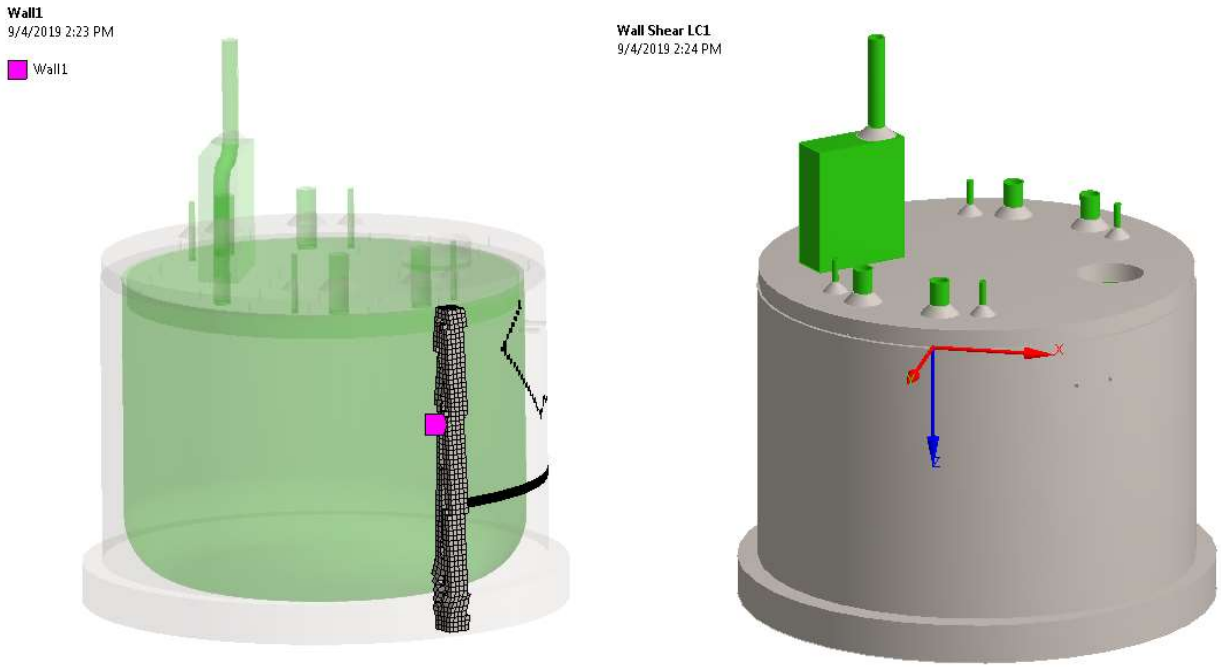

Figure 4.11-10: Wall Vertical Strip for Integrated Stresses for 241-CX-70

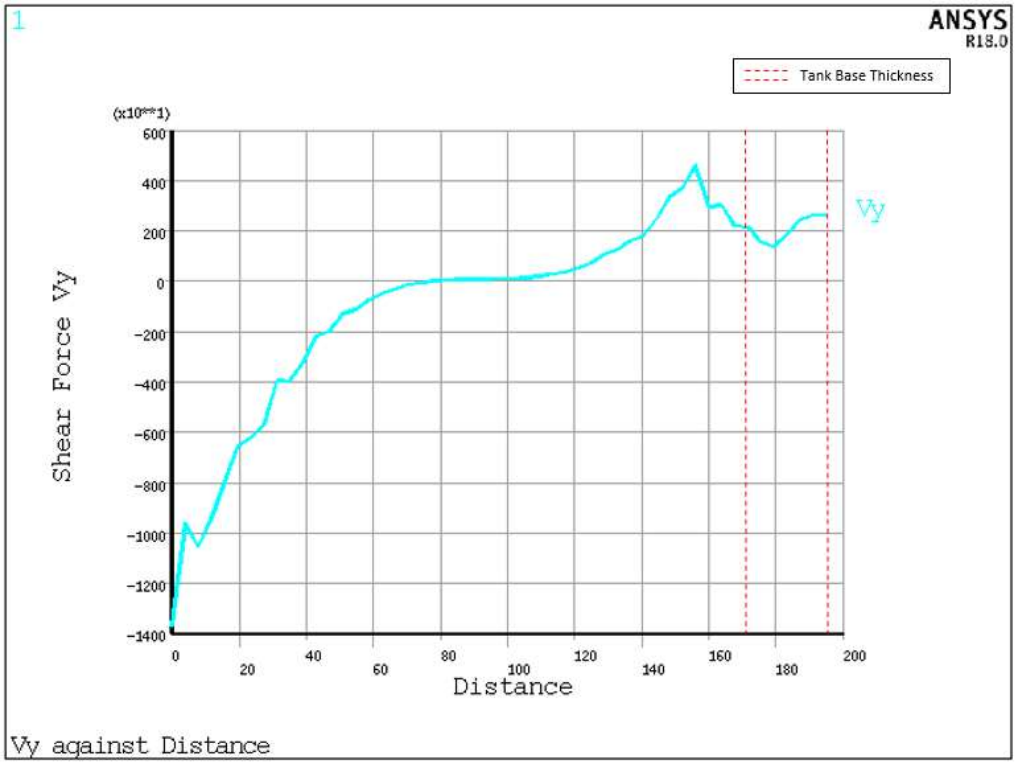

Figure 4.11-11: Graph of Integrated Wall Shear Force (lb) for 241-CX-70

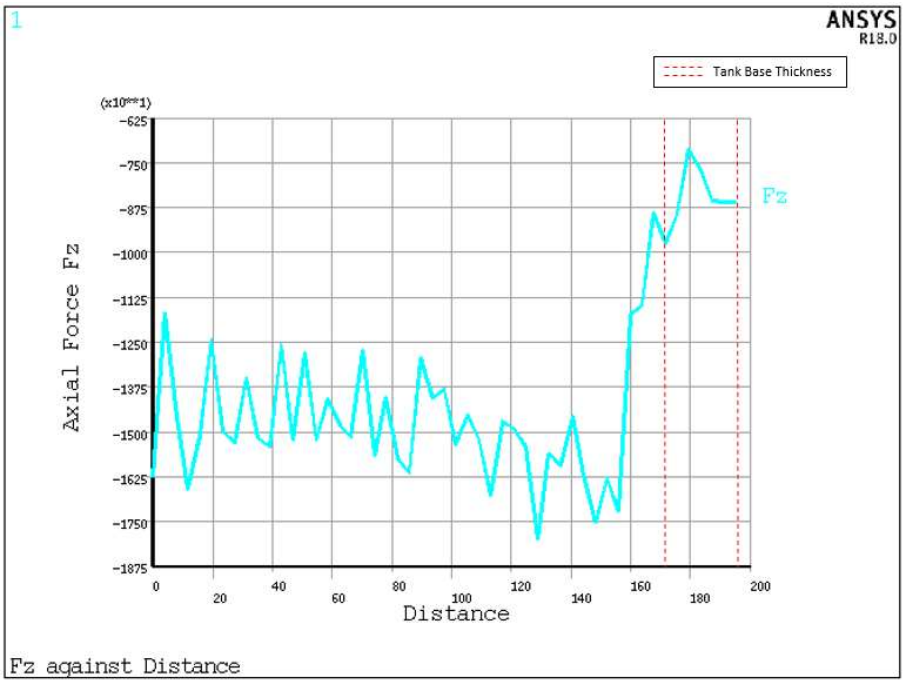

Figure 4.11-12: Graph of Integrated Wall Axial Force (lb) for 241-CX-70

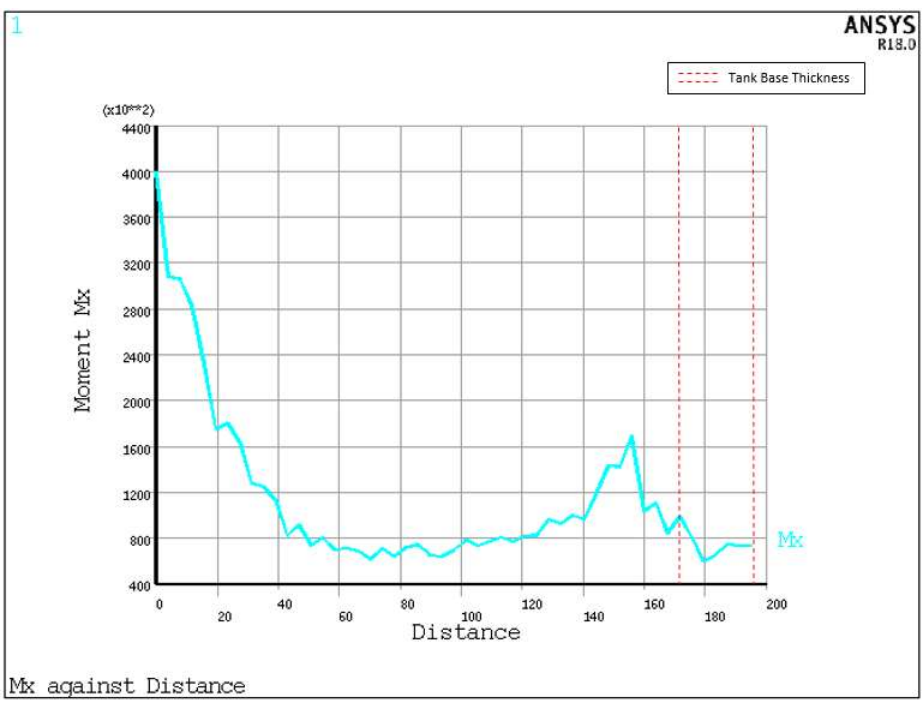

Figure 4.11-13: Graph of Integrated Wall Bending Moment (in.-lb) for 241-CX-70

5. SUMMARY

LPI performed structural analyses of the facilities that were determined to have the highest combined risk and consequence of failure as reported in the "RL-40 Aging Structures Risk Assessment" report [18]. Using a verified and validated version of ANSYS ® software, structural analyses were performed to determine if margin from collapse exists in the structural members. The structural evaluation employed factored load combinations and strength limits based on minimum specified material strength limits to identify the point at which failure is postulated to initiate. Some failures identified may cause only local damage and not necessary lead to larger failures. However, progressive failure analysis was not included in this study. Furthermore, the acceptance strength limits do not represent actual failure limits but, rather, provide some indication of the potential for failure.

As stated above, the evaluations summarized herein are based on current code factored load combinations and strength reductions for steel and concrete. An assessment of the original design requirements was not in the scope of this evaluation. Therefore, the results presented herein should not be used to assess the adequacy of the original design.

Table 5-1 summarizes the results of the present structural evaluation. Results are based on the available information (drawings [2], and "RL-40 Aging Structures Risk Assessment" report [18]), inputs, and assumptions reported herein (see Section 3, 4, and Appendix A). Several assumptions were required in order to perform the structural evaluation, because information was very limited for several of the facilities (e.g., 241-T-361, refer to Table 3-2). The structural calculations presented herein address the overall structural stability of the underground structures in the scope of work and should not be used to justify worker safety. Accordingly, the results presented in this report should be assessed within the context of the available information and applied assumptions.

The impact of structural failure for structures shown in Table 5-2 was qualitatively evaluated in the "RL-40 Aging Structures Risk Assessment" report (Rev. 2) [18].

Table 5-1: Structural Evaluation Margin-to-Failure Results

Group	Structure	Acceptable (Y/N)	Discussion
C1	216-Z-2	Y	-
C2	216-B-12	N	Bending and shear stresses are above failure limit.
C3	216-Z-6	N	Overstress in shear
C4	216-Z-7	Y	-
C5	216-Z-9	N	Overstress in slab and column flexure
T1	241-T-361	Y	No information is available for the prestressing and rebar.
T2	241-Z-361	N	Moment and shear limits are exceeded at bottom of long walls. This will likely cause limited local failure. Failure will not progress due to the redundancy available in the box structure.
T3	241-Z-8	Y	Some yielding may take place.
O1	PUREX deep bed filters	Y	-
O2	REDOX sand filter	Y	-
O3	241-CX-70	N	Local yielding of top radial rebar in the roof at the wall junction and in the wall at the top. The yielding may cause relieving of local stresses and limit damage progression.

Table 5-2: RL-40 Aging Structures Evaluated in [18] (2 Sheets)

Group	Structure	Date Constructed	Caved-In, Subsidence	Depth of Soil Overburden	Type of Construction	Approximate Size (ft)	Facility Hazard Classification
C1	216-B-7A/B	1945	No	24 feet	Timber Crib Box	12W x 12W x 4H	Exempt
	216-B-8	1944	Yes	16 feet	Timber Crib Box	12W x 12W x 7H	Exempt
	216-B-9	1948	No	22 feet	Timber Crib Box	14W x 14W x 7H	Exempt
	216-B-10A/B	1948	Yes	16 feet	Timber Crib Box	12W x 12W x 3.5H	Exempt
	216-T-6	1945	Yes	16 feet	Timber Crib Box	12W x 12W x 4H	Exempt
	216-T-7	1947	No	19 feet	Timber Crib Box	12W x 12W x 7H	Exempt
	216-T-8	1949	Yes	16 feet	Timber Crib Box	12W x 12W x 4H	Exempt
	216-T-19	1950	Yes	21 feet	Timber Crib Box	12W x 12W x 9H	Exempt
	216-T-32	1945	No	22 feet	Timber Crib Box	12W x 12W x 4H	Exempt
	216-U-1	1950	No	16 feet	Timber Crib Box	12W x 12W x 4H	Exempt
	216-U-2	1950	No	16 feet	Timber Crib Box	12W x 12W x 4H	Exempt
	216-U-8	1951	Yes	16 feet	Timber Crib Box	16W x 16W x 10H	Exempt
	216-Z-1	1948	Yes	6 feet	Timber Crib Box	12W x 12W x 14H	Exempt
	216-Z-2	1948	No	6 feet	Timber Crib Box	12W x 12W x 14H	Exempt
	216-Z-5	1945	No	14 feet	Timber Crib Box	12W x 12W x 4H	Exempt
C2	216-B-12	1951	Yes	15 feet	Timber Crib Box	16W x 16W x 10H	Exempt
C3	216-Z-6	1945	Yes	6 feet	Timber Trench Box	50L x 6.5W x 4H	Exempt
C4	216-Z-7	1946	No	6 feet	Timber Trench Box	150L x 8W x 3H	Exempt
C5	216-Z-9	1955	No	None	Concrete Covered Crib	120L x 90W x 20H	2
T1	241-B-361	1944	No	6 feet	Cylindrical Concrete Tank	20D x 19H	Exempt
	241-T-361	1944	No	6 feet	Cylindrical Concrete Tank	20D x 19H	Exempt
	241-U-361	1951	No	6 feet	Cylindrical Concrete Tank	20D x 19H	Exempt
T2	241-Z-361	1948	No	2 feet	Rectangular Concrete Tank	28L x 15W x 19H	2

Table 5-2: RL-40 Aging Structures Evaluated in [18] (2 Sheets)

Group	Structure	Date Constructed	Caved-In, Subsidence	Depth of Soil Overburden	Type of Construction	Approximate Size (ft)	Facility Hazard Classification
T3	241-Z-8	1954	No	6 feet	Cylindrical Steel Tank	40L x 8D	Exempt
O1	PUREX Deep Bed Filters	1954	No	4 feet	Rectangular Concrete Vault	82L x 52W x 13H	2
O2	REDOX Sand Filter	1950	No	None	Rectangular Concrete Vault	85L x 85W x 20H	2
O3	241-CX-70	1951	Yes	11 feet	Cylindrical Concrete Tank	20D x 15H	Exempt

6. REFERENCES

1. TerraGraphics Environmental Engineering, Inc. Master Services Agreement, Subcontract Number: S18-1055, "RL-40 Aging Structures Structural Risk Analysis," October 25, 2018.

2. U.S. Atomic Energy Commission, Richland Operations Drawings
   - H-2-346, Sh. 01, 1973, 216-Z-5 Crib Additional Waste Disposal for Bldg 231-3, Rev. 3, Hanford Engineer Works, Richland, Washington.
   - H-2-353, Sh. 01, 1973, Waste Disposal Cribs 216-T-6, 216-T-8 Cribs & Reverse Wells 216-T-3 & T2, Rev. 3, Hanford Engineer Works, Richland, Washington.
   - H-2-508, Sh. 01, 1973, 216-Z-6 Crib – Temporary Effluent Disposal Trench – 231-Z Bldg, Rev. 2, Hanford Engineer Works, Richland, Washington.
   - H-2-511, Sh. 01, 1973, 216-Z-7 Crib – Permanent Disposal Trench Near 231-Z Bldg, Rev. 4, Hanford Engineer Works, Richland, Washington.
   - H-2-558, Sh. 01, 1973, 216-T-32 & 216-B-7A & 7B & 201 TK Baffle Modifications, Rev. 2, Hanford Engineer Works, Richland, Washington.
   - H-2-578, Sh. 01, 1973, Waste Disposal System Plan & Details 241-T, 216-T-32, T-7, Rev. 5, Hanford Engineer Works, Richland, Washington.
   - H-2-579, Sh. 01, 1973, Waste Disposal System Plan & Details 241-B, Rev. 12, Hanford Works, Richland, Washington.
   - H-2-738, Sh. 01, 1973, Contaminated Pump Run-in Caisson – Located in 216-B-8 Tile Field, Rev. 1, General Electric Co., Hanford Works, Richland, Washington.
   - H-2-806, Sh. 01, 1975, 18 Tank Farm Finish Grading & Facilities, Rev. 6, General Electric Co., Hanford Works, Richland, Washington.
   - H-2-821, Sh. 01, 1973, Timber Crib and Piping Details 216-T-19, Rev. 7, U.S. Atomic Energy Commission, Richland Operations, Richland, Washington.
   - H-2-1031, Sh. 01, 2017, 216-B-5 Reverse Well, 216-B-9 Crib and Tile Field – Plan & Details, Rev. 16, Hanford Works, Richland, Washington.
   - H-2-1124, Sh. 01, 2017, Well Locations 241-T-TX & 361 Areas, Rev. 0, Hanford Works, Richland, Washington.
   - H-2-1649, Sh. 01, 2017, 216-B-10-A & 216-B-10-B Cribs, Rev. 3, General Electric Co., Hanford Works, Richland, Washington.
   - H-2-1722, Sh. 01, 1973, Drain Line for Contaminated Waste 292-B to Cribs 216-B-10-A & B, Rev. 4, General Electric Co., Hanford Works, Richland, Washington.
   - H-2-1748, Sh. 01, 1949, Tanks 241-301 & 361 Riser & Nozzle Elevs., Rev. 0, General Electric Co., Hanford Works, Richland, Washington.

- H-2-1749, Sh. 01, 1949, Tanks 241-301 & 361 Riser & Nozzle Elevs., Rev. 0, General Electric Co., Hanford Works, Richland, Washington.
- H-2-1750, Sh. 01, 1949, Tanks 241-301 & 361 Riser & Nozzle Elevs., Rev. 0, General Electric Co., Hanford Works, Richland, Washington.
- H-2-4108, Sh. 01, 1957, Hot Semiworks Drawing Schedule, Rev. 3, U.S. Atomic Energy Commission, Richland Operations, Richland, Washington.
- H-2-4108, Sh. 37, 1957, Hot Semiworks Drawing Schedule, Rev. 3, U.S. Atomic Energy Commission, Richland Operations, Richland, Washington.
- H-2-4319, Sh. 01, 1952, Hot Semiworks Tank Sections TK-70, Rev. 4, General Electric Co., Hanford Works, Richland, Washington.
- H-2-4320, Sh. 01, 1953, Hot Semiworks Tank Liner TK-70, Rev. 3, General Electric Co., Hanford Works, Richland, Washington.
- H-2-4320, Sh. 02, 1950, Hot Semiworks Tank Liner TK-70, Rev. 0, General Electric Co., Hanford Works, Richland, Washington.
- H-2-4321, Sh. 01, 1950, Hot Semiworks Base & Wall Reinforcing TK-70, Rev. 0, General Electric Co., Hanford Works, Richland, Washington.
- H-2-4322, Sh. 01, 1950, Hot Semiworks Dome Reinforcing TK-70, Rev. 0, General Electric Co., Hanford Works, Richland, Washington.
- H-2-4323, Sh. 01, 1950, Hot Semiworks Details TK-70, Rev. 0, General Electric Co., Hanford Works, Richland, Washington.
- H-2-4335, Sh. 01, 1957, Hot Semiworks Waste Liner Bldg 201 C to TK-70, Rev. 6, General Electric Co., Hanford Works, Richland, Washington.
- H-2-5514, Sh. 01, 1974, Exhaust Air Sand Filter Sampler 2718-S Arrgt & Details, Rev. 3, U.S. Atomic Energy Commission, Richland Operations, Richland, Washington.
- H-2-8454, Sh. 01, 1951, Heat & Vent – Plan & Sections Stack Gas Filter, General Electric Co., Hanford Works, Richland, Washington.
- H-2-15491, Sh. 01, 1966, Architectural Waste Disposal Facility Layout, Rev. 3, U.S. Atomic Energy Commission, Richland Operations, Richland, Washington.
- H-2-15492, Sh. 01, 1983, Architectural Waste Disposal Facility Details, Rev. 5, U.S. Atomic Energy Commission, Richland Operations, Richland, Washington.
- H-2-16024, Sh. 01, 1993, Waste Disposal Facilities 241-Z-361 Settling Tank, Rev. 5, General Electric Co., Hanford Works, Richland, Washington.
- H-2-16108, Sh. 01, 1966, Silica Storage Tank & Vent Filter, Rev. 6, U.S. Atomic Energy Commission, Richland Operations, Richland, Washington.

- H-2-16459, Sh. 01, 1973, 216-Z-1A Tile Field 216-Z-1 & 216-Z-2 Cribs, Rev. 8, General Electric Co., Hanford Works, Richland, Washington.
- H-2-16460, Sh. 01, 1975, Waste Disposal Facilities 241-Z-361 Settling Tank Arrgt & Details, Rev. 7, General Electric Co., Hanford Works, Richland, Washington.
- H-2-16653, Sh. 01, 1973, Silica Waste Storage Tank & French Drain 216-Z-8, Rev. 7, U.S. Atomic Energy Commission, Richland Operations, Richland, Washington.
- H-2-24923, Sh. 01, 1973, 216 Z-1A Modifications – Process Waste Disposal Plot Plan, Rev. 5, U.S. Atomic Energy Commission, Richland Operations, Richland, Washington.
- H-2-24924, Sh. 02, 1973, Plan & Profile Process Waste Disposal to 216-Z-8 Crib, Rev. 5, U.S. Atomic Energy Commission, Richland Operations, Richland, Washington.
- H-2-26532, Sh. 01, 1977, 216-Z-9 Crib Area Detail Topography, Rev. 1, U.S. Atomic Energy Commission, Richland Operations, Richland, Washington.
- H-2-26565, Sh. 01, 1974, 216-Z-9 Crib Area Drainage Control, Rev.0, U.S. Atomic Energy Commission, Richland Operations, Richland, Washington.
- H-2-26566, Sh. 01, 1971, Storm Sewer Re-Routing to 216-Z-11 Ditch, Rev. 2, U.S. Atomic
- Energy Commission, Richland Operations, Richland, Washington.
- H-2-26872, Sh. 01, 1983, Mining Apparatus Risers Installation z-9 Trench Excavation, Rev. 4, U.S. Atomic Energy Commission, Richland Operations, Richland, Washington.
- H-2-27115, Sh. 01, 1973, Block Flowsheet Pu Recovery from 216-Z-9, Rev. 3, U.S. Atomic Energy Commission, Richland Operations, Richland, Washington.
- H-2-27125, Sh. 01, 1977, 216-Z-9 Mining Equip. Conveyor Installation, Rev. 3, U.S. Atomic Energy Commission, Richland Operations, Richland, Washington.
- H-2-27125, Sh. 02, 1976, 216-Z-9 Mining Equip. Conveyor Installation Details, Rev. 2, U.S. Atomic Energy Commission, Richland Operations, Richland, Washington.
- H-2-27503, Sh. 01, 1973, 216-Z-1A Tile Field & Vicinity, Rev. 3, U.S. Atomic Energy Commission, Richland Operations, Richland, Washington.
- H-2-32523, Sh. 01, 1973, “C” Plant Liquid Waste Disposal Sites 216 “C” Series, Rev. 2, U.S. Atomic Energy Commission, Richland Operations, Richland, Washington.
- H-2-32528, Sh. 01, 1973, “Z” Plant Liquid Waste Disposal Sites 216-Z Series, Rev. 6, U.S. Atomic Energy Commission, Richland Operations, Richland, Washington.
- H-2-32582, Sh. 01, 1967, “Z” Plant Liquid Waste Disposal Sites 216-Z Series, Rev. 5, U.S. Atomic Energy Commission, Richland Operations, Richland, Washington.

- H-2-33123, Sh. 01, 1973, 216-Z-7 Crib – Waste Unloading Stations Plan & Details, Rev. 2, U.S. Atomic Energy Commission, Richland Operations, Richland, Washington.
- H-2-36801, Sh. 01, 1973, Crib 216-T-19 By-Pass Line, Rev. 1, U.S. Atomic Energy Commission, Richland Operations, Richland, Washington.
- H-2-37693, Sh. 01, 1974, Crib 216-B-10 (A&B), Abandonment, Rev. 0, U.S. Atomic Energy Commission, Richland Operations, Richland, Washington.
- H-2-37916, Sh. 01, 1977, Civil Plot Plan & Civil Details, Rev. 2, U.S. Atomic Energy Commission, Richland Operations, Richland, Washington.
- H-2-37953, Sh. 01, 1975, 216-Z-9 Trench Mining Grid, Rev. 0, Energy Research & Development Administration, Richland, Washington.
- H-2-38500, Sh. 01, 1976, 216-Z-9 Mining Apparatus Modifications and Details, Rev. 1, U.S. Atomic Energy Commission, Richland Operations, Richland, Washington.
- H-2-43027, Sh. 01, 1974, Waste Crib Structural Details 216-U-8 & 216-B-12, Rev. 6, General Electric Co., Hanford Works, Richland, Washington.
- H-2-43028, Sh. 01, 1974, Waste Crib 216-U-8, General Electric Co., Rev. 6, Hanford Works, Richland, Washington.
- H-2-43029, Sh. 01, 1973, 216-B-12 Crib 200 East Area, General Electric Co., Rev. 5, Hanford Works, Richland, Washington.
- H-2-43057, Sh. 01, 1973, 216-U-8 Waste Crib Line 200 West Area, Rev. 6, U.S. Atomic Energy Commission, Richland Operations, Richland, Washington.
- H-2-44511, Sh. 103, 1983, Area Map 200 West Z Plant Facilities, Rev. 5, U.S. Atomic Energy Commission, Richland Operations, Richland, Washington.
- H-2-50061, Sh. 01, 1964, 216-U-1 & 216-U-2 Cribs Piping, Structural Details & Temporary UNH Line, Rev. 7, General Electric Co., Hanford Works, Richland, Washington.
- H-2-55016, Sh. 01, 1968, Heat & Vent – Plan & Sections – Stack Gas Filter Process Exhaust System – Sheet No. 1, Rev. 2, U.S. Atomic Energy Commission, Richland Operations, Richland, Washington.
- H-2-55017, Sh. 01, 1956, Heat & Vent Plan & Sections Stack Gas Filter Process Exhaust System Sheet No. 2, Rev. 2, U.S. Atomic Energy Commission, Richland Operations, Richland, Washington.
- H-2-55018, Sh. 01, 1956, Heat & Vent Plan & Sections Duct Work Process Exhaust System Sheet No. 1, Rev. 3, U.S. Atomic Energy Commission, Richland Operations, Richland, Washington.

- H-2-55020, Sh. 01, 1965, Heat & Vent Plan & Sections Fan Layout & Piping – Process Exhaust System – SH. No. 1, Rev. 3, U.S. Atomic Energy Commission, Richland Operations, Richland, Washington.
- H-2-58540, Sh. 01, 1966, Civil Plot Plan Outside Lines, Rev. 2, U.S. Atomic Energy Commission, Richland Operations, Richland, Washington.
- H-2-58541, Sh. 01, 1965, PUREX Exhauster Filter #2 Excavation Plan, Rev. 3, U.S. Atomic Energy Commission, Hanford Atomic Products Operation, Richland, Washington.
- H-2-58542, Sh. 01, 1965, Structural Concrete Filter Building Floor Plan EL 692FT-3IN, Rev. 2, U.S. Atomic Energy Commission, Richland Operations, Richland, Washington.
- H-2-58543, Sh. 01, 1965, Structural Concrete Filter Building Sectional Plan EL 700FT-0IN, Rev. 2, U.S. Atomic Energy Commission, Richland Operations, Richland, Washington.
- H-2-58544, Sh. 01, 1965, Structural Concrete Filter Building Roof Plan, Rev. 2, U.S. Atomic Energy Commission, Richland Operations, Richland, Washington.
- H-2-58545, Sh. 01, 1965, Structural Concrete Filter Building Sections, Rev. 2, U.S. Atomic Energy Commission, Richland Operations, Richland, Washington.
- H-2-58546, Sh. 01, 1965, Structural Concrete Filter Building Sections & Details, Rev. 3, U.S. Atomic Energy Commission, Richland Operations, Richland, Washington.
- H-2-58547, Sh. 01, 1982, Structural Concrete Filter Building Misc. Details, Rev. 4, U.S. Atomic Energy Commission, Richland Operations, Richland, Washington.
- H-2-60330, Sh. 01, 1964, Trench 216-B-55, Cond. Waste Lines 221-B to Trench 216-B-55 & B-(?) Crib – Plan & Profile, Rev. 9, U.S. Atomic Energy Commission, Richland Operations, Richland, Washington.
- H-2-71377, Sh. 01, 1978, 216-BCrib Facilities Geologic Characterization Cross Section A-A, Rev. 0, U.S. Department of Energy Richland Operations Office, Richland, Washington.
- H-2-71378, Sh. 01, 1978, 216-B Crib Facilities Geologic Characterization Cross Section B-B, Rev. 0, U.S. Department of Energy Richland Operations Office, Richland, Washington.
- H-2-71379, Sh. 01, 1978, 216-B Crib Facilities Geologic Characterization Cross Section C-C, Rev. 0, U.S. Department of Energy Richland Operations Office, Richland, Washington.

- H-2-71380, Sh. 01, 1978, 216-B Crib Facilities Geologic Characterization Cross Section D-D, Rev. 0, U.S. Department of Energy, Richland Operations Office, Richland, Washington.
- H-2-71632, Sh. 01, 1985, Piping General Notes, Symbols and Legend, Rev. 1, U.S. Department of Energy, Richland, Washington.
- H-2-71676, Sh. 01, 1985, Piping Plans Tanks 241-U-361 & 241-T-361, Rev. 1, U.S. Department of Energy, Richland Operations, Richland, Washington.
- H-2-71679, Sh. 01, 1985, Piping Plans & Elevations 241-Z-8 & 241-Z-361, Rev. 1, U.S. Department of Energy, Richland, Washington.
- H-2-85541, Sh. 01, 1964, Purex Exhaust Filter #2 Excavation Plan, Rev. 1, U.S. Atomic Energy Commission, Richland Operations, Richland, Washington.
- H-2-821407, Sh. 01, 1994, Topographic Map 216-U-1 & 2 Cribs Before Stabilization, Rev. 0, U.S. Department of Energy, DOE Field Office, Westinghouse Hanford Co., Richland, Washington.
- H-2-821407, Sh. 02, 1994, Topographic Map 216-U-1 & 2 Cribs After Stabilization, Rev. 0, U.S. Department of Energy, DOE Field Office, Westinghouse Hanford Co., Richland, Washington.
- H-2-821414, Sh. 01, 1994, Topographic Map 216-T-3 & 6 Before Stabilization, Rev. 0, U.S. Department of Energy Richland Operations Office, Richland, Washington.
- H-2-821414, Sh. 02, 1994, Topographic Map 216-T-3 & 6 After Stabilization, Rev. 0, U.S. Department of Energy Richland Operations Office, Richland, Washington.
- H-2-821419, Sh. 01, 1994, Topographic Map 216-B-9 Before Stabilization, Rev. 0, U.S. Department of Energy Richland Operations Office, Richland, Washington.
- H-2-821419, Sh. 02, 1994, Topographic Map 216-B-9 After Stabilization, Rev. 0, U.S. Department of Energy Richland Operations Office, Richland, Washington.
- H-2-831023, Sh. 01, 2003, U Plant Closure Area Pipeline to 241-U-361 Settling Tank, Rev. 0, U.S. Department of Energy, Richland, Washington.
- H-2-831024, Sh. 01, 2003, U Plant Closure Area Pipeline to 216-U-1 and 216-U-2 Cribs, Rev. 0, U.S. Department of Energy, Richland, Washington.
- H-2-831026, Sh. 01, 2003, Plant Closure Area 200-W-42 Pipeline to 216-U-8 Crib, Rev. 0, U.S. Department of Energy Richland Operations Office, Richland, Washington.
- HNF-4371, 1999, 241-Z-361 Sludge Characterization Sampling and Analysis Plan, Rev. 0, U.S. Department of Energy, Richland, Washington.
- HNF-5231,1999, Historical Vadose Zone Contamination from B, BX, and BY Tank Farm Operations, Revision 0, Flour Daniel Northwest, Inc., Richland, Washington.

- HNF-20611, 2004, Unabated Emissions Estimate for the PUREX 291-A-1 Stack, Rev. 0, U.S. Department of Energy, Richland, Washington.
- HNF-58818, 2016, Documented Safety Analysis for the 216-Z-9 Waste Storage Crib Facility, Revision 0, U.S. Department of Energy Richland Operations Office, Richland, Washington.CH2M HILL Plateau Remediation Company, Richland, Washington.

3. International Building Code, 2006.
4. ACI 318, “Building Code Requirements for Structural Concrete,” 2008.
5. ACI 349, “Code Requirements for Nuclear Safety Related Concrete Structures,” 2001.
6. AISC Manual of Steel Construction, 9th Edition.
7. ANSYS ® General Purpose Finite Element Analysis Software Code, Version 18.0, ANSYS Inc., LPI Report No. V&V-ANSYS-18, Rev. 0, “Verification and Validation of ANSYS Software Program.”
8. LPI Report No. CGD-ANSYS-18, Rev. 1, “Commercial Grade Dedication of ANSYS Software Program – Version 18.”
9. LPI Quality Assurance Procedure LPI 4.1, “Software Control.”
10. LPI Internal Memorandum LA181779-M-002, “Verification of Workbench in ANSYS.”
11. ASCE/SEI 41-13 “Seismic Evaluation and Retrofit of Existing Buildings,” 2010.
12. Wood Handbook, “Wood as an Engineering Material,” Centennial edition, 2010.
13. PRC-PRO-EN-097, Engineering Design and Evaluation (Natural Phenomena Hazards), Revision 3, Change 0, CH2M Hill Plateau Remediation Company, Richland, Washington.
14. CHPRC-03364, 2017, PUREX Tunnel 1 Engineering Evaluation, Revision 0, CH2M HILL Plateau Remediation Company, Richland, Washington.
15. CHPRC-03365, 2017, PUREX Tunnel 2 Engineering Evaluation, Revision 0, CH2M HILL Plateau Remediation Company, Richland, Washington.
16. RPP-RPT-49992, Rev. 0, “Single-Shell Tank Integrity Project Analysis of Record Hanford IV Single-Shell Tank Thermal and Operating Loads and Seismic Analysis,” 2014.
17. RPP-RPT-32237, Rev. 0, “Hanford Double-Shell Tank Thermal and Seismic Project – Increased Liquid Level Analysis for 241-AP Tank Farms,” 2007.

18. TerraGraphics Environmental Engineering, Inc. and LPI, Inc. Report Number 67569-RPT-001, Revision 2, "RL-40 Aging Structures Risk Assessment," Prepared for CH2M Hill Plateau Remediation Company.

19. U.S. Atomic Energy Commission Report No. TID-4500, "Nuclear Reactors and Earthquakes," 22nd edition, prepared by Lockheed Aircraft Corp, & Holmes & Narver, Inc.

20. CHPRC Purchase Requisition No. 312599, Attachment 1, 2018, Crib & Tank Descriptions, U.S. Department of Energy Richland Operations Office, Richland, Washington.

21. Silvan, G.R. "Structural Evaluation of the PUREX No. 1 Burial Tunnel," RHO-CD-1079, dated September 1980.

22. TOC-PRES-14-3313-FP, Rev. 0, January 2015, "Progress of the Enhanced Hanford Single Shell Tank (SST) Integrity Project -15497," prepared for the U.S. Department of Energy Assistant Secretary for Environmental Management.

23. EPRI report No. 3002011710, "Irradiation Damage of the Concrete Biological Shield," May 2018.

24. ASCE 7-10, "Minimum Design Loads for Buildings and Other Structures," Second printing, incorporating errata identified through April 6, 2011.

25. Gaylord, E.H. Jr. and Gaylord, C.H., "Structural Engineering Handbook," third Edition.

26. Cosenza, E; Galasso, C.; Maddaloni, G., "Simplified Assessment of Bending Moment Capacity for RC Members with Circular Cross-Section," 3rd FIB International Congress 2010.

27. Waste Information Data System (WIDS) General Summary Report, March 6, 2017, Richland, Washington.

APPENDIX A

STRUCTURAL LOAD CRITERIA, MATERIAL PROPERTIES AND MODELING ASSUMPTIONS

STRUCTURAL LOAD CRITERIA, MATERIAL PROPERTIES AND MODELING ASSUMPTIONS

1. INTRODUCTION

Structural load criteria for the structural analysis of legacy aging buried cribs and tanks at the Hanford Central Plateau are described herein. The intent of the structural analysis is to determine if margin from collapse still exists in each of the highest-risk crib/tank facilities (one structure from each of the 11 categories). Attachment A of this appendix summarizes the material properties and modeling assumptions employed in the present structural analysis. Attachment B of this appendix includes calculations for the lateral acceleration effects for the tanks that contain waste (categories T1 and T2 as shown in Table A1).

The buried structures addressed in this analysis were classified as Structural Performance Category (PC) 1 for general service structures as defined in [1]. This classification is similar to that used for the evaluation of PUREX Tunnel 1 [2] and is therefore considered appropriate for the purpose of this document. The structures addressed in the structural analysis are listed in Table A1.

2. LOADS

The structures in the scope were analyzed for the following loads:

a. Dead Weight, DW

Dead weight includes self-weight of the material of construction and is based on volumes as shown in drawings and the following unit densities:

- Reinforced concrete[13] = 150 lb/ft^3 (for normal weight concrete to account for weight of reinforcement)
- Steel[14] = 490 lb/ft^3
- Timber = 32 lb/ft^3 (based on specific gravity of 0.5 [2])

[13] Concrete density (without rebar) is 145 lb/ft^3 per [3]

[14] Applies to structural steel and steel liners

- Additional weights of nonstructural items such as steel liner, tiles, and bricks were included using the above steel density and bounding density of 125 lb/ft^3 for tiles and bricks per (based on common bricks in Table 17-12 of [6]).
- Backfill soil = 125 lb/ft^3 [16, Tables 4.2 and 4.3] (conservative bounding value compared to [2] to account for high level of moisture from heavy rain) – refer to Attachment A for dry soil weight and moisture content.
- Filter material (applicable to Groups O1 and O2), weights were based on the construction and material of the filters as described in drawings and [7].

Vertical soil weight on roofs = $\gamma_{soil} * H_r$

where γ_{soil} is soil unit weight defined above, and

H_r is the depth of soil above the roof.

This load was applied as uniform pressure on roof surfaces.

b. <u>Waste Load, F</u>

The buried structures in the Hanford Central Plateau were used for storage of liquid waste [7]. However, several of the structures have been abandoned. The level of waste in each buried structure is described in [7]; the current level of waste is summarized in Table A1 below. The density of the waste is based on a specific gravity of 1.7 [16]. The level of waste in each buried structure is described in [7]. The waste static loading consists of lateral hydrostatic pressure linearly varying from zero at the top of waste level to maximum value at the base, applied to all interior surfaces and on the floor.

Table A1. Waste Level

Group	Structure	Waste Level
C1	216-Z-2	NA
C2	216-B-12	NA
C3	216-Z-6	NA
C4	216-Z-7	NA
C5	216-Z-9	NA
T1	241-T-361	10.8 ft
T2	241-Z-361	8 ft
T3	241-Z-8	Negligible
O1	PUREX deep bed filters	N/A
O2	REDOX sand filter	N/A
O3	241-CX-70	Negligible

c. Earth Lateral Load, LE

Lateral earth pressure was applied along all walls. The earth pressure linearly varied with depth using the following formula for at-rest lateral earth pressure:

Lateral earth pressure at depth Hs = Ko $*\gamma_{soil} *$ Hs $(1 + \sin \theta)$

Where:

Ko = 0.5 = lateral at-rest earth pressure coefficient [2]

Hs = depth of soil

θ = slope of ground surface with the horizontal in degrees (positive for depth increases away from the structure, negative values are not considered)

Water table is considered below the structure and as such no water pressure was applied. This is consistent with the analysis of the PUREX Tunnel 1 [2].

d. Live Load, LL

Consistent with the analysis of the PUREX Tunnel 1 [2] and since barricades (light-duty post and chain fence) and signage (i.e., "Cave-In Potential", and "Caution Underground Radioactive Material" signage) are currently employed at the ground surface for many of these underground structures, a zero live load value was used.

e. Snow Load, S

Snow load was taken as 15 lb/ft^2 on ground surface [1 and 2]. No reduction of this load was credited as it is transferred to the depth of the buried structure. As such, a snow load of 15 lb/ft^2 was applied uniformly on the roof of the buried structure.

f. Seismic Load, E

Seismic loads are in accordance with [1 and 5] for Performance Category PC-1. Seismic accelerations were applied along the two horizontal directions and the vertical direction concurrently. The spectral seismic design parameters are as follows:

S_{MS} = 0.66 [1, Table 6]

S_{M1} = 0.33 [1, Table 6]

S_{DS} = 2/3 S_{MS} = 0.44 [5, para. 11.4.4]

S_{D1} = 2/3 S_{M1} = 0.22 [5, para. 11.4.4]

The seismic spectral acceleration, S_a, is defined as follows where T is the fundamental period of the structural component [5, para 11.4.5]:

For $T \le T_o$ $\quad S_a = S_{DS}\,(0.4 + 0.6\,T / T_o)$

For $T_o \le T \le T_s$ $\quad S_a = S_{DS}$

For $T_s \le T \le T_L$ $\quad S_a = S_{D1} / T$

For $T_L \le T$ $\quad S_a = S_{D1}\,T_L / T^2$

$T_o = 0.2\,S_{D1} / S_{DS} = 0.2 \times 0.22 / 0.44 = 0.1$ (in seconds)

$T_s = S_{D1} / S_{DS} = 0.22 / 0.44 = 0.5$

T_L = ground motion long period transition = 16 [5, Figure 22-12]

The general shape of the seismic response spectrum is shown in Figure A1 below.

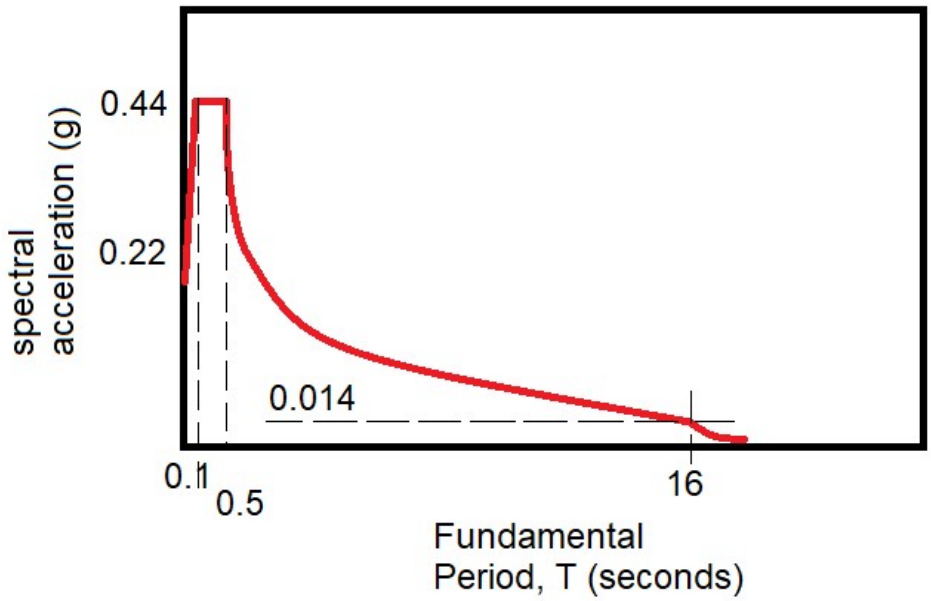

Figure A1 Seismic Response Spectrum [5]

Static analysis was employed for the seismic loading using spectral acceleration based on the dynamic properties (fundamental period) of the structural component. In lieu of determining the natural (fundamental) period of the structural component to obtain the corresponding seismic acceleration, the peak spectral seismic acceleration (Sh) of 0.44g was used.

The seismic loading consists of lateral seismic acceleration, Sh, as defined above, applied along two horizontal orthogonal directions per [5, para. 12.4.2.1] and vertical acceleration, Sv. The vertical acceleration was taken as Sv = 0.2 S_{DS} [5, para. 12.4.2.2], i.e. Sv = 0.2 * 0.44g = 0.088g.

The vertical and horizontal seismic coefficients, Sv, and Sh, defined above were applied to the mass of structural components and attachments (such as tiles, bricks, vents, …etc.). Overburden and lateral earth pressures were factored by the vertical seismic acceleration.

Lateral earth pressure was not adjusted for the lateral seismic acceleration. This was based on the assumption that the soil and structure move in phase and that local displacements of the wall are small and therefore have insignificant impact on the lateral earth pressure based on rigid boundary.

Tanks T1 and T2 contain liquid waste and therefore hydrodynamic loads were considered. Those were calculated separately for lateral and vertical seismic accelerations. The vertical

acceleration effect is the hydrostatic pressure, F, times Sv. The lateral acceleration effects were determined using methods in [8]. Detail calculations are included in Attachment B where it is shown that the lateral hydrodynamic pressures consist of impulsive and sloshing components. The impulsive pressure profile is a quadratic function with height and changes from zero at the free surface of the fluid to a maximum value at the base. The sloshing pressure is a hyperbolic function and is maximum at the free surface of the fluid and reaches a minimum value at the base. Due to the complex non uniform distributions of the pressure, simplified uniform pressure patterns are derived in Appendix A and specified for the finite element analysis. These simplified pressures are equivalent in the total magnitude but distributed over smaller areas and therefore are conservative. The following is a summary of the lateral hydrodynamic loads used in the analysis:

<u>Tank T1</u>

- Impulsive pressure, psi = 1.194 sin (θ)

  Where θ is the circumferential angle from 0 to 360 deg. This pressure acts on a 4 ft wide horizontal band around wall (360 deg), center of band is at height 4.05 ft from bottom of tank. Positive pressure is acting outward and negative pressure is acting inward.

- Sloshing pressure, psi = 0.519 sin (θ)

  Where θ is the circumferential angle from 0 to 360 deg. This pressure acts on a 2 ft wide horizontal band around wall (360 deg), center of band is at height 6.77 ft from bottom of tank. Positive pressure is acting outward and negative pressure is acting inward.

<u>Tank T2</u>

<u>Acceleration along short direction</u>

- Impulsive pressure, psi = 0.426

  This pressure acts on a 3 ft wide horizontal band on the long walls, center of band is at height 3 ft from bottom of tank. Pressure is positive on one wall and negative on the opposite wall according to the direction of the lateral acceleration. Positive pressure is acting outward and negative pressure is acting inward.

- Sloshing pressure, psi = 0.222

  This pressure acts on a 2 ft wide horizontal band on the long walls, center of band is at height 4.92 ft from bottom of tank. Pressure is positive on one wall and negative on the opposite wall according to the direction of the lateral acceleration. Positive

pressure is acting outward and negative pressure is acting inward.

Acceleration along long direction

- Impulsive pressure, psi = 0.477

  This pressure acts on a 3 ft wide horizontal band on the long walls, center of band is at height 3 ft from bottom of tank. Pressure is positive on one wall and negative on the opposite wall according to the direction of the lateral acceleration. Positive pressure is acting outward and negative pressure is acting inward.

- Sloshing pressure, psi = 0.434

  This pressure acts on a 2 ft wide horizontal band on the long walls, center of band is at height 4.29 ft from bottom of tank. Pressure is positive on one wall and negative on the opposite wall according to the direction of the lateral acceleration. Positive pressure is acting outward and negative pressure is acting inward.

In summary, the sloshing and impulsive pressures act over the wet depth of the tank. Application of the total pressure force over smaller length is more conservative. This is similar to comparing simply supported beam with uniform load and same beam with same total load but distributed over smaller length. The sloshing is over a narrower band as compared to impulsive because the significant sloshing pressure is concentrated over smaller depth near the fluid surface. The impulsive pressure on the other hand acts over entire depth. Therefore, the selected band widths are conservative.

3. MATERIAL PROPERTIES

PROPERTIES OF STRUCTURAL MATERIALS ARE AS FOLLOWS (ATTACHMENT A):

	Poisson's Ratio	**Modulus of Elasticity (ksi)**
Concrete	0.15	5,100
steel	0.29	29,700
Timber (1)	0.29	1,765

(1) Properties are along fiber direction (i.e. longitudinal direction)

4. LOAD COMBINATIONS

Load combinations were determined based on the review of applicable documents for the Hanford Central Plateau [1, 2, 16]. Based on this review, it was determined that the proper load combinations will envelope those in ACI 349[15] [4] and ASCE 7 [5] for strength design. The following Load Resistance Factor Design (LRFD) load combinations were used in the evaluation of structural components strength:

U = 1.4 DW + 1.4 F + 1.7 LE + 1.4 S Load Combination 1

U = 1.2 DW + F + LE + 1.2 S + 1.0 E Load Combination 2

U is the required strength (axial, bending moment or shear) of the wood, concrete, or steel structural component.

Snow load was treated as dead weight in load combinations 1 and 2. Where waste pressure (F) and lateral soil pressure (LE) produce opposing results at a specific section, the factor for the load causing the smaller response was reduced to 0.9. It is likely that the load factor reduction could be applied to F except for cases of shallow structures where the load factor for LE is reduced. However, the results should be inspected to apply the load factor reduction appropriately on a case-by-case basis.

5. REFERENCES

1. PRC-PRO-EN-097, Engineering Design and Evaluation (Natural Phenomena Hazards), Revision 3, Change 0, CH2M Hill Plateau Remediation Company, Richland, Washington.
2. CHPRC-03364, 2017, PUREX Tunnel 1 Engineering Evaluation, Revision 0, CH2M HILL Plateau Remediation Company, Richland, Washington.
3. RPP-RPT-49992, Rev. 0, “Single-Shell Tank Integrity Project Analysis of Record Hanford IV Single-Shell Tank Thermal and Operating Loads and Seismic Analysis,” 2014.
4. ACI 349, “Code Requirements for Nuclear Safety Related Concrete Structures,” 2001.

[15] Table C-1 in [1] lists ACI 318 as applicable for PC-1/PC-2 structures and ACI 349 for PC-3 structures. Load combinations in ACI 318 are similar to those in ASCE 7. ACI 349 load combinations that are relevant to this analysis bound the corresponding combinations in ACI 318. Though the structures covered under the scope of this document are categorized as PC1, ACI 349 shall be used herein to be consistent with the evaluation of the Type IV single-shell tank in [16].

5. ASCE 7-10, “Minimum Design Loads for Buildings and Other Structures,” Second printing, incorporating errata identified through April 6, 2011.
6. AISC Manual of Steel Construction, 9th Edition.
7. TerraGraphics Environmental Engineering, Inc. and LPI, Inc. Report Number 67569-RPT-001, Revision 2, “RL-40 Aging Structures Risk Assessment,” Prepared for CH2M Hill Plateau Remediation Company.
8. U.S. Atomic Energy Commission Report No. TID-4500, “Nuclear Reactors and Earthquakes,” 22nd edition, prepared by Lockheed Aircraft Corp, & Holmes & Narver, Inc.

ATTACHMENT A:
MATERIAL PROPERTIES AND MODELING ASSUMPTIONS

Structural calculations and analyses were performed by LPI, Inc. (LPI) to determine the amount of remaining factor of safety in the designs from collapse for the highest combined risk of failure facilities in each of the 11 groups [67569-RPT-001, Rev. 2].

Information was gathered and reviewed for each structure category to determine the different types of material properties the structural evaluations need to consider. Materials representing the 11 structure categories primarily include wood (Douglas Fir, and creosote-treated), concrete, and mild carbon steel. All structures are buried or surrounded in soil. Table A1 through A4 in this attachment summarize the proposed material properties that were used in the finite element modeling of the Hanford aging structures. Majority of properties were obtained from publically available reports, many of which involved previous assessments of Hanford degraded structures including the PUREX Tunnel 1 Engineering Evaluation, Hanford Double-Shell Tanks, and Hanford Single-Shell Tanks. Fig. A1 shows average annual maximum and minimum temperatures between 1996 and 2018 at depths of 2, 4, 8, 20 in., and effective converging temperature of 54 °F for depths beyond 168 in. reported for Lind Coulee, Washington (within 40 miles from the Hanford site).

The literature shows irradiation with gamma rays in doses up to about 1 MegaRad generally do not impact the strength properties of wood [Green, et al., no date]. As dosage exceeds 1 MegaRad, tensile strength parallel to grain and toughness decrease. The gamma radiation threshold for concrete and steel material degradation is significantly higher than that for wood [EPRI Report, 2018].

However, dose rates for the majority of structures in the current scope of work were not reported (and may not be known). Data collection efforts in the project found that only two dose rates were reported, and the higher of the two gamma radiation dose rate reported is 1.7 Rad/hr (216-B-9 Crib in Group C1). Proposed material properties are nominal properties; proposed material properties are not adjusted to account for radiation effects.

Using nominal properties is acceptable for the following reasons:

- The higher of the two gamma radiation dose rates reported is 1.7 Rad/hr for the current scope of work. This rate is less than the reported rates for the PUREX Tunnel 1 containers - initial dose rates ranged between 0.15 Rad/hr (at 50 ft) and 25 Rad/hr (at 150 ft) [Silvan, 1980].

- It would take approximately 67 years to reach a cumulative dose of 1 MegaRad to observe wood degradation due to radiation effects (based on the maximum reported rate of 1.7 Rad/hr, and at a constant rate over this time).
- Preliminary calculations show a 10% degradation in the nominal wood properties would occur if a dose rate approximately 3x higher than 1.7 Rad/hr was used for 75 years (some of these structures were constructed in 1944).
- In 2015, concrete core samples and rebar samples taken from Hanford Single-Shell Tank C-107 showed that material strength results were all higher than original tank design. Petrographic examination of selected cores concluded that the concrete is in good condition and shows minimal carbonation after decades of ground contact [TOC-PRES-14-3313-FP, Rev. 0].
- Hanford Tunnel 1 and Tunnel 2 evaluations recently performed by CHPRC did not account for radiation effects [CHPRC-03364, 2017], and [CHPRC-03365, 2017]. While it is not clear why irradiation effects were not included, it may be likely because actual radiation exposure to the structures was/is not known. There is precedence to assume nominal properties.

Table A1. Soil Properties

Soil Properties	Units	Source (filename)
Ground consists mostly of coarse sand and gravelly areas	-	Hanford map overlaid on top of Soil Survey
Average Yearly soil temperature	see Fig. 1	Lind Coulee data
Soil Moisture yearly average	9.5%	Lind Coulee data
Soil weight	110 lbs/ ft^3	CHPRC-03364_R0_T1_a
Undisturbed soil modulus	70 ksi	RPP-RPT-32237
Backfill soil modulus	25 ksi	RPP-RPT-32237
Cohesion	1.0 psi	RPP-RPT-32237
Friction angle	35°	RPP-RPT-32237
Dilatancy angle	8°	RPP-RPT-32237
Soil-to-concrete coefficient of friction, Dome	0.3	RPP-RPT-32237, Table 2-9
Side Walls	0.005	RPP-RPT-32237, Table 2-9
Base Mat	0.6	RPP-RPT-32237, Table 2-9

Table A2. Concrete Properties

Concrete Properties	Value	Source (filename)
Compressive strength of continous wall footings	3,000 psi	CHPRC-03365_R0_T2
Compressive strength of concrete arched ribs and thrust block foundations	4,000psi	CHPRC-03365_R0_T2
Coefficient of thermal expansion (CTE) *	0.37×10^{-6} in/in/°F	RPP-RPT-32237
Density of concrete	145 lb/ft^3	RPP-RPT-49992
Poisson's Ratio	0.15	RPP-RPT-32237
Temperature	54 F	Average ground temperature from Lind Coulee
Elastic Modulus	5.1×10^6 psi	RPP-RPT-32237 Fig 2-6, Temp < 100 F
Concrete-cast-against-steel coefficient of friction	0.3	RPP-RPT-32237, Table 2-9
Insulating concrete against steel coefficient of friction	0.4	RPP-RPT-32237, Table 2-9

Reinforced Concrete Additional Properties	Value	Source
Yield Strength	40 ksi	ASTM A15-52T Intermediate Grade (per Specification HWS-5638)

* While RPP-RPT-32237 shows this value of CTE, a value of $5x10^{(-6)}$ in/in/°F may be used to be consistent with nominal concrete CTE values (RPP-RPT-49991).

Table A3. Wood Properties

Wood Properties	Value	Source (file name)
Douglas Fir timbers	-	RL-40 Attachment 1.pdf
Preservation / Waterproofing	Creosote	Drawing No. H-2-1031
Average Dried Weight	32 lbs/ft3 (510 kg/m^3)	http://www.wood-database.com/douglas-fir/
Specific Gravity (Basic, 12% MC)	0.48	http://www.wood-database.com/douglas-fir/
Janka Hardness	620 lbf (2,760 N)	http://www.wood-database.com/douglas-fir/
Modulus of Rupture	12,500 lbf/in^2 (86.2 MPa)	http://www.wood-database.com/douglas-fir/
Elastic Modulus: E_{Long}	1,765,000 lbf/in^2 (12.17 GPa)	http://www.wood-database.com/douglas-fir/
E_{Tan}/E_{Long}	0.05	ch4-Mechanical-Properties-of-Wood Handbook.pdf
E_{Rad}/E_{long}	0.068	ch4-Mechanical-Properties-of-Wood Handbook.pdf
Moduli of rigidity: G_{LR}/E_L	0.064	ch4-Mechanical-Properties-of-Wood Handbook.pdf
G_{LT}/E_L	0.078	ch4-Mechanical-Properties-of-Wood Handbook.pdf
G_{RT}/E_L	0.007	ch4-Mechanical-Properties-of-Wood Handbook.pdf
Poisson's Ratio: μ_{LR}	0.292	ch4-Mechanical-Properties-of-Wood Handbook.pdf
μ_{LT}	0.449	ch4-Mechanical-Properties-of-Wood Handbook.pdf
μ_{RT}	0.39	ch4-Mechanical-Properties-of-Wood Handbook.pdf
μ_{TR}	0.374	ch4-Mechanical-Properties-of-Wood Handbook.pdf
μ_{RL}	0.036	ch4-Mechanical-Properties-of-Wood Handbook.pdf
μ_{TL}	0.029	ch4-Mechanical-Properties-of-Wood Handbook.pdf
Crushing Strength	6,950 lbf/in^2 (47.9 MPa)	http://www.wood-database.com/douglas-fir/
Shrinkage: Radial	4.50%	http://www.wood-database.com/douglas-fir/
Tangential	7.30%	http://www.wood-database.com/douglas-fir/
Volumetric: 11.6%	11.60%	http://www.wood-database.com/douglas-fir/
T/R Ratio	1.6	http://www.wood-database.com/douglas-fir/
Density	0.51 g/cm^3	http://www.musterkiste.com/en/holz/pro/1028_Douglas-fir.html
Moisture content in wood	12%	An Evaluation of the Structural Integrity of PUREX Storage Tunnel #1_Hand and Stephens 1991_91-EAB-218
Decay from moisture	None	Moisture < 20%, ch4-Mechanical-Properties-of-Wood Handbook.pdf
Radiation Dose	1.7 Rad/hr	Max value from RL-40 Attachment 1.pdf and Structure Descriptions B&W.pdf
Radiation Decay	None	1.7 Rad/hr => 67 yr/MR (1 MR is limit for degradation)

Table A4. Steel Properties

Steel Properties	Value	Source (filename)
Steel Type	Mild Carbon	H-2-16108-001-06.pdf General notes
Hardness, Rockwell B (Converted from Brinell hardness)	71	https://www.azom.com/article.aspx?ArticleID=6115, "AISI 1018 Mild/Low Carbon Steel"
Strength, Yield	36 ksi	CHPRC-03365_R0_T2
Modulus of Elasticity (Typical for steel)	29700 ksi	https://www.azom.com/article.aspx?ArticleID=6115, "AISI 1018 Mild/Low Carbon Steel"
Bulk Modulus (Typical for steel)	20300 ksi	https://www.azom.com/article.aspx?ArticleID=6115, "AISI 1018 Mild/Low Carbon Steel"
Poissons Ratio (Typical For Steel)	0.29	https://www.azom.com/article.aspx?ArticleID=6115, "AISI 1018 Mild/Low Carbon Steel"
Shear Modulus (Typical for steel)	11600 ksi	https://www.azom.com/article.aspx?ArticleID=6115, "AISI 1018 Mild/Low Carbon Steel"
Density	490 lb/ft^3	https://www.engineeringtoolbox.com/metal-alloys-densities-d_50.html
Steel-to-steel coefficient of friction	0.2	RPP-RPT-32237, Table 2-9

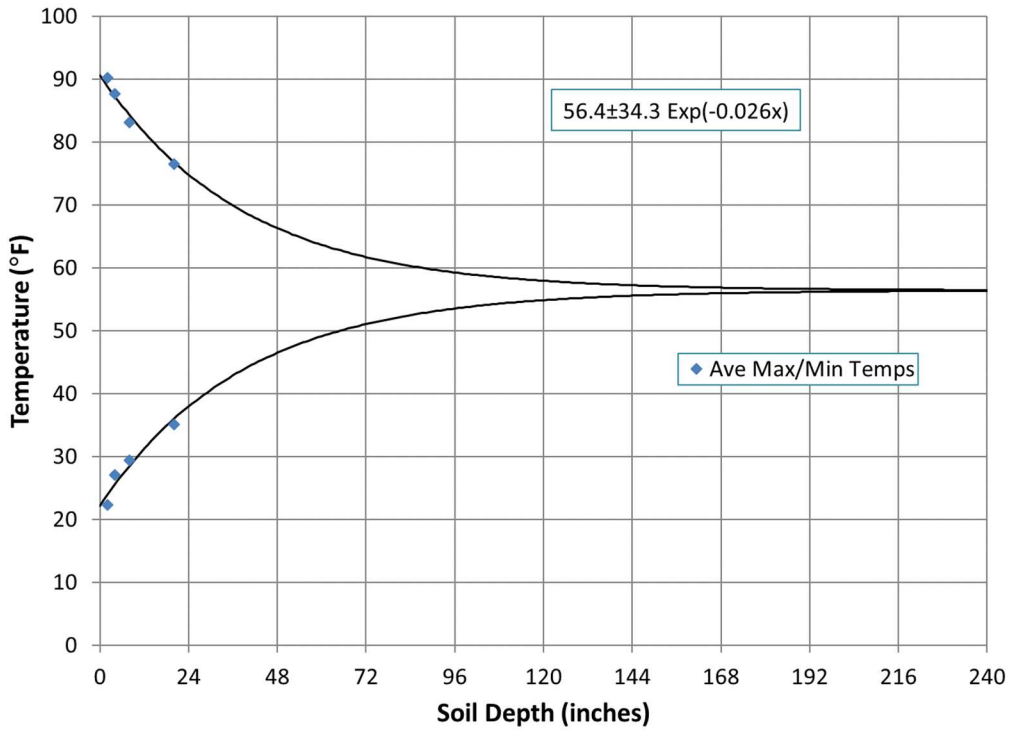

Fig. A1 Average Annual Maximum and Minimum Soil Temperature Data vs. Depth

Some of the models incorporate simulated degradation that is postulated based on the description of current conditions and historical events. The table below summarizes the rational of the assumed degradation:

Group	Structure	Caved-In, Subsidence	Descriptions provided in 67569-RPT-001 Risk Assessment Rev. 2
Group C1	216-Z-2	No	Because the neighbor 216-Z-1 crib (same design as 216-Z-2) already collapsed, an increase factor of 20% shall be applied to the response of the roof components.
Group C2	216-B-12	Yes	Based on the 1973 crib collapse description (gradual subsidence with a final depression of about 5 ft deep), this could be the result of local or more extensive roof collapse. The depth of soil on top of the cribs is 15-17 ft. Other factors such as local soil failure could have contributed to the noted subsidence. Since, the specific location of the subsidence with respect to the crib is also not provided, an assumption is made that some of the roof timber logs collapsed such that the load shared by the adjacent undamaged timber logs increased. This scenario is accounted for by application of increase factor of 20% in the response of the roof elements.
Group C3	216-Z-6	Yes	Based on the descriptions of multiple collapses, and the specific location(s) with respect to the crib is unknown, LPI is not able to quantify/model the structure's degraded state. As such, similar to C2, an increase factor of 20% shall be applied to the response of the roof components.
Group C4	216-Z-7	No	**Damage is not reported**
Group C5	216-Z-9	No	LPI proposes to model the degraded concrete by reducing its thickness by 1 in. (concrete thickness reduced, rebar will stay in place). The weight of the bricks will be included on the cover.
Group T1	241-T-361	No	Based on the available information, there is no indication of damage to this structure. However, due to the harsh environment, degradation was simulated by reducing the concrete thickness and rebar area by 10%.
Group T2	241-Z-361	No	Due to the corroded steel liner, LPI proposes to model the degraded structure by reducing the concrete roof and wall thickness by 1 in. A 20% loss in rebar area will be incorporated to simulate rebar corrosion.
Group T3	241-Z-8	No	**Damage is not reported**
Group O1	PUREX deep bed filters	No	Based on the description of water intrusion, and potential concrete cracking and corrosion of the structural rebar in the concrete cover, LPI proposes to model the degraded concrete cover by reducing its thickness by 1 in. and the rebar cross-sectional area by 10%.
Group O2	REDOX sand filter	No	Similar to the water intrusion concerns for the PUREX deep bed filters and the potential concrete cracking and corrosion of the structural rebar in the concrete cover, LPI proposes to model the degraded concrete cover by reducing its thickness by 1 in. and the rebar cross-sectional area by 10%.
Group O3	241-CX-70	Yes	Although there was a cave-in on the west-side of the tank in 2004, and the 9ft by 9ft (and 7ft deep) subsidence in 2017, a March 2017 Waste Information Data System (WIDS) report suggests that the wood shoring above tank 241-CX-70 is what collapsed - not the tank itself. Therefore, degradation was not included the 241-CX-70 model.

Assumptions:

1)	Per RPP-RPT-49992 , a waste specific gravity (sludge and liquid) of 1.7 will be used for tank waste in Categories T1, T2, and T3.
2)	In the absence of waste temperature information, LPI proposes to use the average annual soil temperature of 56 F for the waste temperature.
3)	Based on the soil samples taken by Dames and Moore (1984), and described in CHPRC-03364 (2017), the average of the range for dry unit weight of soil (111 lb/ft^3), and the average of the range for moisture content (9.6%) were used to determine the soil density of 122 lb/ft^3. A soil density of 122 lb/ft^3 is conservative, yet realistic (typically 110 lb/ft^3 is used for soil density) - this value intends to address increased moisture due to above average snow and/or rain in Richland, Washington. However, 125 lb/ft^3 was used in the structural evaluations as a bounding value to account for high level of moisture.

ATTACHMENT B:
LATERAL ACCELERATION EFFECTS FOR TANKS CONTAINING WASTE

Tank T1 (20ft outside diameter, 6" thick wall):

$Rt := \frac{20 \cdot ft}{2} - 6 \cdot in = 9.5 \cdot ft$ — inside radius of tank

$ht := 10.8 \cdot ft$ — fluid depth in tank

$\frac{ht}{Rt} = 1.137$

The depth/radius ratio is less than 1.5 [8, pg 187]. Thus, the seismic fluid forces consist of sloshing and impulsive components. The sloshing component depends on the horizontal spectral acceleration at the sloshing frequency. The impulsive component depends on the maximum horizontal ground acceleration; this is the acceleration at zero period. From the seismic load, E, definition, this acceleration is 0.4 x 0.44g = 0.18g.

$Wt := \pi \cdot Rt^2 \cdot ht \cdot 62.4 \cdot \frac{lbf}{ft^3} = 191.076 \cdot kip$ — total weight of fluid

$W_o := Wt \cdot \frac{\tanh\left(\sqrt{3} \cdot \frac{Rt}{ht}\right)}{\sqrt{3} \cdot \frac{Rt}{ht}} = 114.041 \cdot kip$ — weight of impulsive fluid [8, eq. 6.12]

$h_o := \frac{3}{8} ht = 4.05 \cdot ft$ — height of impulsive force [8, eq. 6.13]

$P_o := 0.18 \cdot W_o = 20.527 \cdot kip$ — total impulsive force [8, eq. 6.15]

This force is distributed over a <u>four</u> foot high horizontal band with a sine form from 0 degree to 360 degree in the circumferential direction. The seismic acceleration is through the 90 & 270 degree marks. The band center is at h_o from bottom of the tank. The resulting pressure is calculated as follows:

$b_o := 4 \cdot ft$ — height of the impulsive pressure band

$p_o(\theta) := \frac{P_o}{\pi \cdot Rt \cdot b_o} \cdot \sin(\theta)$ — impulsive pressure; positive pressure is outward and negative pressure is inward

$p_o(90 \cdot deg) = 1.194 \cdot psi$ — peak value of the impulsive pressure at 90 deg mark

This pressure is verified by integration of the pressure across the circumferential direction from 0 degree to 360 degree.

$$2\left(\int_0^{\pi} p_o(\theta)\cdot b_o\cdot Rt\cdot \sin(\theta)\,d\theta\right) = 20.527\cdot kip$$

this is equal to the impulsive force, P_o, calculated above

$$W_1 := Wt\cdot 0.318\cdot\frac{Rt}{ht}\cdot\tanh\left(1.84\cdot\frac{ht}{Rt}\right) = 51.843\cdot kip$$

weight of sloshing fluid [8, eq. 6.16]

$$h_1 := ht\cdot\left(1-\frac{\cosh\left(1.84\cdot\frac{ht}{Rt}\right)-1}{1.84\cdot\frac{ht}{Rt}\cdot\sinh\left(1.84\cdot\frac{ht}{Rt}\right)}\right) = 6.772\cdot ft$$

height of sloshing force [8, eq. 6.17]

$$\omega := \sqrt{\frac{1.84\cdot g}{Rt}\cdot\tanh\left(1.84\cdot\frac{ht}{Rt}\right)} = 2.459\cdot\frac{rad}{s}$$

natural frequency of sloshing [8, eq. 6.19]

$$T := \frac{2\pi}{\omega} = 2.556\,s$$

natural period of sloshing

$$S_a := \frac{0.22g}{\frac{T}{s}} = 0.086\cdot g$$

spectral acceleration at sloshing frequency using spectra equation in the seismic load, E, definition.

$$y_{max} := \frac{S_a}{\omega^2} = 0.458\cdot ft$$

maximum horizontal amplitude of sloshing using single degree of freedom approximation

$$\theta_h := 1.534\cdot\frac{y_{max}}{Rt}\cdot\tanh\left(1.84\cdot\frac{ht}{Rt}\right) = 0.072$$

sloshing angle [8, eq. 6.20]

$$P_1 := 1.2\cdot W_1\cdot\theta_h = 4.465\cdot kip$$

maximum sloshing total force [8, eq. 6.21]

This force is distributed over a <u>two</u> foot high horizontal band with a sine form from 0 degree to 360 degree in the circumferential direction. The seismic acceleration is through the 90 & 270 degree marks. The band center is at h_1 from bottom of the tank. The resulting pressure is calculated as follows:

$b_1 := 2 \cdot ft$ height of the sloshing pressure band

$p_1(\theta) := \frac{P_1}{\pi \cdot Rt \cdot b_1} \cdot \sin(\theta)$ sloshing pressure; positive pressure is outward and negative pressure is inward

$p_1(90 \cdot deg) = 0.519 \cdot psi$ peak value of the sloshing pressure at 90 deg mark

This pressure is verified by integration of the pressure across the circumferential direction from 0 degree to 360 degree.

$2\left(\int_0^{\pi} p_1(\theta) \cdot b_1 \cdot Rt \cdot \sin(\theta)\, d\theta\right) = 4.465 \cdot kip$ this is equal to the sloshing force, P_1, calculated above

Tank T2 (26' x 13' inside dimensions):

$Ls := \frac{13 \cdot ft}{2} = 6.5 \cdot ft$ half of short length of tank

$Ll := \frac{26 \cdot ft}{2} = 13 \cdot ft$ half of long length of tank

$ht := 8 \cdot ft$ fluid depth in tank

$\frac{ht}{Ls} = 1.231$ $\frac{ht}{Ll} = 0.615$

The depth/half length ratio is less than 1.5 in both direction [8, pg. 187]. Thus, the seismic fluid forces consist of sloshing and impulsive components. The sloshing component depends on the horizontal spectral acceleration at the sloshing frequency. The impulsive component depends on the maximum horizontal ground acceleration; this is the acceleration at zero period. From the seismic load, E, definition, this acceleration is 0.4 x 0.44g = 0.18g. The sloshing and impulsive components are calculated for the short and long directions.

$Wt := Ls \cdot Ll \cdot ht \cdot 62.4 \cdot \frac{lbf}{ft^3} = 42.182 \cdot kip$ total weight of fluid

Tank T2 Short Direction

$$W_o := Wt \cdot \frac{\tanh\left(\sqrt{3} \cdot \frac{Ls}{ht}\right)}{\sqrt{3} \cdot \frac{Ls}{ht}} = 26.585 \cdot kip$$

weight of impulsive fluid [8, eq. 6.1]

$$h_o := \frac{3}{8} ht = 3 \cdot ft$$

height of impulsive force [8, eq. 6.2]

$$P_o := 0.18 \cdot W_o = 4.785 \cdot kip$$

impulsive force [8, eq. 6.4]

This force is distributed over a three foot high horizontal band on the two opposite faces spaced, Ls. The band center is at h_o from bottom of the tank. The seismic acceleration is along the length Ls. The resulting pressure is calculated as follows:

$$b_o := 3 \cdot ft$$

height of the impulsive pressure band

$$pr_o := \frac{P_o}{2L1 \cdot b_o} = 0.426 \cdot psi$$

impulsive pressure; positive pressure (outward) on one side and negative (inward) on the opposite side.

$$W_1 := Wt \cdot 0.527 \cdot \frac{Ls}{ht} \cdot \tanh\left(1.58 \cdot \frac{ht}{Ls}\right) = 17.338 \cdot kip$$

weight of sloshing fluid [8, eq. 6.5]

$$h_1 := ht \cdot \left(1 - \frac{\cosh\left(1.58 \cdot \frac{ht}{Ls}\right) - 1}{1.58 \cdot \frac{ht}{Ls} \cdot \sinh\left(1.58 \cdot \frac{ht}{Ls}\right)}\right) = 4.916 \cdot ft$$

height of sloshing force [8, eq. 6.6]

$$\omega := \sqrt{\frac{1.58 \cdot g}{Ls} \cdot \tanh\left(1.58 \cdot \frac{ht}{Ls}\right)} = 2.74 \cdot \frac{rad}{s}$$

natural frequency of sloshing [8, eq. 6.8]

$$T := \frac{2 \cdot \pi}{\omega} = 2.293\, s$$

natural period of sloshing

$$S_a := \frac{0.22g}{\frac{T}{s}} = 0.096 \cdot g$$

spectral acceleration at sloshing frequency using spectra equation in the seismic load, E, definition.

$$y_{max} := \frac{S_a}{\omega^2} = 0.411 \cdot ft$$

maximum horizontal amplitude of sloshing using single degree of freedom approximation

$$\theta_h := 1.58 \cdot \frac{y_{max}}{Ls} \cdot \tanh\left(1.58 \cdot \frac{ht}{Ls}\right) = 0.096$$

sloshing angle [8, eq. 6.9]

$$P_1 := W_1 \cdot \theta_h = 1.663 \cdot kip$$

maximum sloshing total force [8, eq. 6.10]

This force is distributed over a <u>two</u> foot high horizontal band on the two opposite faces spaced, Ls. The band center is at h_1 from bottom of the tank. The seismic acceleration is along the length Ls. The resulting pressure is calculated as follows:

$$b_1 := 2 \cdot ft$$

height of the sloshing pressure band

$$pr_1 := \frac{P_1}{2Ll \cdot b_1} = 0.222 \cdot psi$$

sloshing pressure; positive pressure (outward) on one side and negative (inward) on the opposite side.

<u>Tank T2 Long Direction</u>

$$W_o := Wt \cdot \frac{\tanh\left(\sqrt{3} \cdot \frac{Ll}{ht}\right)}{\sqrt{3} \cdot \frac{Ll}{ht}} = 14.88 \cdot kip$$

weight of impulsive fluid [8, eq. 6.1]

$$h_o := \frac{3}{8} ht = 3 \cdot ft$$

height of impulsive force [8, eq. 6.2]

$$P_o := 0.18 \cdot W_o = 2.678 \cdot kip$$

impulsive force [8, eq. 6.4]

This force is distributed over a <u>three</u> foot high horizontal band on the two opposite faces spaced, Ll. The band center is at h_o from bottom of the tank. The seismic acceleration is along the length Ll. The resulting pressure is calculated as follows:

$b_o := 3 \cdot ft$ height of the impulsive pressure band

$pr_o := \frac{P_o}{2Ls \cdot b_o} = 0.477 \cdot psi$ impulsive pressure; postive pressure (outward) on one side and negative (inward) on the opposite side.

$W_1 := Wt \cdot 0.527 \cdot \frac{Ll}{ht} \cdot \tanh\left(1.58 \cdot \frac{ht}{Ll}\right) = 27.083 \cdot kip$ weight of sloshing fluid [8, eq. 6.5]

$h_1 := ht \cdot \left(1 - \frac{\cosh\left(1.58 \cdot \frac{ht}{Ll}\right) - 1}{1.58 \cdot \frac{ht}{Ll} \cdot \sinh\left(1.58 \cdot \frac{ht}{Ll}\right)}\right) = 4.288 \cdot ft$ height of sloshing force [8, eq. 6.6]

$\omega := \sqrt{\frac{1.58 \cdot g}{Ll} \cdot \tanh\left(1.58 \cdot \frac{ht}{Ll}\right)} = 1.712 \cdot \frac{rad}{s}$ natural frequency of sloshing [8, eq. 6.8]

$T := \frac{2 \cdot \pi}{\omega} = 3.67 s$ natural period of sloshing

$S_a := \frac{0.22g}{\frac{T}{s}} = 0.06 \cdot g$ spectral acceleration at sloshing frequency using spectra equation in the seismic load, E, definition.

$y_{max} := \frac{S_a}{\omega^2} = 0.658 \cdot ft$ maximum horizontal amplitude of sloshing using single degree of freedom approximation

$\theta_h := 1.58 \cdot \frac{y_{max}}{Ll} \cdot \tanh\left(1.58 \cdot \frac{ht}{Ll}\right) = 0.06$ sloshing angle [8, eq. 6.9]

$P_1 := W_1 \cdot \theta_h = 1.624 \cdot kip$ maximum sloshing total force [8, eq. 6.10]

This force is distributed over a <u>two</u> foot high horizontal band on the two opposite faces spaced, Ll. The band center is at h_1 from bottom of the tank. The seismic acceleration is along the length Ll. The resulting pressure is calculated as follows:

$b_1 := 2 \cdot ft$ height of the sloshing pressure band

$pr_1 := \frac{P_1}{2Ls \cdot b_1} = 0.434 \cdot psi$ sloshing pressure; positive pressure (outward) on one side and negative (inward) on the opposite side.

APPENDIX B

STRUCTURAL EVALUATION FOR PUREX FILTER WITH 8 IN. OF SHOTCRETE

ADDITIONAL STRUCTURAL EVALUATION FOR PUREX DEEP BED FILTERS

1. INTRODUCTION & ANALYSIS METHOD

An additional structural evaluation of the PUREX deep bed filter was performed based on 4 ft of soil overburden and 8 in. of shotcrete (instead of the existing 4 in. of shotcrete). The purpose of this additional evaluation is to determine whether margin from collapse exists in the structural members of the PUREX Deep Bed filter if 4 in. of shotcrete were added in the future as part of water intrusion mitigation efforts (for a total of 8 in. of shotcrete).

The structural evaluation was performed using the same approach, including inputs, assumptions, and assessment of the structural margin as previously described for the PUREX Filters in Section 3.9, Section 4.9, and Appendix A of this document. Refer to these sections in the body of the document for detailed description of the structure and modeling approach.

2. RESULTS

Detailed structural drawings for the PUREX filters were used to obtain concrete geometry and rebar information. The roof slab was reduced 1 in. in the modeling and in the concrete evaluation to account for degraded conditions. Similarly, the rebar cross section area was reduced by 10%.

Deformation of the structure is shown in Figure B 2-1, which indicates a maximum deflection of 0.08 in. Contour plots of maximum tension and compression stresses are given in Figure B 2-2 and Figure B 2-3. Contour plots of shear stress are shown in Figure B 2-4. The resulting stresses were integrated over concrete sections to obtain section shear force, axial force, and bending moment. Those are shown in Figure B 2-5 through Figure B 2-8. The following table summarizes the maximum demand forces and moments on critical sections of the structure.

Building Component	Size	Shear Force (lb)	Axial Force (lb)	Bending Moment (in.-lb)
Roof slab	16 in. x 11 in. deep	10,000 (1)	-12,000	310,000
Steel Beam (2)	5 I 10	105	--	3,372

(1) Per Figure B 2-6, the maximum shear force of 29,000 lb occurs at the slab terminal supports and does need not be considered for the slab evaluation. Similarly, high shear forces occurring within the intermediate walls do not need to be considered.

(2) The steel beam shear force and bending moment values are the same as previously summarized in Section 4.9, and illustrated in Figure 4.9-9.

Roof Slab:

Detailed evaluation of the concrete section capacities is similar to Section 4.9 of the calculation.

Cross section = 16 in. wide x 11 in. deep

Assume rebar are No. 6 @ 6 in. top (lower rebar between top and bottom is used)

Area of #6 rebar = 0.44 in.^{2} (to be reduced by 10%)

Rebar depth = 11 in. (assuming 1 in. clear cover so that rebar becomes exposed with 1 in. loss of thickness)

Axial compression capacity

Axial compression capacity with no bending (using strength reduction factor of 0.7):

$\phi Pn = 0.7 \times 0.8\ (0.85\ fc\ (A_{cross} - As) + fy\ (As))$

$= 0.7 \times 0.8\ (0.85 \times 3{,}000\ (16 \times 11 - 0.44 \times 16/6 \times 0.9) + 40{,}000\ (0.44 \times 16/6 \times 0.9))$

$= 273{,}500$ lb >> 12,000 lb

The axial compression capacity is significantly larger than the demand axial compression.

Bending Moment Capacity

$\phi Mn = 0.9 \times As\ fy\ \{d - As\ fy / (2 \times 0.85\ fc\ b)\}$

$= 0.9 \times (0.44 \times 16/6 \times 0.9) \times 40{,}000 \times$

$\{11.0 - (0.44 \times 16/6 \times 0.9) \times 40{,}000 / (2 \times 0.85 \times 3{,}000 \times 16)\}$

$= 398{,}497{,}006$ in.-lb >> 310,000 in.-lb

Shear Capacity

Reduced shear stress capacity of the concrete section using ACI Eq. 11-3:

$\phi\tau n = 0.75 \times 2 \times \sqrt{fc} = 82$ psi

$\phi Vn = 82$ psi x 16 x 8 = 14,460 lb > 10,000 lb

Thus, the roof slab is acceptable since additional shotcrete weight has insignificant impact on beam demand. The loads on the steel beam are acceptable by inspection based on the magnitude and size of the 5 x 10 I-beam section.

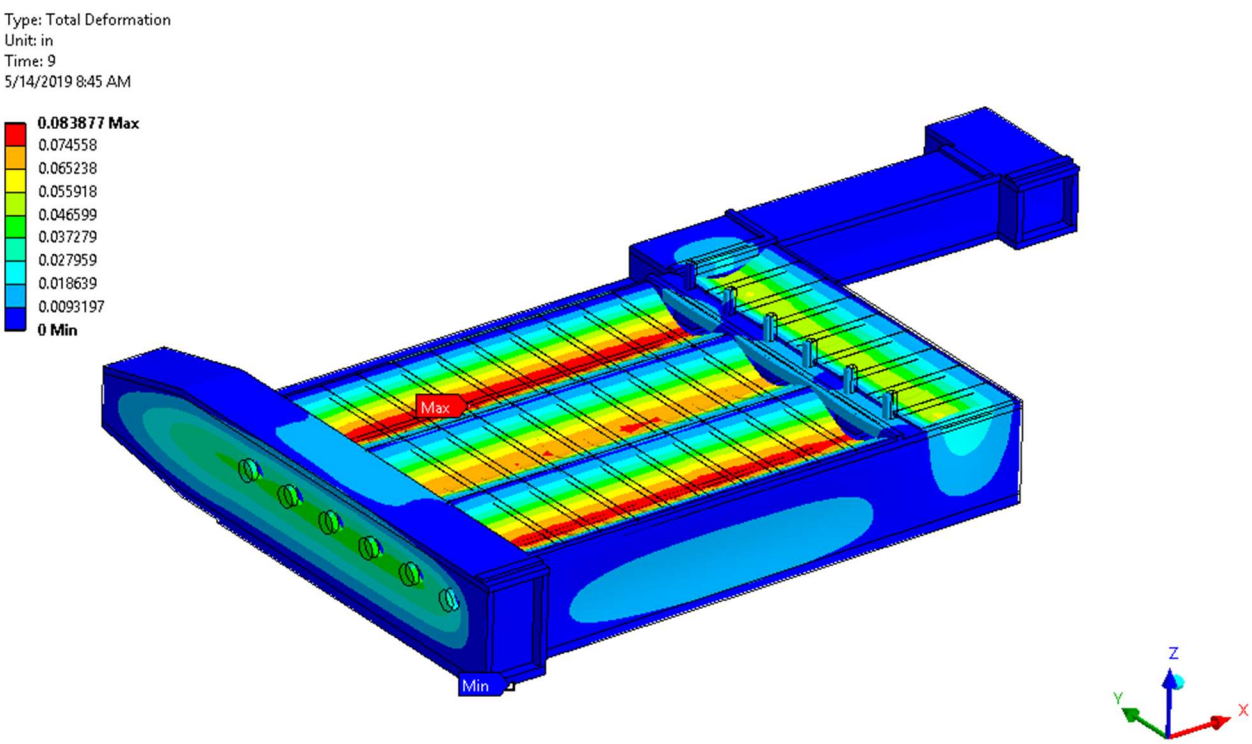

Figure B 2-1: Contour Plot of Deformations (in.) for PUREX Filters

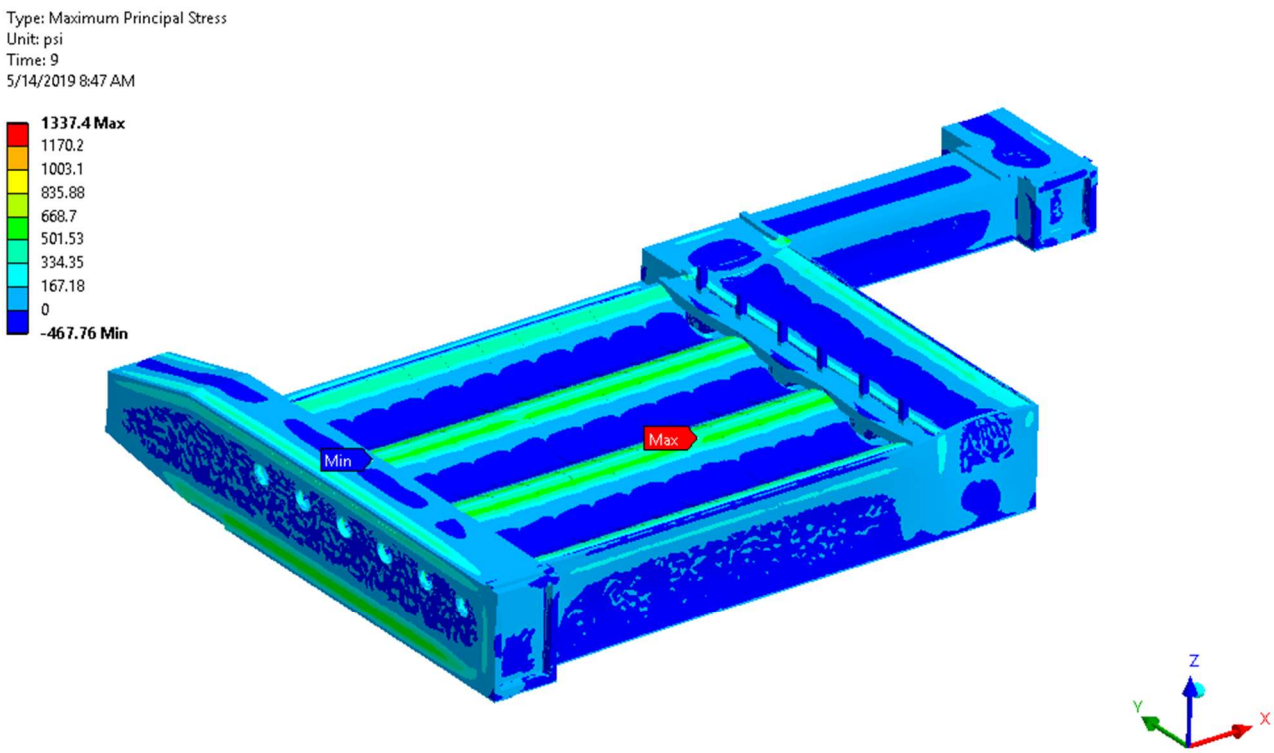

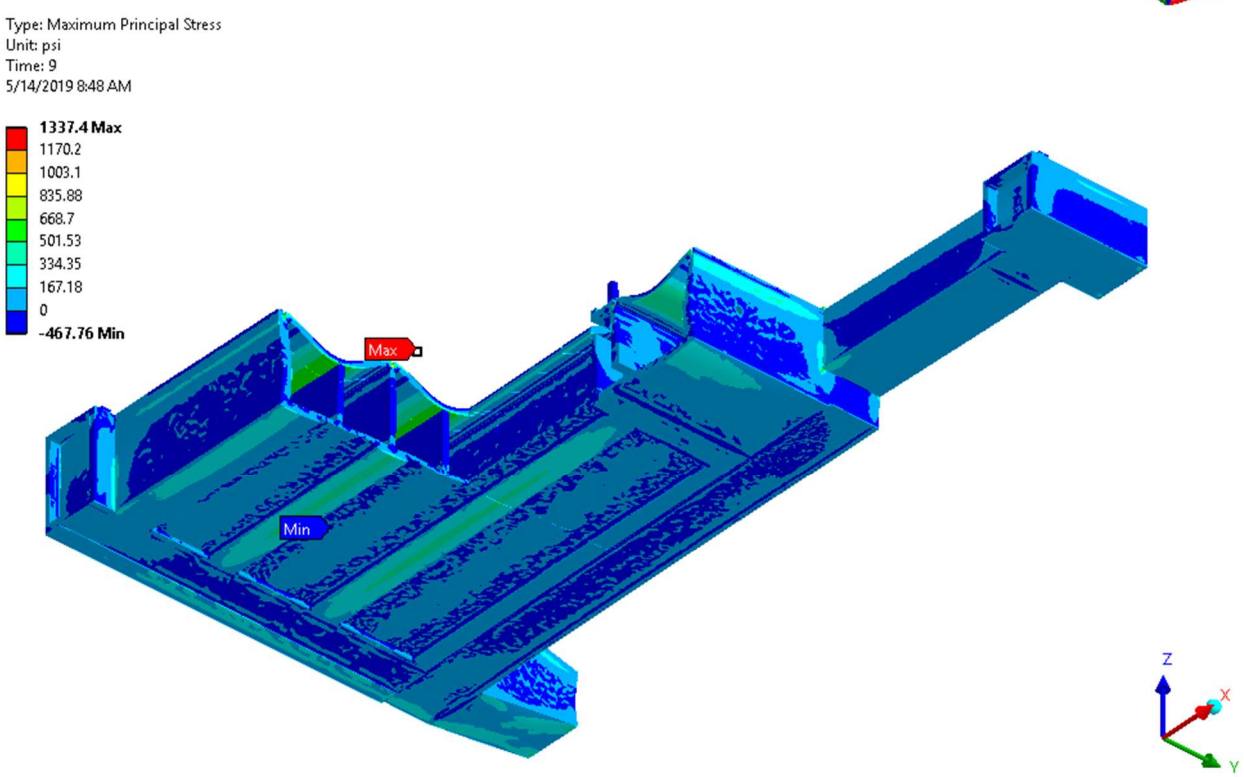

Figure B 2-2: Contour Plots of Maximum Principal Stress (psi) for PUREX Filters

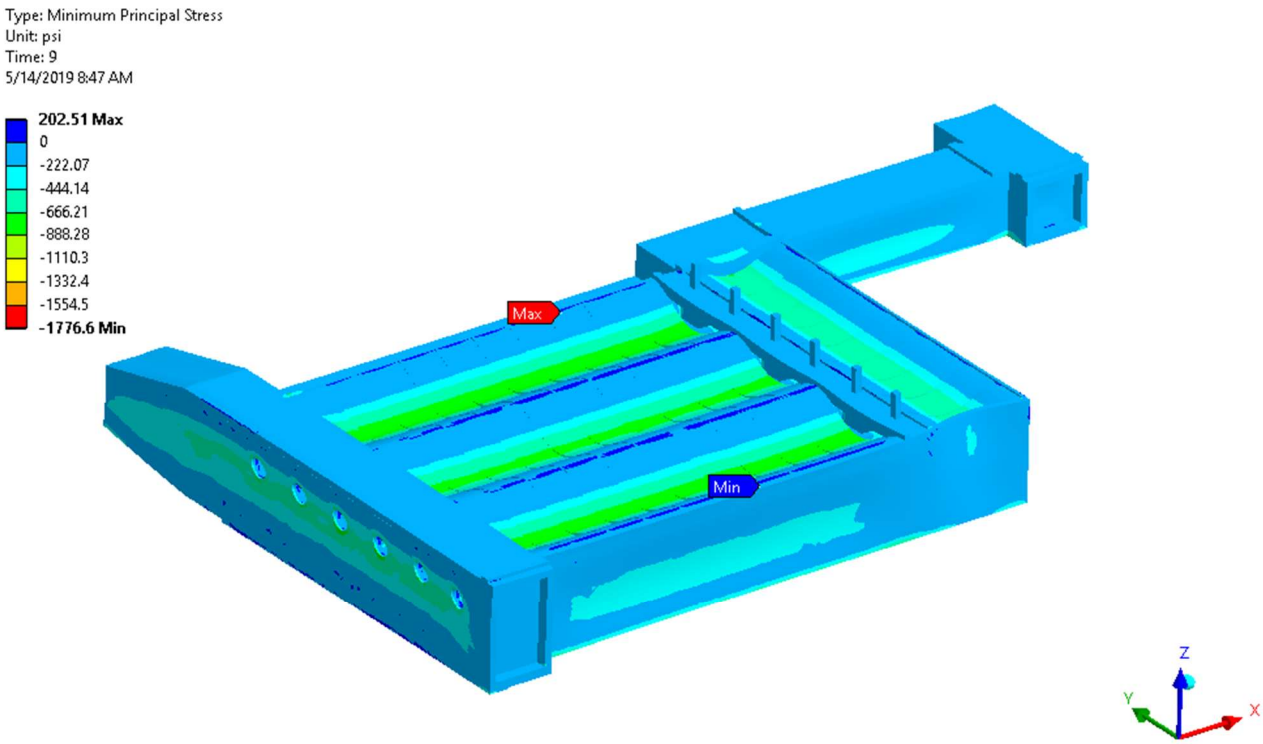

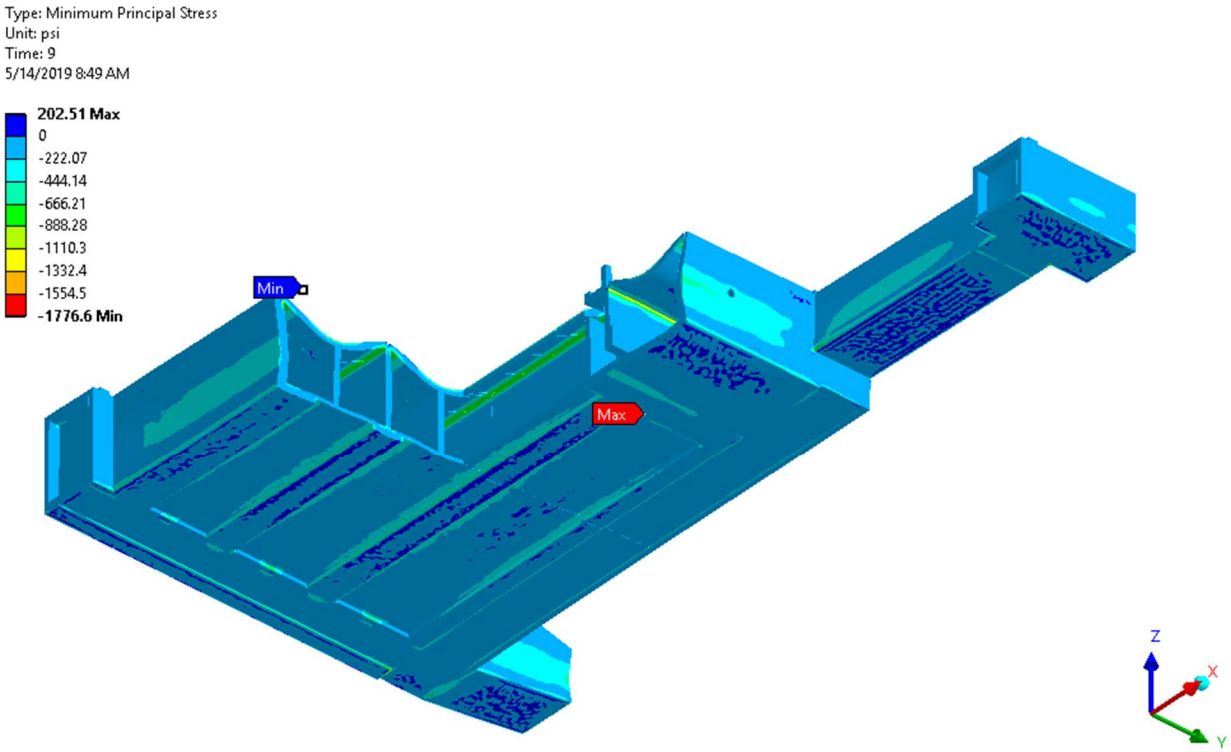

Figure B 2-3: Contour Plots of Minimum Principal Stress (psi) for PUREX Filters

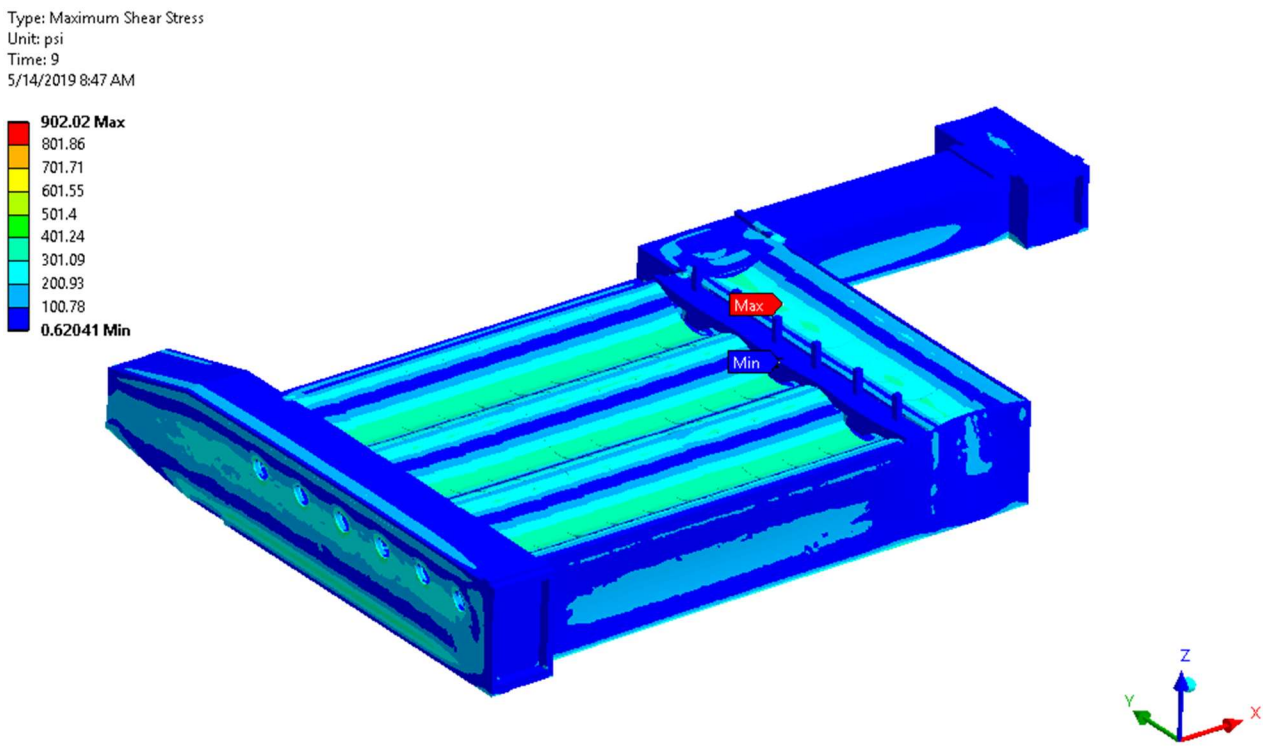

Figure B 2-4: Contour Plots of Shear Stress (psi) for PUREX Filters

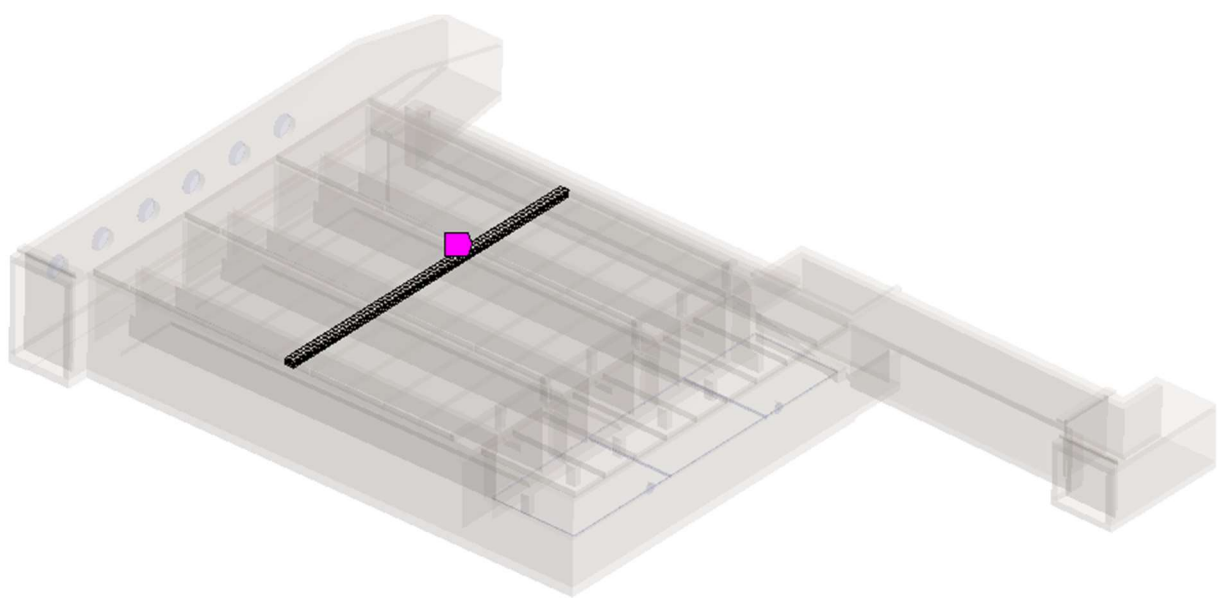

Figure B 2-5: Roof Slab Strip for PUREX Filters

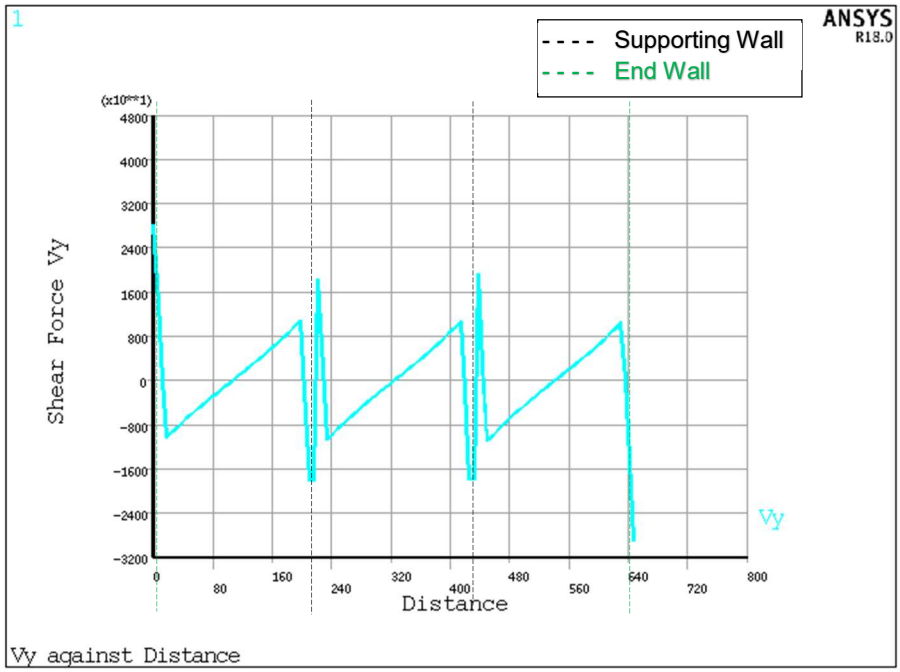

Figure B 2-6: Roof Slab Strip Shear Force (lb) Diagram for PUREX Filters

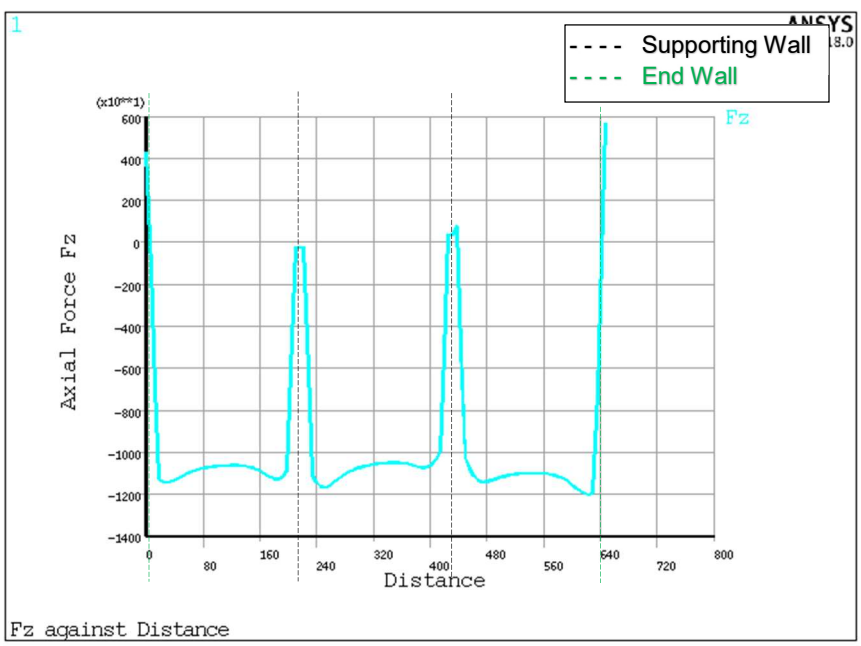

Figure B 2-7: Roof Slab Strip Axial Force (lb) Diagram for PUREX Filters

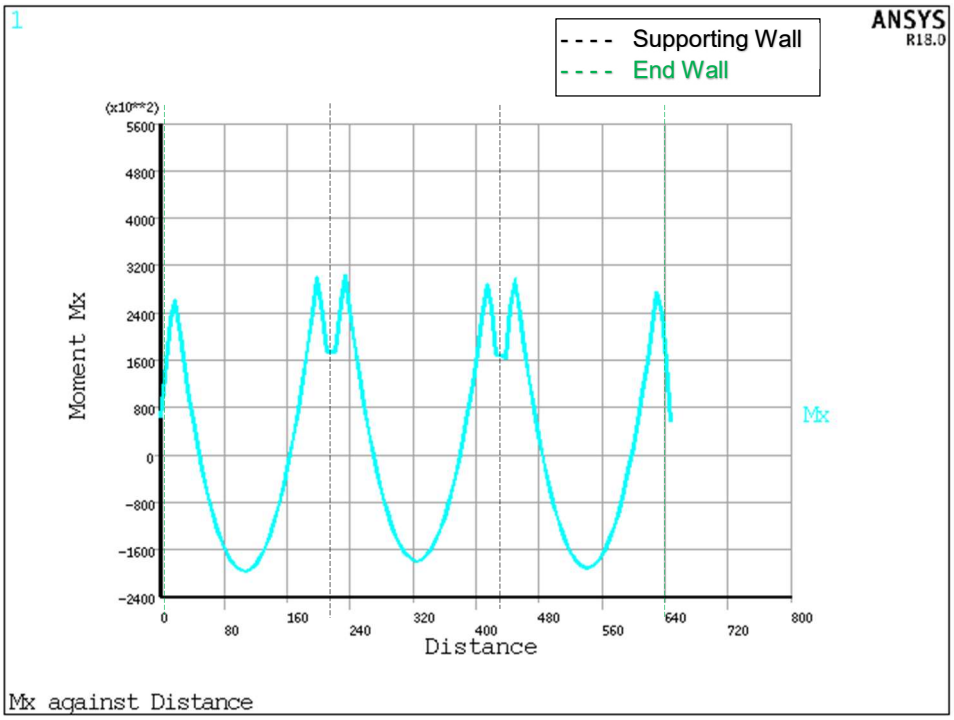

Figure B 2-8: Roof Slab Strip Moment (in.-lb) Diagram for PUREX Filters

3. SUMMARY

ANSYS ® software was used to perform a structural evaluation of the PUREX deep bed to determine whether margin from collapse exists in the structural members of the PUREX Deep Bed filter if 4 in. of shotcrete were added in the future as part of water intrusion mitigation efforts (for a total of 8 in. of shotcrete). The PUREX filter analysis was performed based on current code requirements for load factors, load combinations, and strength reductions for concrete and steel materials, as described in Appendix A. Given the documented evidence of water intrusion for the PUREX filters [18], the structural evaluation simulated degradation in structural members by employing reduced concrete thickness and reduced rebar surface area. The modeling and analysis approach is similar to that used in Sections 3.9 and 4.9 for the current configuration (i.e. with 4 in. shotcrete) analysis.

Results indicate that structural members of the PUREX filters have adequate margin against failure (i.e., margin to collapse is acceptable). The structural evaluation presented herein address the overall structural stability, and should not be used to justify worker safety.

APPENDIX C

RCR DOE COMMENTS
AND
ADDITIONAL PLOTS

Acrobat 9.0

REVIEW COMMENT FORM

Document Reviewed: LA181779-R-001, Structural Assessment of Aging Legacy Buried Cribs and Tanks a the Hanford Central Plateau

Reviewer(s): DOE / Al Farabee

Revision(s)/Rev. #: 0

Reviewing Department: DOE

Review Date: 06/25/2019

Item	Reference Number (Section, Figure, Table, Page)	Comment	Comment Type		Resolution
			Major	Minor	
	COMMENTS 1-10 BELOW ARE BASED on LPI Subcontractor notes taken during 6/25/2019 meeting with DOE. Comments 11-28 are directly from Mr. Farabee's email correspondence.				
1	Entire document.	Change page numbering. Mr. Farabee's exact comment: Consider the value of re-thinking the numbering system the report. Appendix B has a page numbered "Page 166 of 164" and "B-167". Page "B-168" is the first page of Appendix A to Appendix B and is numbered "Page A1 of A23" and "B-168". There is also Attachment A and Attachment B to the Appendix A to Appendix B			The LPI report LA181779-R-001 will be issued separately - this report will not be an Appendix of another report. Therefore, the page numbering issue will be resolved.
2	All figures.	Add units to all figures.			Agreed, change will be implemented.
3	Figures	Explain legend in figures or remove legend on ANSYS plots.			Agreed, legends will be explained.
4	Section 4.11, Tank 241-CX-70	Provide (for one location along the critical strip of Tank 241-CX-70) shear force diagrams through the thickness of Tank 241-CX-70, a curve for each node.			Will be provided as requested. However, these additional plots will be provided outside of the LPI Report LA181779-R-001.

WCH-DC-041 (09/16/2014)

Page 1 of 12

Acrobat 9.0

REVIEW COMMENT FORM

Item	Reference Number (Section, Figure, Table, Page)	Comment	Comment Type		Resolution
			Major	Minor	
5	Figures/graphs throughout document.	Explain "artifacts" in each plot as applicable. These are the "dips" or "blips" in graphs that occur due to numerical modeling techniques (i.e., refined mesh), this may be done via footnotes. Mr. Farabee's exact comment: –Present data in the report submitted to DOE that is representative of the risk addressed by the analysis but does not affect the credibility of the analysis by displaying data that has no physical significance. An example of this issue is graph of Figure 4.7-5 on page 106 of 164 (B-107). As discussed in the last meeting, the first and last 6-10" and the spikes at ~80" and 125" have no physical significance and are an artifact of the numerical analysis technique. The presence of these points on the graph are difficult to explain to a non-technical audience and would only affect the credibility of the product.			Agreed, explanations will be added.
6	Graphs throughout document.	Revise graphs (add dashed vertical lines) to indicate where wall begins and ends to differentiate stresses in roof and base.			Agreed, graphs will be revised.
7	All model runs.	Add the number of nodes for each ANSYS element type or number of nodes through the thickness at critical locations.			Agreed, changes will be implemented.

WCH-DC-041 (09/16/2014)

Page 2 of 12

Acrobat 9.0

REVIEW COMMENT FORM

Item	Reference Number (Section, Figure, Table, Page)	Comment	Comment Type		Resolution
			Major	Minor	
8	Section 4.7, 241-Z-361	For 241-Z-361, Figure 4.7-2, identify location (height along the wall) where maximum deflection occurs. Provide simple sketch or sketches in to explain why maximum deflection occurs at mid height of the wall. It is expected maximum deflection of occur slightly above mid height of the wall. Sketches should show increasing hydrostatic pressure with increasing depth of waste and increasing lateral earth pressure with increasing depth, with and without load factors.			Will be provided as requested. However, these additional plots will be provided outside of the LPI Report LA181779-R-001.
9	Figure 4.7-1	Show opposite face in Figure 4.7-1 to match location of legend ("Max" arrow).			Agreed, change will be implemented.
10	Section 4.7, 241-Z-361 additional modeling	Perform additional modeling on the 241-Z-361 tank to capture noted roof cracking. Suggest assuming 20% reduction in rebar cross-setion area or crack modeling. Mr. Farabee's exact comment: --Provide additional data analysis to recognize the existing crack in 241-Z-361 tank. This crack was discussed on Page 18 (A-29) of Appendix A.			In the absence of crack dimensions and exact location(s) within Z-361, LPI will update results in the report for tank Z-361 by assuming a 20% reduction in rebar cross-section area to account for the observed cracking.
11	References	Change references to mass of Pu from pounds to kilograms.			Accept. Will change reference from pounds to kilograms in 67569-RPT-002.
12	On page 7	please identify the inches of sludge and liquid in the tank			Accept. Will identify sludge depth of sludge in 241-Z-361 on page 7 in 67569-RPT-002.
13	On page 9	does "center of the long side of tank pertain to horizontal and vertical. Pls clarify.			Clarification will be added to the discussion in Section 4.7 for the 241-Z-361 tank.

WCH-DC-041 (09/16/2014)

Page 3 of 12

Acrobat 9.0

REVIEW COMMENT FORM

Item	Reference Number (Section, Figure, Table, Page)	Comment	Comment Type		Resolution
			Major	Minor	
14	On page 9	"...lower end of the long wall..." does not appear to agree with contour plots			Contour plot for vertical axial stress (Figure 4.7-2) in Section 4.7 for the 241-Z-361 tank shows high stresses at bottom of wall. Therefore, statement is consistent with the plot. No change.
15	On page 9	is a negative value for compression the same as a positive value for compression? If the answer is yes, can this be more clearly stated? Is maximum tension directly on the other side of wall from the maximum compression value?			Section 4.7 for the 241-Z-361 tank, no, a positive axial force is tension and a negative axial force is compression. Figure 4.7-4 shows a compressive axial force in the bottom side of the wall and a tensile axial force approaching the top side of the wall.
16		The 2003 EE/CA for Z-361 refers to the Appendix C of the FSAR stating "...the consequences of the tank containing wet sludge are extremely small...". Is there more current document that states otherwise?			CHPRC will address this comment.

WCH-DC-041 (09/16/2014)

Page 4 of 12

Acrobat 9.0

REVIEW COMMENT FORM

Item	Reference Number (Section, Figure, Table, Page)	Comment	Comment Type		Resolution
			Major	Minor	
17	Tank T2 assumptions on Page A7 of A23 (B-174)	Since both zones along short and long directions are below sludge and water, provide rationale in document for zone selection/placement.			The sloshing and impulsive pressures act over the wet depth of the tank. Application of the total pressure force over smaller length is more conservative. This is similar to comparing simply supported beam with uniform load and same beam with same total load but distributed over smaller length. The sloshing is over a narrower band as compared to impulsive because the significant sloshing pressure is concentrated over smaller depth near the fluid surface. The impulsive pressure on the other hand acts over entire depth. Therefore, the selected band widths are conservative. Note in the sketch (provided at end of this review comment form), the impulsive band should be shifted up by about 1 ft.
18	9. Page 6 of LPI presentation and discussion of "241-CX-70 Graphs"	Explain the x-axis number of 250 wrt diameter and height of tank. Also, same question on the "250" wrt Figure 4.7.3 on page B-106 (105 0f 164) -THIS MAY BE ADDRESSED IN COMMENT 6 ABOVE-			The height of 241-Z-361 is 19 ft (228 in.), and the inner diameter of CX-70 is 20 ft (240 in.). The x-axis of these graphs stops at 250 in. since 250 bounds both the height and diameter of these 2 structures.

WCH-DC-041 (09/16/2014)

Acrobat 9.0

REVIEW COMMENT FORM

Item	Reference Number (Section, Figure, Table, Page)	Comment	Comment Type		Resolution
			Major	Minor	
19	Figure 3.11-4	The sides appear to have 3-4 cells. Mesh size is 3.5" and material thickness is 12" (analysis assumed 11"). Were the calculation runs made in center of cell or on the sides of the cell? How many runs were made?			The finite element equation solution was performed at element (cell) integration points interior to the elements and the solution was interpolated at the element boundary nodal point. Two load combinations (Section 4 of Appendix A) were evaluated for the structural analysis, and hence, two runs were performed.

WCH-DC-041 (09/16/2014)

Page 6 of 12

Acrobat 9.0

REVIEW COMMENT FORM

Item	Reference Number (Section, Figure, Table, Page)	Comment	Comment Type		Resolution
			Major	Minor	
20	Page 62	Explain the rebar and stainless steel stiffeners and why they were not modeled WIDS report seems to indicate that 2004 cave-in was due to wood shoring above the manway. Why would this drive the 1" and 10% assumptions? Where is the code evaluation that was addressed outside of ANSYS?			The concrete was modeled as a solid linear elastic material, and cracking was not simulated in the finite element analysis (FEA); therefore, rebar were conservatively not included in the model. The resulting forces and moments from the FEA were evaluated using ACI equations for flexure and shear. The rebar were utilized in the ACI equations. Excluding the stiffeners in the analysis is conservative and adequate since the condition of the stiffeners cannot be verified. The concrete and rebar degradation were conservatively assumed since the condition is unknown. Assumed degradation was based on the data collection efforts as summarized in 67569-RPT-001 report. The WIDS report was not available to the team at the time 7569-RPT-001 was issued; therefore, details of the subsidence were not known. The WIDS report suggest that the shoring surrounding the manway collapsed-not the tank itself. Given the new information, LPI proposes to redo the ANSYS analysis of this tank without degradation of the concrete and rebar. The code evaluation outside of ANSYS ® is provided in Section 4.11.

WCH-DC-041 (09/16/2014)

Page 7 of 12

Acrobat 9.0

REVIEW COMMENT FORM

Item	Reference Number (Section, Figure, Table, Page)	Comment	Comment Type		Resolution
			Major	Minor	
21	Figure 4.11-1	Explain all of legend Relative to question on Figure 3.11-4, which mesh location is this a plot of----------top, bottom, etc? Provide contour plots for each mesh level. It is expected that this is only three or four plots			The legend shows the range of displacement in the structure, where the units of displacement are inches. For example, the maximum displacement of 0.145 in. occurs in the center of the roof. The displacement contours for the outside surfaces (top view) are shown Figure 4.11-1. Similar displacement results on interior surfaces would be observed since changes in the wall and roof thicknesses are negligible. Per previous response, additional displacement plots are not necessary since displacement through the thickness is independent of the mesh level.

WCH-DC-041 (09/16/2014)

Page 8 of 12

Acrobat 9.0

REVIEW COMMENT FORM

Item	Reference Number (Section, Figure, Table, Page)	Comment	Comment Type		Resolution
			Major	Minor	
22	Figure 4.11-6	Explain all of legend Relative to question on Figure 3.11-4, which mesh location is this a plot of----------top, bottom, etc? Provide contour plots for each mesh level. It is expected that this is only three or four plots			Believe the comment shown to the left was not intended for Figure 4.11-6. Per June 4, 2019 meeting, comments and responses for Figure 4.11-6 are as follows: 1)Why is this particular area chosen? --LPI response: Based on stress contour plots, this is the most critical section in the slab. 2) What are units? -LPI response: shear and axial forces are in lb and moments are in lb-in. 3) What is interaction with roof penetration? -LPI response: Penetrations in the roof were included in the model, and their interaction was captured by the FEA as shown in the displacement and stress contour plots (Figures 4.11-1 through 4.11-4). The maximum stress locations in the roof observed at the center and perimeter of the roof are generally not influenced by the penetrations.

WCH-DC-041 (09/16/2014)

Page 9 of 12

Acrobat 9.0

REVIEW COMMENT FORM

Item	Reference Number (Section, Figure, Table, Page)	Comment	Comment Type		Resolution
			Major	Minor	
23	Graphs	Explain shape of graphs relative to graphic figures Explain relationship of "0" on graph to the red/blue/green notation on the figures			This comment applies to 241-CX-70 graphs (Section 4.11 in the report). The graphs follow the coordinate system located at the critical location (strip) shown on Figures 4.11-6 and 4.11-10. The horizontal axis represents the distance along the Z-axis (blue), the shear force is in Y direction (green), axial force in the Z direction (blue), and bending moment is about the X-axis (red). The "0" is at the origin of the shown coordinate system, and the different colors axes are as described above.
24		Show applied forces/pressure diagrams for all structures on the maximally stressed surface.			Will be provided as requested. These additional plots will be provided outside of the LPI Report LA181779-R-001 Or plots can be included as an Appendix in the LPI report. Please advise.
25		Please show the load combinations used for each structure at the maximally stressed surface: o For vertical surfaces, show the values of load combination at 6 different levels o For horizontal surfaces, show the load distribution on the surface.			As described in response to comment #19, two load combinations (described in Section 4 of Appendix A) were evaluated for the structural analysis, and hence, two runs were performed for each structure. The additional plots or values requested will be provided outside of the LPI Report LA181779-R-001 Or can be included as an Appendix in the LPI report. Please advise.

WCH-DC-041 (09/16/2014)

Page 10 of 12

Acrobat 9.0

REVIEW COMMENT FORM

Item	Reference Number (Section, Figure, Table, Page)	Comment	Comment Type		Resolution
			Major	Minor	
26	Figure 4.1-3	does it represent the structure roof? If so, please indicate that. This comment applies to all other structures.			Figure shows shear stress contour for the general cross-section of 216-Z-2 in the top (cover) of the crib. Clarification will be added to other structures as applicable.
27	Figure 4.1-3	What is the difference between the upper and lower figures on Figure 4.1-3? Please explain why the smallest value of the shear stress (548 PSI) was chosen?			The upper plot shows the XZ shear stress component through the thickness, where the maximum average shear stress in that direction is 548 psi. The lower plot shows the resultant maximum shear stress where the peak value of 1,372 psi is at geometric discontinuities. The maximum average shear stress of 548 psi better represents the overall structural demand for the purpose of comparison to strength limits.
28	Page 101 of 164 (B-102) tables	shows the values of bending moment, axial & shear forces, are those the maximum values? What is the location of maximum bending moment, shear and axial forces on the roof?			Tables in Section 4.7 (Z-361) summarize bending moment, axial force, shear force, axial stress and shear stress - values shown are maximum values. The location where these maximum occur will be added to the discussion in Section 4.7.
29					

WCH-DC-041 (09/16/2014)

Page 11 of 12

Acrobat 9.0

REVIEW COMMENT FORM

Item	Reference Number (Section, Figure, Table, Page)	Comment	Comment Type		Resolution
			Major	Minor	

WCH-DC-041 (09/16/2014)

Discussion and Plots Requested for DOE RCR Comment No. 4

For concrete structures, ANSYS-calculated stresses were integrated for selected representative slice (strip) of elements along the critical locations in the roof and walls to obtain the demand axial and shear forces and bending moments (as shown in Section 4). Section 4.11 provides graphs of shear force, axial force, and bending moments along the most critical 12 in. wide strip (of the roof and the vertical wall) for the 241-CX-70 tank. Recall that depending on the selected mesh of the finite element model, the selected strip of elements may have irregular shape (due to refined meshing) – where the irregular shape causes indications (dips/humps) in the 2-D graphs.

To avoid irregularities in the shape of the selected strip in the 241-CX-70 tank model, the method of integrating ANSYS-calculated stresses to obtain a shear force diagram through the thickness of a component was verified by comparing the ANSYS-generated shear force diagram to the explicitly calculated (hand-solution) of a solid element beam (12 x 6 x 120 in.), simply supported (pin-roller) model, and having a concentrated load of 100,000 lb at the center of the beam length (60 in.). Theoretical solutions for maximum shear and moment for this model are:

shear = P_{load} / 2,

where P_{load} = 100,000 lb, or shear = 50,000 lb

max moment = P_{load} x Length / 4,

where Length = 120 in., or moment = 3 x 10^6 in.-lb.

As shown in Figure 1 through Figure 4 below, the shear and moment diagrams generated by ANSYS match those calculated explicitly (hand solution).

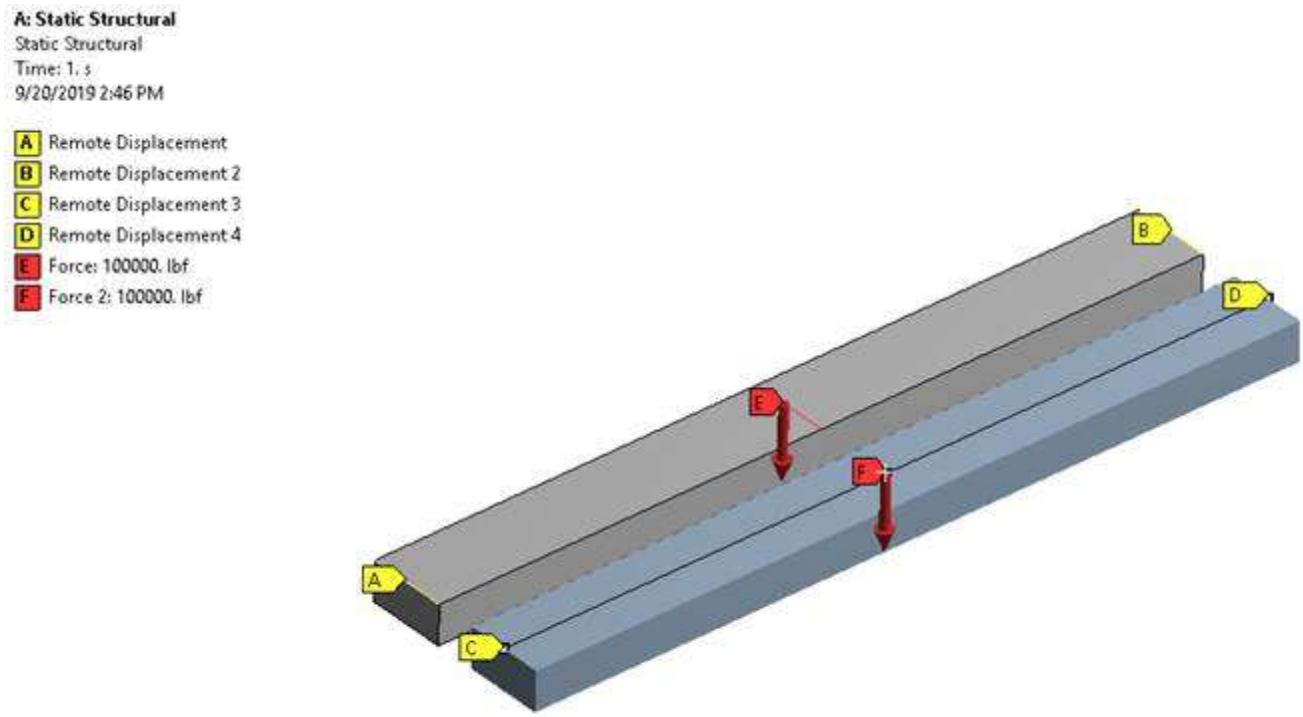

Figure 1. Solid Beam Model with Concentrated Load

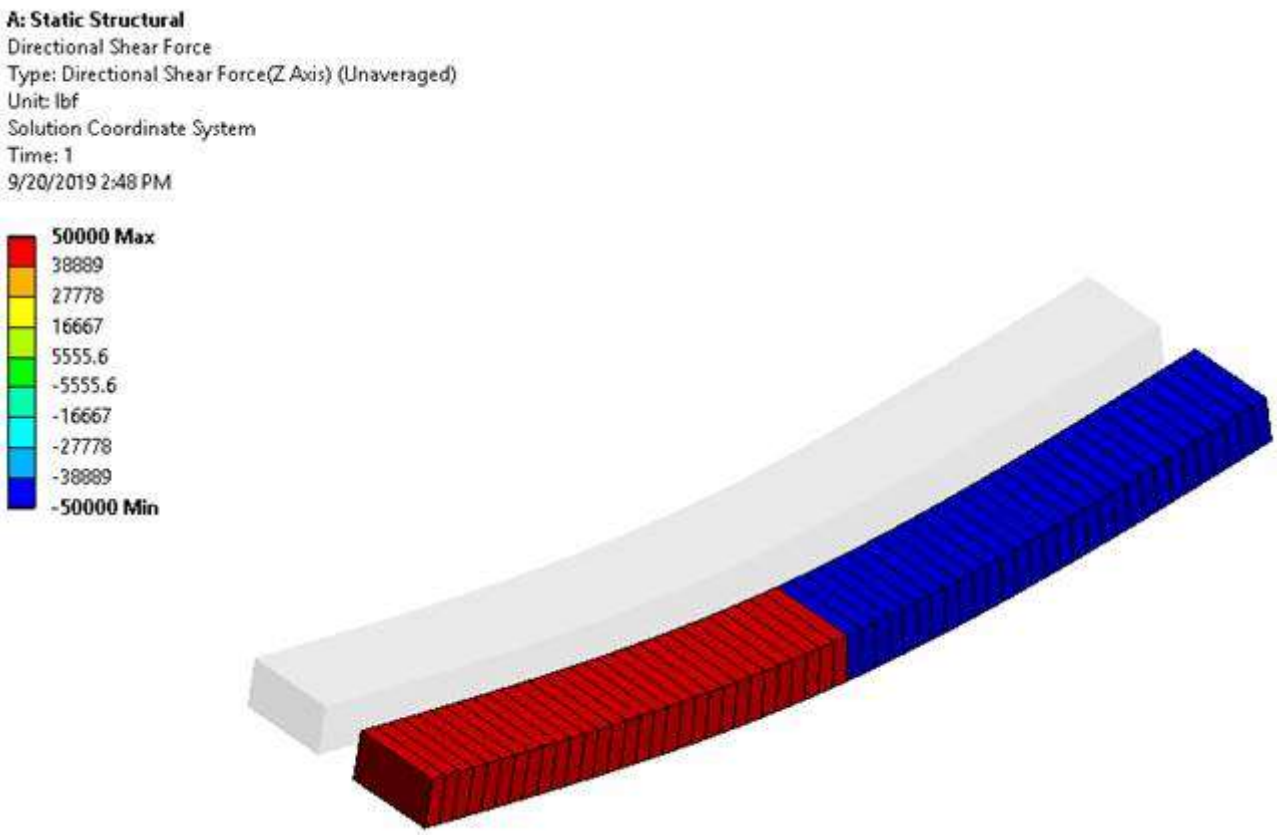

Figure 2. Solid Beam Model Shear Force (lb)

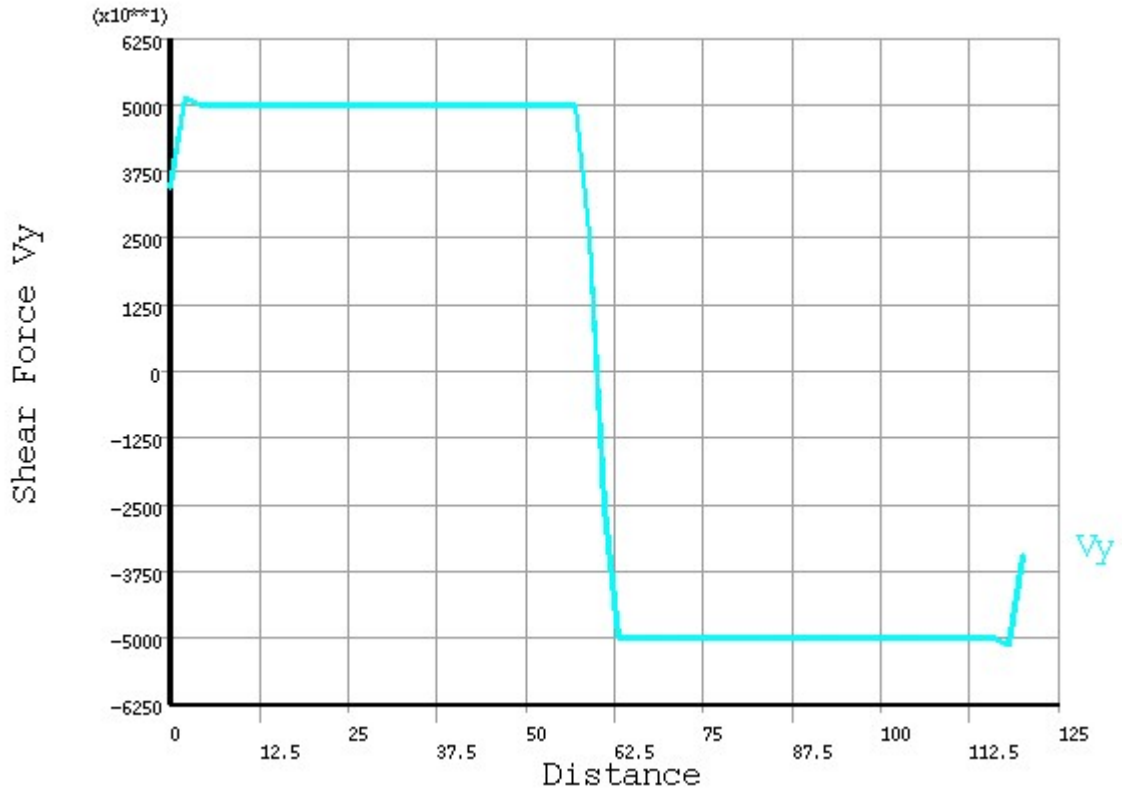

Figure 3. Shear Force (lb) vs. Distance (in.)

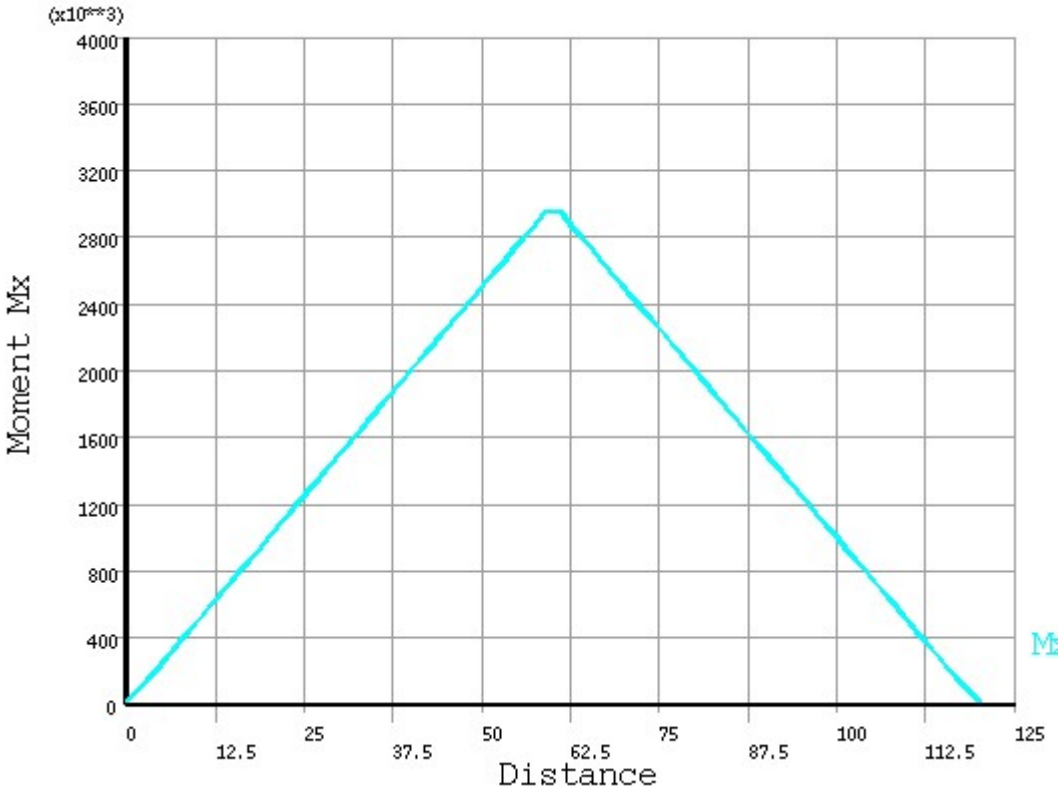

Figure 4. Moment (in.-lb) vs. Distance (in.)

Discussion and Plots Requested for DOE RCR Comment No. 8

Figure 1 below shows the deflection profile of the long wall for 241-Z-361 at mid length resulting from the finite element analysis described in LPI report LA181779-R-001. The general shape of the deflection profile is nearly symmetric about mid height. However, as shown in Figure 1 below, the shape above and below the mid height are different as indicated with the two points at 40 in. above and below the mid height. Asymmetry is also clear in the wall rotation at the top end and bottom end as indicated by the dashed circles. The maximum deflection is slightly above the mid height. So, in summary, the deflected shape can be characterized as nearly symmetric.

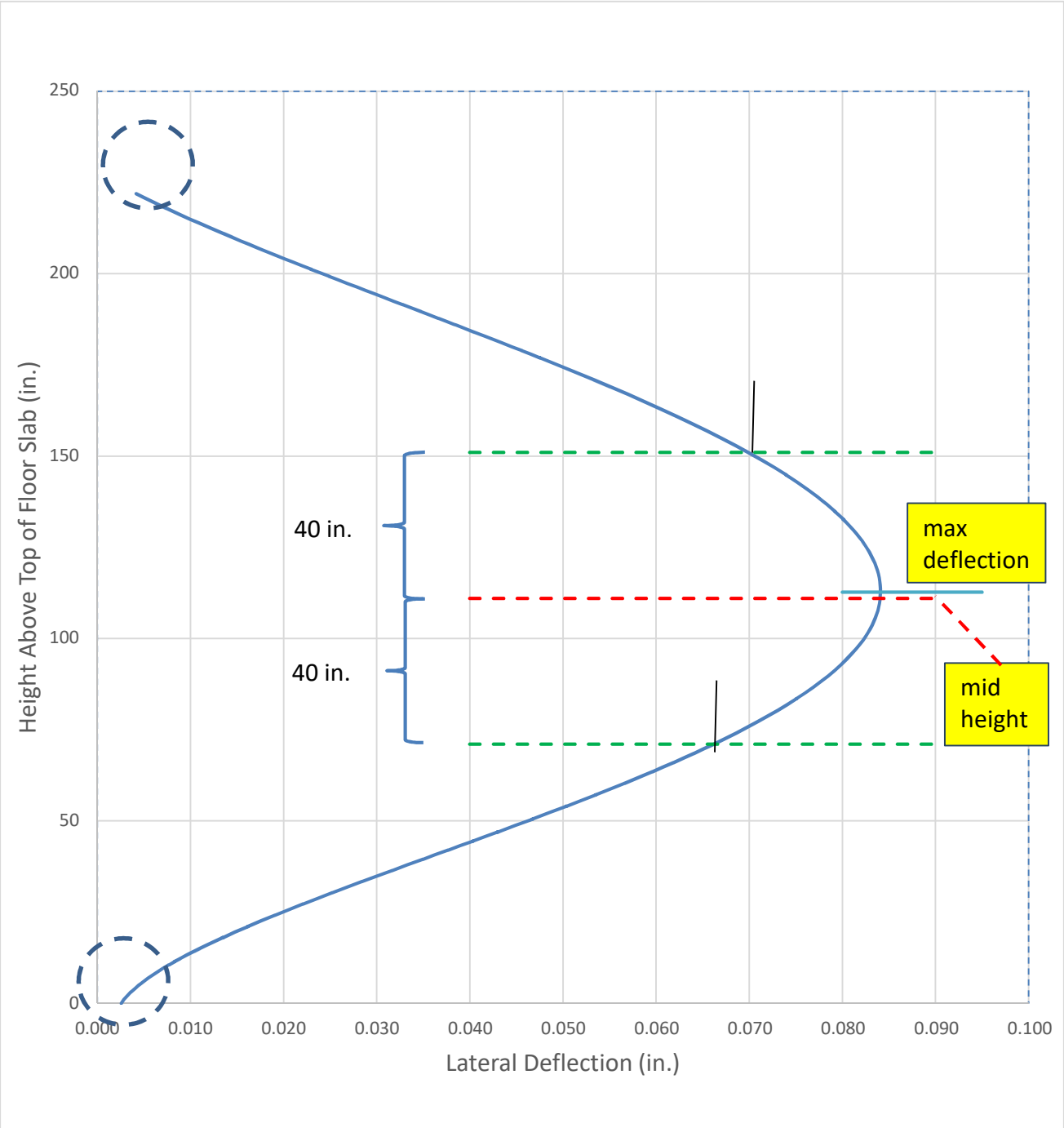
250
200
150
100
50
0
Height Above Top of Floor Slab (in.)
0.000
0.010
0.020
0.030
0.040
0.050
0.060
0.070
0.080
0.090
0.100
Lateral Deflection (in.)
40 in.
40 in.
max deflection
mid height

Figure 1

Lateral deflection of the long wall shown above is governed by the applied pressure loads and the top and bottom end conditions (i.e. rotation restrained at the dashed circles). The applied pressure loads are shown in Figure 2 below where the values are determined by the following equations:

Lateral earth pressure (unfactored) = 0.5 x 125 lb/ft^3 x depth (ft)
Lateral earth pressure (factored) = 1.7 x 0.5 x 125 lb/ft^3 x depth (ft)

> Where depth is from ground surface and is 21 ft at the top of the foundation slab, and
> 1.7 is the load factor for lateral earth pressure in Load Combination 1 (see Appendix A of this report).

Lateral waste hydrostatic pressure (unfactored) = 1.7 x 62.4 lb/ft^3 x waste depth (ft)
Lateral waste hydrostatic pressure (factored) = 0.9 x 1.7 x 62.4 lb/ft^3 x waste depth (ft)

> Where waste depth is from top of waste level at 8 ft above foundation slab, and 0.9 is the load factor for waste pressure in Load Combination 2 (see Appendix A of this report).

The lateral loads are obviously significantly higher on the lower half of the wall and will thus cause the maximum deflection of the wall to move down below the mid height.

The end conditions are wall rotations at the foundation slab and at the top slab. Equal rotations at top and bottom will cause the deflection profile to be symmetric with maximum deflection at mid height. However, the wall rotation at the foundation is restrained more than the rotation at the top slab as can be seen in the deflected shape. This causes the maximum deflection to move up.

Thus, the load pattern and end conditions of the wall have opposing effects on the location of the maximum wall deflection. Based on the near symmetry of the deflection profile, it is deduced that the two effects are nearly of equal magnitude on the location of the maximum deflection. Any variations in the loads or end conditions will change the location of the maximum deflection.

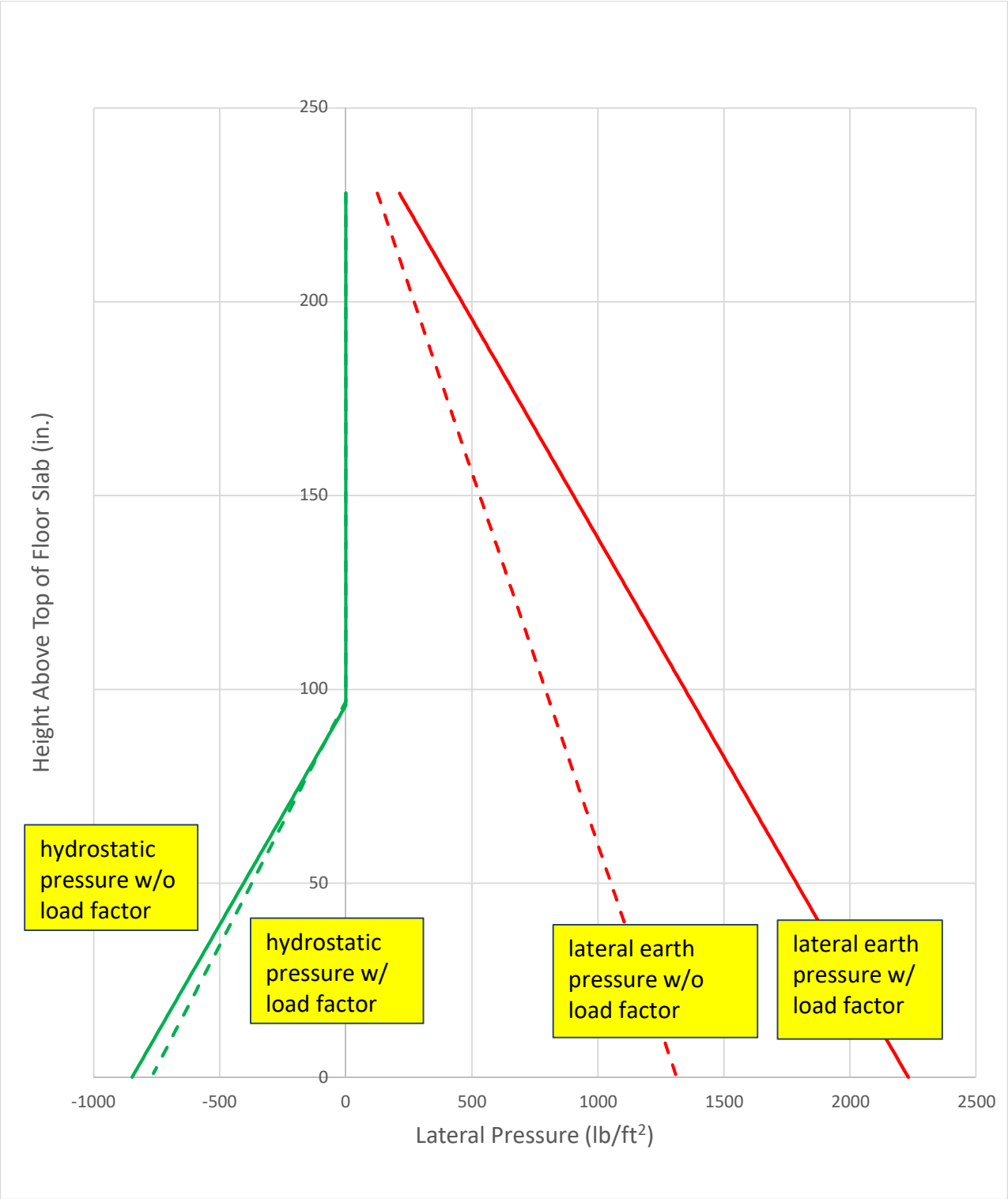
250
200
150
100
50
0
-1000
-500
0
500
1000
1500
2000
2500
Height Above Top of Floor Slab (in.)
Lateral Pressure (lb/ft²)
hydrostatic pressure w/o load factor
hydrostatic pressure w/ load factor
lateral earth pressure w/o load factor
lateral earth pressure w/ load factor

Figure 2

Plot Addressing DOE RCR Comment No. 17

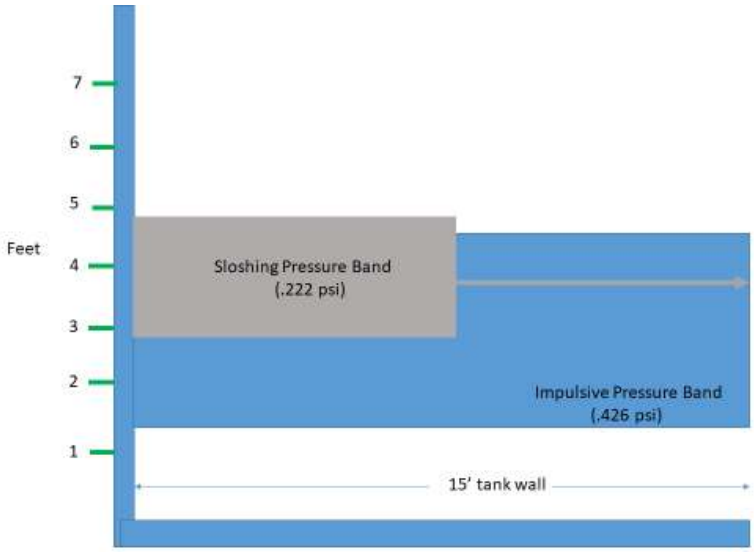

Discussion and Plots Requested for DOE RCR Comment No. 24 & 25

Applied loads on the walls and roofs for each of the eleven structures in the scope of work are tabulated in the subsequent tables. The discrete values for the loads in these tables encompass the maximally stressed surfaces shown in Section 4 of this report; therefore, addressing the review comment record (RCR) Comment No. 24. As requested by RCR comment No. 25, loads are shown at 6 different elevations for the walls of the structures.

Note: lateral earth pressure (LE), Waste Load (F) – as applicable, load factor (LF), and the roof pressure includes the weight of the roof if the roof is concrete.

Structure: 216-Z-2

depth of soil in.	lateral pressure on walls lb/ft^2			
	LE w/o LF	LE w/ LF	F w/o LF	F w/ LF
84	438	744	0	0
118	615	1,045	0	0
151	786	1,337	0	0
185	964	1,638	0	0
218	1,135	1,930	0	0
252	1,313	2,231	0	0

	vertical pressure lb/ft^2	
	w/o LF	w/ LF
Roof	890	1,246

Structure: 216-B-12

depth of soil in.	lateral pressure on walls lb/ft^2			
	LE w/o LF	LE w/ LF	F w/o LF	F w/ LF
180	938	1,594	0	0
204	1,063	1,806	0	0
228	1,188	2,019	0	0
252	1,313	2,231	0	0
276	1,438	2,444	0	0
300	1,563	2,656	0	0

	vertical pressure lb/ft^2	
	w/o LF	w/ LF
Roof	1,890	2,646

Structure: 216-Z-6

depth of soil in.	lateral pressure on walls lb/ft^2			
	LE w/o LF	LE w/ LF	F w/o LF	F w/ LF
72	375	638	0	0
80	417	708	0	0
89	464	788	0	0
97	505	859	0	0
105	547	930	0	0
113.5	591	1,005	0	0

	vertical pressure lb/ft^2	
	w/o LF	w/ LF
Roof	765	1,071

Structure: 216-Z-7

depth of soil in.	lateral pressure on walls lb/ft^2			
	LE w/o LF	LE w/ LF	F w/o LF	F w/ LF
72	375	638	0	0
79	411	699	0	0
86	448	761	0	0
94	490	832	0	0
101	526	894	0	0
108	563	956	0	0

	vertical pressure lb/ft^2	
	w/o LF	w/ LF
Roof	765	1,071

Structure: 216-Z-9

This is a concrete covered crib, with earth walls slanted inward. Therefore, lateral pressure results are not tabulated below as no side loads were applied to the ANSYS model.

	vertical pressure lb/ft^2	
	w/o LF	w/ LF
Roof	128	179

Structure: 241-T-361

depth of soil in.	lateral pressure on walls lb/ft^2			
	LE w/o LF	LE w/ LF	F w/o LF	F w/ LF
72	375	638	0	0
120	625	1,063	0	0
165	859	1,461	0	0
210	1,094	1,859	-350	-315
255	1,328	2,258	-748	-673
300	1,563	2,656	-1,146	-1,031

	vertical pressure lb/ft^2	
	w/o LF	w/ LF
Roof	840	1,176

Structure: 241-Z-361

depth of soil in.	lateral pressure on walls lb/ft^2			
	LE w/o LF	LE w/ LF	F w/o LF	F w/ LF
24	125	213	0	0
72	375	638	0	0
117	609	1,036	0	0
162	844	1,434	-53	-48
207	1,078	1,833	-451	-406
252	1,313	2,231	-849	-764

	vertical pressure lb/ft^2	
	w/o LF	w/ LF
Roof	415	581

Structure: 241-Z-8

depth of soil in.	lateral pressure on walls lb/ft^2			
	LE w/o LF	LE w/ LF	F w/o LF	F w/ LF
72	375	638	0	0
91	474	806	0	0
110	573	974	0	0
130	677	1,151	0	0
149	776	1,319	0	0
168	875	1,488	0	0

	vertical pressure lb/ft^2	
	w/o LF	w/ LF
Roof	765	1,071

Structure: PUREX Deep Bed Filter

depth of soil in.	lateral pressure on walls lb/ft^2			
	LE w/o LF	LE w/ LF	F w/o LF	F w/ LF
48	275	468	0	0
80	442	751	0	0
112	608	1,034	0	0
144	775	1,318	0	0
176	942	1,601	0	0
211.5	1,127	1,915	0	0

	vertical pressure lb/ft^2	
	w/o LF	w/ LF
Roof	715	1,001

Structure: REDOX Sand Filter

depth of soil in.	lateral pressure on walls lb/ft^2			
	LE w/o LF	LE w/ LF	F w/o LF	F w/ LF
0	0	0	0	0
47	245	416	0	0
95	495	841	0	0
142	740	1,257	0	0
190	990	1,682	0	0
236	1,229	2,090	0	0

	vertical pressure lb/ft^2	
	w/o LF	w/ LF
Roof	115	161

Structure: 241-CX-70

depth of soil in.	lateral pressure on walls lb/ft^2			
	LE w/o LF	LE w/ LF	F w/o LF	F w/ LF
132	688	1,169	0	0
168	875	1,488	0	0
204	1,063	1,806	0	0
240	1,250	2,125	0	0
276	1,438	2,444	0	0
312	1,625	2,763	0	0

	vertical pressure lb/ft^2	
	w/o LF	w/ LF
Roof	1,696	2,375